AD NUMBER

AD862599

LIMITATION CHANGES

TO:

Approved for public release; distribution is unlimited.

FROM:

Distribution authorized to U.S. Gov't. agencies and their contractors; Critical Technology; AUG 1969. Other requests shall be referred to U.S. Army Aviation Materiel Laboratories , Fort Eustis , Virginia 23604. This document contains export-controlled technical data.

AUTHORITY

USAAMRDL ltr, 23 Jun 1971

AD

USAAVLABS TECHNICAL REPORT 69-53

ADVANCED ENGINE CONTROL SYSTEM STUDY

By

Joseph Karol
Robert Hatch

August 1969

U. S. ARMY AVIATION MATERIEL LABORATORIES
FORT EUSTIS, VIRGINIA

CONTRACT DAAJ02-68-C-0042
AVCO LYCOMING DIVISION
STRATFORD, CONNECTICUT

Disclaimers

The findings in this report are not to be construed as an official Department of the Army position unless so designated by other authorized documents.

When Government drawings, specifications, or other data are used for any purpose other than in connection with a definitely related Government procurement operation, the United States Government thereby incurs no responsibility nor any obligation whatsoever; and the fact that the Government may have formulated, furnished, or in any way supplied the said drawings, specifications, or other data is not to be regarded by implication or otherwise as in any manner licensing the holder or any other person or corporation, or conveying any rights or permission, to manufacture, use, or sell any patented invention that may in any way be related thereto.

Trade names cited in this report do not constitute an official endorsement or approval of the use of such commercial hardware or software.

Disposition Instructions

Destroy this report when no longer needed. Do not return it to the originator.

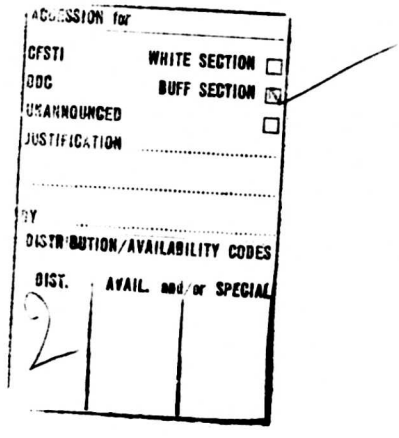

DEPARTMENT OF THE ARMY
HEADQUARTERS US ARMY AVIATION MATERIEL LABORATORIES
FORT EUSTIS, VIRGINIA 23604

The research described herein was conducted by Lycoming Division, AVCO Corporation under U. S. Army Contract DAAJ02-68-C-0042. The work was performed under the technical management of Mr. R. G. Furgurson, Propulsion Division, U. S. Army Aviation Materiel Laboratories.

Appropriate technical personnel of this Command have reviewed this report and generally concur with the conclusions and recommendations contained herein.

The findings and recommendations outlined herein will be considered in planning future programs of engine control development.

Project 1G162203D144
Contract DAAJ02-68-C-0042
USAAVLABS Technical Report 69-53
August 1969

ADVANCED ENGINE CONTROL SYSTEM STUDY

Final Report

Avco Lycoming Report No. 105.5.6

By

Joseph Karol
and
Robert Hatch

Prepared by

Avco Lycoming Division
Stratford, Connecticut

for

U. S. ARMY AVIATION MATERIEL LABORATORIES
FORT EUSTIS, VIRGINIA

ABSTRACT

This report presents the results of a program conducted to design and evaluate an advanced engine control system for a small (2 to 5 pounds per second airflow) turboshaft engine.

The objective of this program was to evaluate the feasibility of a unique engine control system consisting of closed-loop turbine-inlet-temperature limiting, electronic computation and either of two novel fuel metering systems.

Control mode logic and dynamics were analyzed using computer simulation techniques. Control computer logic and circuitry were established, and all elements of the control system were designed.

The efforts of this program produced the following results:

1. Closed-loop turbine inlet temperature control mode logic and dynamics criteria

2. Two electronic control computer designs

3. Two compact fuel metering system designs

4. Design and analysis of a fluidic turbine inlet temperature sensor and averaging system

5. Optimum packaging and cost for each of the control systems

It was concluded that a miniaturized advanced control system, weighing 6 to 9 pounds (including pump), is feasible with either of two fuel metering systems and with either analog or digital electronic computation.

Operation of the closed-loop turbine inlet temperature control mode was satisfactorily demonstrated using computer simulation techniques.

Problems associated with fluidic temperature sensing, such as time response, reliability, and ambient temperature compensation, were resolved either analytically or by testing. Turbine inlet temperature averaging remains the key problem to be solved by hardware development.

The comparison of analog and digital electronic computation favors the analog approach based largely on cost. However, by 1975, the digital

approach should achieve significant cost, weight, accuracy, and flexibility advantages.

Analysis of the weights and costs of the two proposed fuel metering systems slightly favors the centrifugal-pump variable-speed drive approach. More important, the centrifugal pump system offers a number of significant advantages which strongly recommend further development.

All components of the control systems evaluated during this study program are within a reasonable level of technology commensurate with production by the mid-to-late 1970's.

FOREWORD

This program study was conducted under USAAVLABS Contract DAAJ02-68-C-0042 (DA Project 1G162203D144) by the Avco Lycoming Division, Stratford, Connecticut during the period of 1 July through 31 December 1968. The results of work and concepts developed under various Contributing Engineering and Independent Research and Development (IRAD) Programs conducted at Avco Lycoming have contributed to the preparation of this report.

Acknowledgement is made of the following companies and organizations for their assistance in this study program:

Pesco Products Division, Borg Warner
Mechanical Components Division, TRW
Globe Industries Division, TRW
Aeroflex Laboratories, Incorporated
Flow Corporation
D. G. O'Brien, Incorporated
Harry Diamond Laboratories, U. S. Army
Avco Electronics Division
Film Microelectronics, Incorporated
Dielectric Systems, Incorporated
Microelectronics Division, General Instruments Corporation
Oeco Corporation

TABLE OF CONTENTS

LIST OF ILLUSTRATIONS

LIST OF TABLES

LIST OF SYMBOLS

A	area, ft^2
C_1	sensor cavity capacitance, Btu/^oR
C_2	sensor material capacitance, Btu/^oR
Cp	specific heat of the gas at a constant pressure, Btu/lb - ^oF
h	heat transfer coefficient, Btu/hr - ft^2 - ^oF
$I_{1,2,3}$	loop currents (heat flow), Btu/sec
K	heat transfer coefficient, Btu - ft/hr - ft^2 - ^oF
K_I	integral gain
Kp	proportional gain
L_t	plate thickness, ft
N_h	high-pressure engine rotor speed, rpm
N_l	low-pressure engine rotor speed, rpm
Np	engine power turbine shaft speed, rpm
P_k	path transmittance = the path from a source to a node
P_1	ambient absolute air pressure at engine inlet, psia
q	heat transfer from the gas to the duct wall, Btu/hr
Q_l, Q_{loc}	engine output shaft torque, ft-lb
Q_r, Q_{rem}	output shaft torque of remote engine(s) in multiengine applications, ft-lb
R_1	inlet orifice resistance, ^oR/Btu/sec
R_2	inside film resistance, ^oR/Btu/sec

R_3	outside film resistance, ^{o}R/Btu/sec
S	LaPlace Transform
T_a	sensor cooling air temperature, ^{o}R
T_{avg}	average temperature of the gas in the duct, ^{o}F
T_b	sensor body temperature, ^{o}R
T_c	sensor cavity temperature, ^{o}R
T_i	duct inside wall temperature, ^{o}F
T_T	overall transfer function or graph transmittance
T_1	ambient air temperature at engine inlet, ^{o}F
T_5	gas temperature at inlet to high-pressure rotor turbine, ^{o}R
W_a	airflow or gas flow, lb/sec
W_f	fuel flow, lb/hr
Δ	graph determinant = 1 - (sum of loop transmittances) + (sum of pairs of nontouching loops) - (sum of triplets)
Δ_k	path factor = graph determinant of the remaining portion of the signal flow graph when the path transmittance is removed
ΔT	temperature drop across the plate, ^{o}F
ΔT_{gas}	temperature drop of the gas, ^{o}F
β	helicopter rotor collective pitch setting
τ	time constant
ω	frequency, rad/sec

Prefixes and Suffixes for Electronics and Computer Sections

AVG	Average
SEL	Select
MEAS	Measured
LIM	Limit
ACC, ACCEL	Acceleration
DEC, DECEL	Deceleration
COMMAND	Command

BLANK PAGE

INTRODUCTION

Future generations of gas turbine engines will be significantly smaller and more efficient than those in use today. Current advanced technologies permit engine operation at higher speeds, higher temperatures, higher pressure ratios and better component efficiencies. Unfortunately, comparable improvement in engine control system technology has not kept pace with engine technology. The controls that are being developed today continue to be relatively large, heavy, and costly. Furthermore, the controls are custom-designed for a particular type of engine owing to the limitation of control mode and envelope.

Objectively, the design of an advanced engine control system must provide a more flexible control mode and achieve substantial reductions in size, weight, and cost. To accomplish these objectives Avco Lycoming pursued the evaluation of a control system that offers a novel approach to the requirements but uses hardware that is within reasonable reach of current technology.

Flexibility in application of a control system is more likely to result from the initial selection of parameters than from any other subsequent decision. In the absence of a feasible surge detector to limit acceleration fuel, the control designer must retreat a step and attempt to measure an engine parameter that rapidly indicates the effect of overfueling. Such a parameter is turbine inlet temperature, but until recently, sensors having any reasonable environmental life have been too slow to detect the rapid changes that occur in this parameter. Recent developments in miniature fluidic oscillator temperature sensors make feasible further study of turbine inlet temperature acceleration controls. This report concentrates its scope in evaluating this particular mode and the hardware necessary for its implementation.

To a great extent, miniaturization, like flexibility, requires a departure from existing practices in gas turbine fuel control design. The success of the missile industry in miniaturizing solid-state electronic controls is directly applicable to the control problem of future gas turbines. Thus, the report emphasizes the study of both analog and digital electronic circuits and packaging techniques.

Beginning with the proposal for this study, it was felt that any advanced engine controls study should seriously consider the integration and interfacing of accessories, in particular the fuel pump and fuel metering system. In essence, the gas turbine fuel control requires the services of these components to do its job. Additional substantial miniaturization can

be obtained by considering high-speed fuel pumps and integration or elimination of fuel metering components when studying new control concepts. A substantial section of the report is, therefore, devoted to evaluating the design of the most promising pumping and metering systems.

Another major section of the report deals extensively with the temperature sensors, compensation of sensor errors, turbine inlet temperature averaging, and the design of the necessary interface hardware. In any new control concept, such as this, it is necessary to isolate the potential problems and to offer alternatives. Such is the intent of the section on sensors.

Finally, upon completion of the design and analysis of each subsystem, system packaging layouts were prepared and cost and weight estimates were obtained.

SUMMARY DESCRIPTION OF THE CONTROL SYSTEM

The advanced engine control system (Figure 1) incorporates a fuel metering section whose output flow is controlled by an electronic computer. The computer receives command signals from the pilot and inputs from engine parameter transducers. The required engine fuel flow and the status of the engine variable-geometry devices are determined by the computer. During engine start, the computer also controls the combustor ignitor flow and protects the engine from the effects of a hot start by cutting off fuel flow.

The functions performed by the control system are:

1. Controls starting, and acceleration and deceleration fuel flows
2. Controls sequencings of automatic starts
3. Governs full range of gas producer speed (turboprop applications)
4. Protects engine from gas generator and free turbine overspeeds
5. Controls free turbine speed with wide range of speed selection (turboshaft applications)
6. Limits closed-loop turbine inlet temperature
7. Limits closed-loop torque
8. Provides load sharing for multiengine installations via torque control
9. Positions compressor and/or turbine variable geometry
10. Provides input signals to an engine analyzer.

Turbine inlet temperature limiting is used to provide the transient mode of engine control. Acceleration and deceleration temperatures are limited by programming referred turbine inlet temperature against referred gas producer speed as shown in Figure 2.

An isochronous governor provides the pilot with a wide range of power turbine speed control for turboshaft operation. In multiple engine installations, the pilot setting may be modified by the load-sharing function of the computer.

For turboprop operation, engine power level is established by the pilot's selection of gas producer speed. The gas producer governor is also isochronous.

Either speed governor system may be overruled by one or more of the proportional limiting sections of the computer through the "select minimum" logic. Primary limit functions are low-pressure rotor overspeed if applicable, power turbine overtorque, and transient turbine inlet temperature. The computer also contains "select maximum" logic, which insures that fuel flow never drops below that required to sustain combustion.

Under emergency conditions such as power turbine overspeed and overtemperature, the computer will activate a fast-response solenoid valve to shut down all fuel flow to the engine.

Engine variable-geometry systems will be controlled by electrohydraulic or electropneumatic servo systems. The computer generates geometry position schedules as a function of engine parameters. Electrical position transducers mounted on the actuators provide position feedback to the computer, and the resultant position error acts to control the interface devices of the system.

CONTROL MODE STUDY

GENERAL

To imply that fuel flow scheduling is obsolete for future gas turbines would be extremely premature and a gross injustice to this proven method. Yet, in a sense, we do so when we propose to study closed-loop acceleration control via turbine inlet temperature. In doing this, however, we must be careful to recognize the faults and limitations in this mode of control.

Most high-performance military gas turbine engines are limited in their appetite for acceleration fuel by the region of compressor surge which could extend well up into the useful power range. In the high power range and usually during starting, the limitation is established by the maximum allowable turbine inlet temperature. Many of the gas turbine engines in production today have maximum turbine inlet temperature limiters or temperature selection, as in fixed-power turbine engines. Only a few of these, however, provide control of acceleration fuel by this limiting of turbine inlet temperature. Those that have this capability are primarily industrial turbines that operate well away from their compressor surge regions and with less stringent requirements on acceleration time.

The latest tool that permits T_5 acceleration control on military engines is the fluidic oscillator temperature sensor. In essence, its nearly instant response during transients will record the temperature spikes in the combustor when fuel flow is changed abruptly. The temperature spikes and associated pressure changes are related thermodynamically to produce a transient operating point on the compressor map. Thus, rapid measurement of T_5 permits close observance of the compressor surge line.

Certain inherent advantages of the closed-loop turbine inlet temperature control mode are:

1. Interchangeability with regenerator cycle engines
2. Immunity to different fuel types
3. Ability to eliminate the altitude pressure variable

With these advantages in mind, the objectives of this control mode analysis were to:

1. Verify and evaluate control system logic

2. Modify and optimize the system logic

3. Evaluate different hardware approaches

4. Stabilize and optimize system response

5. Define problem areas in the system approach

6. Provide potential alternatives

STUDY APPROACH

To conduct this analysis, it was necessary to use an advanced engine cycle in the 2- to 5-lb/sec airflow class. A representative split compressor configuration with free power turbine was selected. Design points were a pressure ratio of 14:1 and a turbine inlet temperature of 2370° F. A turboshaft engine having approximately 5 lb/sec design airflow was used for the basic studies. Variations to the basic engine configuration were considered, such as a turboprop version, a regenerator with variable power turbine stators, twin turboshafts, reduced airflow, and 16:1 cycle pressure ratio with a turbine inlet temperature of 2500°F.

It was recognized that a split compressor design would require an additional speed sensor and control loop in the system. On the other hand, analysis derived with a split compressor engine provides results which are more comprehensive and universally applicable than for a single-spool design.

The following general requirements were initially established for the control system to provide boundaries on the study:

1. Power turbine speed governing for helicopter applications

2. Full-range gas producer speed governing for turboprop applications

3. Closed-loop turbine inlet temperature limiting during acceleration and deceleration

4. Low-pressure spool overspeed limiting

5. Torque limiting

6. Load sharing in the twin-engine configuration.

These requirements were expanded further, as follows, to provide a control system logic diagram (Figure 3) for linear response studies on the EAI 131R analog computer:

1. The power turbine speed governor should be isochronous to assure constant helicopter rotor speed regardless of load and flight conditions.

2. The gas producer speed governor and maximum steady-state turbine inlet temperature governor should be isochronous to maintain the same limits regardless of flight condition.

3. Acceleration and deceleration control should be performed by comparing the turbine inlet temperature with a reference temperature generated as a function of gas producer speed and compressor inlet temperature.

4. Compressor inlet or discharge pressure sensing should be avoided for altitude and flight speed compensation, since sufficient parameters and isochronous governing are provided for this purpose.

5. Limiting functions should take over from the governing function through a "select minimum" logic. A "select maximum" logic should also be employed to assure that the fuel never drops below that required to sustain combustion.

ANALYSIS METHOD

The control mode analysis was divided into two phases consisting of (1) a linear system response analysis and (2) a nonlinear system response analysis. The first phase individually established system stability for each control loop and was performed using an analog computer. Interaction of different control loops, acceleration control accuracy, and large-scale engine transients were evaluated during the nonlinear response analysis phase using the MIMIC program described subsequently. Modifications to the control system logic were incorporated during and subsequent to each phase.

LINEAR SYSTEM RESPONSE ANALYSIS

Baseline Engine Analysis

Three components comprise the system in a study of this type. Two of these are independent, e.g., the engine and load, but must be reduced to a dynamic model or analog. The third component, the engine control, is dependent and its configuration and dynamics must be varied to suit the other two.

Considering the engine first, a block diagram or model is constructed to represent the mathematical relationships occurring between those parameters received from and delivered to the controller. Quantities contained within the blocks are in the form of partial derivatives and are known as "engine gains". They are obtained by allowing each independent variable to make a 4-percent excursion from the engine steady-state operating line while holding all other variables constant.

By referring the engine gains at lower power level to their corresponding design point value, dimensionless engine gains are obtained. For similar engines of different airflow, but identical design turbine inlet temperature and pressure ratio, the dimensionless gains are comparable as indicated in Table I. Thus, the results of the control analysis at 5 lb/sec design are applicable to a scaled 2 lb/sec engine.

When considering the turboshaft engine, the load was assumed to be a helicopter rotor and power turbine having a torsional resonant frequency of 5 cycles per second. This value is based on earlier Avco Lycoming studies of advanced engines and rotor systems. No lag hinges or dampers were used in the analysis to simulate "worst case" control applications.

When power turbine speed is controlled with a resonant load system, sufficient stability margin must be provided at both the control loop crossover frequency (unity gain) and the resonant frequency. Not only is it important to provide at least 40-degree phase margin at crossover, but the control should attenuate the resonance to at least 50 percent of unity. These were the stability criteria established for the linear system study.

The engine, load, and control logic were simulated on an analog computer to evaluate the system stability, one loop at a time. Single-engine operation was investigated at three power levels, and a twin-engine installation was investigated at 55 percent per engine. Step changes in load and power setting were limited to 10 percent to remain within the linear range of engine gains.

Proportional, integral, and proportional-plus-integral control were investigated. Individually, each has its merits. Proportional control permits a higher crossover frequency than the integral but suffers from steady-state inaccuracy or "droop". Integral control offers high accuracy but can easily become unstable at the crossover frequency by virtue of its basic 90-degree phase lag. The preferred approach is proportional plus integral to obtain the benefits of both and eliminate the need of an altitude compensator for "droop".

The transfer function for a proportional-plus-integral governor may be defined as

$$\frac{K_p}{\tau S + 1} + \frac{K_I}{S}$$

Rearranging terms and allowing τ to become small, the function looks like

$$\frac{K_I \left(\frac{K_p}{K_I} S + 1 \right)}{S}$$

which is shown graphically in Figure 4.

Various gains and shaping networks were investigated at three engine power conditions before each loop was optimized to obtain the desired response.

Table II presents the optimum control gains and sensor time constants at the three engine power conditions. Figure 5 defines the block diagram of the simulation.

With the optimized values, a 10-percent step disturbance was introduced into each control loop.

Tables III and IV present the performance obtained in each loop in response to the indicated disturbance.

As mentioned earlier, the stability criteria for the power turbine speed control loop must be maintained for two frequency modes. The low-frequency (crossover) mode is determined primarily by the engine parameters and the higher frequency mode by the power turbine and rotor

inertias and rotor system torsional stiffness. Since the rotor system is very lightly damped, the system tends to oscillate at the resonant point of 5 cps. The proportional lag of the governor was designed to attenuate the high-frequency mode. This was done by a simple lag network having a time constant of 0.2 second, allowing a gain margin of approximately 50 percent at the 5-cps point.

A frequency response of the power turbine speed loop was conducted. (See Figures 6 and 7.) Note that the crossover frequency of the loop is 0.25 cps with a phase margin of 40 degrees. The gain margin at the load resonance is approximately 50 percent. As in the previous cases, the gain constants were evaluated at three power levels. (Refer to Table III.) The system was excited with a 10-percent step of collective pitch (β) and was allowed to settle. The maximum undershoot was 0.8 percent, and the system settled to within 0.1 percent within 3.0 seconds. Various forms of β reset were investigated to improve the transient droop. One method was $d\beta/dt$, which proved to be unsuccessful and, because the timing and the slope of the signal were very critical, was abandoned. The second form investigated was β position reset which did reduce the transient droop. However, the integrator aids in this area, in that it also eliminates the steady-state droop. Either the β reset could be used as a course corrector and the integrator allowed to act as a fine corrector, or the β reset could be ignored.

Twin-Engine Operation

A twin-engine application in a helicopter was investigated for stability. At the point of interest, each engine produced 55 percent of its available power. Table V presents the transient performance obtained in the power turbine loop.

Regenerator Engine Considerations

A regenerator and a variable power turbine stator area control were added to the single-engine system. The three loops investigated were the power turbine speed loop, the T_5 loop, and the N_h loop. Ten-percent step disturbances were introduced into each loop, and the results are shown in Table VI.

Comparing Table VI with Table III, note that the major difference in performance is the long settling characteristic in gas producer speed. This is not unusual when considering that the fuel flow has ceased to vary but the heat exchanger continues to change its heat input for as much as 4

seconds. This also affects the transient accuracy of the T_5 control since the heat exchanger represents a long time constant in the feedback path to the control.

The results indicated that the gains and shaping networks optimized for the basic engine will produce acceptable performance with a regenerator.

NONLINEAR SYSTEM RESPONSE ANALYSIS

After the control parameters of each loop were optimized independently, using the linear analysis, it was necessary to perform large-scale acceleration and deceleration transients to observe the interactions between loops as control was passed from one to the other.

To facilitate this study, a simulation program (MIMIC) was created for the engine and load. (See Figure 8 and 9.) Essentially MIMIC is a program for digital computers written in analog form (refer to Appendix I). The engine is stored in the form of component maps to provide any station temperature, pressure, flow, or speed throughout the transient calculation. A MIMIC representation of the control computer and MIMIC simulations of the fuel metering systems, Nos. 1 and 2, are provided in Figures 10, 11, and 12, respectively.

Turboshaft and turboprop versions of the engine were studied. Large-scale acceleration and deceleration transients of 50 and 100 percent power change were performed on the complete control system. This was done with a nonresonant load to minimize computer time.

During preliminary studies, it became apparent that the control had to be altered to eliminate interaction between the loops. Initially, each governor had its own individual integral path, and severe transient excursions ensued when mode switching occurred. The control was modified to incorporate one common integrator for all the proportional governors. This dramatically reduced transient excursions.

Further studies showed that transients which did not approach the acceleration temperature reference tended to transfer control back and forth between the speed and temperature governing modes. To correct this undesirable effect, the temperature control loop was converted from a governor to a limiter, as indicated in the final system logic diagram (Figure 3).

For the turboshaft application, 1-second ramps of 3 different collective pitch magnitudes were introduced to the system (0 to 50 percent, 50 to 100 percent, and 0 to 100 percent). The system responses to the disturbances are displayed in Figures 13 through 18. For the smaller excursions, the temperature did not reach its acceleration limit. The response noted in the other parameters is typical of turboshaft operation. For the 100 percent excursion, the temperature did reach the acceleration limit and limited the temperature to within 1 percent of the desired schedule. The reduction of fuel is evident in the trace. Again, the response noted in the other parameters is typical of turboshaft operation. The initial delay noted on the traces is attributed to the 1-second ramp input and the use of a resonant load equilizer.

For the turboprop application, a 0.3-second ramp of N_h select from flight idle to takeoff power was introduced to the system. The system responses are shown in Figures 19 and 20. The temperature did reach the acceleration limit and controlled the temperature to within 5 percent of the desired value in the low power region but within 1 percent in the higher power region. With further optimization of the system for a specific engine, this value can be reduced. The responses noted are typical of turboprop engine operation. Decelerations were checked for proper operation, as were smaller disturbances.

The final control logic for a turboshaft engine utilizes a wide-range power turbine speed governor selected by the pilot, with all other functions operating as limiters. For the turboprop engine, the gas producer is controlled by an all-speed governor, and all other features operate as limiters. The control can be used interchangeably with minor modification.

The multiple-function fuel handling valve with a positive displacement pump and a VSD with a centrifugal pump were evaluated within the control system. The results indicated that the control will accept the dynamics of either fuel metering system with little or no modification of the computer.

START-FUEL SCHEDULING

One of the most serious deficiencies in automatic controls for gas turbine engines is their inability to generate the highly empirical start-fuel schedules required with any real degree of accuracy. This control is no exception, although it has one distinct advantage. Limiting the fuel rate by sensing turbine inlet temperature avoids the major problem of starting with cold fuel and restarting with a hot engine.

Regarding the accuracy of determining fuel rate by this method, the weak link lies in the fluidic oscillator temperature sensor itself. The sensor requires choked airflow through its cavity to generate a frequency proportional to the square root of absolute temperature without pressure effects. Below the choking condition, the generated frequency falls off much the same as the flow function through a nozzle. Avco Lycoming's experience with fluidic oscillators has been mostly with those having a threshold pressure level of 1.0 psig. Between this level and choking, they will generate a frequency which is related to temperature but is erroneous due to pressure level. Down to about 30 percent high-pressure spool speed, the 1.0 psig threshold sensor can hold its own (including temperature averaging and fuel flow sensor errors) with the best of today's 3D cam controls. However, between 30 and 20 percent N_h, at which speed the minimum fuel flow setting occurs, the sensor, averaging and metering errors combined climb to about 16 percent.

A recent development at Harry Diamond Laboratories holds the promise of greater sensor accuracy at or near engine firing conditions. This is a fluidic oscillator having a 0.1-psig threshold level. Characteristics of this sensor should provide improved accuracy at lower speeds.

The intent of the subject matter in this section was to highlight the fact that a problem of temperature sensing and averaging errors exists in the starting region. Any subsequent hardware development program must address itself to the solution of this problem if the goal of developing a truly workable closed-loop temperature control is to be achieved.

ELECTRONIC COMPUTER

CIRCUIT DESIGN

The object of the circuit design effort was to produce the best computer design possible, incorporating the latest of a rapidly changing electronic technology. Other factors being equal, the test design is the one which is the simplest and results in the smallest package. To achieve this goal, two distinctly different computer designs, one analog and the other digital, were prepared for comparison.

Analog circuitry is being used extensively for similar control applications. Digital circuitry, while quite promising, is relatively new to this type of application, and the merits of this approach have not yet been established. Most of the circuit design effort was spent on the digital design because the unknowns were principally in this area.

Both designs were successfully completed and are discussed in detail in the following paragraphs of this section. The relative merits of each design are presented in a final comparison summary.

The power supply circuit is discussed first because it is essentially the same for both designs.

POWER SUPPLY CIRCUIT

The power supply circuit (Figure 21) converts ac generator voltage to the dc voltage required by the computer and its external elements. Accuracy of the regulation required for the computer is 1 percent of the voltage; however, the voltage required for the external loads such as solenoids and servos can vary by $\pm$ 10 percent.

While several designs of a power supply circuit were considered, the final design is based on the use of a regulated (excited field) generator. (Refer to Appendix VI.) The terminal voltage of the generator is controlled by a computer-supplied excitation current V_{exc} and is controlled to $\pm$ 10 percent. The regulation required for the external loads is accomplished at the generator. The ac voltage is then rectified in the computer before transmission. This configuration results in a minimum of power-handling regulator circuits and minimum internal power dissipation. With the $\pm$ 10 percent rectified voltage applied to the regulating circuit, the regulator requires only a simple power amplifier operating on a fixed reference voltage.

ANALOG CIRCUIT

General

Computation is generally performed by the use of operational amplifiers and feedback circuitry (consisting of resistors and capacitors). The operational amplifier itself is a high-gain (of the order of 2000) voltage amplifier to which external components are connected in a negative feedback arrangement. This reduces the net gain of the device but improves overall performance.

Inaccuracies in an operational amplifier circuit result from both gain and zero offset errors which result from changes in ambient temperature. The accuracies given are those to be expected over the required temperature range. All accuracies specified are in percentage of full scale. It should be noted that in a closed-loop control mode, gain variations do not significantly contribute to performance degradation.

For simplicity, potentiometers are shown as command and position transducers in the diagrams. Linear variable differential transformers (or equivalent devices) and their associated conditioning circuitry would actually be used in applications where reliability is critical such as the high-pressure spool speed select function.

Signal Conditioning Circuits

Engine Speed and T_5 Signal Conditioning Circuit

This circuit converts the variable frequency signal from a magnetic pickup or a fluidic temperature sensor to a proportional dc voltage.

The signal to be measured is converted to a square wave by a high-gain amplifier (see Figure 22). The square wave is differentiated, and the resulting pulses trigger a one-shot multivibrator whose output is a constant-duration pulse at a rate equal to the frequency of the source. The generated pulses are then amplitude regulated and integrated to obtain the dc voltage proportional to signal frequency.

This circuit is capable of $\pm$ 1 percent accuracy under all operating conditions.

Turbine Inlet Temperature Averaging Circuit

This circuit (Figure 23) computes the average turbine inlet temperature, T_5 AVG, based upon measurements taken on 8 individual temperature sensors. Each sensor frequency is converted to a proportional dc voltage. The 8 signals are connected through solid-state switches to the averaging circuit. Each switch is controlled by a comparator, which opens the switch in the event of a failure of the associated sensor. The averaging circuit will continue to generate the average of the remaining active sensor outputs.

The averaged output of all 8 sensors is normally transduced with an accuracy of $\pm$ 1 percent. This accuracy changes to $\pm$ 1-1/4 percent with 7 active sensors, and $\pm$ 2 percent with just 4 active sensors.

Fuel Control Mode Circuits

Power Turbine Speed Governor with Load Sharing Circuit

This circuit (Figure 24) represents the proportional section of the power turbine speed governor. It corrects errors in power turbine speed caused by sudden speed-select changes or fast external perturbations. The complete power turbine speed governor consists of this proportional circuit, the mode select, and the integrator.

The desired power turbine speed is selected by positioning the N_p SEL potentiometer. The N_p SEL voltage applied to the control circuit is compared with a voltage representing the power turbine speed, N_p MEAS. The difference (error) voltage is amplified by A1 and A2 to obtain a voltage representing the amount of fuel required W_f (N_p) to correct N_p MEAS.

For twin-engine applications, load sharing has been incorporated. The local engine torque (Q_{loc}) refers to the engine being controlled by the circuit under consideration. When the remote (other) engine torque Q_{rem} is greater than Q_{loc}, W_f (N_p) is changed in a direction to raise the level of the engine at lower power. Under no circumstances will the control reduce the power of either engine.

Noise immunity is afforded by the feedback capacitor in the A1 circuit which reduces the high-frequency response.

This circuit is capable of the following performance over the operating temperature range:

Loop Accuracy, $\pm$ 1-1/2 percent

Gain Variation, $\pm$ 1 percent

High-Pressure Spool Speed Governor Circuit

This circuit (Figure 25) represents the proportional or "fast path" section of the high-pressure spool speed governor. Its purpose is to correct errors in high-pressure spool speed caused by sudden speed-select changes or fast external perturbations. The complete high-pressure spool speed governor consists of this proportional control, the mode select, and the integrator.

The desired high-pressure spool speed (N_h SEL) voltage is compared with a voltage representing measured high-pressure spool speed (N_h MEAS). The difference (error) voltage is amplified by A1 and A2 to obtain a voltage representing the amount of fuel W_f (N_h) required to correct N_h MEAS.

This circuit is capable of the following performance over the operating temperature range;

Loop Accuracy, $\pm$ 1 percent

Gain Variation, $\pm$ 1 percent

Power Turbine Torque and Low-Pressure Spool Speed Limiter Circuits

These circuits (Figure 26) prevent overtorque and overspeed of the controlled engine. The complete limiters consist of these circuits: the mode select and the integrator.

The fixed design limits of torque and speed are represented by fixed voltages Q_{loc} LIM and N_1 LIM. The limit voltages are compared with voltages representing the measured torque, Q_{loc} MEAS, and measured speed, N_1 MEAS. The error voltages are amplified to obtain voltages representing the amount of fuel required to keep the levels of the measured parameters below the design limits.

These circuits are capable of the following performance over the operating temperature range:

Loop Accuracy, $\pm$ 2 1/2 percent (torque limiter)

$\pm$ 1 percent (speed limiter)

Gain Variation, $\pm$ 1 percent

Acceleration and Deceleration Limit Circuit

This circuit (Figure 27) maintains upper (acceleration) and lower (deceleration) limits of flow to prevent engine surge, overtemperature, and flameout. The complete circuit consists of the proportional sections, the mode select, and the integrator.

Acceleration and deceleration fuel flows are determined as functions of the proximity of turbine inlet temperature (T_5 MEAS) to surge and flameout levels, T_5 ACCEL REF and T_5 DECEL REF, respectively. T_5 ACEL REF and T_5 DECEL REF, having been computed as functions of high-pressure spool speed and compressor inlet temperature, are compared with T_5 MEAS. The difference voltages are amplified to obtain voltages representing acceleration and deceleration fuel flow limits, W_f (ACC) and W_f (DEC), respectively.

Improved loop stability results from a level-dependent loop gain which is higher for large errors.

This circuit is capable of the following performance over the operating temperature range:

Loop Accuracy, $\pm$ 1 percent

Gain Variation, $\pm$ 1 percent steady state

$\pm$ 3 percent transient

Control Mode Selector Circuit

This circuit (Figure 28) selects the fuel control mode and passes the command fuel flow demanded by that mode to the integrator.

The selector first chooses, on a "least wins" basis, among the outputs of the power turbine governor, the torque limiter, the high-pressure spool speed governor, the acceleration limit control, and the low spool speed limiter. For example, if the acceleration limit fuel, W_f (ACC), is the least output, then the "least wins" section will select W_f (ACC). The signal selected is passed to the next section of the circuit, where it is compared on a "most wins" basis to the deceleration limit and a fixed starting fuel flow level, LOW W_f LIM. If all signals are at a lower level than that of the deceleration limit, the output of the control mode selector will be the deceleration limit W_f (DEC).

This circuit is capable of the following performance over the operating temperature range:

Loop Accuracy, $\pm$ 2 percent

Gain Variation, $\pm$ 1 percent

Integrator Circuit

This circuit (Figure 29), common to all control modes, minimizes steady-state control errors by providing high gain under steady-state conditions. Under transient conditions, the circuit presents a low gain proportional path. The output of the integrator is the final computed value of command fuel.

A voltage representing high-pressure spool speed, N_h MEAS, drives a function generator, the output of which is G (N_h). The output of the linear ramp generator and G (N_h) are inputs to a comparator C1. Output voltage of the comparator is positive when G (N_h) is greater than the ramp voltage and zero when G (N_h) is less. The output of the comparator is, therefore, a rectangular wave signal whose duty cycle is proportional to G (N_h). This signal is used to switch the output voltage of the mode selector, $\dot{W}_f$ COMMAND, resulting in a rectangular wave signal whose duty cycle is proportional to G (N_h) and whose amplitude is proportional to $\dot{W}_f$ COMMAND. When this signal is acted upon by integrating amplifier A1, the resulting output is a voltage proportional to the product of G (N_h) and $\dot{W}_f$ COMMAND.

Under normal operation, G (N_h) X $\dot{W}_f$ COMMAND is the input to integrating amplifier A3, which provides the high gain to low frequency inputs. The output of A3 is added in summing amplifier A4 to the output of the low-gain proportional A2 path.

For the A3 integration operation, $\dot{W}_f$ COMMAND can be considered to represent a measure of the command rate of change of engine fuel flow. Since a constant fuel flow is desired in steady state, $\dot{W}_f$ COMMAND is the system error. Gross error reset is accomplished by comparing $\dot{W}_f$ COMMAND with preset high and low error limits and, when the limits are exceeded, switching the input to the integrator to zero through field effect transistor Q1. This allows only fast-path operations to be performed on the gross error inputs experienced during transients.

This circuit is capable of the following performance over the operating temperature range:

Loop Accuracy, $\pm$ 2 percent

Gain Variation, $\pm$ 4 percent

Fuel Metering Control Circuit

This circuit (Figure 30) monitors and trims the fuel metering system such that the fuel delivered to the engine is equal to that of command fuel.

A voltage representing command fuel ($\dot{W}_f$ COMMAND), having been computed at the integrator output, is compared with a voltage representing the actual fuel being delivered, W_f MEAS. The difference voltage is power amplified and is applied to either the positive or the negative displacement motor winding. The motor displacement results in a change in W_f MEAS which cancels the difference voltage.

Negative feedback around the operational amplifier is obtained from the complementary power output stage, rather than the output of the operational amplifier. Overall offset drift and deadband are thus minimized.

This circuit is capable of the following performance over the operating temperature range:

Loop Accuracy, $\pm$ 1 percent

Gain Variation, $\pm$ 2 percent

Acceleration and Deceleration Limit Generator Circuits

These circuits (Figure 31) compute the design levels of the acceleration and deceleration schedules. These computed outputs are compared with the measured average turbine inlet temperature to determine the error.

T_5 ACCEL REF and T_5 DECEL REF are known functions of high-pressure spool speed and compressor inlet temperature. Straight-line approximation functions are generated from voltages representing measurements of high-pressure spool speed (N_h MEAS) and compressor inlet temperature (T_1 MEAS). For simplicity, it may be considered that for each reference, a single function of N_h MEAS is generated and that the function is biased by T_1 MEAS as required.

T_5 DECEL REF is approximated as a single straight-line function. T_1 MEAS is added as a linear function. The slope of the straight-line function of N_h MEAS is represented by the gain of the operational amplifier in the T_5 DECEL REF circuit. The change of the function, with respect to T_1 MEAS, determines the input resistance to the operational amplifier from T_1 MEAS.

T_5 ACCEL REF is approximated by several straight-line segments. The negative slope portion of the function of N_h MEAS is generated by operational amplifiers A2, A3, and A4; the positive slope portions, by A5, A6, and A7. The required "shift right" change with T_1 MEAS is accomplished by an input voltage addition at operational amplifier A1, while the required "shift up" change is generated by an output voltage addition at A8. While each straight-line voltage segment is generated over the entire range of N_h MEAS, the desired portion of the segment is selected by "most" and "least wins" logic circuits.

The circuits are capable of the following performance over the operating temperature range:

T_5 ACCEL Loop Accuracy, $\pm$ 3 percent

T_5 DECEL Loop Accuracy, $\pm$ 2 percent

Inlet Guide Vane Control Circuit

This circuit (Figure 32) generates a signal which positions the inlet guide vanes as a function of referred low-pressure spool speed. A voltage representing the desired inlet guide vane position as a function of low spool speed, N_1 MEAS, and compressor inlet temperature, T_1 MEAS, is generated. This voltage is compared with a voltage representing the actual guide vane position, MEASθ_{IGV}. The error or difference between the two is power-amplified and applied to the winding of a proportional solenoid, which corrects the error.

The circuit is capable of the following performance over the operating temperature range:

Loop Accuracy, ± 1 percent

Gain Variation, ± 5 percent

Power Turbine Overspeed and Abort-Start Shutoff Control Circuit

This circuit (Figure 33) provides a means of rapidly reducing delivered fuel in the event of an aborted start or power turbine overspeed. The driver circuit of the main fuel shutoff solenoid can be driven by either an abort-start signal from the autostart section or by the output of a comparator that is active only when a voltage representing power turbine speed, N_p MEAS, is greater than a fixed voltage representing an upper limit of power turbine speed, N_p LIMIT.

Automatic Starting System

The automatic starting system (Figure 34) programs the starting sequence, monitors engine parameters, and controls the engine starting accessories.

When a starting sequence is initiated from the autostart switch, power is applied to the ignition and starting fuel valve control line and the starter motor. During a normal start, when the high-pressure spool speed attains 10 percent, the starting fuel valve is opened and ignition begins. When this speed increases to 40 percent, a successful start has been accomplished, and the starting system is automatically reset and de-energized.

The system can be reset and de-energized during the starting sequence either by an undervoltage condition of the airframe dc supply or manually by depressing the autostart switch a second time.

Depressing the autostart switch depicted in Figure 34 energizes the set coil (S) of a latching relay whose contacts (in the positions shown) turn on the regulator to arm the starting system and also energize relay K2 through its driving silicon-controlled rectifier (SCR).*

*For the sake of simplicity both in text and in Figure 34, solid-state switches shall be referred to as relays.

Relay K1 can be energized to initiate the aborted starting sequence by a positive output from either the overtemperature shutdown circuit or the 40-second timer before a normal start reset is effected.

Relay K2 can be de-energized to de-energize the starter relay either by switching off the regulator normally supplying the coil voltage (terminating a successful start) or by a positive output from the 10-second dry-crank timer during an aborted starting sequence.

The reset coil (R) of the latching relay can be energized either by depressing the autostart switch while K2 is energized or by receiving positive outputs from the 40-percent speed circuit, the undervoltage circuit, or the 10-second reset timer.

The timer circuits consist of temperature-compensated unijunction oscillators, whose periods are determined by resistor-capacitor combinations. The application of a positive input voltage will result in a positive output voltage following a fixed time delay.

The undervoltage detection circuit is a high-gain voltage amplifier stage operating upon the difference voltage between the airframe supply and a low limit reference.

The speed trip circuit monitors the period of an ac input, the frequency of which is proportional to high-pressure spool speed N_h. When the input period is less than an internally generated reference, a positive output pulse is produced.

The overtemperature shutdown circuit is a Schmitt trigger, which consists of a two-stage amplifier employing positive feedback, such that an output is produced when the input exceeds a predetermined level.

The regulator supplies the power for the starting system control circuits. This regulator is provided to allow complete shutdown of the starting system independent of the fuel control circuitry. The regulator is a dc voltage control circuit employing feedback to maintain its output voltage constant over fixed ranges of input voltage and output current change.

DIGITAL CIRCUIT

Digital designs for the required circuit functions were investigated. In digital computation, the value of a parameter (word) is expressed as a number of bits, each of which has one of two values, zero or one. The bits may all be registered at one time (parallel) or in time sequence (serial).

The digital design was pursued because it offers the following potential advantages over the analog design:

1. Performance improvements in accuracy and temperature stability

2. Hardware compatibility with large-scale monolithic integration packaging

While the second advantage may not be feasible today, it will become feasible in the future. Converting from film to monolithic fabrication will require little redesign.

Several computation techniques were examined, each of which involves the use of a basic element or small group of elements. Trade-off studies were conducted to select various alternative methods of performing digital computation, such as incremental versus whole word methods and serial versus parallel methods. The functions performed by the digital circuits are the same as for the analog circuits previously described. The major performance difference is in the improved tolerances which can be achieved by the use of the digital techniques.

Computation techniques are discussed in this section, and circuit description is provided for those circuits for which supplemental information is appropriate.

Computation Technique

Serial Versus Parallel Computation

Investigation of both serial and parallel computation techniques revealed (1) that the serial method has the advantage of requiring less hardware and (2) that the parallel method permits higher computing speed. The serial method was chosen because the feature of faster computation is not required.

In the serial computation technique, quantities are represented by binary numbers (words), the digits (bits) of which are interrelated by time. Each bit is located in the time between two successive negative transitions of a clock's square wave. As shown in Figure 35 , each word is bounded by a TMI (beginning of word) pulse and a TSN (end and sign of word) pulse. The word begins on the negative transition of TMI and ends when TSN is equal to 1. The order of the bits increases in significance with respect to time. The sign of the word is defined during TSN time. If the sign bit of the word is logic zero, the word is positive and is evaluated by converting each binary digit to its decimal equivalent and adding directly. (For the example given, $2^0 + 2^4 = +17.$) If the sign bit is at logic 1, the word is negative in two's complement form and, for a seven bit word, is evaluated by subtracting 2^7 from the addition of the decimal equivalents. (For the example given, $2^0 + 2^1 + 2^2 + 2^4 + 2^5 + 2^6 - 2^7 = -9.$)

In general, the tolerance capabilities of the digital circuits are plus or minus the least significant bit. Close tolerance can, therefore, be achieved at the expense of additional hardware and increased computation time. Hence, optimum circuit design requires careful specification tolerance studies to keep the hardware and computation time at a minimum. Accuracies of $\pm$ 1 percent are typical of the digital circuits.

Computation Hardware

Computing elements examined were general-purpose computer logic elements in a basic logical approach and are as follows: the Digital Differential Analyzer (DDA), the Binary Rate Multiplier (BRM), and the recently developed Digital Incremental Computer (DIC) elements.

The DIC elements combine many of the features of the others and were, therefore, selected as the main computing element hardware.

In the DIC category, four types of integrated circuits have been made available. Each of these circuits performs a particular serial incremental computation function. Various interconnections among these elements result in a variety of arithmetic and transfer functions involving whole-word addition and subtraction, and incremental multiplication and division. Whole-word arithmetic is performed on entire quantities, while incremental computation is performed only on small changes in the quantities. The outputs of an incremental operation

are accumulated to form a whole-word result. The symbols for the four elements defined below are depicted in Figure 36 . The Scale Factor Array converts a parallel number to serial form and is used to insert numbers, either functions of measured variables or permanent constants, into the computations. The Variable Storage Array is an accumulator chip that converts increments into whole-word variables. The Incremental Multiplier performs multiplication of a whole word by an increment and also provides for whole-word addition. The Incremental Selector is a magnitude comparator normally used for incremental division. While the circuits described show the Incremental Selector used as a whole-word comparator, ambiguities resulting from input sign changes must be resolved before the element can actually be used in this manner. Within the Increment Multiplier is a decoder chip (D) which decodes an increment into whole-word form prior to addition.

Signal Conditioning

Speed Measuring Circuit

This circuit (Figure 37) generates a binary number representative of engine speed. Requirements are a resolution of one part in one thousand and a computation time of 10 milliseconds maximum.

For an assumed input frequency range of 400 to 4000 Hertz, use of the conventional counting technique of counting pulses over a period of time would require a computation time of 250 milliseconds to achieve satisfactory resolution. Therefore, it is necessary to compute the frequency as the reciprocal of its measured period (T), or interval between similar points on the input signal as a function of time.

This circuit uses a read-only memory (ROM) as a reciprocal function generator. The ROM element is a storage device that can be arranged with an input of eight bits. The relationship between the input and output will result in an output that satisfies the predetermined relationship. The device is employed to generate any function of an input variable with eight-bit accuracy.

The best ROM element currently available can process a maximum of eight bits of information. Therefore, an approximation that satisfies the resolution and accuracy requirement has been implemented by this design.

With the approximation, the counter and register are shifted with respect to the ROM such that the ROM is operating only on the most significant bits of the computation, and the least significant bits are simply subtracted. The number of shifts is determined by the input period (T). As T increases (for decreasing frequencies) to values requiring more than ten bits for its evaluation, the shifting begins. By successive shifting, the circuit can handle order-of-magnitude changes of input.

Analog-to-Digital (A/D) Converter Circuit

This circuit (Figure 38) converts an analog dc voltage to a digital signal by a technique in which the analog input is compared with an analog-equivalent to the digital output. The comparator allows the triggering clock pulses to increase the binary number in the counter during the time when the analog input is greater than the analog output. When the output is equal to the input, the counting process is interrupted. The digital number in the counter is then equal to the input. The switching circuit and the resistive ladder network function as a digital-to-analog converter to obtain the analog-equivalent of the digital number. The circuit is sampled and reset at a rate low enough to allow the largest analog input to be digitized.

Turbine Inlet Temperature Signal Averaging Circuit

This circuit (Figure 39) computes the average turbine inlet temperature (T_5 MEAS) from measurements taken by eight individual sensors, S1 through S8.

The input frequency of the sensors is in a range that allows the use of conventional counting techniques. Pulses from each sensor are gated to a counter for a constant time interval (T). Sensor operation is verified by a circuit that monitors the highest order bits of the counter; the presence of logic 1's in these bits means that the associated sensor is operational and that the number in the counter can be gated to the averaging circuit. The monitoring circuit outputs are summed and decoded to form N, the number of operational sensors. The average turbine inlet temperature is computed by multiplying each reading by 1/N and then adding. In the event of sensor failure, the path in which the failure occurs is opened, and N is corrected. The output represents the average of the remaining operational sensors.

Control Mode Selector

Dual input comparators require iterative "pairing off" of inputs in order to confine the problem to a selection between two variables. (See Figure 40 .)

Integrator

High-pressure spool speed, N_h MEAS, is used to program the integrator's time constant through a read-only-memory (ROM) circuit. The transfer function is thus continually adjusted to remain optimized over the entire operating range. (See Figure 41 .)

T_5 Acceleration and Deceleration Limit Generators

An ROM circuit is used to generate the basic acceleration reference as a function of referred high-pressure spool speed (N_h MEAS and T_1 MEAS). This results in an overall accuracy of $\pm$ 1 percent. (See Figure 42.)

Inlet Guide Vane and Fuel Handling System Control Circuit

The nature of the inlet guide vane control and fuel handling system requirements is such that simple proportional controls are satisfactory. The more economical analog implementation is sufficient. (See Figures 30 and 32 .)

Automatic Starting System

Time measuring, speed detection, overtemperature shutdown, and sequencing can be performed by digital circuitry. (See Figure 43.) Regulation and under-voltage detection are more practically performed by the analog circuits previously described.

The start reset logic is a three-state sequential circuit. When the master dc switch is closed, the logic enters state "zero", in which it supplies control signals to hold the regulator in the off position and clear the system. Depressing the autostart switch puts the circuit into state "one", wherein it switches the regulator on. Releasing the switch causes the circuit to enter state "two", in which the regulator is kept on, the clear pulse is removed, and the starting sequence is initiated. A positive speed

signal, autostart, under-voltage, or 40-second timer pulse returns the circuit to its "zero" state, where, as before, the regulator is off and the system is cleared.

The speed detection logic consists of a two-stage counter that is activated for intervals equivalent to the period of a 20-percent speed signal. If two counts are registered during any interval, then the speed is at least 40 percent and an output pulse is generated.

The clock, counter, and decoder perform the timing functions for the system. The counter circuit counts the number of pulses supplied from the clock at a constant frequency. The number of counter stages and the clock frequency are arranged such that the last stage registers a positive output after 40 seconds of operation. The end of the 40-second interval is thus decoded by the last stage of the counter itself. Two successive 10-second intervals are decoded by monitoring an additional counter stage for each interval. A positive decoder output marks the end of each time interval.

Overtemperature is sensed by detecting the binary number from the fuel control circuitry representing the critical T_5 for starting, and also a 5-percent range of T_5 above the critical level to prevent a missed reading during fast temperature rises. The circuit consists of a serial-in, parallel-out register and logic circuitry to decode the range of interest.

The driver circuits are dc power amplifiers, which provide sufficient voltage and power gain to the logic element outputs to drive the starting accessories. Each of these circuits contains four stages and is designed for minimal dissipation while the associated accessory is de-energized.

ELECTRONIC COMPUTER PACKAGING

General

The objective of the computer packaging study is to establish a design that represents a balanced trade-off between cost, size, and weight, while providing prime reliability and easy maintainability.

Rapid evolution in electronic technology over the past few years has opened the door to a multitude of design techniques. This variety of techniques evolves from the ability to use one or any combination of four

basic electronic technologies: (1) monolithic integrated circuits (IC), (2) thin film, (3) thick film, and (4) discrete components. From this study it has been concluded that the thin-film method combined with the use of miniature discrete components is the most desirable approach for this application. The approach permits the high density required for small size, while maintaining change flexibility and reasonable cost. All-monolithic integrated circuitry, the ultimate technology for miniaturization, is inflexible and expensive at present. It does, however, hold high promise for the future.

Two important areas have received special attention in this study. The first involves cooling requirements necessary for the computer to operate reliably in the difficult engine environment. The second is the need for relatively high power and accurately regulated voltage over the entire engine speed range. These considerations normally require a large, bulky power supply.

Cooling has been accomplished by a unique design using dielectric fluid cooled by both fuel and forced air. Power and voltage regulation requirements become dramatically simplified by (1) taking advantage of the limited speed range of the variable-speed drive output of fuel metering system No. 2, and (2) using an externally regulated generator.

In the following paragraphs, the packaging requirements are defined and the various electronic technologies are discussed. Cooling system studies and analog and digital packaging designs are then presented. Finally, hardware costs and radio frequency interference (RFI) are discussed.

Environmental Requirements

The operating environment is specified by Military Specification MIL-E-5007C, supplemented by applicable requirements of Military Specification MIL-E-5272C.

To supplement the military specification definition of temperature requirements, measurements of accessory section temperature versus time were made at Lycoming on a bailment Mohawk aircraft. This aircraft may be considered a "worse case" type because of its tight cowling. The test is described in detail in Appendix V.

Electronic Technology Discussion

Packaging methods encompassing various technologies were considered for the electronic circuits. Because of the size requirement, the need for microelectronic film packaging concepts was obvious at the outset of the program.

A completely monolithic approach was briefly considered in the study. Costs associated with these semiconductor integrated circuits, in both design and manufacturing, were found to be prohibitive today for anticipated computer production rates.

The technologies evaluated in depth were the thick-film and thin-film approaches, which are briefly explained. Both technologies use a basic ceramic substrate, usually having a 96-percent alumina content, on which are deposited conductive paths, resistive and capacitive elements, and provisions for mounting semiconductors in "chip" form. A "chip" is a semiconductor device, such as a transistor or a diode, without its protective case and mounting and connecting provisions. The methods used to form the circuits differ between the thick- and thin-film technology.

Thick-film circuits and components are deposited on the substrate by using a screening process. The process is accomplished by using a fine-mesh steel screen through which a paste, with proper electrical properties, is passed, using a squeegee-type device. The deposited elements are then baked at high temperature to develop the desired properties. Finally, the circuit is packaged in a protective enclosure.

Thin-film circuits and components are formed by first vacuum depositing a conductive material over the basic ceramic substrate. The circuits and circuit-resistive elements are formed by photographically etching away unwanted material from this base material. Successively, precious metals are then plated on the original etched pattern to protect the base material and to provide a uniform conductive coating. The circuit is then packaged in a protective enclosure, such as the TO-8 configuration shown in Figure 46 .

The thin-film method was selected for the electronic computer for the following reasons:

1. Materials used to vacuum-deposit components result in greater circuit package density.

2. Vacuum-deposited components have better temperature characteristics.

3. Vacuum-deposited components have better long-term stability.

4. Manufacturing processes to obtain thin-film circuits are less complex.

5. The processes are adaptable to high-volume automated assembly techniques.

6. Continous film deposition used in manufacturing eliminates junctions between the interconnects and the deposited components, and results in inherently higher circuit reliability.

Cooling System

The computer cooling system design must provide adequate cooling during normal operation and protection for the computer components from radiated, conducted, and convected heat transfer at the ambient soaking temperature limit of 275°F.

Development of electronic components has advanced to a point that now allows silicon semiconductor devices to operate continously at temperatures up to 257°F. This temperature, however, is considered to be the maximum allowable, and reliability is greatly enhanced as the operating temperature is reduced. Figure 47 shows how reliability is affected by temperature. The design philosophy, therefore, was to achieve the lowest practical operating temperature.

Methods considered to cool the computer included:

1. Thermoelectric cooling devices

2. Vacuum-jacket insulation

3. Plastic foam insulation

4. Air cooling

5. Fuel cooling

6. Dielectric-fluid cooling

Typical thermoelectric devices were studied early in the program. The devices are efficient, but high power requirements during operation and their large inherent size made them impractical for this application.

The vacuum-jacket approach, shown schematically in Figure 48, was best from a thermal standpoint. The disadvantages of high cost and difficult servicing, however, obviated this approach.

The mechanical-insulation technique (Figure 49) is similar to the vacuum-jacket approach, but, it is not as efficient thermally and requires a circulating cooling fluid and external condensor, which would add size and weight to the system. This approach was also dropped.

The air-cooling technique (Figure 50) uses airflow to form a cooling and insulating jacket around the computer assembly.

Fuel cooling is accomplished by simply passing system supply fuel directly through the center of the computer.

The use of the dielectric fluid as a coolant provides an efficient conductive path for the computer-generated heat.

The final cooling scheme selected uses a dielectric-fluid-filled computer cooled by both fuel and air (Figure 50). It consists essentially of a light sheet-metal jacket, surrounding the computer section, through which airflow is maintained. This provides cooling at the external computer surface. The computer is also mounted concentrically on the inlet fuel line, which provides fuel cooling at the internal surface. The air jacket insulates the computer section from the high-temperature environment and removes heat generated within the computer. In addition, the exhaust air from the jacket is allowed to discharge over mating metal assemblies to help lower the metal temperature and reduce conductive heat transfer into the computer.

The concept of using a noncirculating dielectric fluid in direct contact with semiconductor elements without their protective cases was examined. It provides a method to obtain maximum heat transfer from semiconductor elements to the cooling surfaces. Tests conducted at Avco Lycoming to verify the effectiveness of this concept showed that heat transfer was improved and that operation of the elements without protective cases was not adversely effected. Disadvantages are that clean fluid is required and the computer assembly must be sealed. Long-term effects

beyond those shown by the accelerated aging tests performed in the laboratory are under investigation at Avco Lycoming. Details of the test are presented in Appendix IV.

A thermal analysis was made of the performance of the selected cooling system under various conditions. It was assumed that a supply of cooling air of approximately 1 percent of the total engine air was available at 125°F, and that the system was subjected to environmental air moving at 100 feet per second. Taking the maximum internal dissipation as 40 watts, and assuming it to be distributed uniformly throughout the system, temperatures within the computer system were calculated for fuel flow rates of 0.1 and 5.0 gallons per minute for an environmental air temperature of 275°F.

The study showed that for a flow rate of 0.1 gallon per minute, the average dielectric fluid temperature is 205°F. With the flow increased to 5.0 gallons per minute, the dielectric temperature is reduced to 195°F. The results are conservative because convection within the dielectric fluid was not included in the analysis.

The study also showed that at shutdown, in an ambient temperature of 275°F, the maximum temperature rise within the dielectric fluid will be less than 25°F after 15 minutes. This rise added to the highest operating temperature previously computed (205°F) results in a temperature of 230°F, still well below the maximum allowable.

Analog Package

General

The analog computer design uses microelectronic packages mounted on ceramic discs in conjunction with discrete electronic parts. The essential difference between this design and the digital design discussed later is in the basic electronic elements used. The remaining packaging characteristics are similar.

Figure 44 shows the interior layout of the analog package design and points out the major computer items, which include the support frame, the ceramic component discs, the input receptacle, and the electronic packages and components.

Mechanical Assembly

The computer housing is designed to mount on the fuel line at the input to the fuel pump housing. This housing is enclosed by an outer housing or jacket and functions as a can within a can. The outer can is an air jacket that easily separates into two parts like a "clam shell." When the air jacket is removed, easy access is provided to the computer assembly within.

The air jacket has baffles to control the airflow about the inner computer assembly. The rear support for the computer is provided by a mating surface on the jacket when joined with the air manifold and computer mounting locknut assembly.

The entire computer assembly is secured to the fuel line by the fuel line locknut. To remove the outer air jacket, the locknut is loosened to allow the air jacket to be disengaged from the front support assembly (fiber insulator) as shown in Figure 44. The jacket will now separate into two halves, exposing the inner computer, which can be lifted from its seat on the fuel line and removed.

To replace the computer, a thermally conductive grease is applied to the fuel line heat sink. The computer is reassembled by reversing the above disassembly process.

Advantages of the mechanical package design include the following:

1. Small size
2. Simple construction; contains a minimum number of parts
3. No special tools required for servicing
4. Easy removal and replacement
5. Simple cooling system; requires no moving parts
6. Cylindrical shape; less vulnerable to small-arms fire

The inner can computer housing assembly shown in Figure 44 is a sealed unit. A brass alloy was chosen for this assembly for four major reasons:

1. Corrosion resistance

2. Good thermal conductance

3. Good deep-draw capabilities

4. Adaptability to solder sealing operations

A support frame assembly is included in the computer package to function as a heat sink and disc mounting support. One end of the support assembly functions as the support for the computer input receptable and end cap.

Disc Assembly

The disc assembly is the basic structure on which the microelectronic packages are mounted. The discs are fabricated from alumina ceramic material approximately 0.060 inch thick, and they are equipped with pins that connect to the flexible wiring harness. The ceramic disc was selected over a plastic printed-circuit disc because it has more efficient heat transfer properties, is more stable with temperature, has higher dielectric properties, and is inert to the dielectric fluid used as a coolant for the computer assembly.

The deposited-film techniques similar to those used for thin-film fabrication are used for forming conductive paths on the discs to interconnect the individual circuit packages and the discrete components.

The design also includes the use of a unique method of dovetail slots in conjunction with mating nylon strips to retain the discs in the computer assembly. The nylon absorbs stresses set up by the thermal expansion of the ceramic and brass materials and provides some shock and vibration isolation. The slip-fit type of assembly allows for easy installation and removal of the computer discs.

Microelectronic Assemblies

Types of microelectronic assemblies considered to house the circuit elements were the TO-8 round can with attached header, the TO-8 square can concept with header, and the square flat-pack type assembly. The TO-8 round can and the flat-pack are electronic industry standard containers for packaging microelectronic circuits. The

square TO-8 configuration is merely a modification of the round series. The TO-8 round can configuration (see Figure 46) offers several advantages which include easier handling and mounting and, most importantly, a feature that allows the substrates to be stacked to increase package density. The flat-pack package (see Figure 51) considered offers some package density advantages due to its low profile; however, the package configuration is not adaptable to stacking of substrates. The round can TO-8 configuration was selected in preference to the square unit for packaging the thin-film microelectronic circuits because it is an industry-approved design and one more widely used in thin-film circuit manufacture.

The internal construction used in the round can TO-8 packages is shown in Figure 51. The typical microelectronic resistor elements are vacuum deposited on the ceramic substrate as shown in Figure 52. Semiconductor and capacitor chip elements are mounted on the substrate using eutectic bonding techniques, with wiring subsequently accomplished by ultrasonic or thermocompressional welding methods.

To achieve maximum reliability, the selection of a welding method was given special attention. The ultrasonic method excells in joining soft metals such as aluminum, copper, silver, and gold, metals that would be used extensively in the assembly of integrated circuit networks. The thermocompressional joining technique requires that closer controls be exercised in preparing the surfaces to be joined. Close control must also be exercised during the joining process, with particular stress placed on time and temperature.

Both the ultrasonic and thermal compressional welding methods produce highly reliable joints for the electronics industry (Figure 52). Selection of the ultrasonic technique was based on several favorable factors: (1) Objects to be joined are not subjected to a preheating process. The heat that is obtained during the ultrasonic "rubbing" action is strictly localized to the joint and never reaches the components being joined. (2) There are no required welding controls, i.e., temperature, time, oxide free surfaces, etc. (3) Reliability is greater. Failure rates compiled by the USAF show 0.00005 percent per 1000 hours for the thermocompressional method and 0.00003 percent per 1000 hours for the ultrasonic technique.

Discrete Components

The computer uses a number of large discrete components for power supply and other high-power functions. These components have been

grouped together in one end of the computer and within a gap created by the horseshoe shaped discs to achieve maximum compactness within the cylindrical envelope (Figure 44).

Interconnection Cable

Electrical interconnection of the control elements (disc subassemblies, discrete components, and interface devices) is accomplished by a flexible printed wiring cable similar to that shown in Figure 53. The flexible cable uses "KAPTON" as the base material. The wiring terminates in pretinned solder areas, which are connected to mating pins on the ceramic mounting discs by soldering. The advantages of this wiring design are: (1) The assembly is preformed and pretinned for easy installation by low-skill personnel. (2) It is very efficient; a large number of conductors can be installed in areas where individual wiring harnesses could not be used. (3) It is highly resistant to vibration-type failures.

Digital Package

MOSFET Semiconductor Devices

In the digital design, the circuit functions require extensive use of MOSFET semiconductor devices. The MOSFET device (metal oxide semiconductor field effect transistor) is essentially a number of field effect devices integrated and manufactured on one silicon chip. These integrated chips are designed to perform various control functions in the digital computer system. The digital package layout (Figure 45) shows the major features of the design. The digital package is more compact than the analog package due to the absence of the bulkier discrete components used in the latter design.

Mechanical Assembly

The digital package mechanical features are the same as those presented in the analog design described earlier. Only minor physical changes in the disc mounting features have been made.

Disc Assembly

The disc shown in Figure 45 is typical of the type of assembly used to mount and wire the chip-type microelectronic elements. The disc material is similar to that used in the analog concepts; however,

an interconnection technique known as "multilayer" is used in place of surface-deposited interconnects between the semiconductor elements. The multilayer concept is illustrated in Figure 54.

Advantages gained by using the multilayer interconnection concept include:

1. Increased package density gained by crossing conductors within the disc

2. Reduced assembly costs achieved by the use of repetitious manufacturing processes

3. Increased reliability as a result of the protected wiring

4. Easy and economical replacement of faulty elements

This approach, as evaluated in military handbook MIL-HDBK-175, "Microelectronic Device Data Handbook," is rated best when compared with other methods used for interconnection.

Microelectronic Assemblies

Microelectronic assemblies similar to those shown in the lower portion of Figure 52 are used to perform the electrical function of the digital control. These assemblies are interconnected through the multilayer wiring disc discussed above. The devices are used in uncased "chip" form (basic silicon MOSFET element less its protective case). This method is unique in applying these devices and offers the following advantages:

1. Smaller size resulting in maximum package density

2. Direct contact with dielectric cooling fluid resulting in excellent thermal transfer

3. Cost savings realized by discarding hermetic case

4. Reduction in the number of different chip types

Interconnection

Evaluation of methods of interconnecting the various circuit components of the digital computer included analysis of several schemes

directly associated with the semiconductor chip elements themselves, and methods of interconnecting the ceramic disc assemblies.

The "flip-chip" technique of connecting the microelectronic elements to the ceramic disc utilizes elements equipped with raised connection pads.

The chip is installed inverted on the deposited wiring pattern by ultrasonic welding. This technique was discarded because of difficulties in obtaining satisfactory welds and in developing adequate inspection methods.

The "beam lead" approach utilizes semiconductor elements with special flat leads attached that are used to mount the devices to the supporting substrate. This method was also discarded because of attachment and inspection problems.

The method selected to mount the microelectronic elements utilizes chip "carriers." The semiconductor chips mounted and wired in the carrier can be inspected and tested easily prior to bonding the carrier onto the ceramic disc ultrasonically using volume production assembly methods.

The ceramic disc assemblies with chips in place are connected to other discs and accessory system components by a KAPTON flexible wiring harness similar to the one used in the analog computer design.

Discrete Components

The digital computer utilizes a number of large discrete components. These components are similar to those used in the analog computer and are packaged in a similar manner as depicted in Figure 45.

COST

The analog and digital computer designs discussed above were evaluated to determine an estimated cost for each system in production quantities. The analog assemblies in 1200-unit quantities were estimated to cost $2,152 each. The digital assemblies in 1200-unit quantities were estimated to cost $3,970 each. The cost difference is $1,818. These figures are based on the use of existing manufacturing facilities; individual microelectronic element costs are based on early 1971 projections. Factors such as increased use by the electronic industry of the particular circuit

elements, and cost projections based on improved assembly techniques expected in the middle 1970's, should decrease the computer costs shown. It is predicted that costs will change to favor the digital computer approach.

RADIO FREQUENCY INTERFERENCE

Radio frequency interference radiated by the computer is minimized by the shielding afforded by the double-case design and relatively low radio frequency impedences at the outside terminations. The possibility of conducted interference into the aircraft electrical wiring is eliminated by the self-powered feature in the design.

The computer designs are not considered to be susceptible to high field radio frequency energy induced into the unit. The digital circuits switching occurs at a higher voltage level than would be induced, and the analog signals do not respond to low-level radio frequency voltages.

Conventional external bypass filtering and shielding techniques may be required in specific installations. These radio frequency interference problems can be solved only at the specific installation and are not considered a part of this study.

RELIABILITY

General

The objective of the reliability study is to establish a design Mean Time Between Failure (MTBF) goal and to insure that the design meets that goal. This established goal represents a substantial improvement over the computing function of existing fuel controls. Microcircuit manufacturers, the FARADA (The Bureau of Weapons Failure Rate Data Program), and military handbooks were consulted for microcircuit reliability data, which were found to be limited because of the very newness of microcircuit use.

Reliability diagrams, which place the individual computing functions affecting reliability in proper orientation, were prepared. The overall reliability goal was divided among the computing functions (apportioned), taking into account factors such as relative complexity. This subdivision allows a detailed comparison of each circuit with the goals.

The overall computer MTBF was calculated for both the analog and digital designs. Where the design did not meet the goal, a method of improving the reliability was established.

Finally, failure modes were analyzed and methods of avoiding them were considered.

Establishment of Reliability and Maintainability Goals

The most up-to-date reliability estimate for the fuel controls used by Lycoming, (T53 and T55 data) including both fuel metering and computer function, is a failure rate, λ, of 486 failures per million hours, or an MTBF of about 2,058 hours. Approximately one-third of the failures consist of "No Acceleration", "Fast Acceleration", "Discrepant Fuel Schedule", etc., and may be directly assigned to the computation function of the fuel control. Accordingly, the present failure rate for the computation function is 167 failures per million hours, or an MTBF of 6,000 hours. This is the basis for establishing a reliability goal for the electronic computer subsystem of the USAAVLABS control.

Improvements in design and hardware technology permit substantial improvement in reliability. An improvement by a factor of five was applied as a minimum goal, giving a failure rate of 33.333 failures per million hours, or an MTBF of 30,000 hours. The results of this reliability study indicate that this is a realistic goal with which to start. If the 1975-1980 failure rates for the individual building-block hardware improve - and the predictions are for an order of magnitude improvement - then the established goal will also be uprated.

From a maintenance standpoint, the current fuel controls are adjusted and replaced at the field level (third echelon), with overhauls performed at depot level (fifth echelon). Fuel control replacement rates for all causes for the T53 and T55 engines are 0.546 and 1.291 per 1000 flying hours, respectively. The higher replacement rate for the T55 fuel controls is attributable to the greater number of available field adjustments, which expose the control to more handling and consequent mishandling. Thus, the fewer the available field adjustments, the less troublesome the control. The objective of eliminating field adjustments, or keeping them to a absolute minimum, shall be the maintainability goal for the USAAVLABS control.

Subsystem Reliability Goals

Reliability goals for subsystems have been assigned according to an apportionment analysis.* The total system is logically divided into subsystems for this purpose, and each of them is evaluated with respect to the other subsystems in terms of complexity, state of development, past experience, and importance to mission success. Each subsystem was assigned an apportioned failure rate based on both this evaluation and the established system reliability goal. A detailed description of the apportionment is given in Appendix II. The apportioned failure rates for each of the subsystems are compared with the predicted failure rates for the proposed subsystem designs in Tables VII and VIII. Any discrepancy between the apportioned and the predicted failure rates is evaluated for its effect on the total system goal and for possible design improvements.

Development of Reliability Block Diagrams and Mathematical Models

Reliability block diagrams and mathematical models were developed for both the analog and the digital electronic computer designs and are shown in Appendix II. The block diagram for the analog system is based on the logical subsystem assignment used for the apportionment analysis. Two power supplies, one for the plus and the other for the minus voltage, not shown in the logic diagram are included in the block diagram. The block diagrams and mathematical models represent the worst-case analysis; that is, with no adjustment for a component, circuit, or subsystem redundancy scheme or for a manual backup system that may be used.

Performance of Iterative Studies and Reliability Prediction

A summary of reliability prediction studies for the electronic computer portion of the USAAVLABS control is included in Tables VII and VIII. Prediction studies are given for two designs: one for an analog and the other for a digital design. The apportionment goals and the predicted failure rates shown for the analog apportionment and analog failure rate prediction, respectively, are based on the analog circuits that correspond to the analog function reliability block diagram (see Appendix II). The apportionment goals and the predicted failure rates for the digital design are based on the digital reliability block diagram and the number of

---

*A COMPREHENSIVE RELIABILITY ENGINEERING PROGRAM, Brimley, Donald B., Paper presented 5-9 July, 1966, at UCLA, during a course on "System Approach to Reliability".

digital elements needed to realize each function represented in the digital reliability block diagram. Appendix II gives some of the detailed work for the analog and digital predictions and the assignment of component failure rates.

The failure rate predicted for the analog design is better than that for the digital design by a factor of approximately 2.7. Although both fall short of the adopted goal, there are methods of improving the failure rates. Specially designated high-reliability components with lower failure rates can be specified for some of the components, and reliability screening on the component, subsystem, and system level can be used to weed out the potential failures. The reliability screening, particularly the environmental and the burn-in tests, is very effective for semiconductors and integrated circuits. These screens result in an improvement factor of up to three in the failure rate for standard microcircuits. Moreover, investigators have reported that once the deviates are weeded out, the remaining integrated circuits exhibit a decreasing failure rate.* This means that the system failure rate diminishes. Consequently, the MTBF for the system increases. Redundancy can also be used to improve the system failure rate. For example, the power supply having discrete components with the highest failure rates could profit by the use of circuit or power source redundance. Aircraft electrical system power is a logical redundant source. Extensive use of redundancy was not considered because it will increase the size and cost of the computer.

Failure Mode, Effects, and Criticality Analysis

A failure mode, effects, and criticality analysis procedure is useful for determining, evaluating, and analyzing potential failures in an operating system. The potential failure modes of each subsystem function in the electronic computer portion of the system block diagram (Appendix II) are examined for their effect on associated computer functions and are evaluated to ascertain their effect and criticality on the success of the mission. The analysis assumes that a circuit function output fails, either gradually or catastrophically, thus causing too little or too much fuel to be metered to the engine.

*Peralta, Ben C., SCREENING SILICON INTEGRATED CIRCUITS, Proceedings of 1967 Symposium on Reliability, pp. 337-348.

Troxel, D. I., and Tiger, B., PREDICTING INTEGRATED CIRCUIT RELIABILITY VIA FAILURE MECHANISM, Proceedings of the 1968 Symposium on Reliability, pp. 217-225.

Heer, E., Baker, D., and Fox, A., THE TEG-A TEST ELEMENT FOR THE CONTROL OF QUALITY AND RELIABILITY OF INTEGRATED CIRCUITS, Proceedings of the 1968 Symposium on Reliability, pp. 201-216.

Output signal failures for the mode selector, the proportional-plus-integral, and the fuel handling functions have a direct effect on engine operation. The flow chart (Figure 55) illustrates these possible failure modes and effects. Although drift or offset can be compensated for by an adjustment in the command signal, with a corresponding decrease of the control's range in the direction of drift, Figure 55 shows that this type of failure will not necessarily cause an aborted mission.

Signal failures for the functions to the mode select are shown in Figures 56, 57, and 58. Figure 56 shows that a hardover maximum fuel signal from the deceleration limit signal function is most severe, while a hardover minimum fuel signal can be tolerated. Similarly, a hardover maximum fuel signal can be tolerated for the acceleration limit signal function (see Figure 57), while a hardover maximum signal output for any of the four functions shown in Figure 58 renders that function inoperative but does not necessarily cause an engine failure.

Figures 55 through 58 point out the problem areas where a special effort is required to assure reliable system operation. A more detailed failure mode, effects, and criticality analysis for the final circuits in each subsystem function, should be performed to evaluate techniques for avoiding these failures. The goal would be to achieve a fail-safe function, possibly by the use of passive or active redundancy on a component or circuit level.

COMPARATIVE EVALUATION OF ANALOG AND DIGITAL DESIGNS

The most significant factor influencing a comparison of the two designs is the rapidly changing electronic technology, which has made the digital design feasible but whose future course must be judged to render a proper comparison of the two. The advances in electronics have benefitted both designs, resulting in a small size for both designs.

The digital design would have been out of the question a few years ago because the amount and size of hardware required would have been prohibitive. Microelectronics has now overcome that disadvantage.

The ideal microelectronic fabrication process is monolithic because it is a pure process requiring no hand assembly. Complex circuits can be produced as a tiny chip with incredible density. The ultimate goal is to form the entire computer on a single chip, but this has not been economically feasible because of the large initial costs and low yields in production for very complex circuits. Manufacturers make monolithic devices of limited complexity and wide appeal, although more complex

devices are becoming available. When it will be practical to go entirely monolithic is a subject of controversy. However, it is our judgement that it should be within the next four years.

The film technology may be considered to be the interim technology, and it was selected because it is the most practical for today and the immediate future.

The digital circuit is much more adaptable to the entirely monolithic process, because the analog circuit requires many capacitors of values impossible to fabricate by the monolithic process.

With the foregoing in mind, a point-by-point comparison of the two designs is presented below.

Size and Weight

The difference between the two designs is not judged to be significant; both are remarkably small. The adaptability of the digital design to an all-monolithic fabrication will permit a further significant reduction in size as conversion to that method becomes feasible.

Accuracy

The digital design is vastly superior to the analog design, accuracies of .01% or less being possible. No further improvement in analog accuracy is likely, beyond that obtainable today.

Function Generation

The availability of monolithic memory elements has made it possible to "store" an entire univariant curve on a single chip, thus making the digital method much more superior than the analog method. The disadvantage of the analog method is that the curve must be approximated by a series of straight-line segments. A complex curve can require prohibitive circuitry.

Simplicity and Reliability

The digital design is more complex, based on an individual parts count. A result of this greater complexity is that the statistical reliability of the digital unit is lower than the analog, again based on an individual parts count.

A widely accepted premise is that the reliability of a monolithic chip is the same regardless of the individual parts contained therein. As the consolidation of the circuit functions into fewer chips becomes feasible, the digital complexity will decrease and reliability will increase.

Costs

The cost data obtained show the digital design to cost $1,800 more than the analog design, based on 1971 projections. This estimate is judged to be high by today's standards. However, there was insufficient cost data projected into 1975.

One factor contributing to the high digital cost is the newness of the devices used. A factor that will benefit the digital design cost is the digital design's adaptability to automatic assembly methods now under development.

Finally, the adaptability of the digital design to all-monolithic fabrication should ultimately reduce its cost considerably.

Radio Frequency Interference (RFI)

The digital design is less susceptible to radio frequency interference because transistors operate by switching on or off at relatively high-voltage-level signals. The analog is more susceptible because the "normal" operating condition of many circuits is at a very low voltage, subject to interference.

Conclusion

After a review of the above factors, it is Lycoming's judgement that the digital design is superior and that by the time this design is ready for production, the disadvantages of the digital design will no longer exist, and it will be clearly superior to the analog design in every respect.

FUEL METERING SYSTEM

GENERAL

Two methods of fuel metering were studied. The first method, identified as Fuel Metering System No. 1, uses a multiple-function fuel valve, a positive-displacement pump, and a servo motor. The multiple-function valve combines the five conventional functions (metering, bypass, relief, pressurizing, and shutoff) of handling flow into a single compact unit. The second method, Fuel Metering System No. 2, uses a centrifugal pump and miniature variable-speed drive (VSD) to achieve both pumping and metering functions. The input side of the VSD is driven at compressor shaft speed. Modulation of the VSD speed ratio by the computer output controls pump speed and, hence, fuel flow to the engine.

Both methods appear to be feasible and to offer significant reductions in size and weight over currently available systems. Studies made during the program include computer simulations of the systems, component and system design, engine test evaluations, and weight and cost predictions.

REQUIREMENTS

The two systems described above were designed to meet the fuel pumping and metering requirements of engines in the 2-to-5-lb/sec airflow range, including regenerative and nonregenerative versions, without adjustments or component changes. The basic design requirements were:

1. High tolerance to fuel contaminants
2. Compatibility with all fuel types without system adjustment
3. Efficient packaging to provide a small low-weight system
4. High system reliability and reduction of maintenance procedures
5. Design configuration for ease of servicing and quick installation and removal
6. Low vulnerability to small-arms fire
7. Low unit cost potential
8. Provision for variable-geometry actuator fuel supplies

9. Incorporation of emergency manual metering system

10. Satisfactory performance when subjected to environmental temperature, vibrations, and shock levels as specified by Military Specification MIL-E-5007C

11. Satisfactory performance at all altitudes from sea level to 35,000 feet and ambient temperatures from -65° to 160°F

All requirements of Military Specification MIL-E-5007C were considered to be applicable.

Fuel pump flow range and maximum discharge pressure requirements were predicted for the engine range under study and are shown in Figures 59 and 60. The dynamic response of the system should provide an effective time constant of 0.025 second and must provide stable flow regulation in all engine control modes. The accuracy of flow metering shall be ±2.5 percent of the nominal value for satisfactory control during engine starting (up to 45 percent maximum gas producer speed).

FUEL METERING SYSTEM NO. 1

System Description

System No. 1, shown schematically in Figure 61, consists of a positive-displacement pump; a multiple-function fuel valve assembly, which provides all the required fuel handling functions in a single compact unit; and an electrical servo motor, which positions the metering valve portion of the multiple-function valve. The multiple-function fuel valve is being developed at Avco Lycoming as part of an Army-sponsored Contributing Engineering Program.

The following functions performed by the multiple-function valve are illustrated schematically in Figure 62. As determined by the computer, the position of the metering valve is proportional to desired flow. A pressure regulating valve maintains a constant pressure-drop across the metering valve to establish metered flow that is proportional to valve position. Other functions include a pressurizing valve to establish a minimum servo pressure during starting, a high-pressure relief valve for over-pressure protection, and a cutoff valve for engine shutdown.

The multiple-function fuel valve, in addition to providing a more compact valving arrangement, eliminates a large amount of housing, housing machining, and passages. Further, since the metering piston is completely pressure-balanced, computer forces are kept low, eliminating the need for a high-power servo motor.

System Design

General

Design and analysis of Fuel Metering System No. 1 included:

1. Revision of the multiple-function fuel valve to adapt it to the advanced control application
2. Establishment of interface requirements to permit servo motor selection and integration
3. Packaging of the complete system, including pump, computer, and servo motor
4. Cost and weight analysis

Multiple-Function Fuel Valve Design

The multiple-function fuel valve design was studied for adaptation to the advanced control system requirements. The changes in requirements were:

1. Lower metered flow
2. Elimination of fuel temperature compensation and fuel density adjustment

The multiple-function fuel valve was originally designed to accommodate fuel flow to 1000 pph. With the lower flows required by the 2-to-5-lb/sec W_a engines (600 lb/hour maximum), portions of the valve could be scaled down to provide minimum size. The pressure regulator was reduced in diameter and length, and the metered flow transfer passage area was reduced to provide reduction in total valve assembly size.

The closed-loop control mode obviates the need for fuel temperature compensation and fuel density adjustment. The bimetal disc stack and the fuel density adjustment, therefore, have been eliminated.

Packaging

Figure 63 represents the results of the Fuel Metering System No. 1 packaging study. Included in the package are the multiple-function valve, the metering valve servo motor, the fuel pump, the electrical speed pickup, and the digital electronic computer.

A 15,000-rpm, balanced-vane pump was incorporated to permit system packaging and a valid weight and size comparison with Fuel Metering System No. 2. This particular pump, which is being developed by Avco Lycoming under a Contributing Engineering Program, was chosen because it represents a level of development equivalent to the other components of this advanced control.

All components are packaged in an aluminum housing. The fuel inlet passage runs through the center of the electronic computer, providing mechanical support and fuel-cooling to the electronics. The multiple-function valve and servo motor are located against the pump and computer and are installed through appropriate access covers. The metering valve and servo motor shafts are connected by a three-bar linkage.

Engine mounting is accomplished by a three-bolt flange with keyhole type of clearance holes for quick installation. Spot faces at the bolt head location prevent inadvertent disengagement.

Other quick-connect arrangements were considered, including the Marmon Clamp and threaded ring, but were found to be excessively bulky.

Weight and Cost

Weight and cost estimates for the control system incorporating Fuel Metering System No. 1 are presented below.

The costs for many components are based on similar items currently in production. An order for 1000 assemblies is assumed at a delivery rate of 100 per month.

Basic Metering System	Weight (lb)	Cost ($)
Fuel Pump Assembly	1.85	596
Multiple-Function Fuel Valve	0.90	572
System Housing and Covers	0.85	452
Servo motor and Gearbox	0.70	75
Valve Position Transducer	0.40	50
Power Lever and Position Transducer	0.80	110
No. 1 Fuel Metering System Total	5.50	1855
Emergency System Components		
Changeover Valve	0.70	55
Metering Valve and Pressure Regulator	0.75	180
No. 1 Emergency System Total	1.45	235

Emergency Manual Metering System No. 1

The emergency manual metering system is shown schematically in Figure 64. The solenoid-operated changeover valve shuts off fuel pump discharge flow to the multiple-function fuel valve and directs it to the parallel emergency metering system. The emergency metering valve is permanently connected to the power lever shaft. The pressure drop across this valve is held constant by the action of the emergency pressure regulator valve, thus providing proportional flow control from the power lever.

The solenoid changeover valve would be a bistable latching device energized from the airframe power system.

FUEL METERING SYSTEM NO. 2

System Description

In Fuel Metering System No. 2, a high-speed centrifugal pump with an integral inducer stage is driven by a miniature variable-speed drive (VSD).

The input side of the VSD is driven from the engine at compressor shaft speed, and the VSD ratio is modulated to control pump speed and, hence, fuel flow to the engine. The system is shown schematically in Figure 65.

Fuel flow to the combustor is measured by a mass flow sensor for comparison with the flow command signal in the computer. Any resultant error is used to modulate transmission ratio via a torque motor. Fuel shutoff is performed by an inline valve with solenoid and power lever actuated pilot stages. For emergency manual control, the VSD may be locked in a fixed-ratio position and the output of the pump throttled by an emergency metering valve.

The following advantages are anticipated over other metering systems:

1. Resistance to contaminants - Since the steel pump impeller is the only active component in contact with the fuel, the system is compatible with all fuel types, including emulsions, at high contaminant levels. Service life of the system should be in excess of 3000 hours without fuel filtration.

2. Closed-loop flow control creates an adaptive flow handling section, compensating for pump and drive deterioration and changes in fuel characteristics.

3. The centrifugal pump is an inherently high-speed device, which can be greatly reduced in size, and yet is simple in design and manufacture.

4. No engine fuel boost pump is required, since the pump and inducer stage are capable of meeting all current military requirements without external assistance.

5. No additional control system valves are required except for a simple fuel shutoff valve, which may "dead-end" the pump.

6. There is no recirculation of fuel around the pump, thus reducing fuel-temperature rise and contaminant accumulation.

7. Pump and VSD package size would not increase for high flow applications. The proposed system could meet the requirements of a 25-lb/sec airflow engine by increasing pump impeller depth and discharge passage dimensions. The VSD design would remain unchanged.

Design Considerations

General

Detailed analyses of flow, pressure, and speed relationships for the centrifugal fuel pump and VSD system were performed to insure that the best choice of component speed ranges would be used and that all performance requirements could be met.

Fuel Pressure Rise

Fuel pressure rise requirement for the pump is determined by the engine combustor pressure, combustor nozzle system pressure drop, line pressure drops, and pump inlet pressure. The only undetermined factor for the application is the nozzle system pressure drop, and it was necessary to assume a particular system type. A dual-orifice nozzle system with flow divider and manifold drain valve was selected since it required the highest pressure drop. Figure 66 depicts typical pressure drop versus flow characteristic for this system together with the characteristic of an air-assist nozzle system with pressurizing and manifold drain valve. The low-pressure nozzle system could be made compatible with a pump designed for the dual-orifice nozzle system by raising the pressurizing valve setting and increasing its resistance to flow. Figure 67 shows schematically a pressurizing and manifold drain valve which would allow system pressures to be selected in this way. It is desirable to operate at high fuel pressures, to hold actuation systems to minimum size and weight, and to prevent vaporization in engine fuel lines. Curves representing maximum and minimum fuel pressure rise versus engine speed were used in preparing the pump operating map (Figure 68).

Fuel Flow Range

Transient and steady-state flow ranges were obtained for all engine applications, and predictions were made of the fuel flow required for variable-geometry actuation. Additional flow was considered for combustor igniter nozzles at engine starting speeds.

A maximum transient flow of 1.75 gpm was predicted. Figure 59 shows the maximum and minimum flow requirements versus engine shaft speed.

Fuel Pump Speed

Available pump speed range is determined by the VSD input speed and ratio range. Assuming that the VSD could be driven at engine shaft speed, 60,000 rpm was selected as the maximum speed typical of the baseline engine. Operation with different input speed ranges would require resizing of the pump impeller. The ratio range of a single-stage toroidal drive is 0.316:1 to 3.162:1, providing a 10:1 pump speed range at any engine speed. Actual pump speed will be determined by the fuel flow and pressure requirements of the system.

Fuel Pump Sizing

Based upon the data presented above, design points for the pump element were selected. To determine impeller diameter, it is necessary to fix a speed and pressure rise point. In low specific speed units such as this, the pressure rise versus speed characteristic is virtually constant over the entire flow range. To establish the impeller size, two extremes were considered:

1. At 10 percent engine speed, a minimum pressure rise of 95 psi is required to achieve fuel atomization. If the vapor/liquid ratio at the pump inlet is 0.45, an additional 10 psi rise must be provided to offset the loss in the inducer stage caused by this condition. At this engine speed, the maximum pump speed is 19,000 rpm and the minimum pressure rise required is 105 psi.

2. At 100 percent engine speed, the limitation comes from the minimum pump speed, which is also 19,000 rpm. At this speed, pump pressure rise must be less than 155 psi to reduce fuel flow to the deceleration limit in the most unfavorable conditions.

Using these limitations, an impeller was selected to give 125 psi rise at 19,000 rpm, providing a significant pressure margin for both design points. To determine the absolute speed range of this pump over the range of applications, curves of minimum and maximum pressure rise were plotted. These curves were converted to pump speed curves, which were then superimposed on the output speed range plot for the VSD. This plot, shown in Figure 69, illustrates that the system can meet the most adverse range of pressure conditions with a significant margin of pump speed to deal with poor vapor/liquid conditions and

component deterioration. A maximum transient pump speed of 45,000 rpm is predicted in normal operation.

Pump flow capacity must be designed for the maximum predicted steady-state flow requirements. If the unit is significantly over or under capacity, overall efficiency will become unacceptably low in some regions of operation. Consequently, the design capacity was selected as 1.3 gpm at 42,000 rpm.

The flow, pressure, and speed requirements are summarized on a performance map (Figure 68), on which transient and steady-state operating envelopes are superimposed.

System Service Life

For design purposes, an initial service life target of 3000 hours was set. This is a significant advance over current small gas turbine practice and would reduce maintenance time and cost considerably. It is felt that the system should ultimately be capable of 10,000 hours without servicing.

System Design

General

Design and analysis of Fuel Metering System No. 2 included the following effort:

1. Basic design requirements were established for the system, including pressure rise, flow, and speed ranges.

2. Designs were obtained for the fuel pump and VSD using two different approaches for each component.

3. The dynamic response of the system was determined using digital computer simulation programs.

4. Designs were prepared for additional system components, including the power lever and shutoff valve assembly and an emergency metering valve.

5. System packaging studies were performed, incorporating the component designs into complete control system assemblies.

Centrifugal Fuel Pump Design

The flow versus pressure and speed map for the pump was submitted to two pump manufacturers for review. Both vendors responded by submitting pump designs with performance predictions.

In addition to the performance map, the manufacturers were given requirements for overall efficiency, contaminant resistance, and service life. The efficiency had to be such that the fuel temperature rise would not exceed 50°F under steady flow conditions and that the required shaft power would not exceed 3 hp. The pump was required to operate satisfactorily with fuel contaminated according to paragraph 3.4.1.3 of Military Specification MIL-E-5007C for the full service life of 3000 hours without maintenance.

The two manufacturers took significantly different approaches, but the performance predictions were similar. Vendor A proposed a forced-vortex pump (Figure 70), consisting of an inducer located at the inlet passage, a straight radial four-bladed open impeller, and a collector ring with discharge venturi. The impeller and inducer are integral with the pump shaft, which is supported by two bearings. One bearing is a fuel-lubricated carbon journal at the inducer shroud. The other is an oil spray-lubricated angular contact ball bearing that is "shared" with the VSD. Carbon-cartridge-face-type shaft seals are installed between the impeller and ball bearing to provide fuel-to-air and oil-to-air sealing. Vendor A claims that the forced-vortex configuration is more efficient at low specific speeds than conventional pumps due to reduction in disc friction and seal drag. The pump design is simple and rugged, with the components requiring far less machining than a conventional unit with shrouded impeller and discharge volutes.

The pressure rise versus flow characteristics, which are extremely flat over the design flow range, add to the stability of the proposed system. With the inducer stage, the pump will be capable of operating under the specified vapor/liquid ratio conditions and will have satisfactory dry-lift capability. Vendor A submitted temperature rise versus flow and pressure curves and power consumption figures. Also provided was a report describing tests on a similar pump to determine contaminant tolerance, efficiency, and dry-lift ability. The results indicated that the proposed pump could meet the specified requirements.

The design of Vendor B features a shrouded impeller with integral inducer stage. The rotating assembly is suspended on two oil-lubricated ball bearings, which also carry thrust and radial loads from the transmission section. Fuel-to-air and oil-to-air face-type seals are arranged concentrically behind the impeller to reduce pump length. An additional seal is provided on the inlet side of the impeller to eliminate recirculation of fuel within the pump. The impeller discharges fuel to a collector ring in the aluminum pump housing. Vendor B considered that a conventional discharge volute did not provide a sufficient gain in hydraulic performance to justify the additional complexity and space that it would require in the pump.

Overall efficiency was of prime importance in the design of the pump. The work accomplished in pumping fuel is almost insignificant in comparison to the work expended in overcoming frictional losses. Consequently, both manufacturers attempted to reduce these losses and minimize heat transfer into the fuel. Vendor A reduces disc friction by eliminating impeller shrouds and reduces seal drag by eliminating the need for a seal at the impeller. The hydraulic efficiency of the unit is probably lower than that of a conventional pump, but the overall efficiency is acceptable. Vendor B minimizes losses due to recirculation by placing a seal on the front face of the impeller and holds disc friction to a minimum by careful control of impeller side clearances. The location of both bearings in the oil side of the pump eliminates them as a cause of fuel-temperature rise and avoids the fuel recirculation necessary with a fuel-lubricated bearing. A curve of predicted fuel-temperature rise versus flow and pump speed for the Vendor B design is presented in Figure 71. The curve shows a maximum steady-state temperature rise of 54°F, which only slightly exceeds the target value.

Both vendors concluded that the performance and life requirements for the pump were feasible and did not represent an extension of current technology.

Mechanical Transmission Design

The mechanical transmission design was based on the well known toroidal design manufactured by Avco Lycoming for use in constant speed alternator drives, control devices, and mechanical servos. Recent programs have featured miniature, high-speed versions of this transmission lubricated by engine oils such as MIL-L-7808. The reliability, response, and low cost of these devices make them attractive for this application.

The transmission arrangement selected is illustrated in the system design (Figure 72). The aluminum transmission housing supports the input side thrust bearing and carries the required preload for power transmission. The housing also supports and locates the transmission ratio change control assembly, the control torque motor, and the fuel pump housing. The output side bearing is located in the fuel pump housing and carries both the transmission preload and the radial and axial pump loads. Both bearings are of an angular contact-ball type designed specifically for this application. The outer race of the input side bearing is loaded by a Belville washer system that provides the compressive force between the transmission toroids and rolls. The transmission roll-toroid section was sized to transmit 4 hp at 100 percent input speed and 45,000 rpm output speed. Surface velocities and compressive Hertz stresses are within the present design practices of Avco Lycoming. The geometry of the transmission was designed to provide a 10:1 ratio range (0.316 to 3.162:1). The transmission ratio change control assembly supports three gimbal-mounted rolls and their bearings on a machined aluminum cage. Each roll is bearing-mounted on a shaft that is supported in a gimbal and is free to rotate about an axis perpendicular to the transmission axis (θ axis). The gimbal positions are synchronized by gear segments, as shown in Figure 73. The roll shafts are free to pivot about an axis (α) that is perpendicular to the θ axis. Transmission ratio is changed by tilting the roll about the α axis, causing the rolls and gimbals to rotate about the θ axis, changing transmission ratio. The rate of θ rotation is related to the applied steer angle, the input speed, and the position of the rolls in the θ plane. The two methods of applying steer angle are discussed below. Since the motions involved are not easily defined, Figure 74 has been provided as reference to supplement the description of both methods. In both methods, the θ position of one master roll is transmitted to the two slave rolls via the interconnecting gear segments.

The first method, referred to as direct α control, uses an electrical torque motor to modify the master roll bearing position through a mechanical linkage. As shown in Figure 73, the torque motor rotational output would be converted to a linear motion of a pushrod via a crank. The pushrod is concentric with the gimbal axis and rotates with the gimbal. One end of the pushrod is attached to the roll shaft which pivots about the α axis. Steer angle applied to the master roll would then be proportional to torque motor deflection. Very small displacements ($\pm$ .006 in.) are required, and torque motor power consumption would be low (less than 5 watts). The motion of the master-roll about the θ axis is transmitted to the gimbals of the

slave rolls via the gear segments. The slave rolls cannot be forced to rotate about the θ axis but must be steered as is the master roll. This is accomplished by mounting the roll shafts between diagonal slots in the gimbals. When the gimbal is rotated about the θ axis, the forces within the transmission hold the slave roll fixed in the θ plane but allow it to rotate about the α axis. The diagonal mounting slots in the gimbal tilt the roll about the α axis, the displacement being proportional to the difference in θ angle between the gimbal and the roll. The applied α angle makes the roll steer itself toward the same angle as the gimbal, creating a closed-loop position control of the slave rolls.

In the θ control method (Figure 75), all gimbals use a diagonal slot for positioning the roll bearings. The shaft of the master gimbal is extended through the transmission housing and is positioned by an electrical torque motor. The motion of the master gimbal is again transmitted to the slave gimbals by the gear segments.

The θ method of control was selected for the following reasons:

1. Safety - In the event of an electrical power failure or computer malfunction, the gimbals will remain in one position until the pilot assumes manual control. With direct α control, the ratio of the drive would probably drift to a hard-over condition, either direction being catastrophic.

2. Simplicity - the transmission control assembly is much simpler and more robust with the θ control mode. This simplicity provides a more reliable device at lower weight and cost than the α control assembly.

3. Performance - Elimination of the control linkage reduces backlash and hysteresis in the control assembly, leading to improved response and stability. Another advantage is that the rate of change of ratio is directly proportional to torque motor angular velocity. With direct α control, the ratio change rate is proportional to torque motor displacement and is influenced by drive speed and roll position.

The transmission design is based on well-proven design features from previous experiemental and production units. The current MTBF for similar roll and toroid components is 5500 hours.

Transient and frequency response tests on a similar device have demonstrated that adequate dynamic performance can be achieved in the design. The acceleration of the drive is directly dependent on inertia loading of the components on the output end of the drive. A preliminary inertia analysis of the VSD-centrifugal fuel pump combination indicates that the system response-time design objective of 0.03 second is feasible. However, a detailed system inertia study, including any additional accessories, will have to be thoroughly analyzed once a final configuration is established.

A variable-speed test transmission, design for high-speed operation and conventional gas turbine lubricating fluids (i.e., MIL-L-7808 and MIL-L-23699), is currently being evaluated as part of an Avco Lycoming Independent Research Program. The transmission has successfully completed engine cold starts (-30°F) using engine-supplied lubricant MIL-L-7808 and has run continuously at toroidal speeds of 25,000 rpm. The unit is capable of transmitting up to 3 horsepower at a constant output speed over a 20:1 input speed range. Design schemes generated under this program are directly applicable and are reflected in the design of the transmission for this study. Figure 76 shows the power section of the test transmission after 22 hours of development testing. Components in the ratio change section are similar to the proposed drive. Research of high-speed transmissions is being continued. The planned test program includes operation up to 40,000 rpm toroidal speeds and investigation of α and θ control methods and interface devices. The results of this research will be applied to the centrifugal fuel pump transmission.

Dynamic Response Analysis

Digital and analog computer simulations were made of the variable-speed drive and pump system. Satisfactory response and stability were obtained at all operating conditions examined.

Under a previous independent research and development program, in which the feasibility of a similar metering system was studied, a MIMIC digital computer program was constructed to simulate the dynamic performance of the VSD and pump in conjunction with an engine. The program was also duplicated on an analog computer to allow rapid evaluation of parameter changes. In this study, these simulation programs were updated to include the design parameters of the proposed system, and test runs were performed to determine stability and transient response. The Control Mode Studies section

of this report includes block diagrams and results of the simulations.

Although the simulation studies predicted stable operation, they were not capable of predicting possible fuel system pressure resonances and difficulties in establishing stable flow control with a centrifugal pump. Such fuel pressure oscillation could cause combustion instability or "rumble". To investigate these possibilities, tests were performed on an Avco Lycoming T55-L-11 engine using a forced-vortex pump that discharged directly to the engine manifolds. The pump was driven by a variable-speed electric motor at speeds up to 27,000 rpm. During the test, the engine was operated at gas producer speeds between 40 and 80 percent while pressures and flows were observed using high-speed CEC recorders. No instabilities in control occurred. In an attempt to induce combustion instability, the flow divider valve was removed and primary flow was controlled manually. It was impossible to induce any kind of instability by varying primary to secondary flow ratio or by inducing sudden primary flow changes. Engine speeds could be controlled accurately by manual variation of pump speed over the range of the test.

Power Lever and Fuel Shutoff Valve Assembly

The power lever and shutoff valve are included in a single assembly, which can be installed at any convenient point in the fuel control discharge line. The power lever is mechanically connected to the pilot's lever and positions the engine speed select transducer and the manual fuel shutoff pilot valve. The assembly also contains the main fuel shutoff valve and a solenoid-operated pilot valve. For applications requiring an emergency system, an additional bolt-on package would provide an emergency metering valve and stepdown pressure regulator as described below in the paragraph Emergency Manual Metering System. The complete assembly is illustrated schematically in Figure 77.

System Packaging Study

Following the initial sizing of pump and transmission components, packaging studies were made to select the interfaces and envelope requirements. Two design layouts of the system were prepared using alternative pump and transmission assemblies. Design criteria were minimum size, maintainability, provisions for accessory integration, and ease of manufacture.

The first layout, depicted in Figure 72, included the Vendor A fuel pump, the VSD with α control mode, and the digital electronic computer. The aluminum transmission housing supports the VSD input bearing, the VSD control section (including α control torque motor), and the fuel pump assembly. A three-bolt flange with nut clearance holes is provided on the housing for quick engine installation and removal of the control assembly. The fuel pump assembly features a two-part aluminum housing, which is bolted to the transmission housing. To achieve close mechanical integration, the transmission output toroid is mounted on the pump shaft, and the pump bearings carry loads from the transmission. Oil and fuel face-type seals are provided in the pump housing with an interseal drain. The pump inlet tube is integral with the impeller housing and supports the electronic computer assembly, allowing some heat transfer from the electronics to the inlet flow.

This arrangement permitted the major system components to be contained in a cylindrical package, 3.25 inches in diameter and 8.0 inches in length. Additional components required for an engine system would be the power lever and shutoff valve assembly and the fuel flow sensor. These items may be located at any convenient location in the discharge fuel line and are described above in the paragraph Power Lever and Fuel Shutoff Valve Assembly.

The second layout, shown in Figure 78, included the Vendor B fuel pump design, the VSD with θ control mode, a flux switch generator, a digital computer, a flow sensor, and a power lever and shutoff valve assembly. (Note that the generator was added to this layout as discussed below.) This represents a complete control system for dual-engine applications without variable-geometry systems. The package configuration is the same as that in the first layout but illustrates major component differences. An additional 0.25 inch of length is required for inclusion of the generator.

Ease of servicing is provided by the modular package construction. The electronic computer may be removed for testing without removing the system from the engine or disconnecting any fuel lines. The pump assembly can be removed from the VSD by disassembling four bolts and may be tested as a separate unit by installing a drive spline adapter in place of the VSD output toroid. Evaluation of the VSD can be made with the pump assembly attached. The pump may be used to load the transmission in production testing. Other items which may be replaced without removing the system from the engine include the transmission control device, the flow sensor, and the

power lever and shutoff valve assembly. The condition of the pump and VSD assemblies may be checked by measurement of pump speed and fuel pressure rise at ground idle engine speed.

The addition of engine accessories on the VSD output shaft was studied, since the small, high-speed band of operation would enable the size of other pumps and electrical generators to be reduced in comparison with units driven at engine shaft speed. To illustrate the concept, an electrical generator that is capable of providing sufficient power for the control system and its interface devices was designed. The design and installation of a flux-switch generator are described in Appendix VI of this report. Power supply is a major problem in gas turbine electronic controls, and this system provides a unique solution to reduction of the generator size and simplification of power conditioning.

Emergency Manual Metering System No. 2

To provide emergency manual metering, the VSD ratio control would be locked in one position by a cartrige-driven actuator, and the output of the pump would be throttled by a pressure regulator and emergency metering valve. The system is depicted schematically in Figure 77.

System components would be available in kit form for use in single-engine applications. Two assemblies would be provided: (1) the θ shaft lock assembly and (2) the emergency metering valve (EMV) assembly. The θ shaft lock would attach to the VSD housing, and the EMV assembly would bolt to the power lever and shutoff valve assembly.

The system would be actuated by a pilot-operated manual switch, which applies airframe current to the θ shaft lock cartride and the EMV bypass latching solenoid valve. The cartridge provides gas to the actuator, which drives the VSD θ shaft to a predetermined position and locks it. A constant VSD ratio of 0.884:1 was selected for the emergency condition in order to provide adequate fuel pressure for acceleration at all conditions above 50-percent engine speed. This fixed ratio will result in a maximum pump speed of 53,000 rpm at 100-percent engine speed. This pump speed, which is higher than the maximum design speed of 45,000 rpm, will not impose undue loads on the pump and transmission components.

Energizing the bypass solenoid valve closes part of the normal flow path and actuates the stepdown pressure regulator. Normally, fuel from the valve inlet flows through both the regulator valve and the regulator

bypass valve and then out of the assembly via the fuel shutoff valve. The emergency metering valve is permanently connected to the power lever but has no effect on flow in normal operation. When the regulator bypass valve is open (deenergized), pressures across the stepdown regulator piston are equalized, and the regulator spring moves the regulator valve to the fully open position. When the bypass valve is closed (energized), all flow must pass through the regulator valve and emergency metering valve (EMV). The pressure drop across the EMV is then applied to the sensing areas of the stepdown regulator piston, causing the regulator valve to move toward the seat and to restrict flow. The regulator then acts to maintain a constant pressure drop across the emergency metering valve. Since the flow area of the EMV is controlled by power lever position and pressure drop is held constant, the pilot may select steady-state flow directly with the power lever.

The fuel shutoff valve is part of the normal fuel system and is described above in the paragraph Power Lever and Fuel Shutoff Valve Assembly. In manual operation, fuel shutoff is achieved by closing the EMV and by manual operation of the shutoff pilot valve from the power lever shaft.

A design layout for the emergency metering valve assembly, together with the solenoid and manually operated fuel shutoff valve, was prepared.

Weight and Cost Estimates

Weight and cost estimates were obtained for all system components studied. The cost predictions are based on an order for 1000 units with a delivery rate of 100 units per month.

Basic Metering System	Weight (lb)	Cost $
VSD (with θ Control Mode) Assembly	1.9	1050
Vendor B Fuel Pump Assembly	1.3	175
VSD Control Servo Motor	0.6	75
Fuel Flow Sensor	0.3	135
Power Lever and Shutoff Valve Assembly	0.8	150
No. 2 Fuel Metering System Total	4.9	1585

Alternative System Components	Weight (lb)	Cost $
VSD (with a Control Model) Assembly	1.9	1200
Vendor A Fuel Pump Assembly	1.1	277
VSD Control Torque Motor	0.4	105
Emergency System Components		
θ Shaft Lock Assembly	0.15	35
EMV Assembly	0.75	95
No. 2 Emergency System Total	0.90	130

COMPARISON OF SYSTEMS

A comparison of the main features of the two proposed fuel metering systems is as follows:

	System No. 1	System No. 2
Weight of Basic System (lb)	5.50	4.90
Additional Weight of Emergency System (lb)	1.45	0.90
Cost of Basic System ($)	1855	1585
Additional Cost of Emergency System ($)	235	130
Weight of Optional Electrical Generator (lb)	1.50	0.50
Cost of Optional Electrical Generator ($)	400	50
Service Life with Contaminated Fuel (hr)	300	3000
Potential Service Life, Clean Fuel (hr)	3000	10,000
Maximum Potential Pad Speed (rpm)	25,000	85,000
Electrical Power Requirement, Maximum (watts)	17	23

Fuel Metering System No. 1

Advantages

1. Uses established technology

2. Requires less electrical power for actuation

Disadvantages

1. Requires low pad speed

2. Has severely limited pump life with contaminated fuels

Fuel Metering System No. 2

Advantages

1. Long service life

2. High tolerance to fuel contaminants

3. Operates at engine shaft speed

4. Adaptable to engines up to 25 lb/sec airflow without increase in package size, weight, or cost

5. Allows other engine accessories to be integrated with the control system and permits significant size reduction of components (Accessories may include generators, lubrication pumps, and air-assist system compressors or hydraulic pumps.)

Disadvantages

1. VSD and fuel flow sensor require development

2. Requires connections to engine oil system

In summary, Fuel Metering System No. 1 provides a method of achieving the specified requirements without undue technological risk or cost in a package of size and weight comparable to System No. 2. Its service life, reliability, and maintainability would be comparable with present-day systems. Fuel Metering System No. 2 offers advantages in many areas but requires a greater component development effort.

The most significant advantages are (1) the ability to operate at engine shaft speed, (2) the facility for driving the system electrical generator over a high-speed band of operation, thereby reducing the generator size, and (3) simplifying the power-conditioning circuitry. For larger engine applications, Fuel Metering System No. 2 would have unsurpassable advantages in size, weight, and cost.

SENSORS

TURBINE TEMPERATURE SENSORS

Introduction and Background

In the past, the temperature sensing element has been the limiting factor inhibiting the widespread use of closed-loop turbine temperature controls for gas turbine engines. Normally these sensors would be required to live, uncooled, in the turbine region of the engine where turbine blades and vanes are air-cooled. Furthermore, the sensors must respond rapidly to changes in gas temperature. These are diverse requirements. Recently, however, technological developments with fluidic temperature sensing elements and circuitry have fostered renewed interest in closed-loop turbine inlet temperature controls.

Under an Army-sponsored Contributing Engineering research and development program and a company-sponsored independent research and development (IRAD) program, Avco Lycoming has studied and evaluated several different types of temperature sensing devices. These included fluidic oscillators, fluidic and electronic thermistors, thermocouples, radiation sensors, and ultrasonic sensors. Two sensors from this list, the fluidic oscillator and the fluidic thermistor, were selected for further extensive investigation. These two types of sensors were evaluated on the bench and on production versions of Avco Lycoming engines to determine their accuracy and response.

The need for fast dynamic response and accuracy of the sensed temperature becomes more evident when one considers the manner in which the sensor and its related signal circuitry are incorporated into the overall control system block diagram (Figure 79). The fluidic temperature sensor and its signal circuitry are located in the feedback path of the closed-loop controller. If the static gain of the forward loop element G(S) is very much greater than unity, then the response and accuracy of the overall system C(S)/R(S) are directly related to the response and accuracy of the feedback elements H(S).

During 1968, Avco Lycoming completed a preliminary engine evaluation of a miniature (dime-size) fluidic oscillator temperature sensor. This testing was intended to establish the feasibility of using this type of sensor in the hollow turbine stator vanes of the first turbine nozzle. Figure 80 is a schematic of this engine test setup showing the sensors installed in the stator vane. The pneumatic frequency generated by the sensor was ducted from the engine by a 1/8-inch-diameter line, and the pneumatic frequency was converted to an electronic frequency by a piezoelectric pressure transducer. Two prototype sensors were installed and tested simultaneously; however, no attempt was made to average the two readings. With the sensors installed in this manner, cooling air passed over the outside surface of the sensors throughout the entire test; therefore, the effect of this cooling air must be considered when evaluating the output signal. This preliminary test work has led to the discovery that the fluidic oscillator retains the ability to sense supply gas temperature while being deliberately cooled externally. The paragraph Signal Error Compensation in this section describes a method of error compensation whereby the sensed temperature error due to cooling is compensated.

The rest of this section describes the operation of the fluidic oscillator and the fluidic thermistor temperature sensors, and the proposed method of incorporating the oscillator temperature sensors into a typical 2- to 5-lb/sec engine.

Fluidic Oscillator Temperature Sensor

Description

The fluidic oscillator temperature sensor is defined as a jet-edge-resonator device. The oscillator can simply be described as containing two orifices in series with an intermediate volume or resonant cavity, where an acoustic frequency is generated as a function of the temperature of the gas within this cavity.

The fluidic oscillator is unlike other temperature sensing devices since it does not require measurement through a material interface, i.e., the supply gas is ducted directly into the sensor. The sensor material and its mass effect only the steady-state gas temperature measurement by heat-energy transfer from the gas stream to the sensor material; i.e., steady-state accuracy cannot be established until the sensor material is at the same temperature as the

supply gas. If the sensor is not surrounded by supply gas, a temperature gradient will exist across the sensor wall, causing an error in the output signal. This error must be compensated in the final system, and the paragraph Signal Error Compensation discusses this.

Location and Installation

The oscillator will be located in a cooled region of the engine with its inlet orifice located essentially at Station 5, the initial turbine inlet. Figure 81 shows the sensor installed in a typical 2- to 5-lb/sec engine and indicates the relative size of the sensor with respect to the engine. The sensors can not be designed into the hollow, air-cooled, stator vanes because the vanes for this class of engines are too small to accommodate the signal tube. Burner exhaust gas is ducted through the sensor and discharges to ambient air, such that the sensor is referenced to the maximum attainable engine pressure ratio. A Pitran pressure transducer, which is shown mounted to the outside wall of the diffuser housing, is fed by a pneumatic signal tube directly from the temperature sensor. Eight individual fluidic oscillators are proposed for this program to obtain an adequate temperature average that is within approximately 1.2 percent of the calculated thermodynamic average. The electronic frequency signals from each of the eight Pitran transducers are directed, respectively, to each of the eight frequency-to-dc convertors located in the cooled portion of the electronic controller.

Materials and Manufacturing Techniques

The fluidic oscillators should be made from Inconel alloy 702 material, which possesses good oxidation resistance to over 2000°F and has a softening temperature of approximately 2450°F. With the sensor installed in a region of compressor discharge air, the maximum sensor material temperature should be less than the softening temperature when subjected to T_5 transients to 3000°F.

The sensor design configuration can be successfully machined into super-alloy steels by either milling, electrical-discharge machining (EDM), or electrochemical milling (ECM). Assembly of these miniature sensors has been successfully performed using diffusion bonding techniques and heliarc welding.

Advanced sensor designs of the miniature size might ultimately be made from high temperature ceramic materials such as alumina oxide.

Sensor Dynamics

This paragraph defines the operation of the fluidic oscillator by the use of an electrical analogy and will derive the equations that predict the dynamic performance. It will be shown that the fluidic oscillator has an initial fast-path response with respect to changes in the inlet gas temperature, i.e., the sensor responds rapidly to about 80 percent of a step temperature change and responds slowly to the remaining 20 percent of the temperature change because of the mass of the sensor material.

Consider the electrical circuit description of the oscillator shown in Figure 82 . Four discrete temperatures are relevant to the operation of the device: the supply gas temperature (T_5), the sensor cavity temperature (T_c), the sensor body temperature (T_b), and the sensor ambient temperature or cooling air temperature (T_a). The temperature drop between T_5 and T_c is caused by the inlet orifice resistance (R_1) and the sensor cavity capacitance (C_1). The temperature drop between T_c and T_b is caused by the inside film resistance (R_2) and the sensor material capacity (C_2). The temperature drop between T_b and T_a is a function of only the outside film resistance (R_3). The oscillator is subjected to transient temperatures from both T_5 and T_a; the output frequency which is a measure of T_c is influenced by these changes.

Considering a step change in T_5 temperature, the effect will be an immediate change in T_c temperature which is attenuated by the resistance (R_1 and R_2) and the sensor capacitance (C_1). The resistance (R_3) is short circuited by C_2 and the sensor material does not respond. As time increases, the three resistances are in series, and T_c will track T_5 with only a slightly lower amplitude, equivalent to the steady-state error.

Figure 83 is a signal flow graph of the fluidic oscillator temperature sensor and will be used to derive the transfer function (T_c/T_5 This transfer function will aid in an understanding of the effect of the change in the input variable on the output frequency.

In the signal flow graph, the values of the nodes (the circled elements) are equal to the sum of all the incoming signals, and the path functions define the transfer from one node to the next. A tool used in analyzing this type of circuit is Mason's expansion, which permits the transfer function to be written directly from the signal flow graph, i.e., using Mason's expansion and solving for T_c/T_5 for small purturbations about a given steady-state point.

$$T_T = \frac{T_c}{T_5} = \sum_{K=1}^{K=n} \frac{P_k \Delta_k}{\Delta} \tag{1}$$

where T_T = Overall transfer function or graph transmittance

P_k = Path transmittance = the path from a source to a node

Δ = Graph determinant = 1 - (sum of loop transmittances) + (Sum of pairs of nontouching loops) - (sum of triplets)

Δ_k = Path factor = the graph determinant of the remaining portion of the signal flow graph when the path transmittance is removed.

Therefore,

$$P_k = \frac{1}{R_1 C_1 S} \tag{2}$$

$$\Delta = 1 - \left[\left(-\frac{1}{R_1 C_1 S}\right) + \left(-\frac{1}{R_2 C_1 S}\right) + \left(-\frac{1}{R_2 C_2 S}\right) + \left(-\frac{1}{R_3 C_2 S}\right)\right] + \left[\left(-\frac{1}{R_1 C_1 S}\right)\left(-\frac{1}{R_2 C_2 S}\right) + \left(-\frac{1}{R_2 C_1 S}\right)\left(-\frac{1}{R_3 C_2 S}\right) + \left(-\frac{1}{R_1 C_1 S}\right)\left(-\frac{1}{R_3 C_2 S}\right)\right] \tag{3}$$

and,

$$\Delta_k = 1 - \left[\left(-\frac{1}{R_2 C_2 S}\right) + \left(-\frac{1}{R_3 C_2 S}\right)\right] \tag{4}$$

Combining equations (2), (3), and (4) and simplifying the equation results in the transfer function $\hat{T}_c/\hat{T}_5$.

$$\frac{\hat{T}_c}{\hat{T}_5} = \frac{\frac{1}{R_1C_1}\left[S + \frac{1}{R_2C_2} + \frac{1}{R_3C_2}\right]}{S^2 + \left(\frac{1}{R_1C_1} + \frac{1}{R_2C_1} + \frac{1}{R_2C_2} + \frac{1}{R_3C_2}\right)S + \left(\frac{1}{R_1R_2C_1C_2} + \frac{1}{R_2R_3C_1C_2} + \frac{1}{R_1R_3C_1C_2}\right)} \quad (5)$$

Equation (5) will now be used to define the dynamic behavior of the sensor. For simplicity in estimating the sensor performance, relative numerical values will be assigned for the parameters; i.e., $R_1 = 0.1$, $R_2 = 1.0$, $R_3 = 1.0$, $C_1 = 0.1$, and $C_2 = 1.0$.

Substituting these values into equation (5) yields the following results,

$$\frac{\hat{T}_c}{\hat{T}_5} = \frac{100\ (S + 2)}{S^2 + 112\ S + 210}$$

$$= 0.95\ \frac{(0.5\ S + 1)}{(0.59\ S + 1)\ (0.009\ S + 1)} \quad (6)$$

Equation (6) shows conclusively that the transfer function of $\hat{T}_c/\hat{T}_5$ is a lag-lead-lag function, where the lag terms are a result of the sensor material inertia and the cavity purge efficiency, and the lead term is the fast-path transfer from T_5 to T_c. It also indicates that the low-frequency lag and lead will effectively cancel, by proper choice of design conditions, and the sensor mass does not affect the response.

Figure 84 is a Bode plot or frequency response diagram for the fluidic oscillator temperature sensor. The results shown in this figure are those of an experimental study performed on an Avco Lycoming T55-L-7 engine and compare closely with the theoretical predictions for the sensor, substantiating the analytical approach. The block diagram representation of a fast- and slow-path signal (Figure 84) will aid in an intuitive understanding of

the problem and follows from a partial fraction expansion of the transfer function in equation (6).

The fluidic oscillators appear to have excellent dynamic response and should be well suited for acceleration fuel limiting.

Sensor Design

The proposed sensor design was supplied to Avco Lycoming by the Harry Diamond Laboratories (HDL), which, in the past, successfully supported Avco Lycoming research and development work when the original miniature temperature sensor design was evaluated in the engine. For the sensor design, it was necessary to specify only the required operating conditions and the overall sensor size. Figure 85 shows the frequency-temperature relationship of the proposed sensor. The high normal operating frequency (30-60 kHz) should permit the sensor to operate out of the frequency range of engine-generated noise. The sensor threshold of operation will be approximately 1.0 psig supply pressure,which should occur at approximately 20 percent N_h speed during engine cranking. At these conditions, the sensor error due to pressure sensitivity should be approximately 15 percent of the final steady-state value. After the engine has fired and attained approximately 40 percent N_h, the sensor operating point should be at 47 kHz with a sensed temperature error, due to pressure effects, of about 6 percent. At 50 percent N_h speed, the pressure sensitivity error will be reduced to about 2 percent; at 75 percent N_h, the error will be down to about 0.1 percent. These errors are based upon ideal frequency versus supply pressure predictions, and do not reflect possible errors caused by supply-temperature level and ambient pressure changes.

Signal Error Compensation

A method of signal error compensation has been devised which will reestablish steady-state accuracy in a cooled fluid oscillator. The method involves measuring the cooling air temperature at a suitable location and automatically adding a correction to the oscillator output based on this measured temperature. Details of this development are presently under study.

Turbine Temperature Averaging

Before a temperature control system would be accepted to replace the present mode of scheduled acceleration fuel, it must be shown that a directly measured turbine temperature average can be provided. Two presently known methods of averaging turbine temperatures are multiple unit averaging and gas averaging. Both methods will be discussed in this section and the salient features of each will be presented.

Multiple unit averaging has been selected for incorporation into the proposed control system simply because the solutions to the gas averaging problems have not been resolved in sufficient depth. The final temperature averaging system might ultimately incorporate features from both of these approaches.

A study was performed at Avco Lycoming to determine the character of the engine temperature distribution which must be measured and averaged. Various thermocouple arrangements were installed at the tailpipe location of T53 and T55 engines, and a total of 144 individual temperature readings on 9 engine models were taken. Following these tests, statistical analyses developed the temperature distribution that could be expected at the power turbine inlet (T_7) location and showed the average T_7 temperature and the deviation from this average. Nine different thermocouple probe configurations were studied, including even and uneven circumferential locations at 3 different radial depths. From this information, an approximate temperature spread could be determined as a function of the number of evenly spaced probes. These data were used in this program to determine the number of fluidic oscillators necessary to give the percentage of accuracy required. For example, five evenly spaced probes in the system can be expected to give a temperature variation of approximately 85°F, and twelve evenly spaced probes can be expected to give a temperature spread of approximately 17°F. The temperature distribution and spread at the initial turbine inlet station (T_5) are expected to be considerably greater than those indicated for T_7. The radial and circumferential temperature distributions are a result of hot spots and cold spots that develop within the engine. These hot and cold spots, or isotherms, are characteristic signatures of the particular engine; therefore, their locations are expected to vary between engine models and between engines of the same model. The only type of analysis that could possibly predict these isotherms is a statistical analysis based upon past performance.

Multiple unit averaging of temperature is defined as a method whereby a number of sensors are placed strategically in the turbine region of the engine to detect both the circumferential and the radial temperature distributions. Summation of the individual signals and averaging would be performed after the temperature is transduced by the sensors. This method of averaging is proposed for the advanced engine control because it currently is the only method that can be expected to provide the degree of accuracy necessary for temperature control.

Eight individual temperature sensors are proposed at eight different evenly spaced circumferential locations. This arrangement can be expected to give a measured temperature average at T_5 within $\pm 30^{\circ}F$ of the calculated average temperature at design point conditions. This assumes that the T_5 average increases 50 percent from station T_7, where the measured temperature average is estimated to be within $\pm 20^{\circ}F$ of the calculated average. A maximum of $2500^{\circ}F$ turbine inlet temperature has been assumed for this study; therefore, the measured temperature should be within approximately ± 1.2 percent of the true calculated thermodynamic average.

Figure 86 shows a typical multiple unit average system, with each of the eight sensors having the same circuitry. The pneumatic frequency generated by the fluidic oscillator is converted by the Pitran transducer into an electronic frequency. The output from the Pitran circuit is amplified, and then the signal is converted to an analog, dc level by the frequency-to-dc converter. An optional noise filter has been shown in the circuit, but the need for signal filtering has not been resolved. After leaving the frequency-to-dc converter, the signal goes through a preset switch that eliminates a failed sensor from the system when the output level of the faulty sensor falls below the preset value. The signal then goes to the summing junction and averaging system, where the eight signals are compared and averaged. The output of this system then would be a dc voltage which is a function of the measured average from eight separate fluidic oscillators.

Gas averaging of temperature involves the admittance of multiple gas samples from various locations around the turbine inlet into a

gas manifold duct, as shown schematically in Figure 87. These samples then mix and average in the manifold prior to sensing by a single temperature transducer. Preliminary studies of temperature control systems have indicated that the method of gas averaging would be superior to the method of multiple unit averaging if problems such as conduction heat-loss and transient temperature-lag could ultimately be resolved. The final gas averaging configuration, one that could be used with a turbine temperature controller, would be a sophisticated system that would incorporate all the following features:

1. A minimum of eight sampling points, to provide an accuracy of the average sensed temperature

2. Two or more fluidic temperature sensors, for fail-safe protection

3. A bypass orifice in parallel with the temperature sensors to increase gas flow through the averaging duct, thereby minimizing conduction heat losses in the duct and reducing the averaging system transport lag

4. A minimum duct-length to reduce heat loss and to reduce time delay

The applicable heat transfer equations used in the study of gas averaging are presented below.

As the gas flows through the averaging manifold, some of its heat is transferred to the duct walls because of the difference in the temperature between the gas and the wall. The duct walls then conduct the heat away from the system to a region of colder temperature. The amount of heat lost by the gas during this process can be found from the equation

$$q = hA\,(T_{avg} - T_i) \qquad (14)$$

where h = the heat transfer coefficient, Btu/hr - ft^2 - ^oF

A = the wetted area of the duct, ft^2

T_{avg} = the average temperature of the gas in the duct, ^{o}F

T_i = the duct inside wall temperature, ^{o}F

q = the heat transfer from the gas to the duct wall, (Btu/hr)

The amount of heat lost by the gas is related to the temperature drop of the gas as it flows through the duct by the formula

$$q = W_a C_p \Delta T_{gas} \tag{15}$$

where W_a = the mass flow of gas, lb/sec

C_p = the specific heat of the gas at a constant pressure, (Btu/lb - ^{o}F)

ΔT_{gas} = the temperature drop of the gas, ^{o}F

Substituting equation (14) into equation (15) and solving for ΔT_{gas} gives

$$\Delta T_{gas} = \frac{hA\,(T_{avg} - T_i)}{W_a C_p} \tag{16}$$

In addition to the equation for heat transfer from the gas to the duct walls, the equations for heat flow through the duct walls must also be considered. These equations are derived from the standard formula for conductive heat flow through a flat plate, which is

$$q = \frac{KA\Delta T}{L_t} \tag{17}$$

where K = the heat transfer coefficient, (Btu - ft/hr - ft^2 - ^{o}F)

q = the amount of heat transferred per unit time, Btu/hr

A = the flat plate area, ft^2

L_t = the plate thickness, ft

ΔT = the temperature drop across the plate ^oF

The anticipated gas temperature drop can be estimated by assuming a typical ducting system and estimating the gas flow characteristics. Assume that the ducting system samples gas at eight points in a typical 5-pound-per-second engine and that a total of 0.050 pound per second (1.0 percent) of gas can be sampled without overly compromising engine efficiency. Furthermore, assume a gas velocity of 50 feet per second through the duct, which is approximately the velocity necessary for adequate response during transients. The temperature drop of the gas flowing through a 1-inch length of duct is approximately 5 percent of the difference between the gas temperature and the duct wall temperature at design conditions, i.e., the gas will change temperature at the rate of $0.05 (T_{avg} - T_i)$ per inch of duct length.

Under transient and steady-state conditions, the temperature drop of the gas passing through the duct must be negligible for the sensor to read an accurate turbine inlet temperature. Therefore, the temperature of the inside of the duct walls should be as close to the gas temperature as possible. This can be accomplished by several methods: (1) the outside of the duct can be insulated from the ambient, (2) the duct itself can be made out of an insulating ceramic, (3) the duct can be placed in the T_5 region of the engine and totally surrounded by turbine inlet gas, or (4) the duct can be surrounded by a heat pipe. Each of these methods would require that the duct material withstand the T_5 temperature for extended periods of time.

Deliberate cooling of the gas averaging manifold is presently under consideration. If duct cooling is employed, then a method of compensation similar to signal error compensation will be required. To illustrate the need for compensation, the following analysis will show the magnitude of the temperature loss when the averaging system is subjected to a step change in turbine inlet temperature (T_5). Assume that flow through a 6-inch length of duct is required to average temperatures prior to sensing by the temperature transducer. During the transient, the gas will lose 5 percent per inch for 6 inches or 30 percent of the difference between T_5 and T_i. Hence, the temperature that the sensor will experience is

$$T_5 \text{ (sensed)} = T_5 - 0.3 (T_5 - T_i)$$

$$= 0.7 T_5 + 0.3 T_i$$

During a typical transient such as engine "light-off" conditions, the sensor will be indicating T_5 gas temperatures that are several hundred degrees lower than the actual T_5 temperatures. Compensation, therefore, will be required on gas averaging systems to prevent overheat conditions in the engine during transient operation and to reestablish an accurate steady-state value.

A test model was made to verify the applicability of the gas averaging equations. The model had the dimensions as shown in Figure 88 and was instrumented with thermocouples at the duct inlets, at the point where the fluidic oscillator would be located, and at various points along the duct. Hot air entered the duct at points A and B, flowed through the duct, and had its temperature measured as it exited from the system. The effect of artifically cooling the duct walls was studied to see if a correlation existed between average T_5 and ambient temperature. Additional preliminary studies included evaluation of the effect of pressure drop across the inlet orifices and determination of the accuracy of the sensed average temperature.

It was found that a definite correlation existed between T_5, duct wall temperature, and sensor inlet temperature or averaged T_5 as predicted by the equations, and that this system could average multiple gas inputs accurately. These equations can now be used to design a full-size prototype gas averaging system for the study of compensation schemes.

Pneumatic-To-Electrical Conversion

The fluidic oscillator output must be converted to an electrical signal for use with the electronic control. Two types of pressure transducers have been successfully evaluated in this application and are described in the following paragraphs.

The Pitran transducer is a pressure-sensitive silicon transistor in which the emitter-base junction is mechanically coupled to a diaphragm located in the top of the standard transistor can. A force or pressure acting on the diaphragm produces a large, reversible change in the characteristics of the transistor. The Pitran output is a linear voltage which is approximately 20 percent of the supply voltage for input power levels from 1 to 50 volts.

A circuit diagram of the Pitran system evaluated at Avco Lycoming is shown in Figure 89. This circuit had been modified from that suggested by the manufacturer to reduce the low-frequency (steady-state) drift and to incorporate a simple electrical noise filter. The Pitran transducer was evaluated during a 50-hour bench test while mated with a fluidic oscillator; satisfactory dynamic performance was achieved.

The present units are recommended for a temperature range of -40° to +175°F, which is not sufficient for engine installation. The manufacturer, however, has indicated that proper design could extend this range to -65° through +275°F.

A Kistler transducer system has been used for most of the development work performed with the fluidic oscillators. The Kistler quartz pressure transducer is a dynamic electrostatic or piezoelectric device that requires a charge amplifier with each system. The Kistler system is excellent for laboratory instrumentation but is too expensive to use as a prime element in the temperature control subsystem.

Fluidic Oscillator Subsystem Evaluation

Based upon the experience gained from this study and the experimental work that supported it, control of turbine inlet temperatures by the direct measurement of this parameter appears to be feasible. Considerable development work remains to be performed both with the sensors and with the averaging system. These two areas are considered to be of high risk because of the high operating temperatures of the sensors and the complex averaging system required to deliver an accurate signal to the control loop.

Fluidic Thermistor Temperature Sensor

The fluidic thermistor was originally proposed as an alternate method of sensing turbine gas temperature. A prototype unit has been developed for Lycoming by the Avco/Space Systems Division. This section describes the operation of the fluidic thermistor and discusses the results of thermistor response-testing performed on an Avco Lycoming T55 engine.

A schematic representation of the fluidic thermistor system is shown in Figure 90. The thermistor is a laminar orifice or flow tube, made from 310 stainless steel, which is 0.66 inch in length, has an inside diameter of 0.016 inch, and has a wall thickness of 0.004 inch. The thermistor is used as one leg of a bridge network with a standard proportional fluid amplifier as the active element. The amplifier is initially balanced by means of a sharp-edge orifice in the second leg. The resistance-to-flow as a function of gas temperature through these two orifices follows different operating equations. Therefore, as the gas temperature increases, the ΔP across the output of the proportional fluid amplifier increases. It is then only necessary to rapidly change the gas temperature on the inside of the thermistor as a function of the gas temperature on the outside. This is accomplished by making the tube wall extremely thin.

The prototype sensor was tested in the exhaust duct of the gas producer of an Avco Lycoming T55-L-7 engine and was exposed to maximum temperatures of about 1200°F for eight hours. This testing determined the response time of the thermistor when subjected to transient gas temperature. The results indicated a time constant of between 0.08 and 0.2 second, depending on mass flow past the sensor. This response time is presently considered too slow for acceleration/deceleration temperature control but might be improved through additional development work.

FUEL FLOW SENSOR

General

The control mode analysis showed that a fuel flow feedback inner control loop might be required for engine starting. To achieve feedback in Fuel Metering System No. 2, an electrical flow sensor is required as the feedback element. Consequently, a survey of available flow sensors was made, and the more promising ones were investigated to establish the following criteria:

1. Dynamic response characteristics
2. Accuracy, including temperature, pressure, and viscosity effects
3. Tolerance to fuel types and contaminants
4. Reliability and service life
5. Compatibility with electronic computer design
6. Cost and weight

Configuration Requirements

The following configuration requirements were included in a preliminary specification that was submitted to manufacturers of flow sensors:

Apparent Time-Constant (sec)	< 0.005
Accuracy of Mass-Flow Measurement (Percent of Reading)	± 2.5
Flow Range (lb/hour)	20 to 500
Service Life Without Recalibration (hr)	3000 minimum
Electrical Output	Analog voltage or frequency
Electric Power Consumption (watts)	< 3.0
Maximum Weight (lb)	0.25

The fuel flow sensor must be compatible with all types of fuel and contaminants specified for use in the Fuel Metering System No. 2 and must withstand the same environmental conditions.

Types of Flow Sensors

Initially, a fluidic oscillator sensor was selected for investigation. The unit, based on the Vonnegut Whistle principle, creates a rotating oscillation in the fluid. The frequency of oscillation, detected by a suitable transducer, is proportional to volume flow rate. Large-flow-capacity units have been built for industrial applications, and in theory, the principle should be applicable to smaller units. Detailed investigation of the sensor, however, showed it to be impractical, the main problem being the interface transducer. Pressure sensors do not provide an adequate signal-to-noise ratio, and thermistors are used in the larger units to detect fluctuations in total energy level. In a smaller unit, the frequency has to be higher and no thermistor can respond adequately. Also, the accuracy and range of the smaller units are questionable. These factors, combined with its insensitivity to density, proved the fluidic oscillator sensor to be unsuited for this application.

Other devices investigated were turbine flow meters, orifice pressure-drop units, the magnetic-resonance flow meter, and a heat-transfer anomometer device. Volume-flow devices were considered because their simplicity and ruggedness might outweigh the loss of mass-flow reading accuracy. The turbine meter can provide adequate response but is difficult to make contaminant-resistant, while orifice pressure-drop devices cannot provide the required accuracy over the 20:1 flow range. The magnetic resonance flow-meter, would meet the response, accuracy, range, and service life requirements, but the size of the sensor and complexity of the electronics are unacceptable.

A mass-flow sensor has been selected which appears to be capable of meeting all specified requirements. Described below is the proposed fuel flow sensor.

Fuel Flow Sensor Description

The flow sensor is a hot-film, anemometer device which is capable of compensating for fuel temperature, thus providing an output voltage

proportional to mass-fuel flow. The sensor element consists of two film elements that are deposited on a ceramic cone. Protection against film erosion may be provided by a thin overlay of quartz. The support cone is located in the aluminum sensor housing together with a temperature-sensing resistance element. Associated electronic circuitry is included in the control computer package.

The resistance films form two elements of a four-element bridge, a fixed current ratio being maintained in the films. It can be shown by conventional anemometer theory that a voltage output proportional to mass flow can be obtained. The principle has been demonstrated in commercially available units that measure gas and liquid flows. The requirements and limitations of this application, however, will require the development of a specialized unit.

Fuel Flow Sensor Evaluation

The requirements for a rugged, accurate, fast-response fuel flow sensor were met by the mass-flow sensor described above. The best alternative would be a turbine flow-meter that is tolerant of contaminants.

SPEED SENSOR

Magnetic reluctance type pickups will be used to provide engine shaft speed signals to the control computer. The unit selected is a miniature pickup approximately 1.0 inch long and 0.3 inch in diameter.

These devices are extremely rugged and are not subject to deterioration or wear. Similar pickups are being used successfully by Avco Lycoming in other applications.

INTERFACE DEVICES

GENERAL

The following electromechanical interface devices were studied:

1. Rotary actuator for the multiple-function fuel valve of Fuel Metering System No. 1
2. Rotary actuator for VSD ratio control in Fuel Metering System No. 2
3. A proportional electrohydraulic servo system for positioning of engine variable-geometry systems
4. A two-position electropneumatic actuator for engine variable-geometry control

Each application was studied to determine response, accuracy, and power requirements for its interface device. Environmental conditions, service life, and reliability requirements were assumed to be the same as for the fuel metering system. Devices were selected to meet the specified requirements with minimum power consumption and weight.

MULTIPLE-FUNCTION FUEL VALVE ACTUATOR

The multiple-function valve actuator is part of an accurate, fast-response servo system that is continuously modulated by the engine control computer. Basic design requirements were:

1.	Angular stroke	24 degrees
2.	Resolution	$\pm$ 0.20 degrees
3.	Maximum slew rate	6 rads/sec with 0.5 in.-lb load
4.	Maximum acceleration with load	300 rads/sec^2
5.	Mechanical system time-constant	0.030 sec
6.	Stall torque	1.0 in.-lb
7.	Duty cycle	Continuous modulation with instant reversals

The estimated friction torque of the load was 0.45 in.-lb and the load inertia was 0.015 lb-in^2. A specification describing these requirements was submitted to several motor manufacturers. Following discussions with the manufacturers, it was concluded that a dc motor with integral reduction gears would be the most suitable device. A unit featuring a split series-wound field motor with a planetary gear train was incorporated in the Fuel Metering System No. 1 design (See Figure 63).

The use of a wound field enables the motor to be reversed instantaneously, whereas a permanent magnet field may be demagnetized by rapid reversal of current. The split winding of the field simplifies the motor-driver circuits in the control computer by eliminating the need for switching logic for motor reversal. The motor operates on 18 volts dc with a maximum power consumption of 15 watts. The estimated weight of motor and gearbox is 0.6 pound.

VSD RATIO CONTROL ACTUATOR

Ratio control actuator requirements were:

1.	Angular stroke	90 degrees
2.	Resolution	$\pm$ 0.4 degrees
3.	Maximum slew rate	25 rads/sec with 0.75 in.-lb load
4.	Mechanical system time constant	0.03 sec
5.	Maximum continuous torque	1.0 lb-in.
6.	Duty cycle	continuous modulation with instantaneous reversals

Estimated frictional torque at the load was 0.3 lb-in., and predicted load inertia was 0.012 lb-in.^{2}. Following discussions with motor manufacturers, two devices were considered for the application: (1) a dc servo motor with reduction gearbox and (2) a brushless dc torque motor. The cost, weight, and power consumption of the units are similar, and both can meet the specified performance. The brushless torque motor, however, offers the possibility of a 10,000-hour service

life and does not require a gearbox or slip clutch. Installations of both devices were studied, and the torque motor envelope was found to fit in the package configuration more conveniently. Consequently, the torque motor was selected for use in the proposed system.

A suitable torque motor unit was selected and is included in Fuel Metering System No. 2 (Figure 75). The torque motor has a permanent magnet rotor and toroidal field windings. Maximum torque is obtained at 18 volts with a power consumption of 20 watts. The motor will be designed to retain its instantaneous position in the event of a system power failure, insuring that a hardover failure condition can not occur in the fuel metering system.

PROPORTIONAL ELECTROHYDRAULIC SERVO ACTUATOR FOR ENGINE VARIABLE-GEOMETRY CONTROL

In order to define the requirements of an interface device for variable-geometry systems, a specific actuator was studied. The following assumptions were made for the system:

1.	Maximum actuator load	$\pm$ 30 lb
2.	Linear stroke	0.75 in.
3.	Maximum slew rate	3.0 in./sec
4.	System time constant	less than 0.05 sec
5.	Working medium	engine fuel
6.	Available fuel pressure drop over operating range	300 to 700 psi

To meet these requirements, it was assumed that a differential area actuator would be used in conjunction with a proportional solenoid valve and that electrical position feedback would be used to close the servo loop. The system is shown schematically in Figure 91 . To obtain the specified performance, an actuator with the following dimensions is required:

Cylinder and piston diameter	0.59 in.
Rod diameter	0.47 in.
Diameter of orifice in piston	0.025 in.
Effective orifice diameter of proportional flow control valve when fully open	0.055 in.

The maximum fuel flow consumed by the system would be 0.35 gpm. A proportional solenoid valve for this system would require a maximum current of 0.2 ampere at 28 volts.

The valve consists of a pressure-balanced poppet valve positioned by the force from a solenoid. The solenoid armature is flexibly connected to the valve and is spring-loaded to the closed position. By careful design of the solenoid coil, armature, and valve, the restriction to flow can be made linear with current. Hysteresis and linearity deviation typically reach $\pm$ 5 percent of the nominal level, which is satisfactory for this closed-loop type of application. The contaminant resistance of the valve is acceptable due to the lack of close clearances and the inherent tolerance of the poppet valve. However, the system may be protected against fuel contaminants by a wash-flow filter element at the fuel pump discharge to insure maximum operational life and reliability.

A similar valve assembly designed for higher flow rates has been tested by the contractor as part of an experimental servo system. Despite relatively high valve hysteresis and poor linearity, system performance was satisfactory for the intended applications. No electronic compensation or "dither" was required to achieve the required accuracy, response, or stability in the demonstration system.

TWO-POSITION ELECTROPNEUMATIC ACTUATOR

A two-position pneumatic actuator is often required to control the operation of a compressor interstage bleed valve. In an electronic engine control system, the actuator would be controlled by a solenoid-operated pilot valve; and for fail-safe engine operation, the solenoid would be energized when the bleed valve was open. The bleed valve would have to open, however, for engine starting when there is no

electrical power available to energize the solenoid-operated pilot valve. Consequently, the system has to keep the bleed open until sufficient electrical power is available for solenoid operation. This is achieved by using an actuator as shown in Figure 92, which changes the logic from bleed normally-open to normally-closed when the supply air pressure from engine compressor discharge reaches a preset level. This level would cause the pressure-drop across the control plunger orifice to move the plunger against its spring. When the solenoid pilot valve is energized to the closed position, pressures on either side of the control plunger are equalized, allowing the spring to move it back to the bleed-open position.

Assumed actuator requirements were:

Maximum force	+ 20 lb, -2 lb
Stroke	1.0 in.
Operating time	0.025 sec
Available air pressure drop	50 to 220 psi

On the basis of these requirements, it was determined that the actuator cylinder diameter should be 0.8 inch and that the effective orifice diameter of the control valve seat should be 0.18 inch. The pilot valve seat diameter will be 0.040 inch, requiring a minimum solenoid force of 5.0 ounces. The solenoid will require 0.25 ampere at 28 volts.

SYSTEM WEIGHT AND COST

Estimates of the weight and cost for the various possible configurations of the two fuel metering systems and miscellaneous components studied are tabulated below. The cost figures are based on manufacturing costs in quantities of 1000 units at a delivery rate of 100 per month. G & A and profit have not been included.

Fuel Metering System No. 1

Analog Computer	Weight (lb)	Cost ($)
Electronic Control Computer (Analog)	1.60	2152
Fuel Pump Assembly	1.85	596
Multiple-Function Valve	0.90	572
Servomotor	0.70	75
Valve Position Transducer	0.40	50
Power Lever and Position Transducer	0.80	110
Fuel Dump Valve	0.25	63
Fuel System Housing	0.85	452
Total	7.35	4070
Digital Computer		
Substitute for Analog Computer above:		
Electronic Control Computer (Digital)	1.35	3970
Total	7.10	3888
Manual Metering System		
If required, add to either of the above totals:	1.45	235

Fuel Metering System No. 2

Analog Computer	Weight (lb)	Cost ($)
Electronic Control Computer (Analog)	1.60	2152
Variable Speed Drive (VSD)	1.90	1050
Centrifugal Fuel Pump	1.30	175
VSD Control Torque Motor	0.60	75
Power Lever and Shutoff Valve Assembly	0.80	150
Fuel Flow Sensor	0.30	135
Total	6.50	3737

Digital Computer	Weight (lb)	Cost ($)
Substitute for Analog Computer above:		
Electronic Control Computer (Digital)	1.35	3970
Total	6.25	5555
Manual Metering System		
If required, add to either of the totals above:	0.75	95

Miscellaneous

Sensors	Weight	Cost ($)
8 Fluidic Oscillators with Pressure Transducers	1.2	600
3 Speed Sensors	0.3	45
Variable-Geometry Components (as required)		
Hydraulic Actuator with Proportional Solenoid	1.15	138
Position Feedback Transducer	0.32	62
Pneumatic Actuator and Solenoid Valve	0.95	116

Each of the possible systems configurations tabulated above offers substantial reduction in weight when compared with present-day systems. Depending, of course, upon the selected configuration, the weights of complete control systems, including fuel pump, range from 6 to 9 pounds.

Fuel Metering System No. 2 has relatively small (10 percent) weight and cost advantages over Fuel Metering System No. 1. These particular advantages, therefore, would not be a dominant factor in system selection.

The digital electronic control computer is slightly lighter (0.25 lb) but is appreciably more expensive ($1818) than the analog electronic control computer. The estimates of weight and cost, however, are based upon current technology, and the potential for reduction in the future heavily favors the digital version of the computer.

TECHNICAL RISK

When considering technical risk, the degree of risk pertinent to development lead time must be judged. All elements of the proposed control system are considered to be within reasonable reach of today's technology when considering a 5- to 7-year development cycle.

The highest risk areas are defined below in order of their magnitude:

The fluidic oscillator temperature sensor, although highly promising, requires considerable development work in three areas: first, development of durability and reliability of the sensor hardware at the very high operating temperatures of the newer engines; second, establishment of an accurate engine temperature averaging technique without undue hardware complexity; and third, lowering of the sensor's operating threshold pressure to permit the sensor to close the loop on starting fuel flow.

The digital electronic computer implementation requires extensive effort because of the newness of the technology and the need to establish prime reliability in an engine environment.

The variable-speed drive, the key element of the recommended fuel system, presently enjoys a high level of development. However, operation at 60,000 RPM and above, although theoretically feasible, has not yet been accomplished. Therefore, the VSD must still be considered an element of risk.

CONCLUSIONS AND RECOMMENDATIONS

Within the scope of this study, the technical feasibility of the proposed advanced control system has been demonstrated. Practical logic and dynamic criteria for the closed-loop T_5 control mode selected for this study have been established. The problems associated with the fluidic oscillator temperature sensor appear to be soluble. Turbine inlet temperature averaging remains as one of the most difficult problems.

Each of four possible combinations of computation and fuel metering systems studied offers substantial reduction in weight and size while still achieving technical and performance objectives. The four combinations evolved from choices between analog and digital electronic computation and between two novel fuel metering systems. Inevitably, the choices offering the most technical advantages also incur the greatest technical risk. Selection, therefore, must be based upon a balance of factors including, where necessary, a prediction as to the future course of a technology.

It is recommended that the digital electronic computer be selected in preference to the analog computer. Although the digital technology is newer and costs are currently higher, it offers greater accuracy, function flexibility, and smaller size. More important, it is felt that digital microelectronic fabrication is coming of age, and future advancements in microcircuit technology will heavily favor the digital approach. Order-of-magnitude improvements are anticipated in size, cost, and reliability within a 4- to 5-year period.

It is recommended that Fuel Metering System No. 2 (VSD/centrifugal pump) be selected over the more conventional System No. 1. The centrifugal pump approach, in addition to weight and cost advantages, provides several significant system advantages. It is felt that the advantages provided by this novel approach fully justify the degree of increased technical risk.

TABLE I. DIMENSIONLESS ENGINE GAINS AT DESIGN CONDITIONS*		
PARTIALS % Design / % Design	5 lb/sec	2 lb/sec
$\partial T_5 / \partial N_l$	0.360	0.353
$\partial T_5 / \partial N_h$	0.045	0.046
$\partial T_5 / \partial W_f$	0.505	0.402
$\partial Q_p / \partial N_l$	1.450	1.420
$\partial Q_p / \partial N_h$	0.320	0.320
$\partial Q_p / \partial W_f$	0.800	1.000
$\partial W_f / \partial N_l$	6.100	7.250
$\partial W_f / \partial N_h$	3.750	3.030
$\partial W_{fx} / \partial N_l$	0.704	0.795
$\partial W_{fx} / \partial N_h$	4.550	4.102
*$T_5 = 2370^{\circ}F$ $P_3/P_1 = 14:1$		

TABLE II. OPTIMUM CONTROL GAINS AND SENSOR TIME CONSTANTS AT THREE ENGINE POWER CONDITIONS

Gains or Time Constants	100% N_h	90% N_h	80% N_h
K_{t5} ($\%W_f/\%T_5$)	3.0	2.5	1.5
$K_{t5meas.}$ ($\%W_f/\%T_5$)	1.0	1.0	1.0
K_{1t5} ($\%W_f/\%T_5$/sec)	7.0	5.0	3.0
τ_{t5}(sec)	0.01	0.01	0.01
K_{nh} ($\%W_f/\%N_h$)	8.0	6.0	4.0
τ_{nh} (sec)	0.01	0.01	0.01
K_{inh}($\%W_f/\%N_h$/sec)	40.0	30.0	20.0
K_{nl} ($\%W_f/\%N_1$)	5.0	4.0	3.0
τ_{nl} (sec)	0.01	0.01	0.01
K_{inl} ($\%W_f/\%N_1$/sec)	15.0	12.0	9.0
K_p ($\%W_f/\%N_p$)	3.0	3.0	3.0
τ_p (sec)	0.2	0.2	0.2
K_{ip} ($\%W_f/\%N_p$/sec)	6.0	5.0	3.5
K_{qld} ($\%W_f/\%Q$)	2.5	2.5	2.5
τ_{qld} (sec)	0.3	0.3	0.3

TABLE III. SINGLE-ENGINE, HIGH-POWER-CONDITION TRANSIENT RESPONSE TO A 10% STEP DISTURBANCE IN EACH LOOP

Governing Loop	Disturbance	Peak Over or Undershoot (% of variable)	Time to Peak Over or Undershoot (sec)	Settling Time to Within ± 0.1% of Change (sec)
N_p (Turboshaft)	Collective Pitch	0.8	0.8	3.0
T_5 (Both Engines)	T_5 Sensed	0.1	0.5	0
N_h (Turboprop)	N_h Select	1.0	0.25	0.7
N_l (Turboprop)	N_l Select	0.1	0.5	0.7
Q (Turboshaft)	Turbine Torque	0.5	0.5	0.7

TABLE IV. SINGLE-ENGINE, LOW-POWER-CONDITION TRANSIENT RESPONSE TO A 10 STEP DISTURBANCE IN EACH LOOP

Governing Loop	Disturbance	Peak Over or Undershoot (% of variable)	Time to Peak Over or Undershoot (sec)	Settling Time to Within ± 0.1% of Change (sec)
N_p (Turboshaft)	Collective Pitch	1.2	1.2	5.6
T_5 (Both Engines)	T_5 Sensed	0.1	0.5	0
N_h (Turboprop)	N_h Select	1.0	0.25	0.7
N_l (Turboprop)	N_l Select	0.5	0.5	0.6
Q (Turboshaft)	Turbine Torque	0.5	0.5	0.7

TABLE V. DUAL TURBOSHAFT ENGINES - EACH AT 55% MAXIMUM POWER - TRANSIENT RESPONSE TO A 10% COLLECTIVE PITCH DISTURBANCE

Governing Loop	Disturbance	Peak Over or Undershoot (% of variable)	Time to Peak Over or Undershoot (sec)	Settling Time to Within ± 0.1% of Change (sec)
N_p	Collective Pitch	0.75	0.8	2.5

TABLE VI. SINGLE TURBOSHAFT ENGINE WITH REGENERATOR - TRANSIENT RESPONSE TO A 10% DISTURBANCE

Governing Loop	Disturbance	Peak Over or Undershoot (% of variable)	Time to Peak Over or Undershoot (sec)	Settling Time to Within $\pm$ 0.1% of Change (sec)
N_p	Collective Pitch	0.75	0.7	3.0
T_5	T_{t5} Sensed	1.2	0.5	1.1
N_h	N_n Sel	0	0	4.0

TABLE VII. RELIABILITY APPORTIONMENT VERSUS PREDICTION STUDY FOR THE ANALOG RELIABILITY BLOCK DIAGRAM

Analog Block Diagram Designation	Analog System Function	Circuit Failure Rate Apportionment (Failures per 10^6 hours)	Circuit Failure Rate Prediction (Failures per 10^6 hours)
A	N_h Actual	0.8	.618
B	Accel Limit Function Generator	1.5	1.451
C	Accel Limit Amplifier	0.6	.476
D	Temperature Multiplier	2.5	2.677
E	N_h Select	2.6	2.077
F	Temperature Amplifier	0.6	.507
G	Decel Limit Function Generator	0.6	.562
H	N_p Select	4.0	3.330
J	N_h Expand	0.8	.487
K	Airbleed Trigger Control	2.6	2.345
L	Inlet Guide Vane Circuit	1.2	1.026
M	N_h Temperature Bias	0.8	1.073
N	Authority Circuit	1.0	.250
P	Flow Element Amplifier	3.0	2.819
O	N_1 Measuring Circuit	1.6	1.864
R	Power Supply	6.0	22.863
S	Torque Amplifier Circuit	1.0	.902
T	T_5 Measuring Circuit	1.6	2.585
U	Wiring and Connections	0.5	.585
Failure Rate (Total):		33.3	48.63
MTBF:		30,030 $\frac{\text{Hours}}{\text{Failures}}$	20,563 $\frac{\text{Hours}}{\text{Failures}}$

TABLE VIII. RELIABILITY APPORTIONMENT VERSUS PREDICTION STUDY FOR THE DIGITAL RELIABILITY BLOCK DIAGRAM

Digital Block Diagram Designation	Digital System Function	Circuit Failure Rate Apportionment (Failures per 10^6 hours)	Circuit Failure Rate Prediction (Failures per 10^6 hours)
A	Signal Conditioner (N_h, N_1, N_p)	2.260	7.2
B	Signal Conditioner (B)	0.575	1.6
C	Select (Limit) (N_h & N_p)	1.145	3.2
D	Load Sharing (Q_r & Q_1)	1.145	3.2
E	Signal Conditioner (N_1, Q_1, T_5)	1.720	4.8
F	Signal Conditioner (T_5 & W_f)	1.146	20.0
G	Signal Conditioner (T_1)	0.575	2.0
H	Function Generator	1.585	6.4
J	Operational Amplifiers	1.145	5.2
K	Summing Point	6.735	11.2
L	Least Voter	0.895	3.2
M	Most Voter	0.750	2.4
N	Integrator	4.010	28.8
O	Limiter	1.445	2.4
P	Low Limiter	0.485	0.8
Q	Proportional-Variable Gain	0.615	1.2
R	Comparator (Hysteresis)	0.750	2.4
S	Wiring and Connections	0.350	3.445
T	Power Supply	6.0	22.863
Failure Rate (Total):		33.331	132.308
MTBF:		30,002 $\frac{\text{Hours}}{\text{Failures}}$	7,558 $\frac{\text{Hours}}{\text{Failures}}$

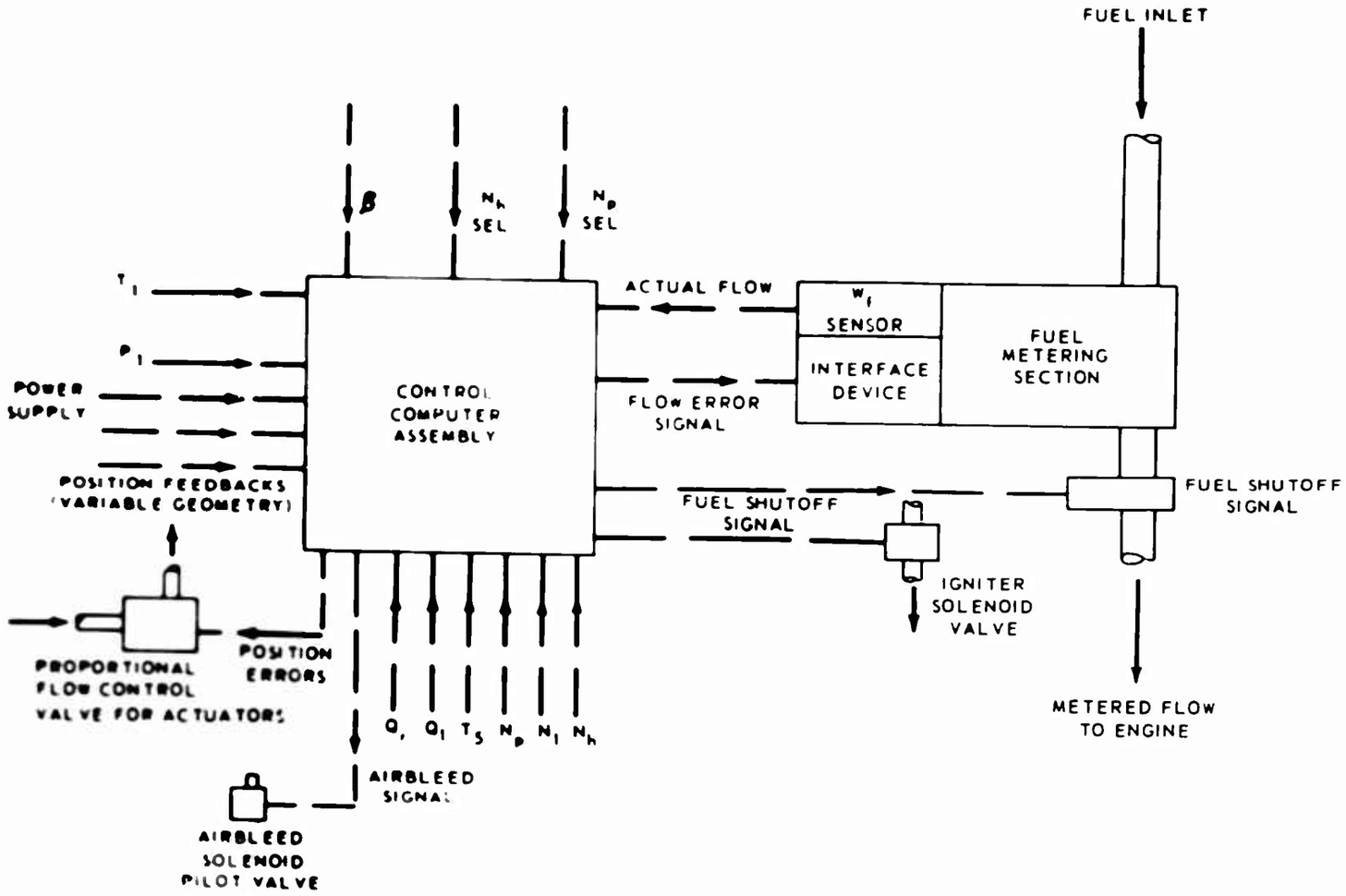

Figure 1. Schematic of Advanced Engine Control System.

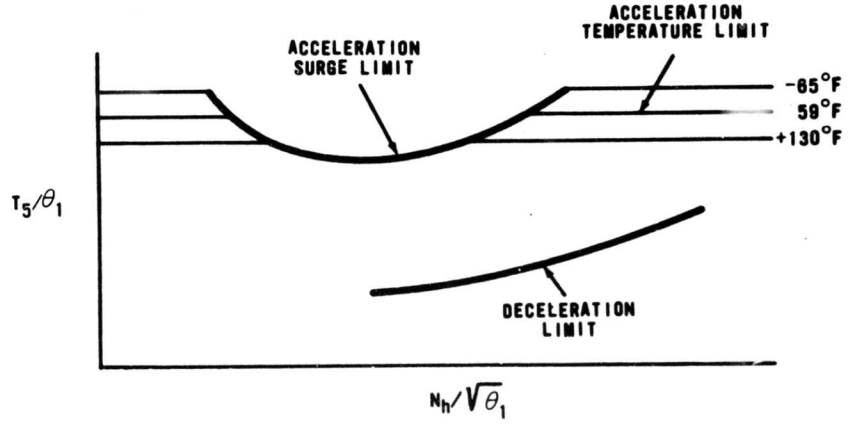

Figure 2. Acceleration and Deceleration Reference Limits.

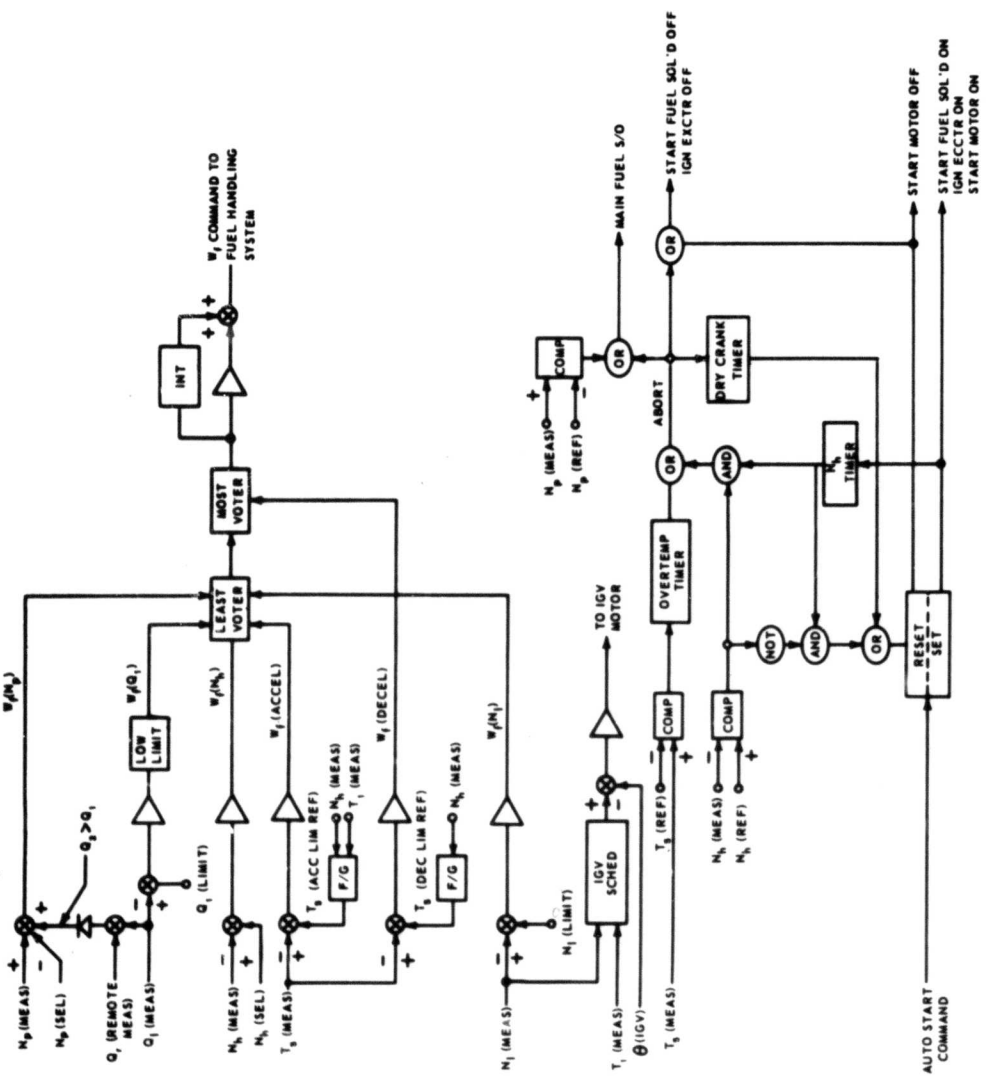

Figure 3. Control Computer Logic Diagram.

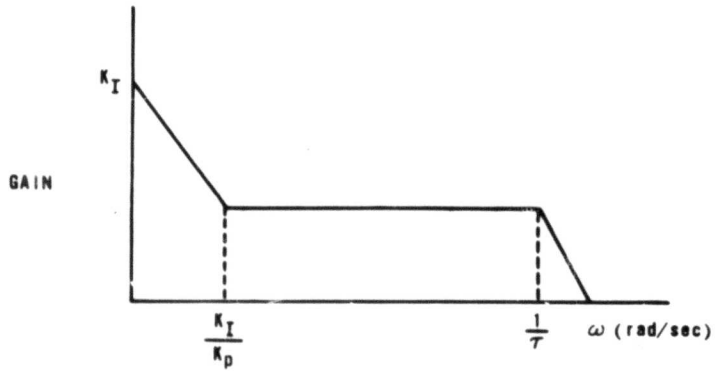

Figure 4. Frequency Response Representation of a Proportional-Plus-Integral Governor.

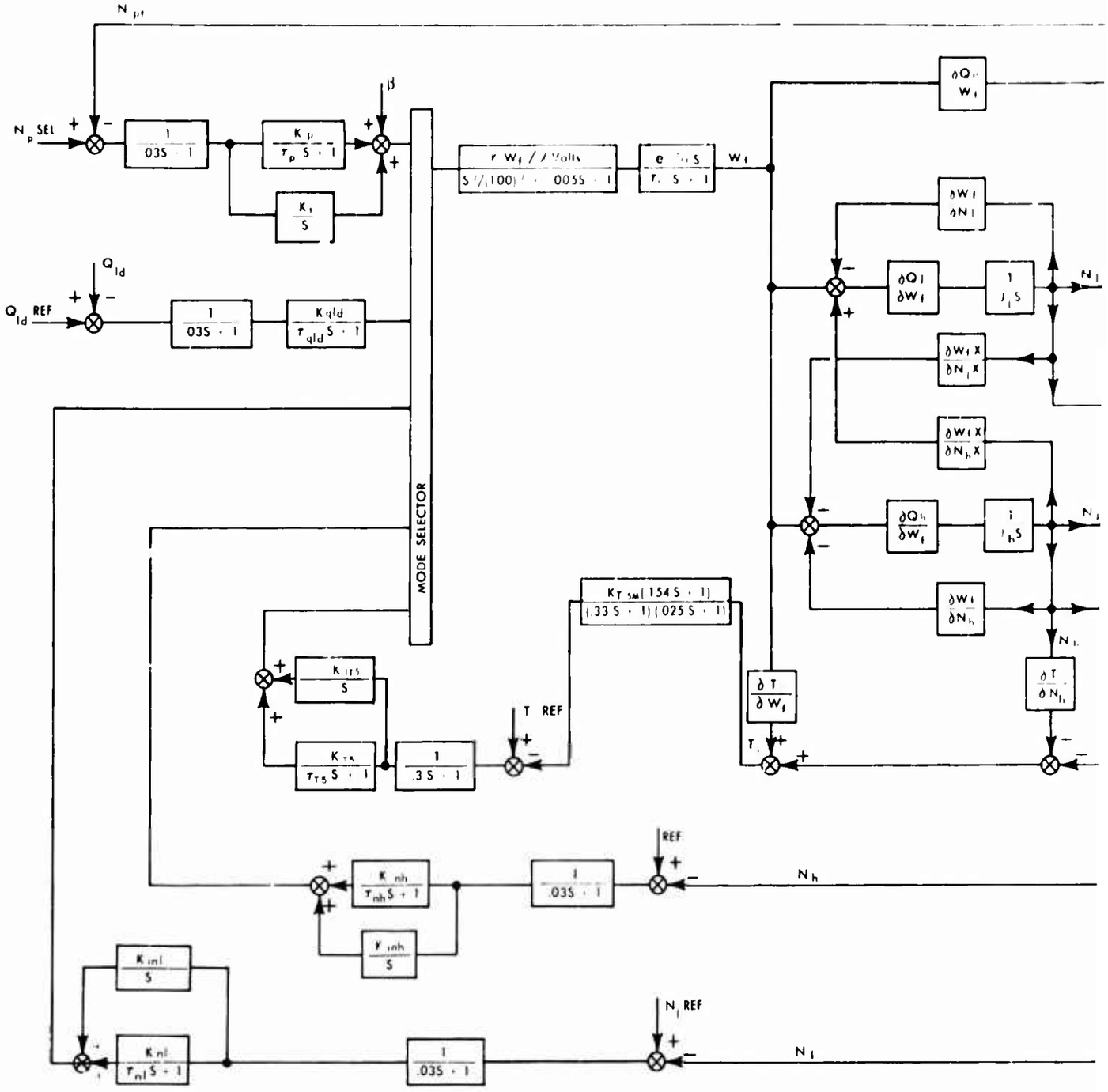

Figure 5. Analog Block Diagram for Engine, Control, and Load.

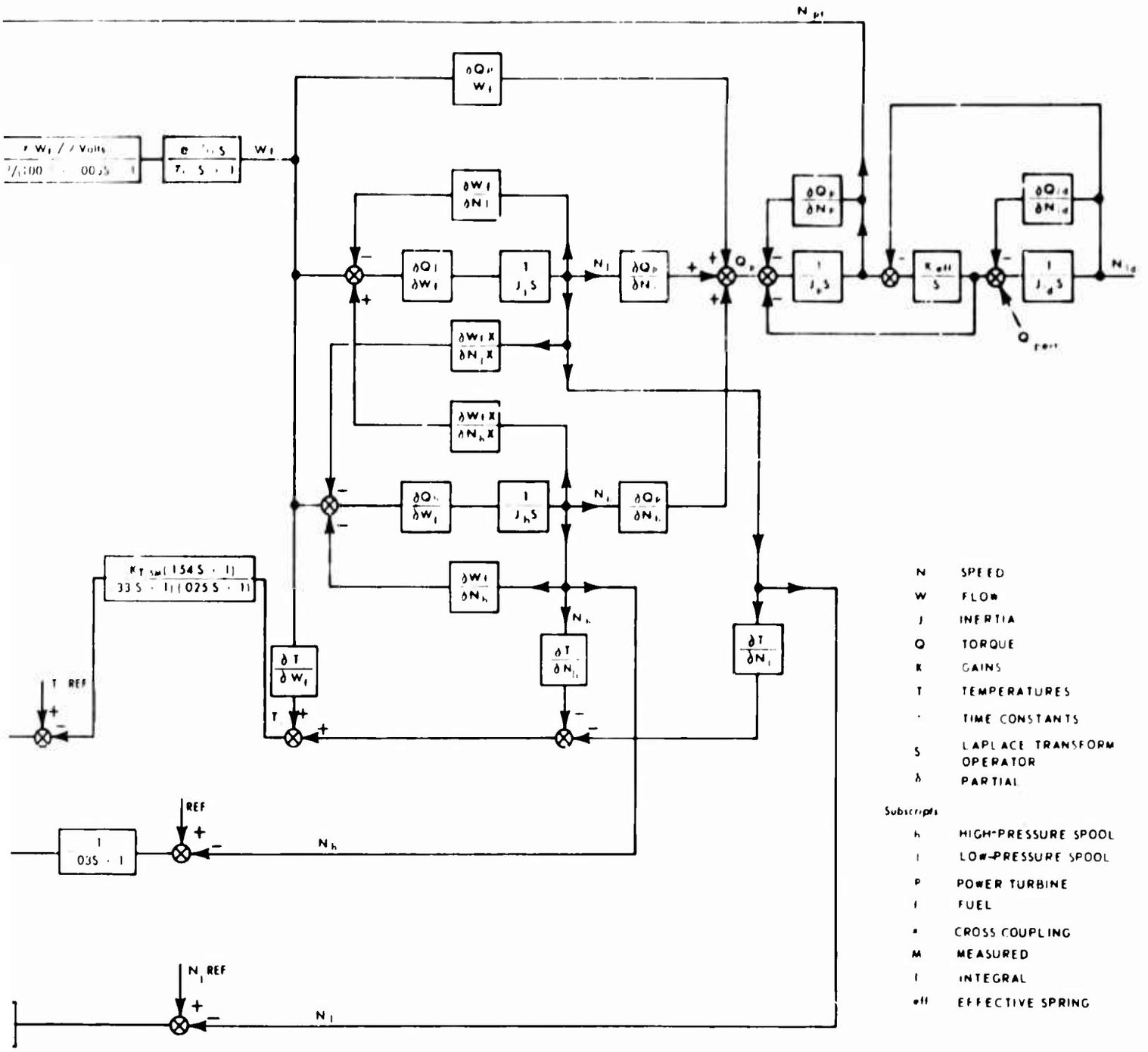

ngine, Control, and Load.

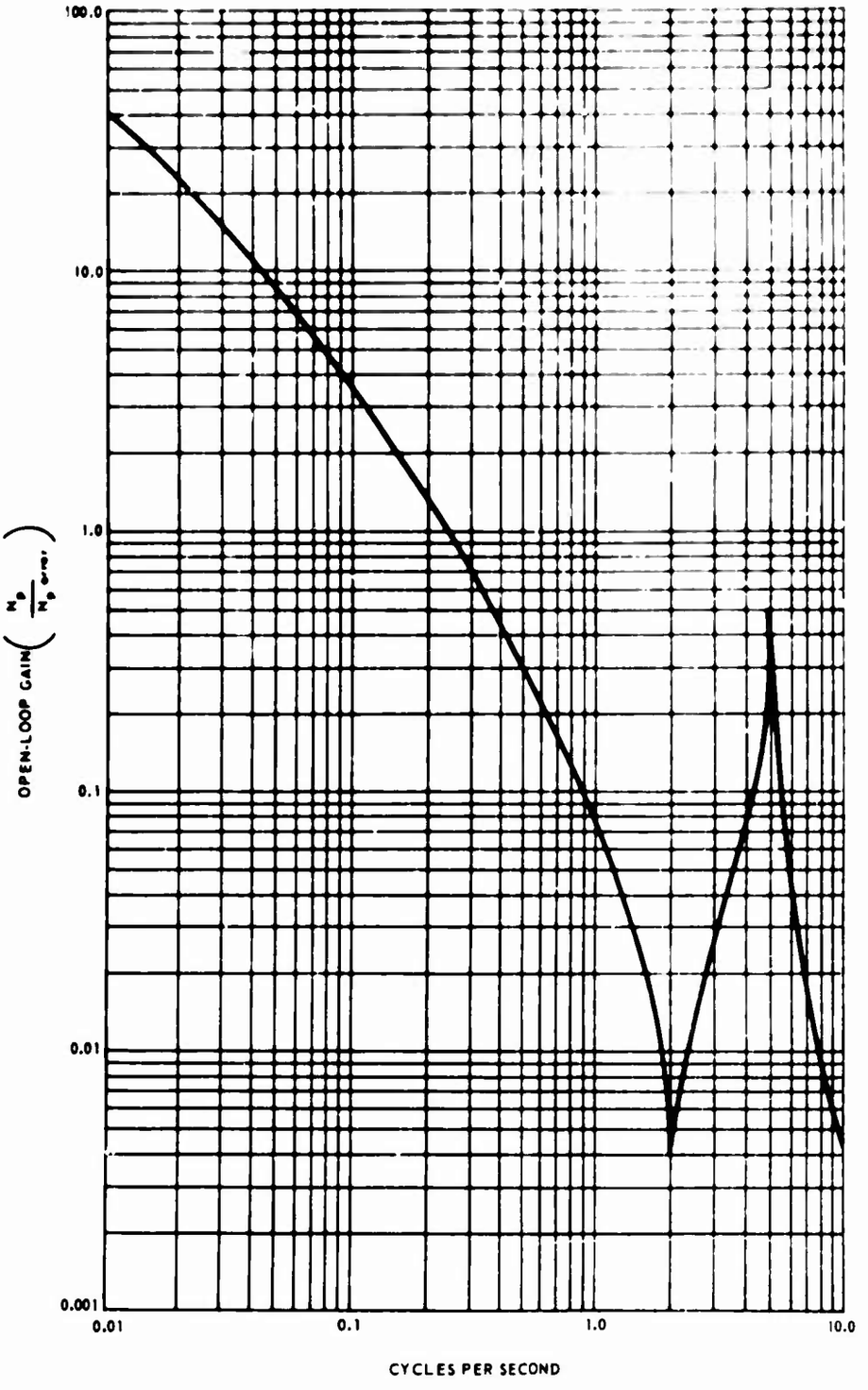

Figure 6. Amplitude Frequency Response - Engine Plus N_p Control at 100% Power.

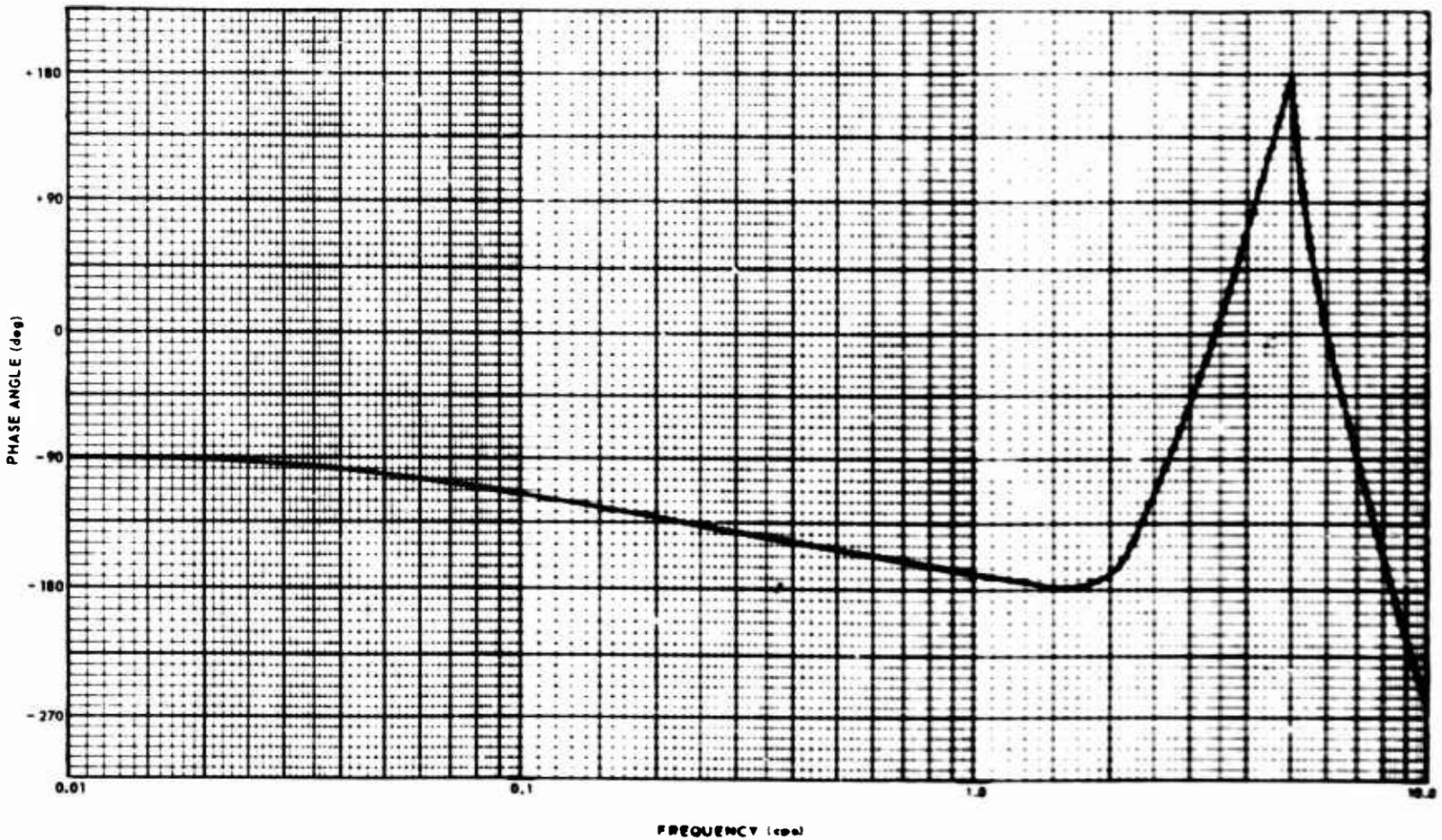

Figure 7. Phase Angle - Engine Plus N_p Control at 100% Power.

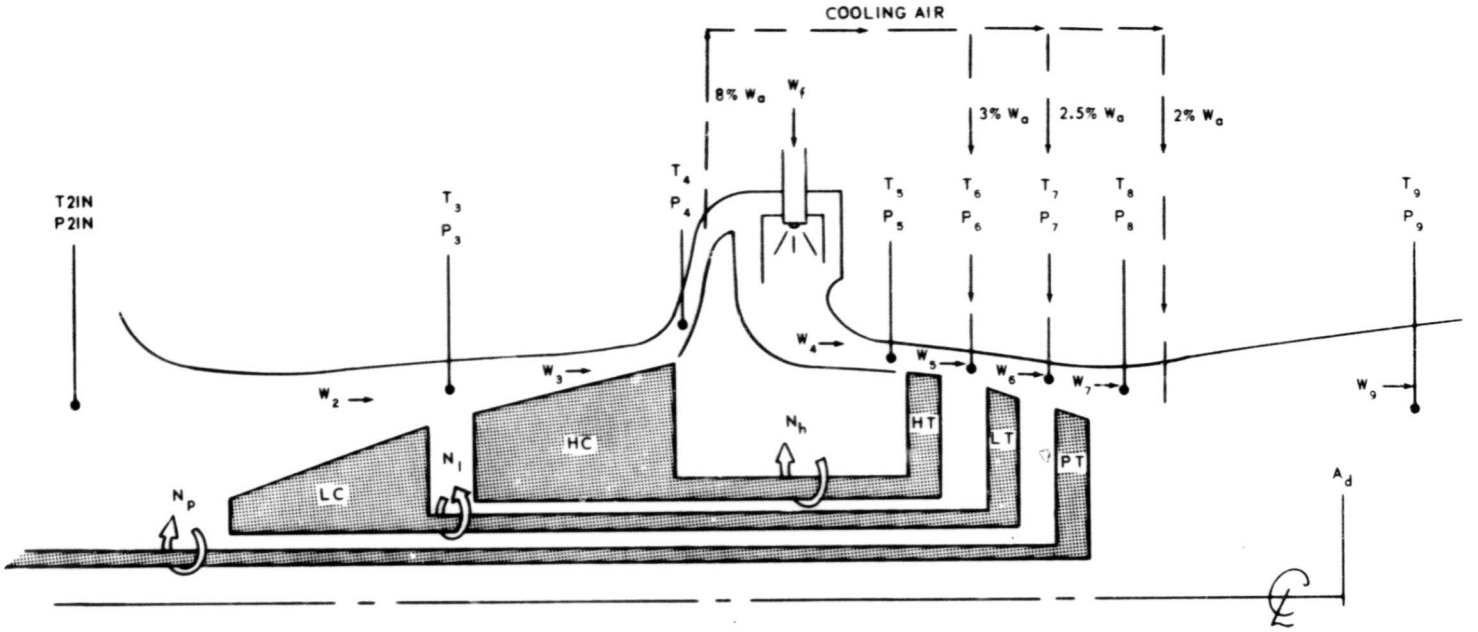

LC = LOW COMPRESSOR
HC = HIGH COMPRESSOR
HT = HIGH TURBINE
LT = LOW TURBINE
W_f = FUEL FLOW
N_h = HIGH SPOOL SPEED
N_l = LOW SPOOL SPEED
N_p = POWER TURBINE SPEED
A_d = DISCHARGE NOZZLE AREA

Figure 8. Engine Station Representation.

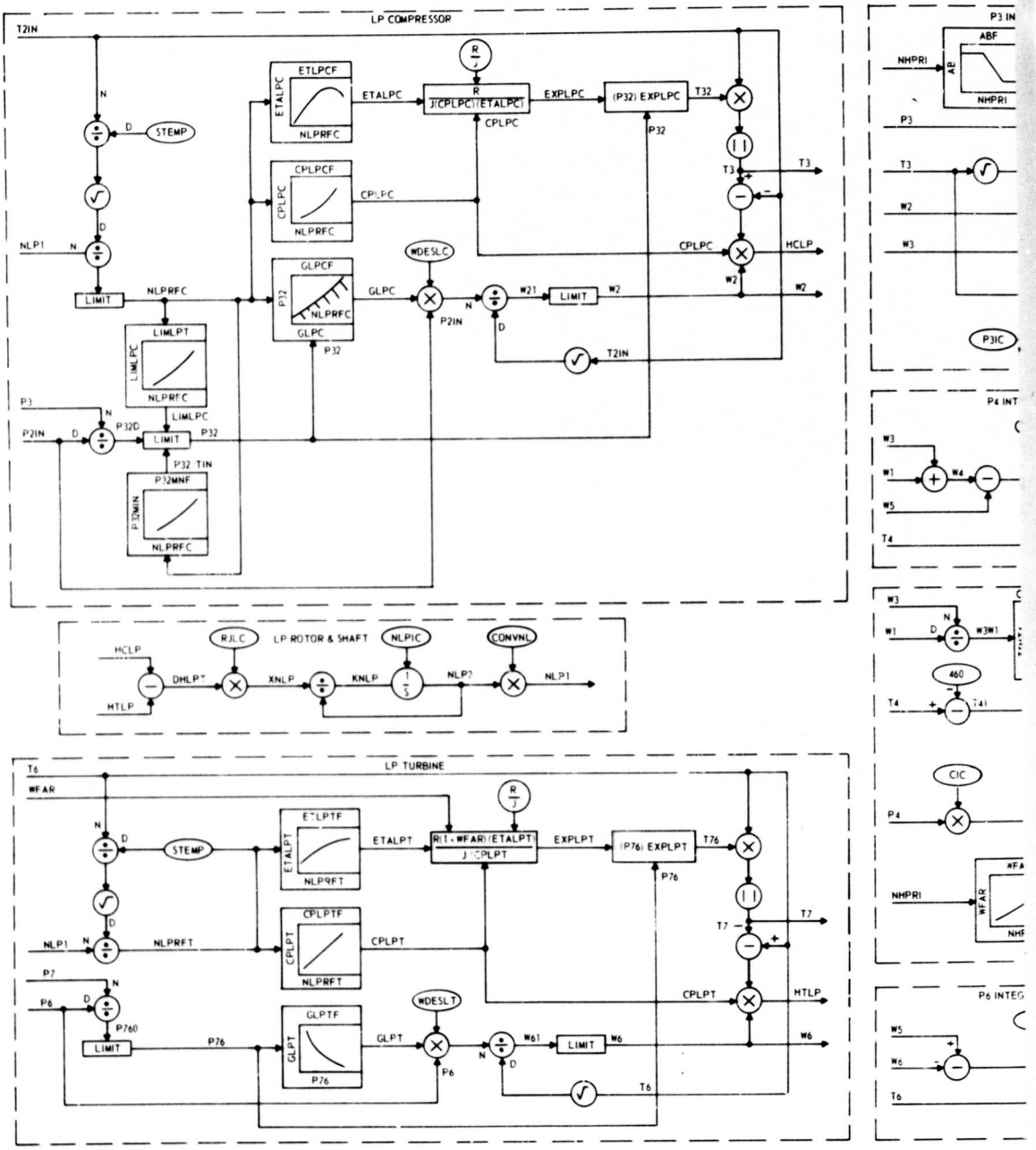

Figure 9. MIMIC Representation - Engine and Load.

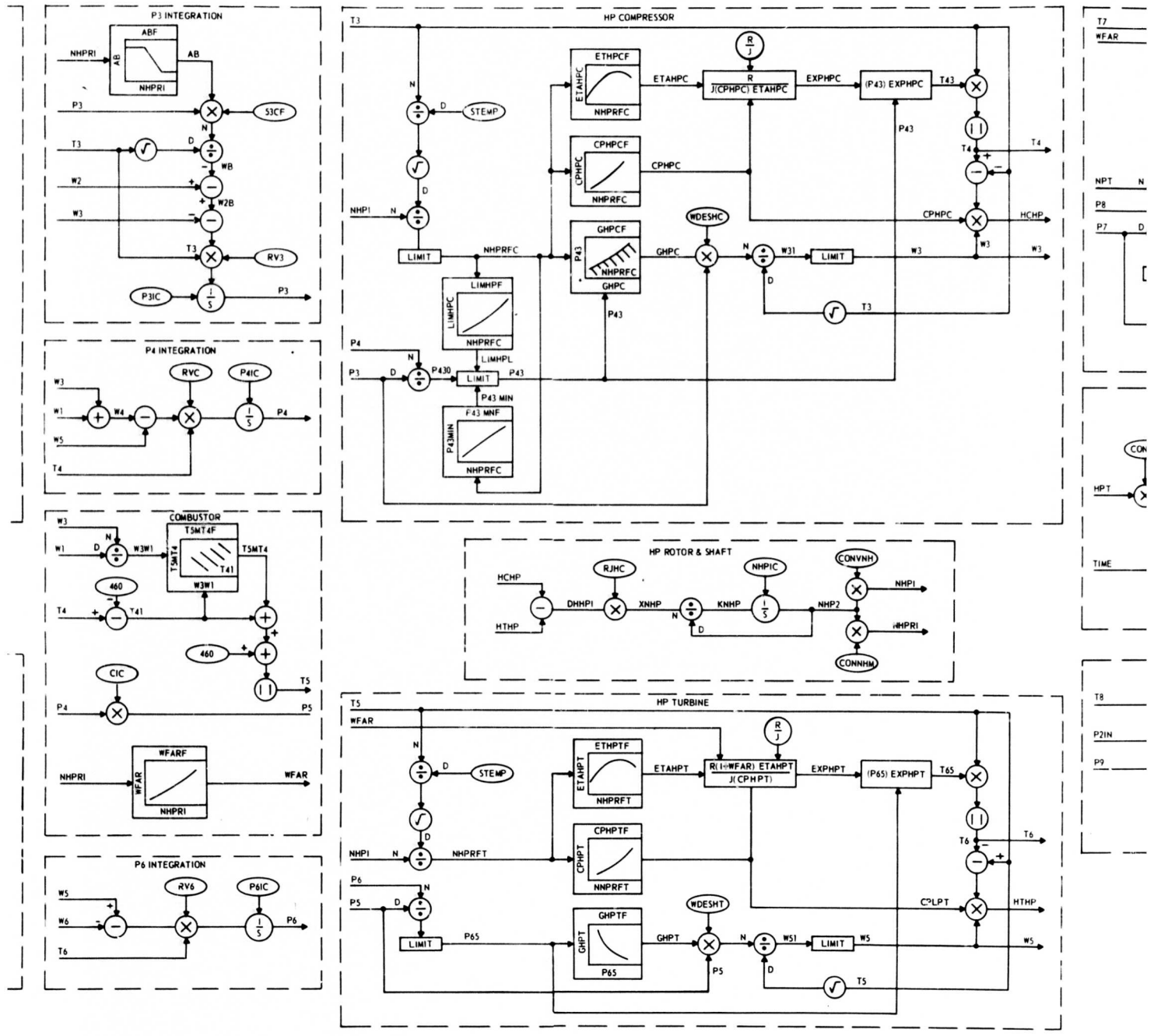
P3 INTEGRATION
ABF
AB
NHPRI
S3CF
WB
W2B
RV3
P3IC
P3
P4 INTEGRATION
RVC
P4IC
W4
P4
COMBUSTOR
T5MT4F
T41
W3W1
460
CIC
P5
WFARF
WFAR
P6 INTEGRATION
RV6
P6IC
P6
HP COMPRESSOR
STEMP
ETHPCF
ETAHPC
CPHPCF
CPHPC
GHPCF
GHPC
NHPRFC
LIMIT
LIMHPF
LIMHPC
LIMHPL
P43 MIN
P43MIN
WDESHC
W31
R/J
J(CPHPC) ETAHPC
EXPHPC
(P43) EXPHPC
T43
T4
HCHP
HP ROTOR & SHAFT
RJHC
NHPIC
CONVNH
CONNHM
DHHPI
XNHP
KNHP
NHP2
NHPI
HTHP
HP TURBINE
ETHPTF
ETAHPT
CPHPTF
CPHPT
GHPTF
GHPT
NHPRFT
WDESHT
W51
R(1-WFAR) ETAHPT
J(CPHPT)
EXPHPT
(P65) EXPHPT
T65
T6
CPLPT
P65
T7
WFAR
NPT
P8
P7
HPT
TIME
T8
P2IN
P9

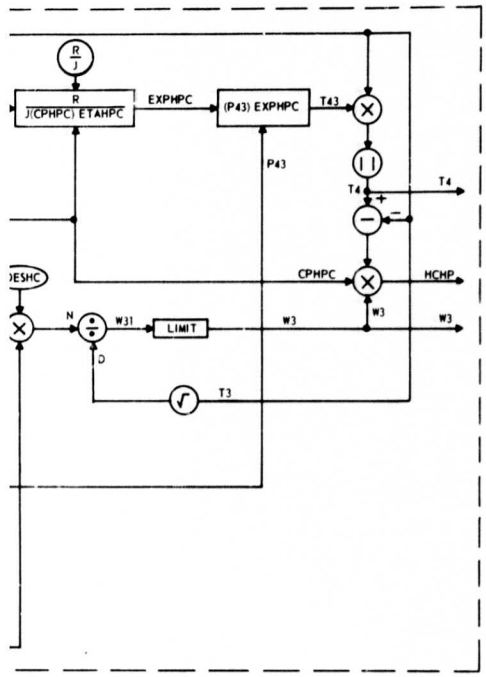
R/J
R / J(CPHPC) ETAHPC
EXPHPC
(P43) EXPHPC
T43
P43
T4
CPHPC
HCHP
W3
W31
LIMIT
T3

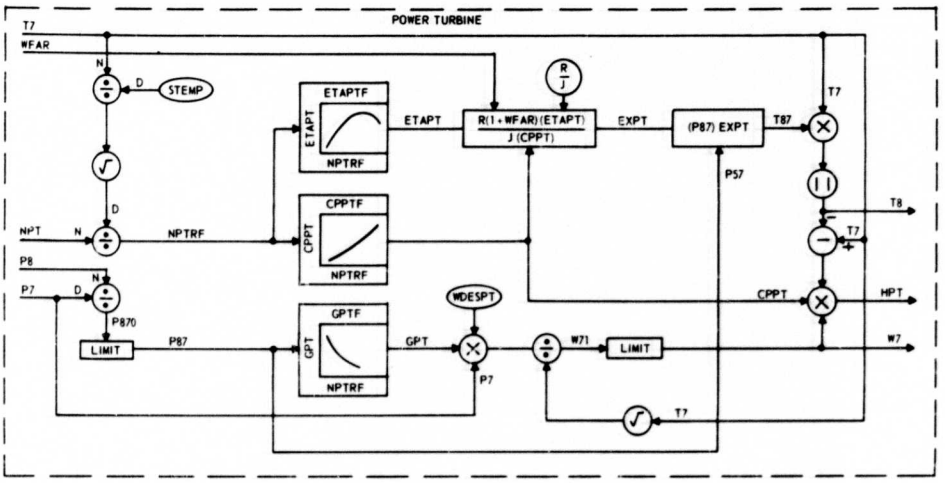
POWER TURBINE
T7
WFAR
STEMP
ETAPTF
ETAPT
NPTRF
R(1+WFAR)(ETAPT) / J(CPPT)
EXPT
(P87) EXPT
T87
P57
T8
NPT
NPTRF
CPPTF
CPPT
P8
P7
P870
LIMIT
P87
GPTF
GPT
WDESPT
W71
HPT
W7

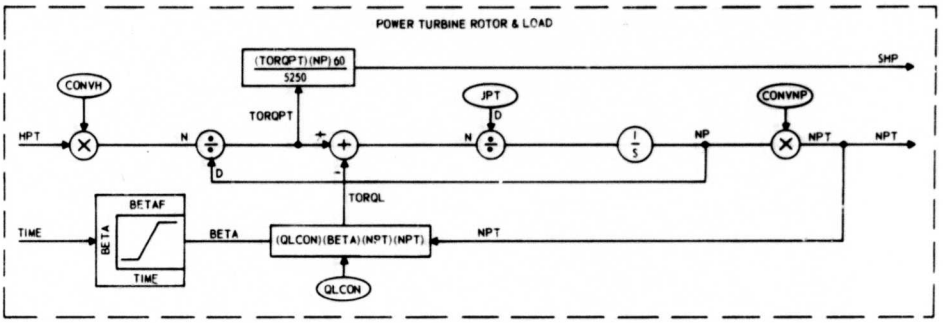
POWER TURBINE ROTOR & LOAD
(TORQPT)(NP)60 / 5250
SHP
CONVH
TORQPT
JPT
CONVNP
HPT
NP
NPT
TORQL
TIME
BETAF
BETA
(QLCON)(BETA)(NPT)(NPT)
QLCON

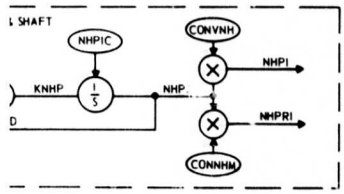
SHAFT
NHPIC
CONVNH
KNHP
NHP
NHPI
NHPRI
CONNHM

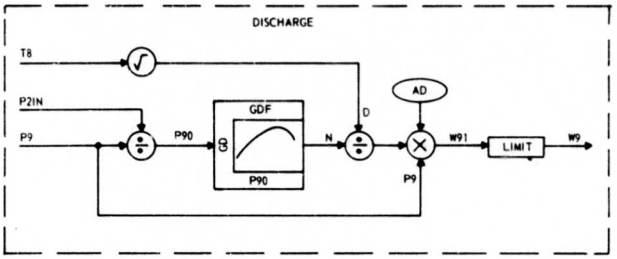
DISCHARGE
T8
P2IN
P9
P90
GDF
AD
W91
LIMIT
W9

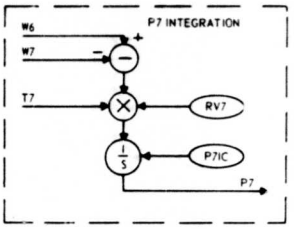
P7 INTEGRATION
W6
W7
T7
RV7
P71C
P7

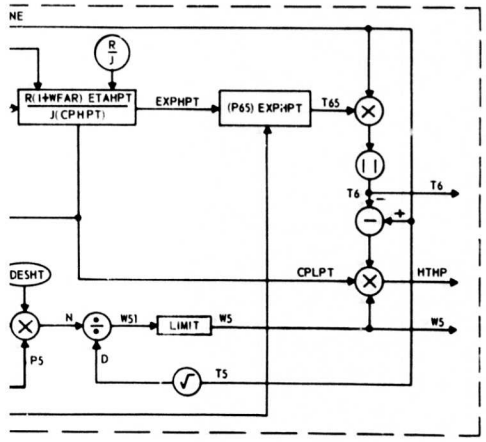
R(1+WFAR) ETAHPT / J(CPHPT)
EXPHPT
(P65) EXPHPT
T65
T6
CPLPT
HTHP
W5
W51
LIMIT
P5
T5

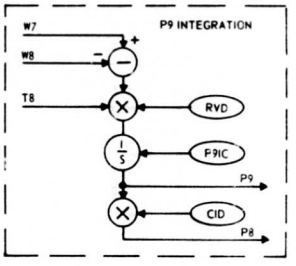
P9 INTEGRATION
W7
W8
T8
RVD
P91C
P9
CID
P8

BLANK PAGE

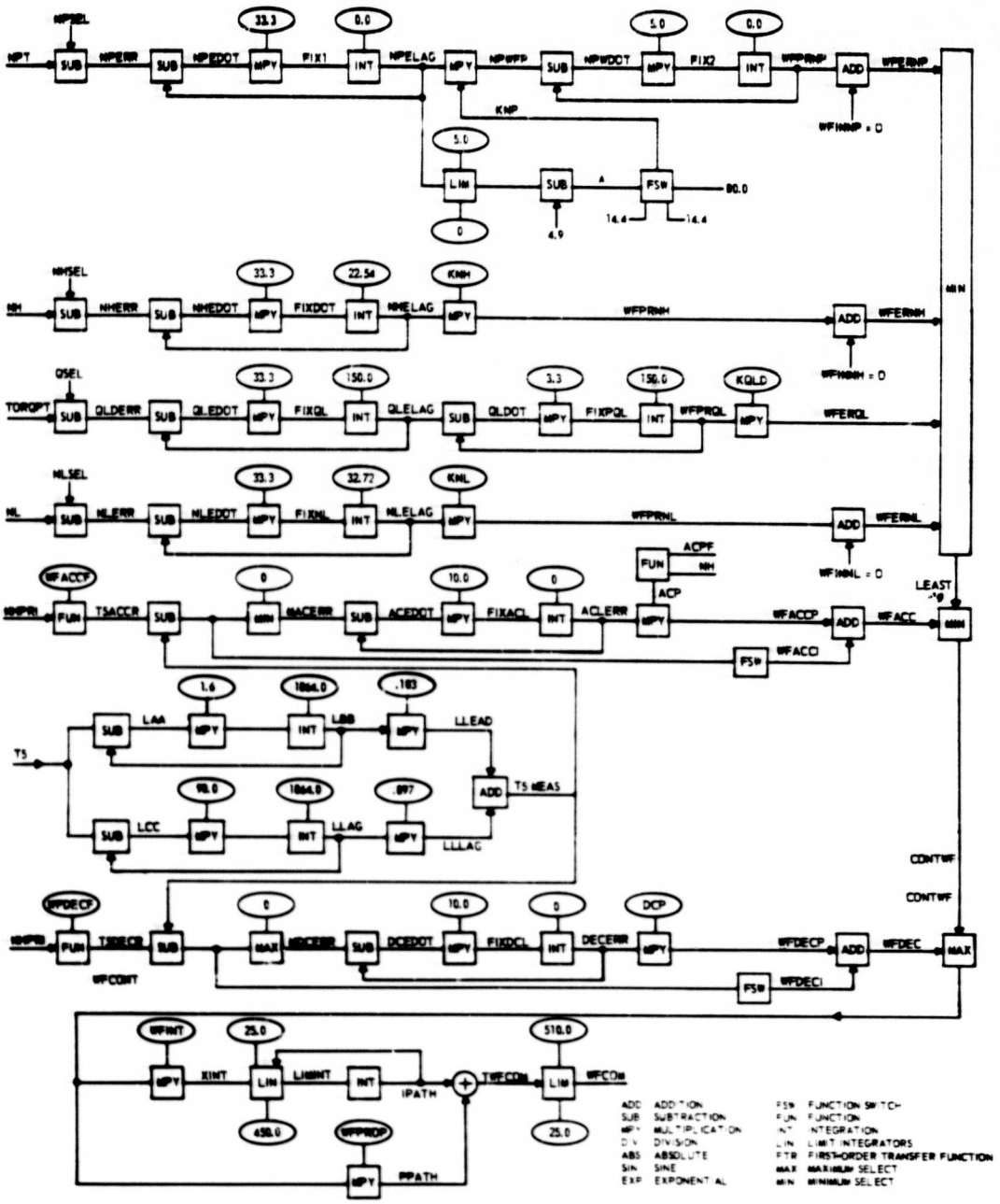

Figure 10. MIMIC Representation - Control Computer.

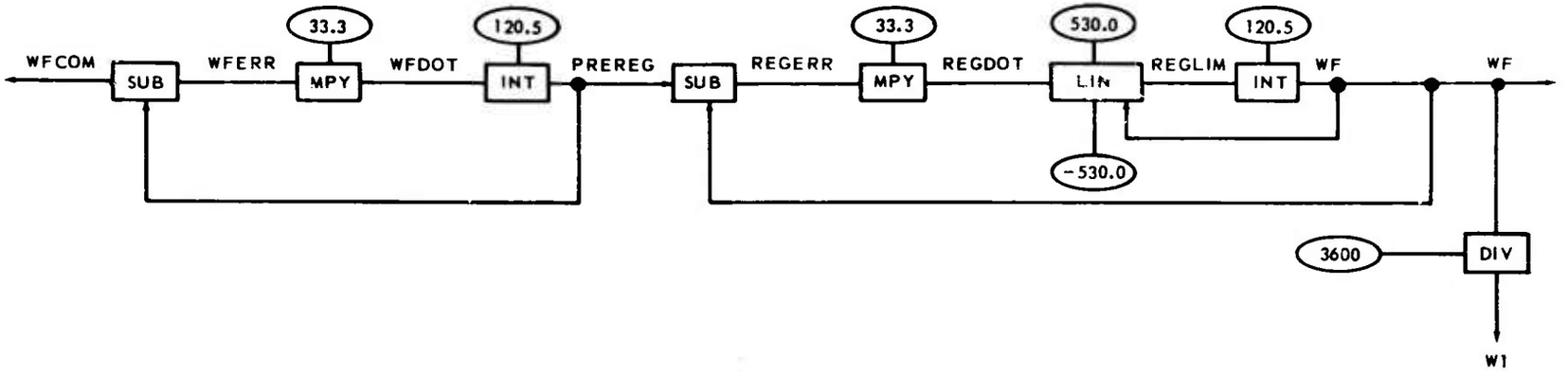

Figure 11. MIMIC Representation - Fuel Metering System No. 1.

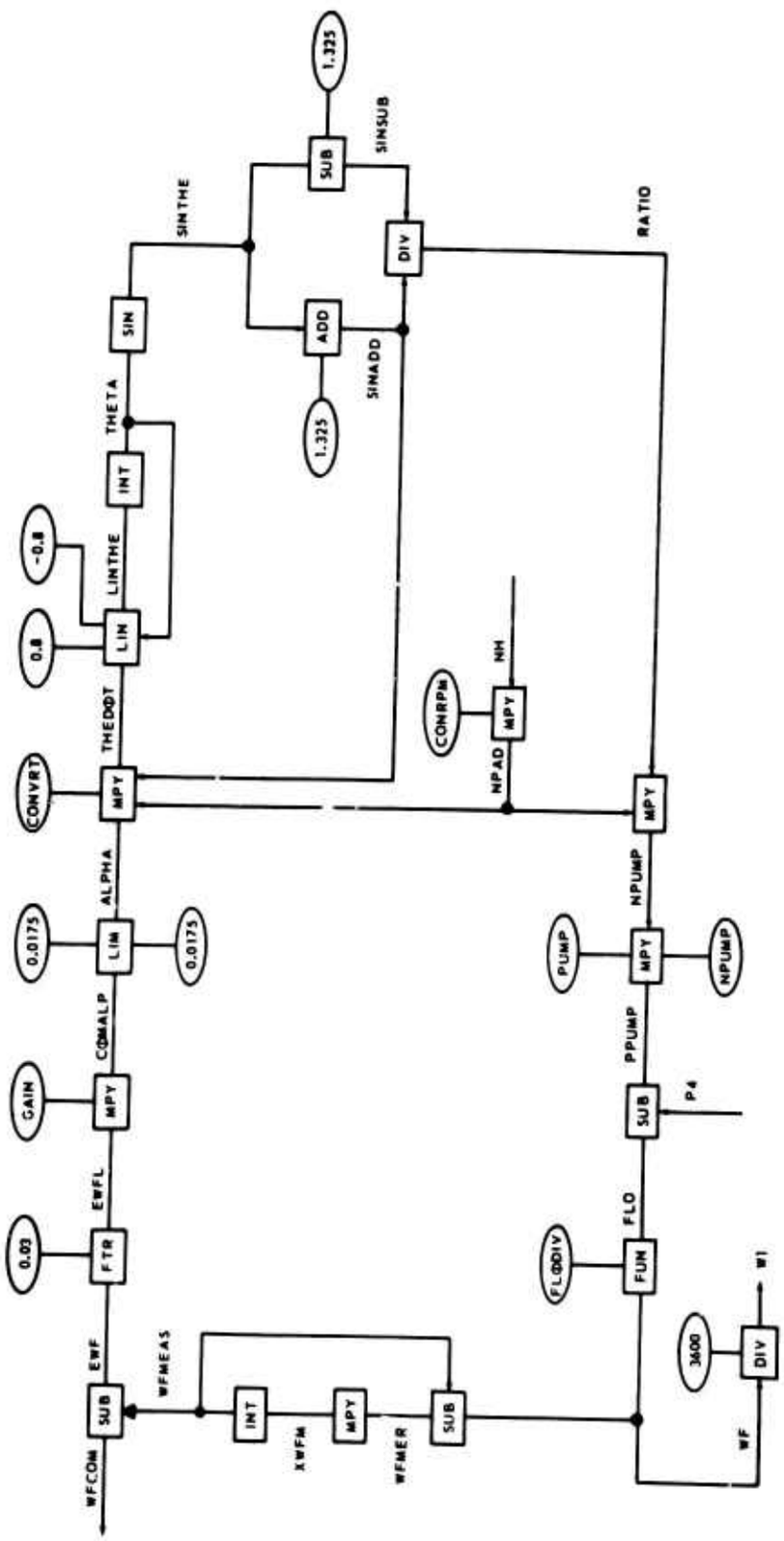

Figure 12. MIMIC Representation - Fuel Metering System No. 2.

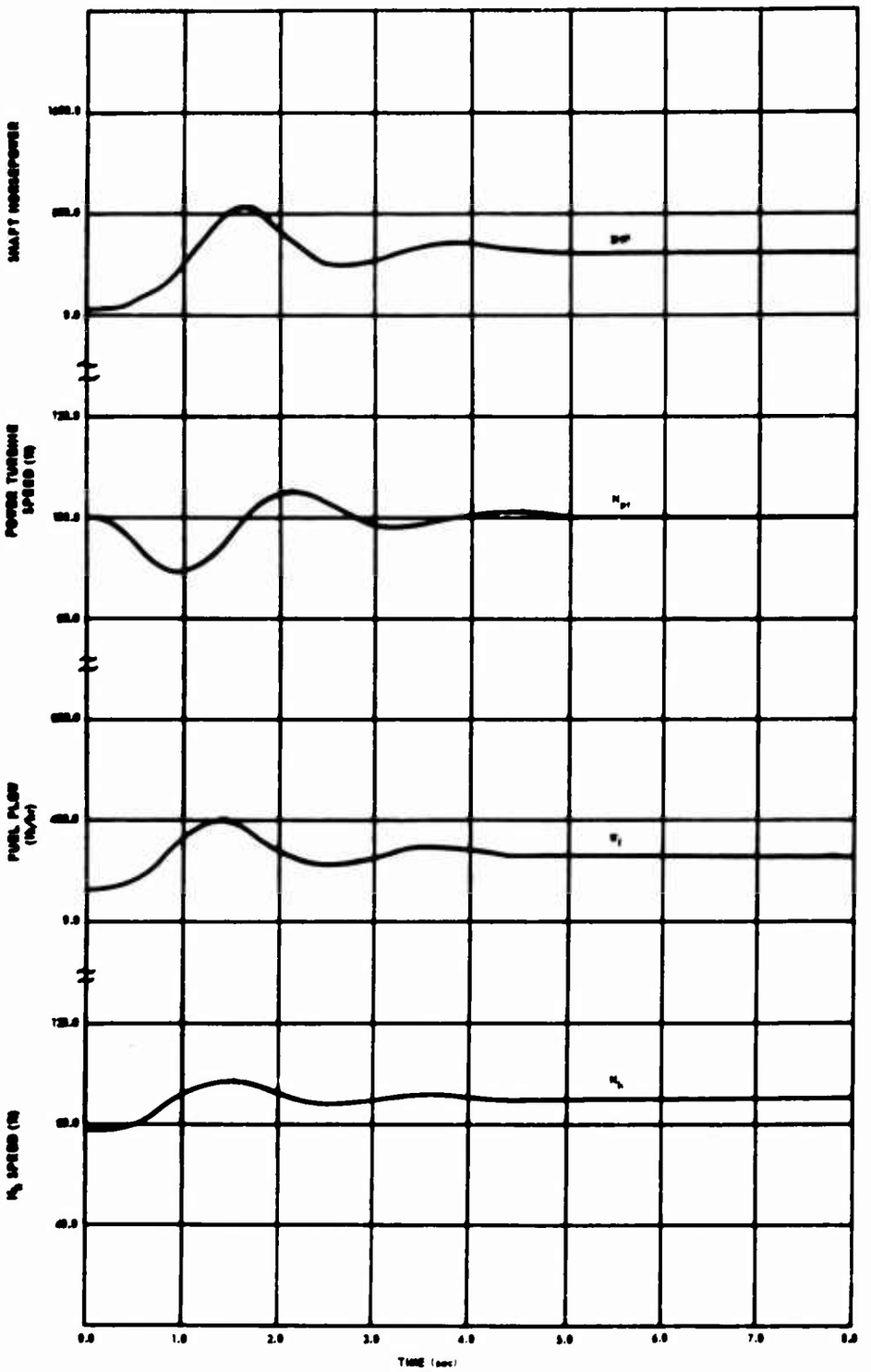

Figure 13. System Response to 1.0-Second Ramp in Collective Pitch - Zero to 50% Load (Turboshaft Engine).

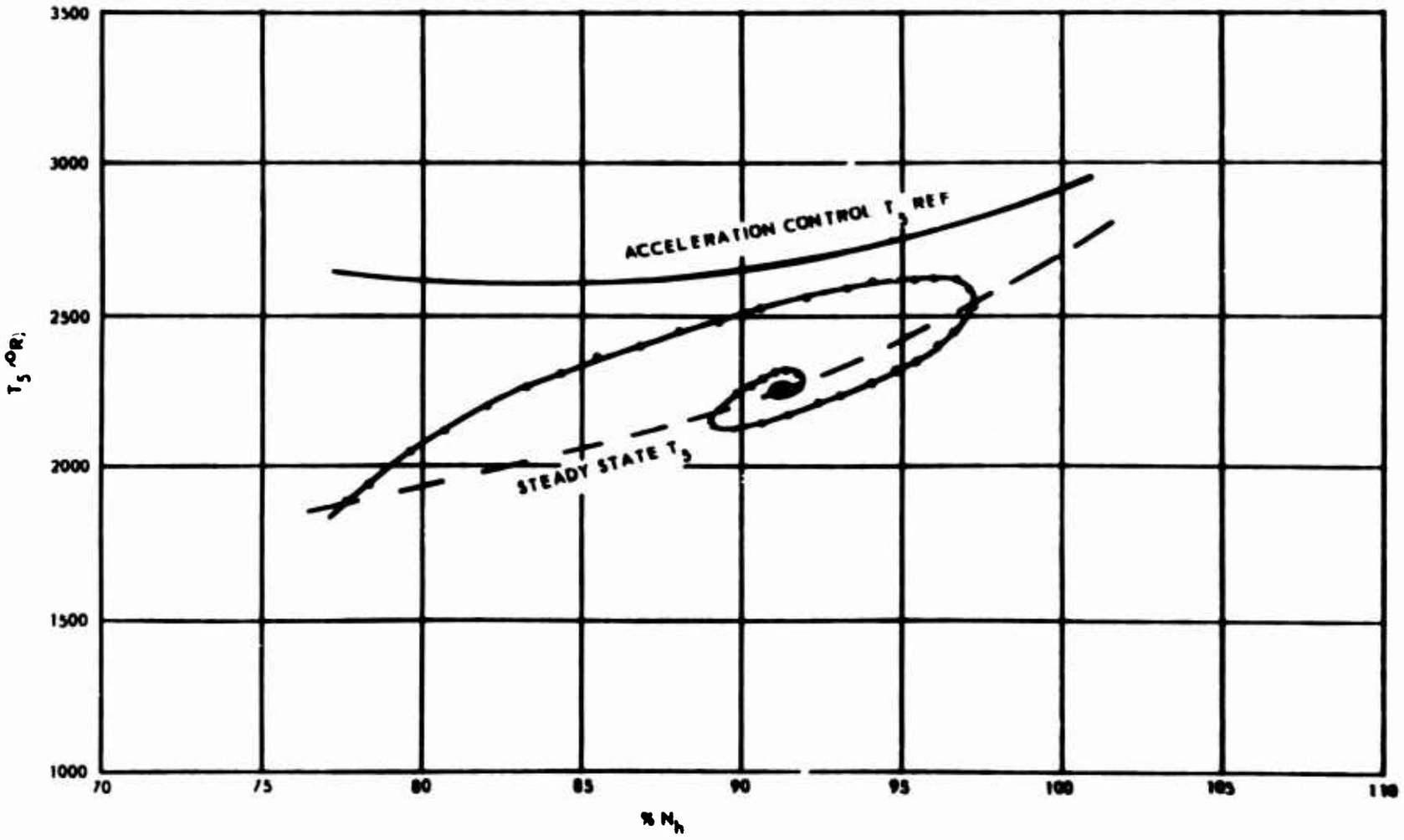

Figure 14. T_5 Response to 1.0-Second Ramp in Collective Pitch - Zero to 50% Load (Turboshaft Engine).

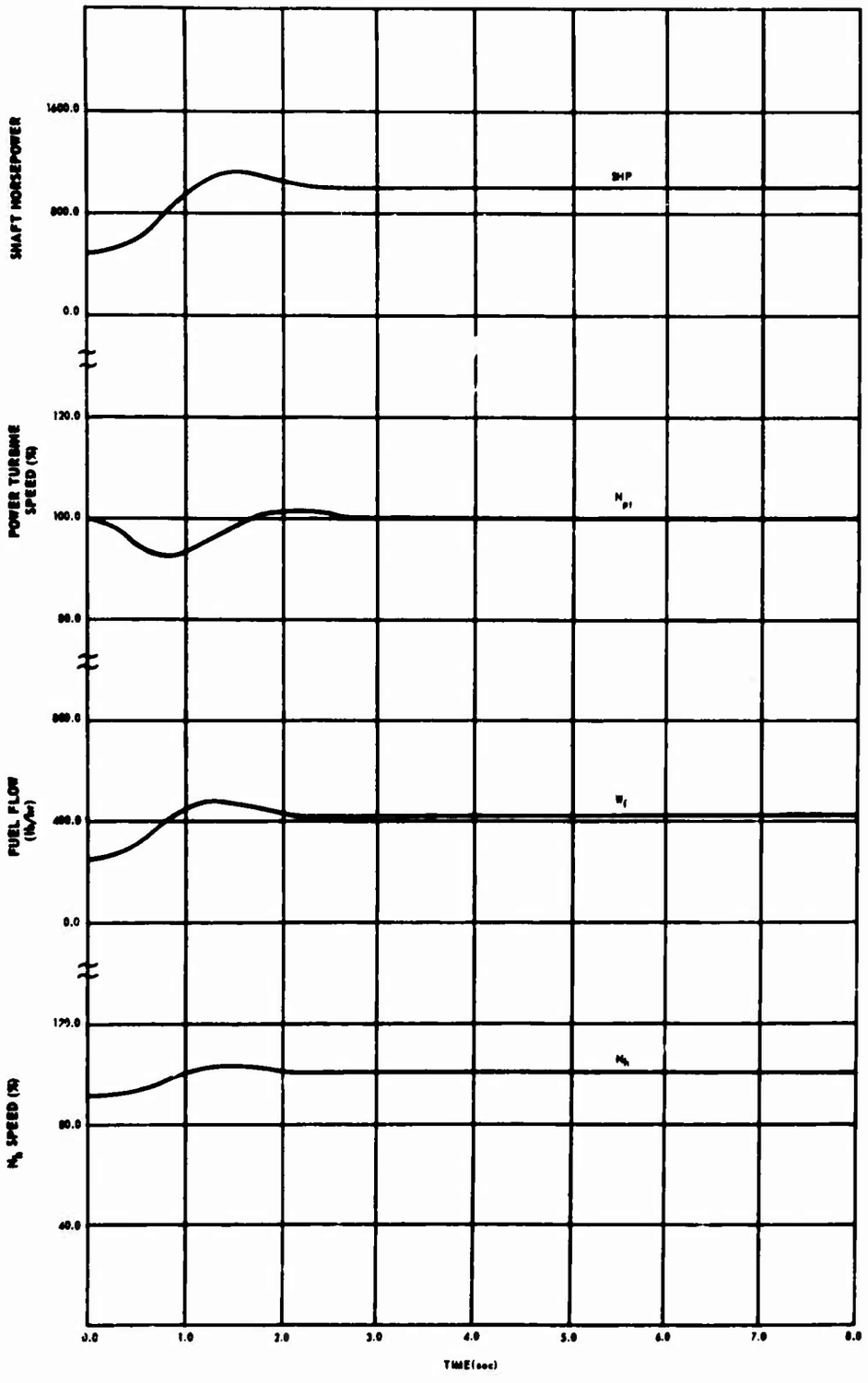

Figure 15. System Response to 1.0-Second Ramp in Collective Pitch - 50% to 100% Load (Turboshaft Engine).

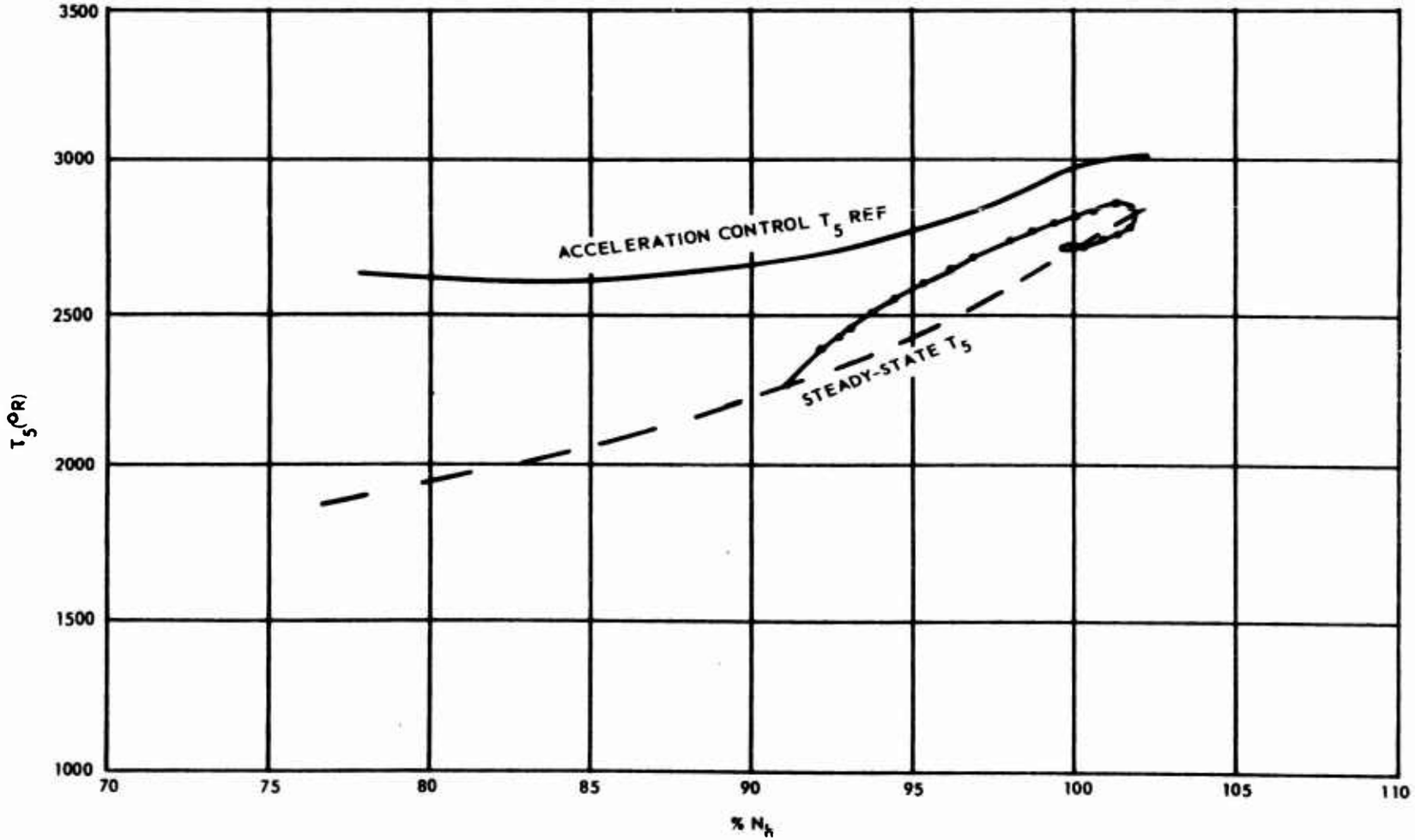

Figure 16. T_5 Response to 1.0-Second Ramp in Collective Pitch - 50% to 100% Load (Turboshaft Engine).

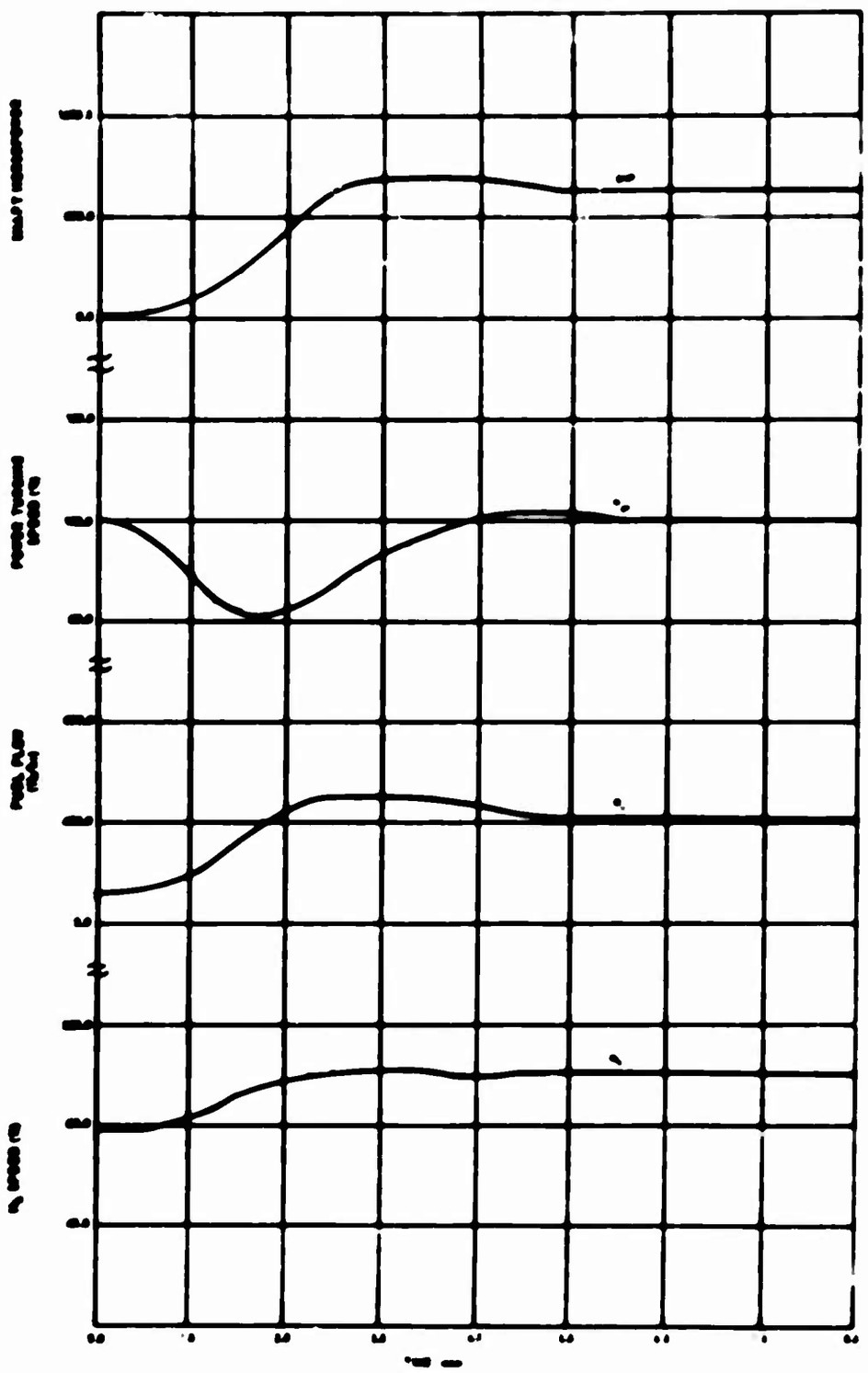

Figure 17. System Response to 1.0-Second Ramp in Collective Pitch - Zero to 100% Load (Turboshaft Engine).

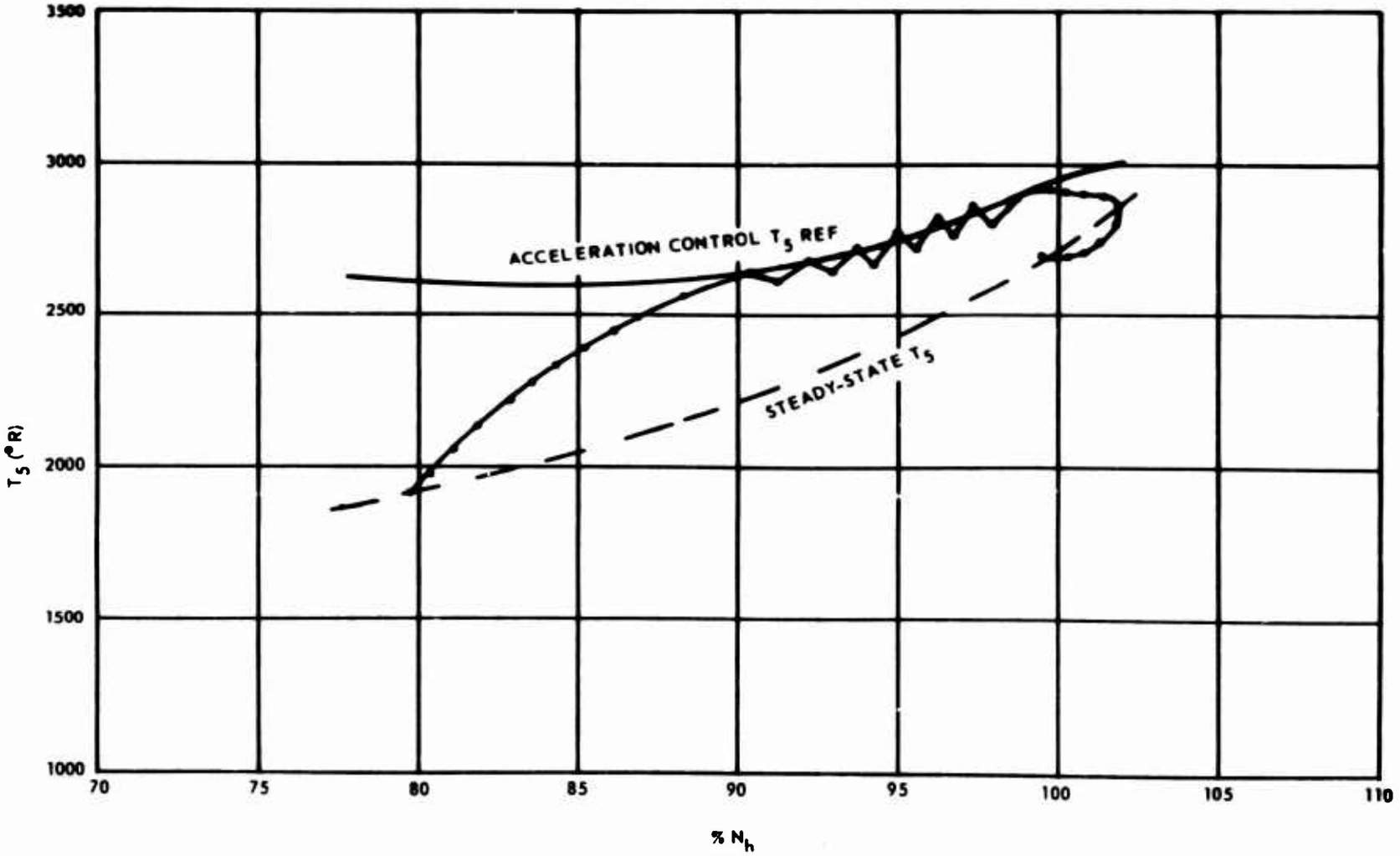

Figure 18. Response to 1.0-Second Ramp in Collective Pitch - Zero to 100% [illegible] (Turboshaft Engine).

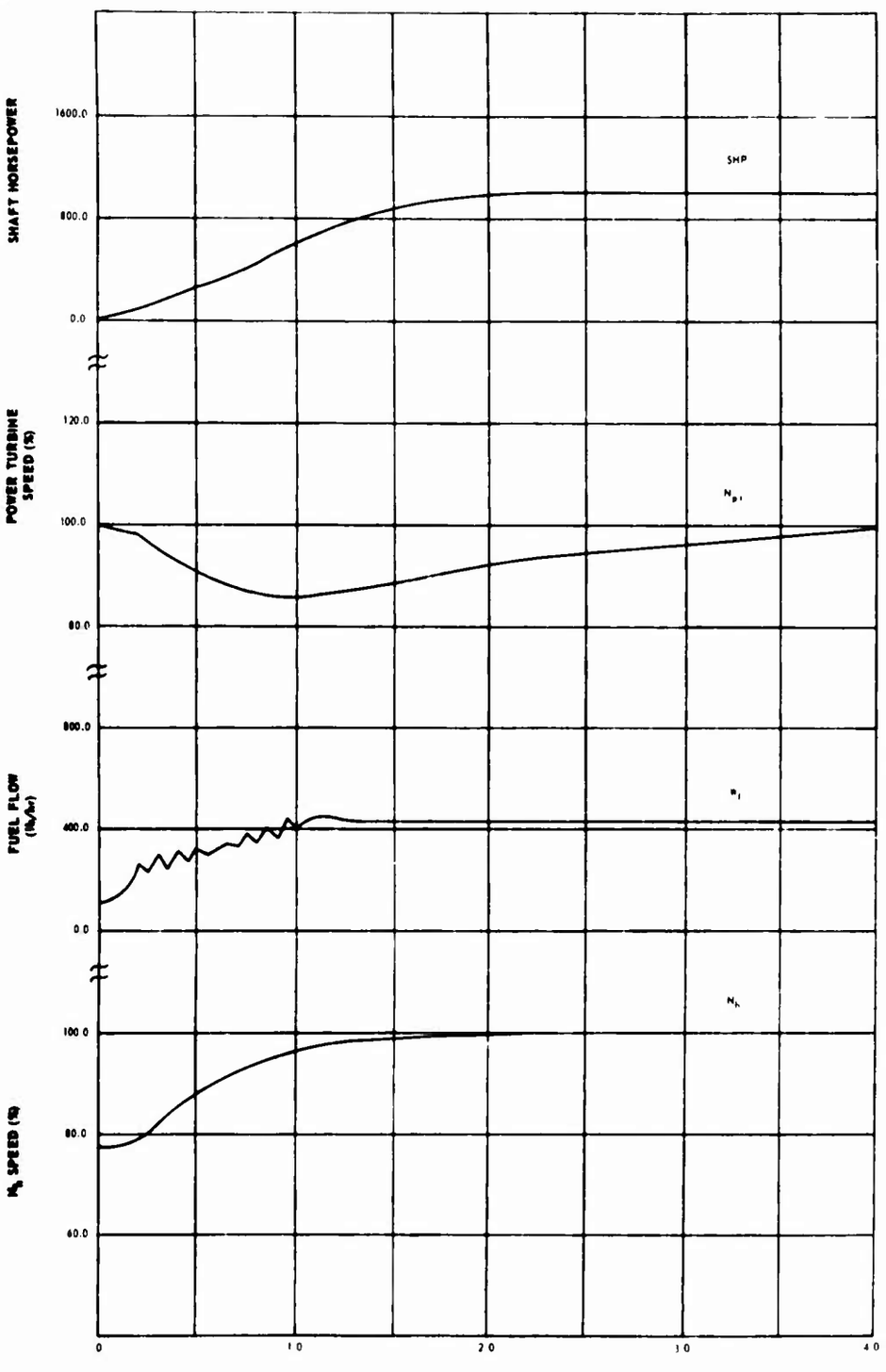

Figure 19. System Response to 0.3-Second Ramp N_h Select From Flight Idle to Takeoff Power (Turboprop Engine).

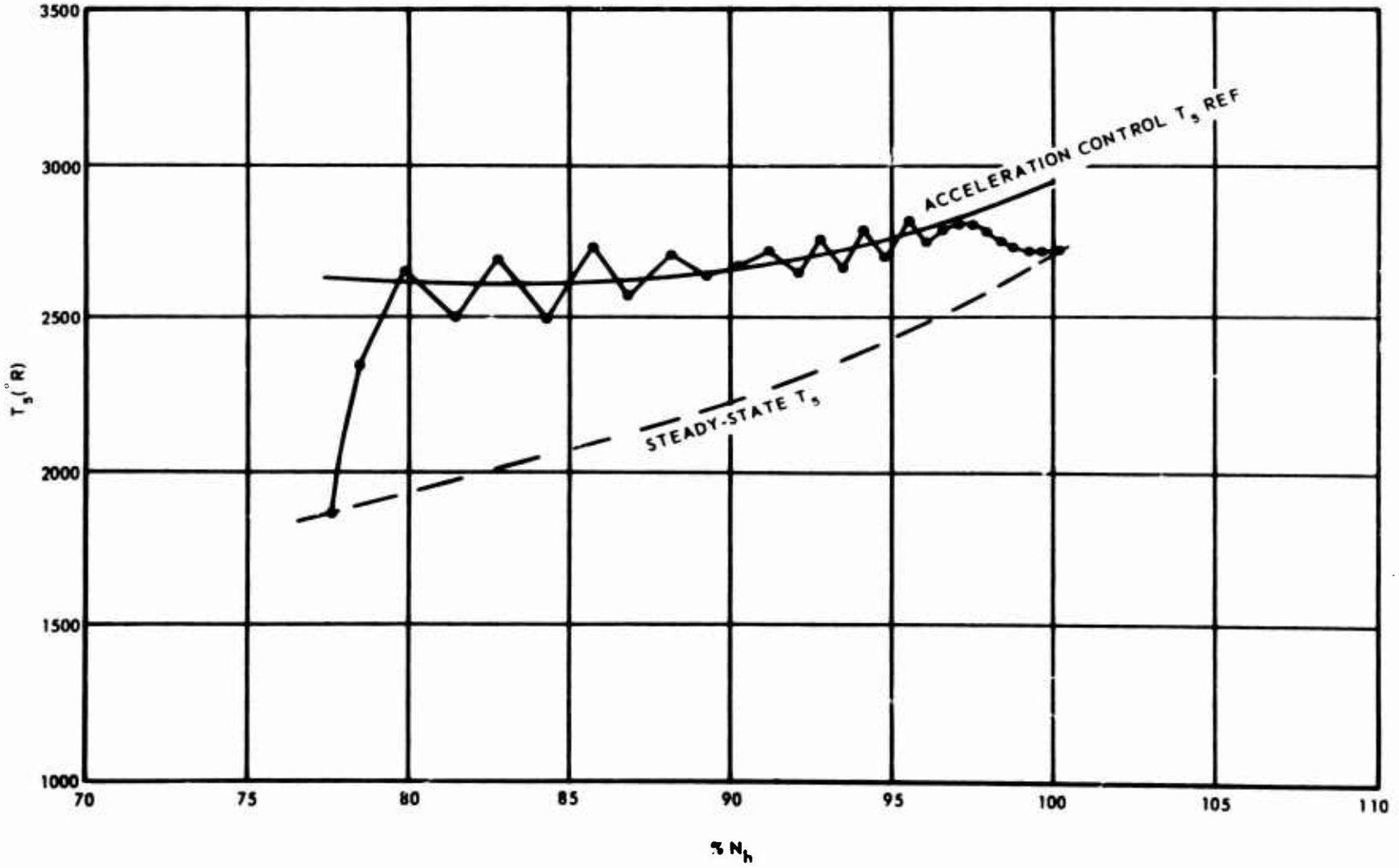

Figure 20. T_5 Response to 0.3-Second Ramp N_h Select From Flight Idle to Takeoff Power (Turboprop Engine).

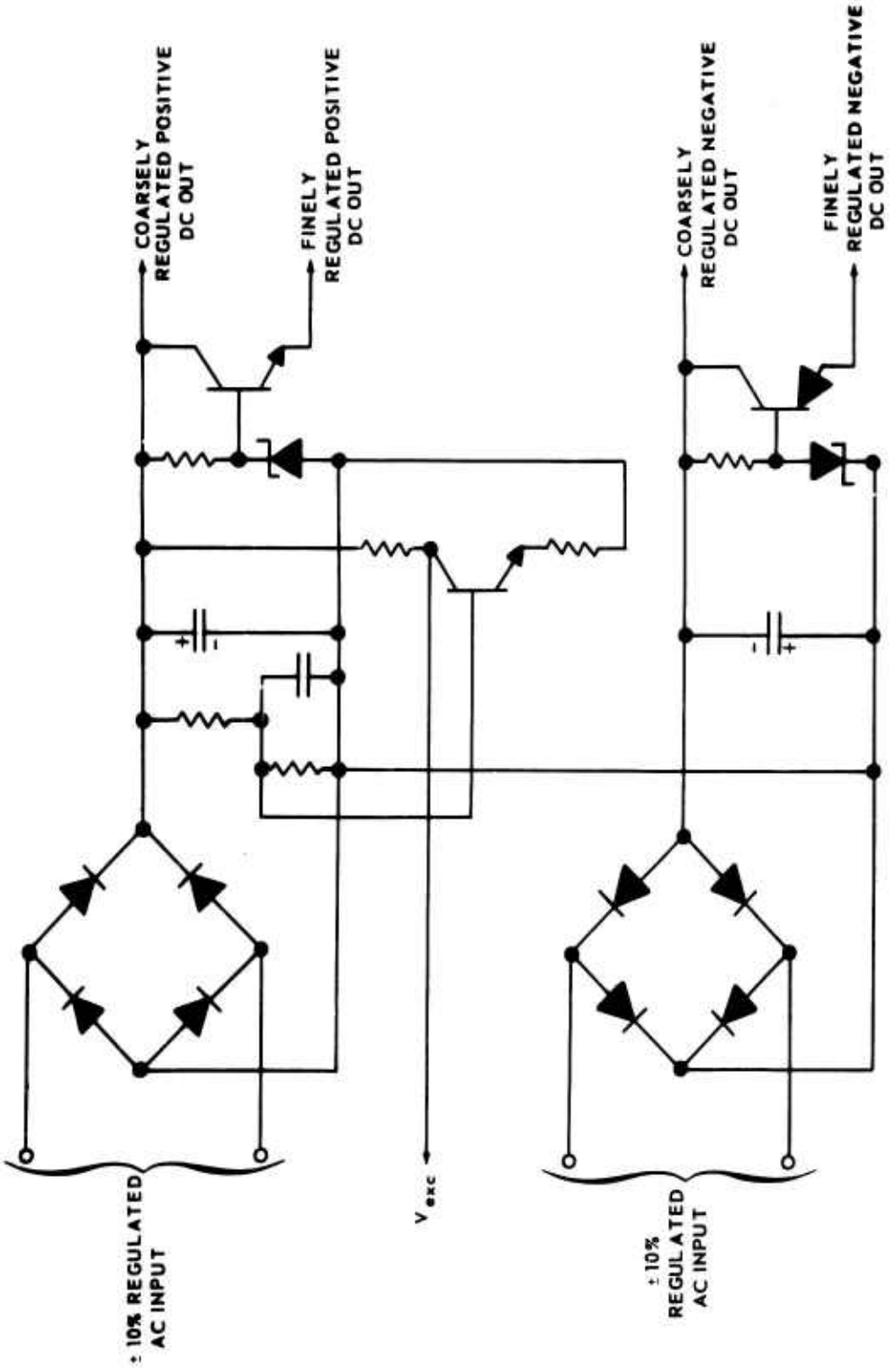

Figure 21. Power Supplies.

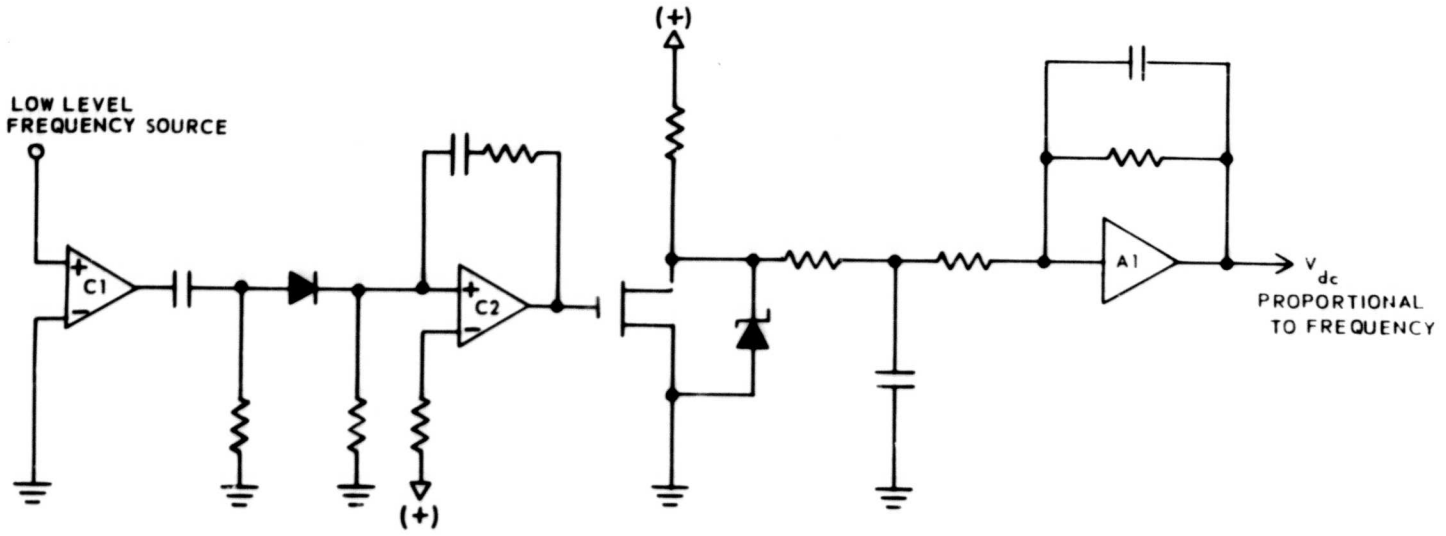

Figure 22. Engine Speed and T_5 Signal Conditioning Circuit (Analog).

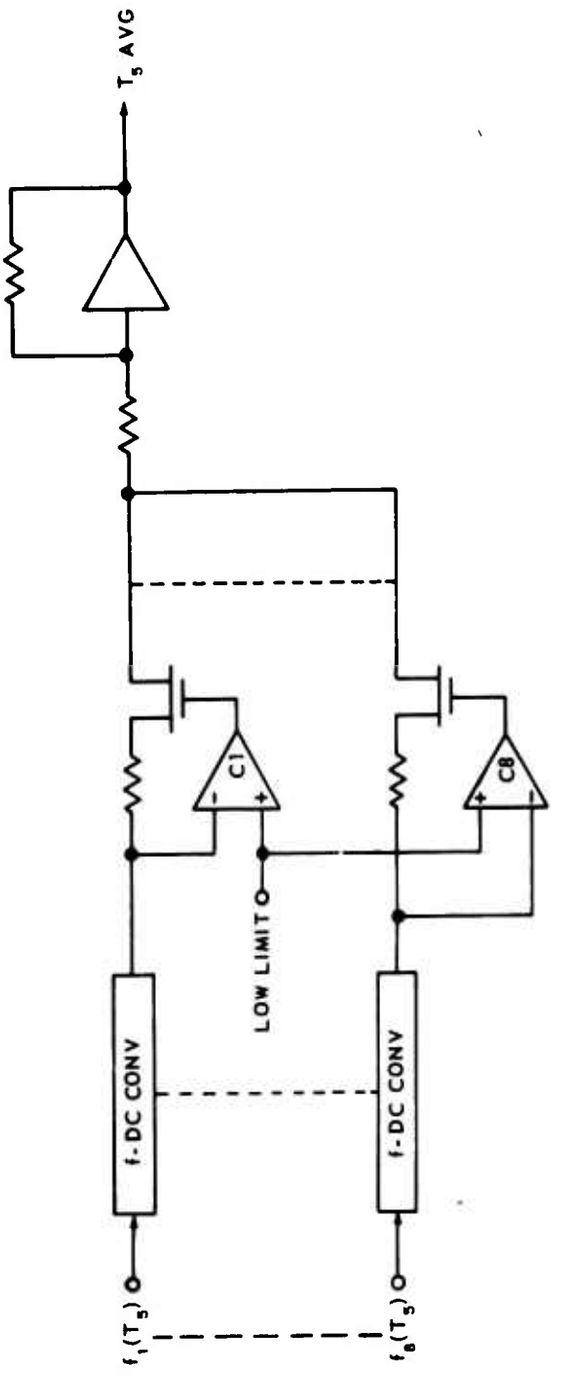

Figure 23. Turbine Inlet Temperature Averaging Circuit (Analog).

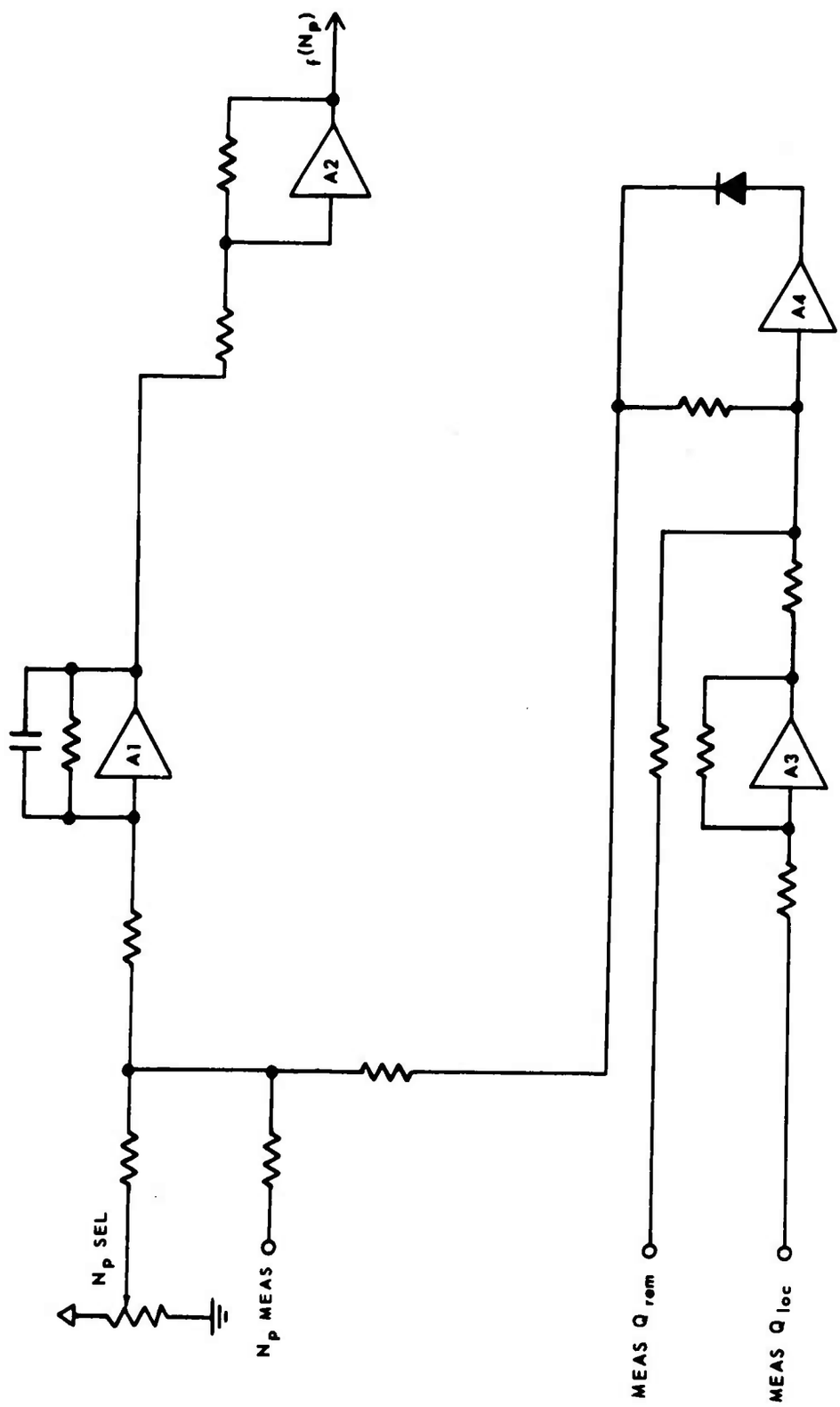

Figure 24. Power Turbine Speed Governor and Load-Sharing Circuit (Analog).

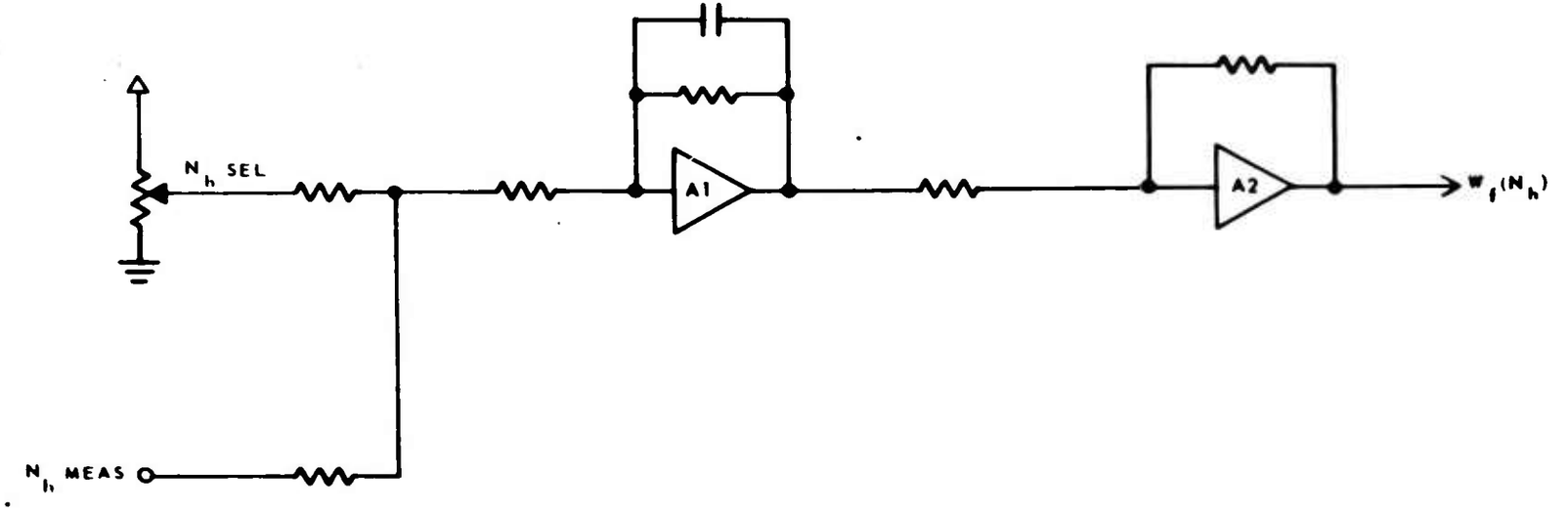

Figure 25. High-Pressure Spool Speed Governor Circuit (Analog).

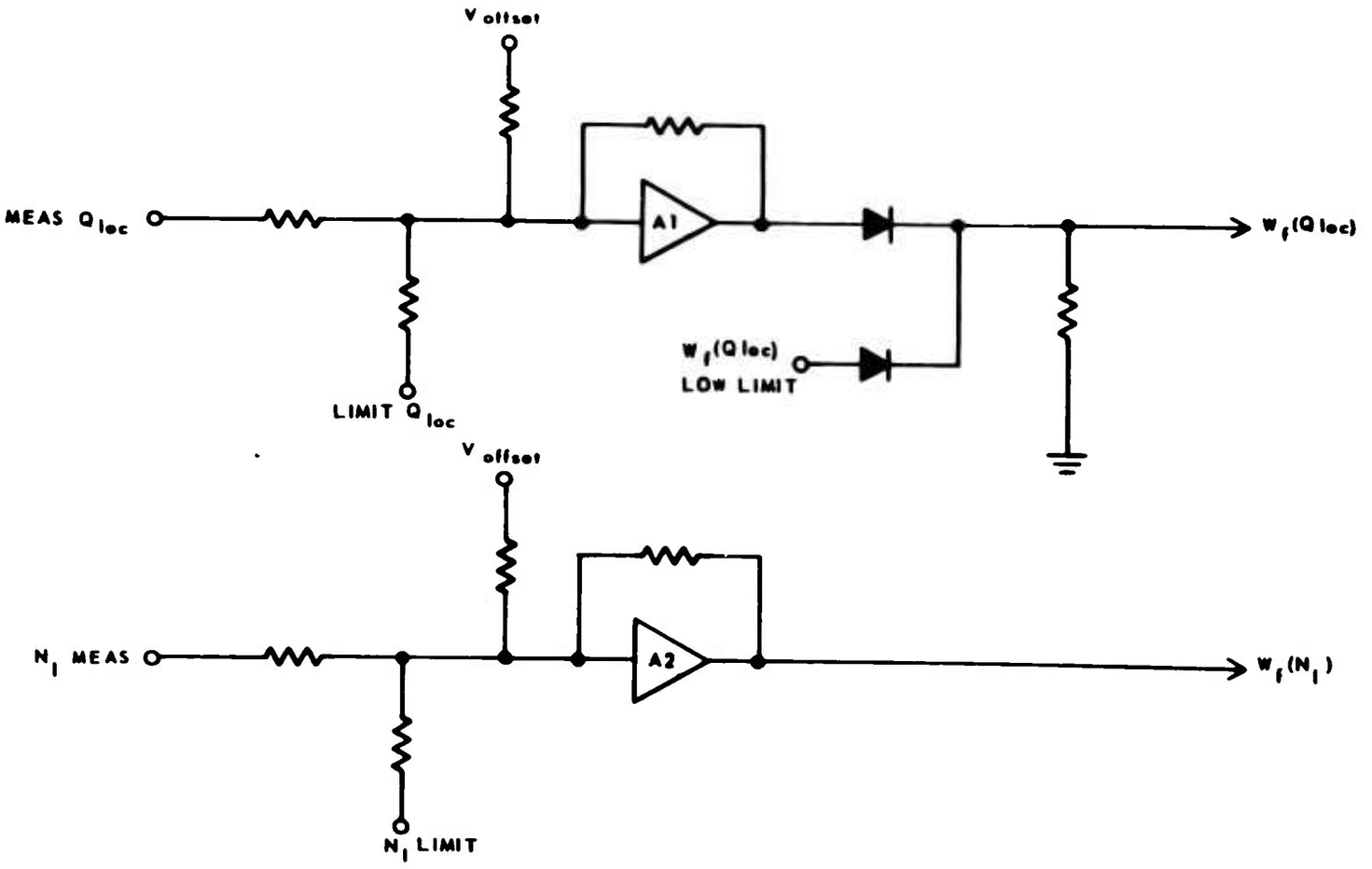

Figure 26. Power Turbine Torque and Low-Pressure Spool Speed Limiter Circuit (Analog).

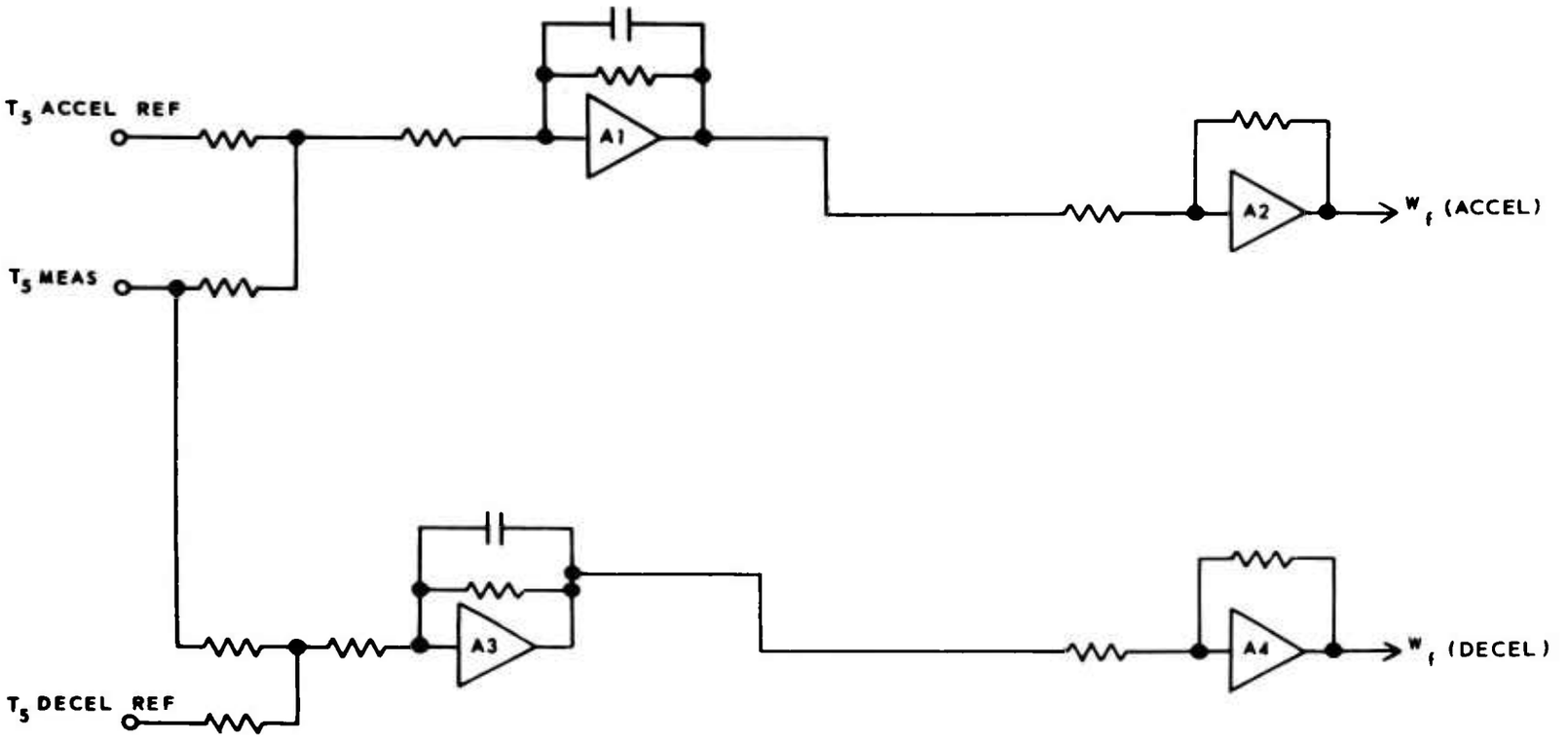

Figure 27. Acceleration and Deceleration Limit Circuit (Analog).

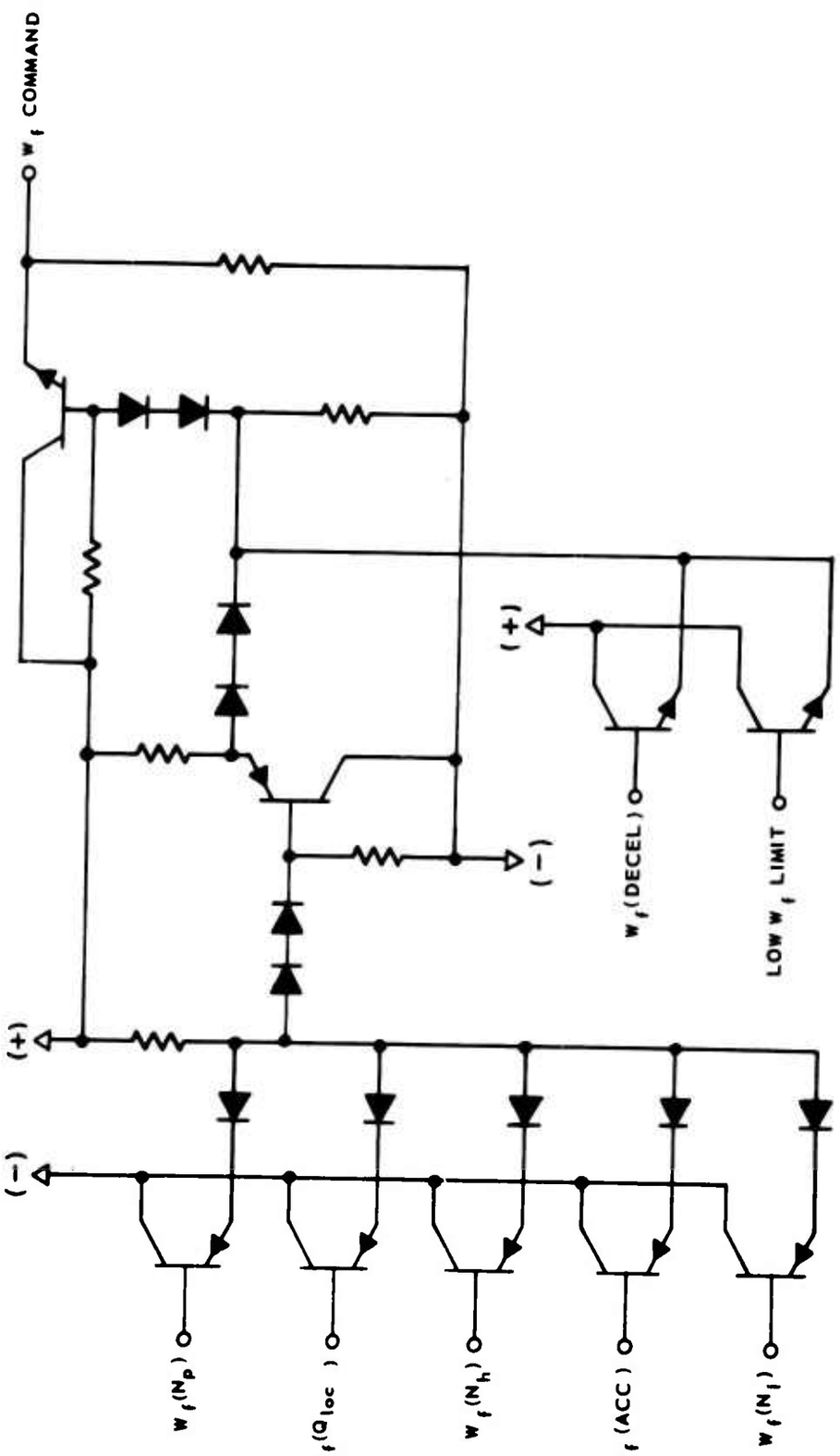

Figure 28. Control Mode Selector Circuit (Analog).

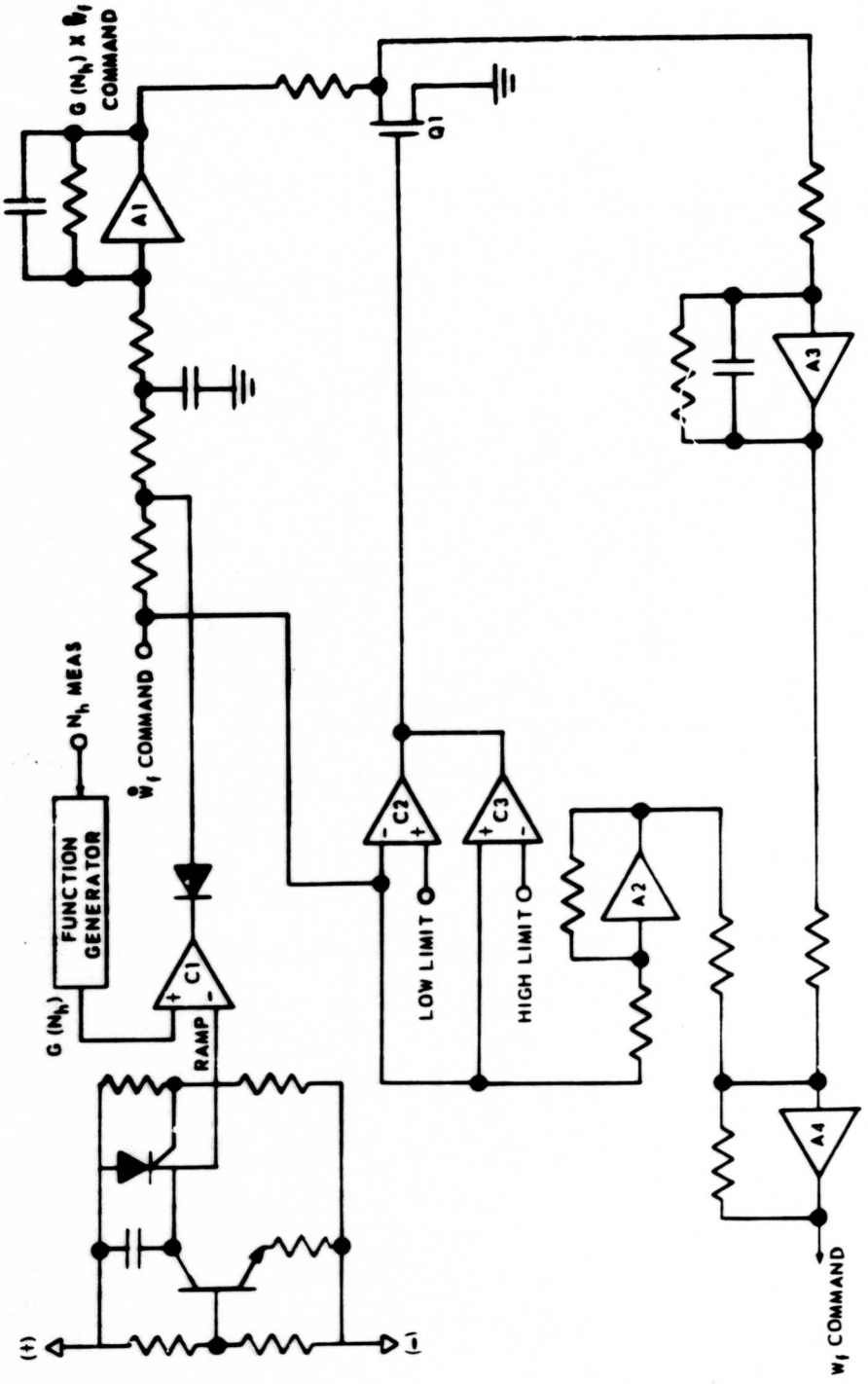

Figure 29. Integrator Circuit (Analog).

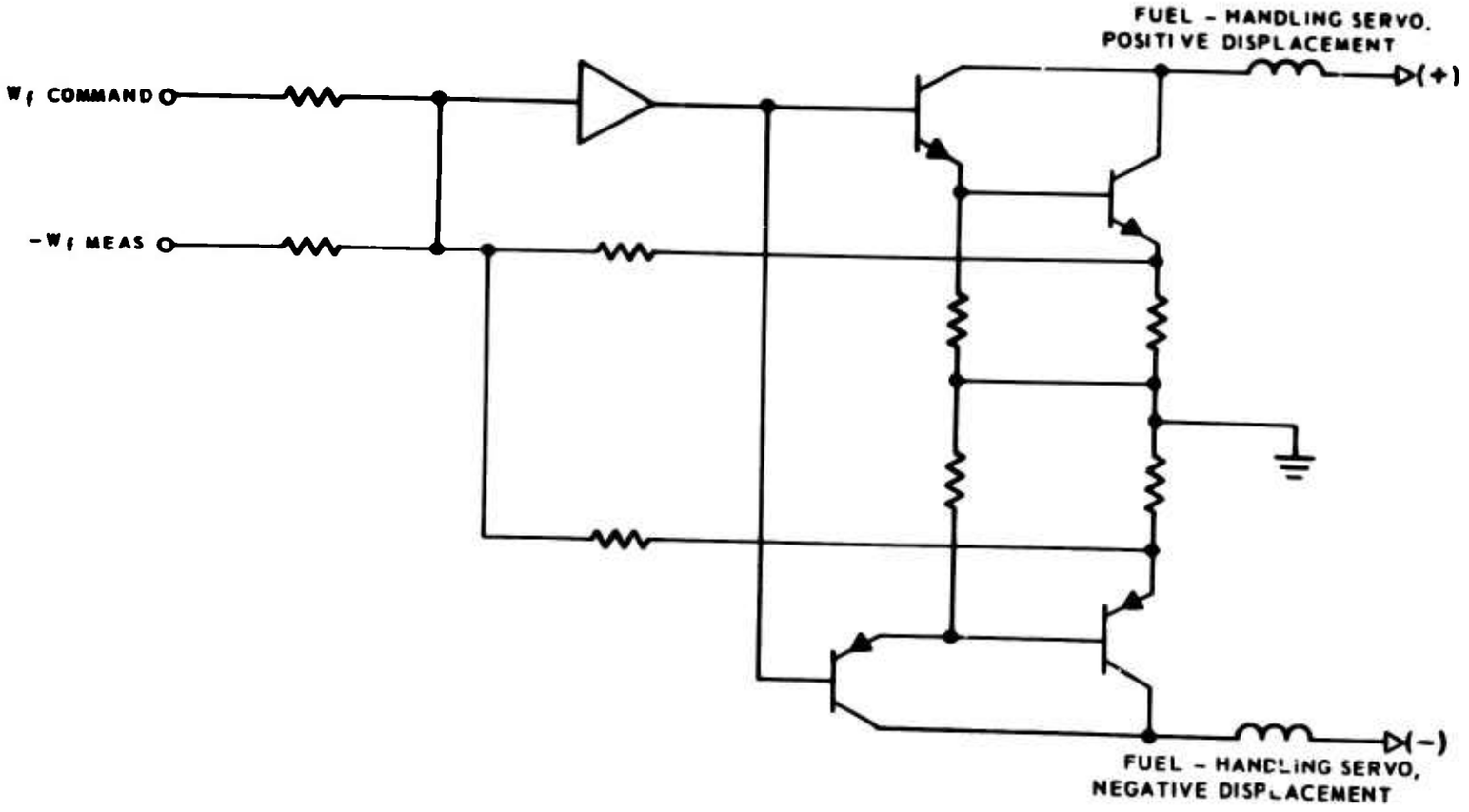

Figure 30. Fuel Metering Control Circuit (Analog).

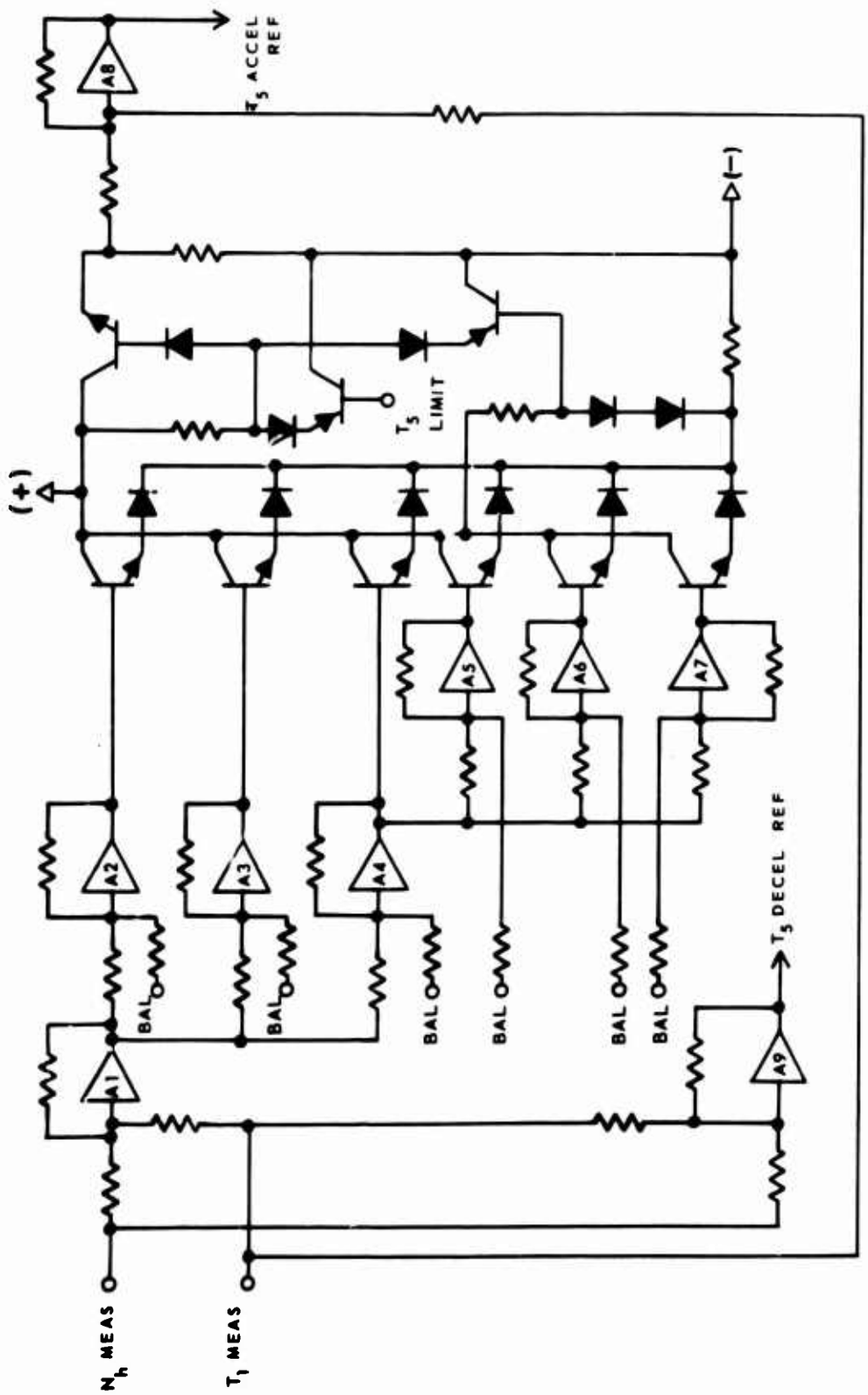

Figure 31. Acceleration and Deceleration Limit Generator Circuit (Analog).

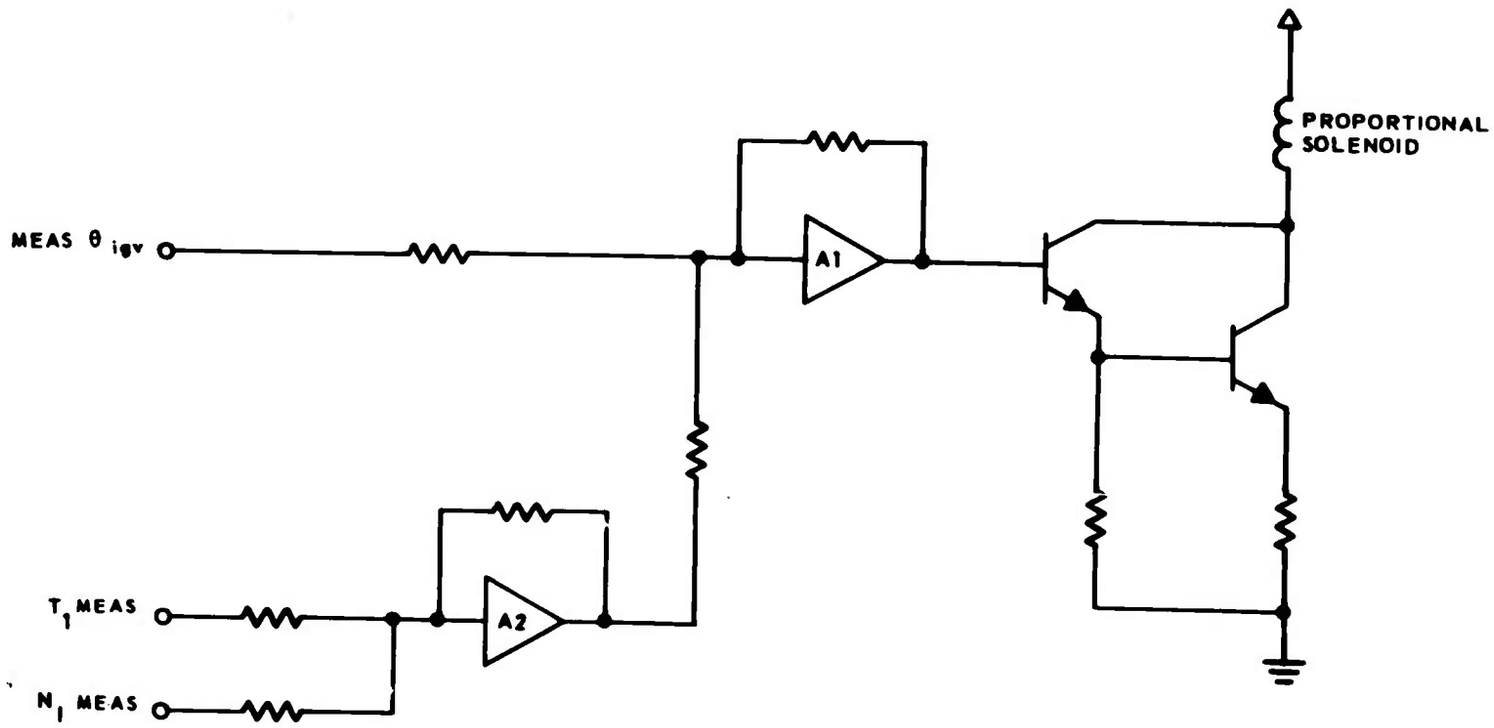

Figure 32. Inlet Guide Vane Control Circuit (Analog).

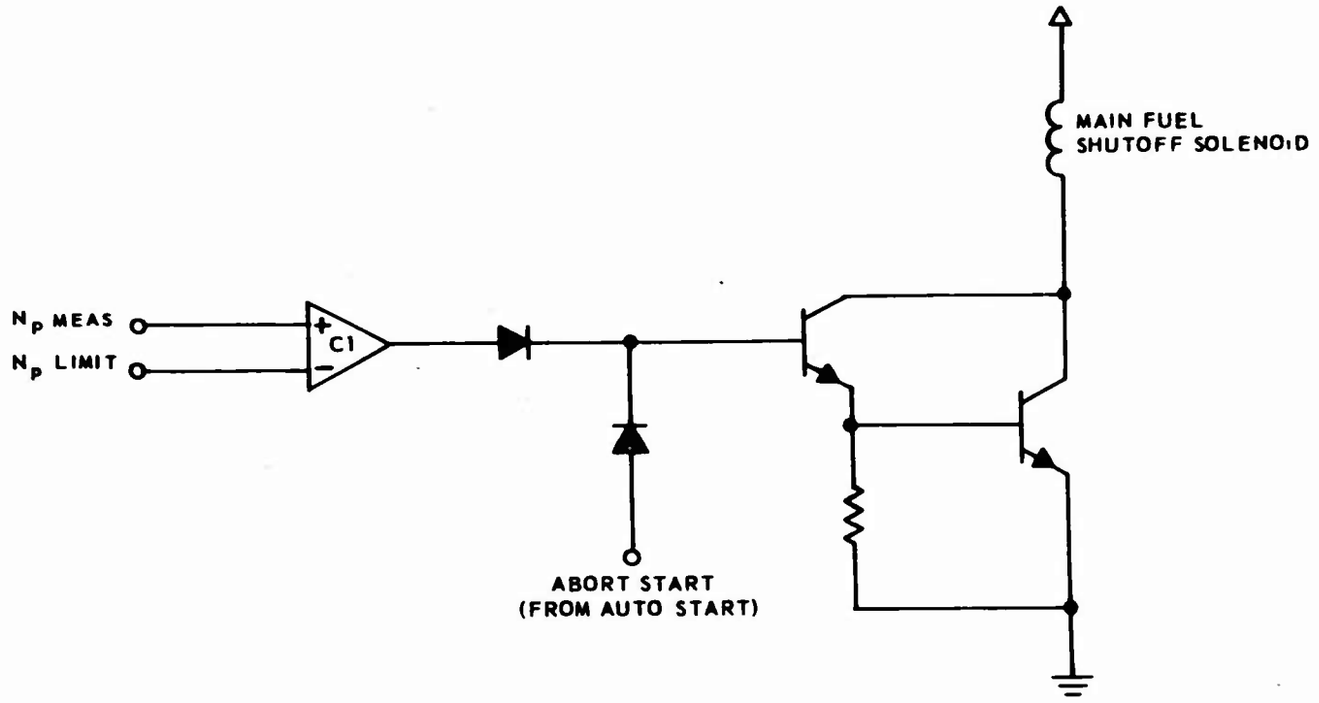

Figure 33. Power Turbine Overspeed and Abort-Start Shutoff Control Circuit. (Analog).

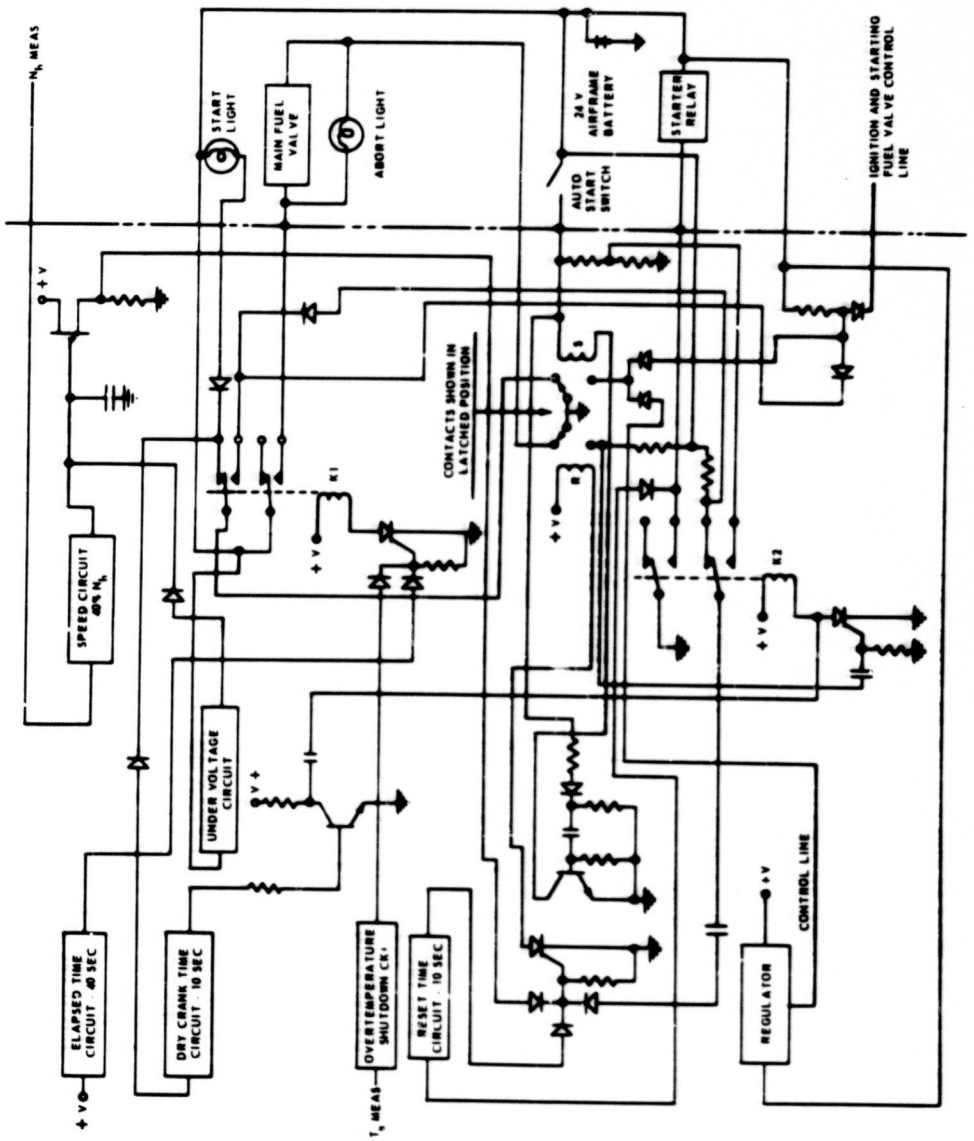

Figure 34. Automatic Starting System Circuit (Analog).

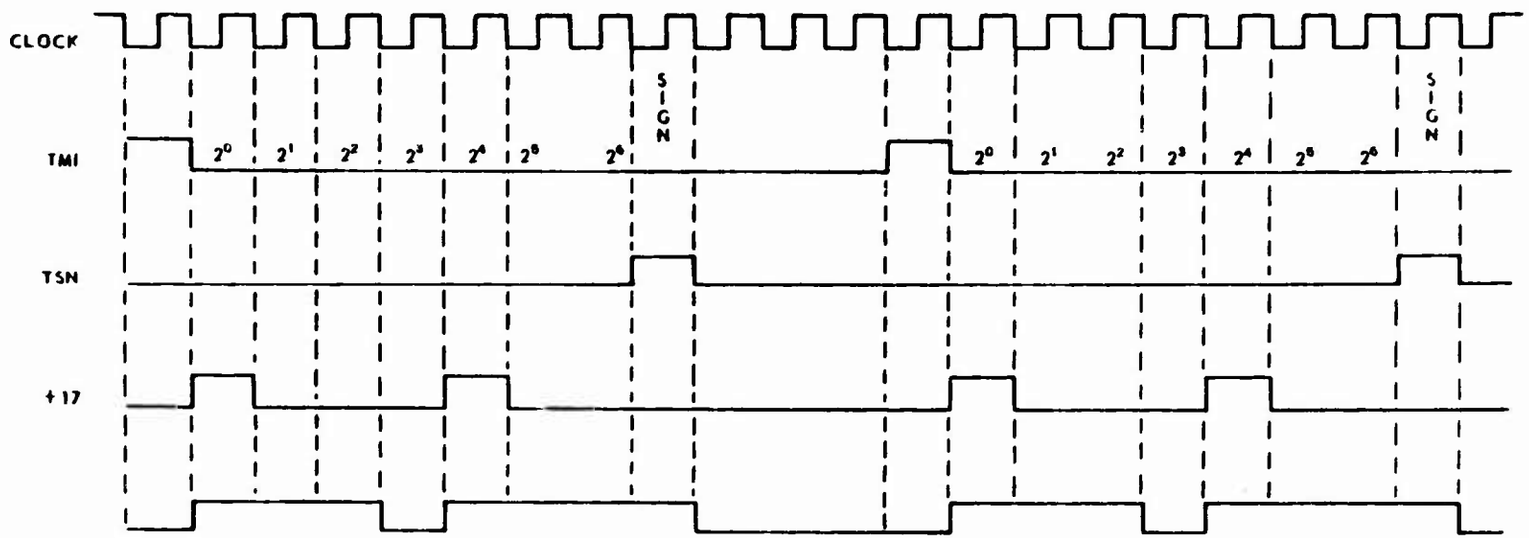

Figure 35. Digital Timing Diagram for Word Definition.

Figure 36. Symbols for Digital Incremental Computer Elements.

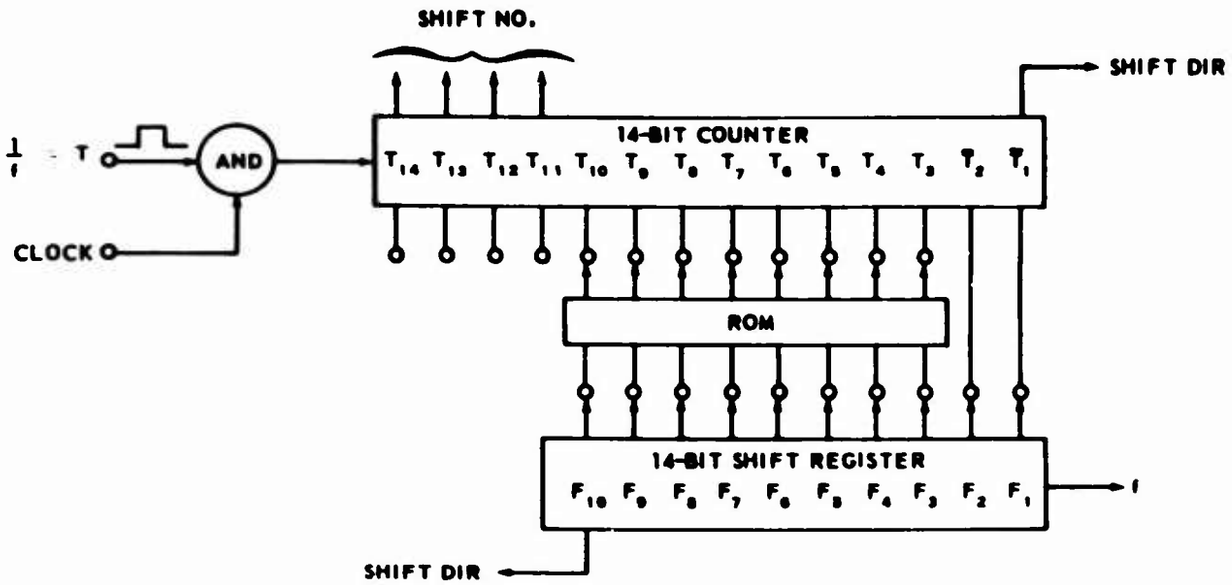

Figure 37. Speed Measuring Circuit (Digital).

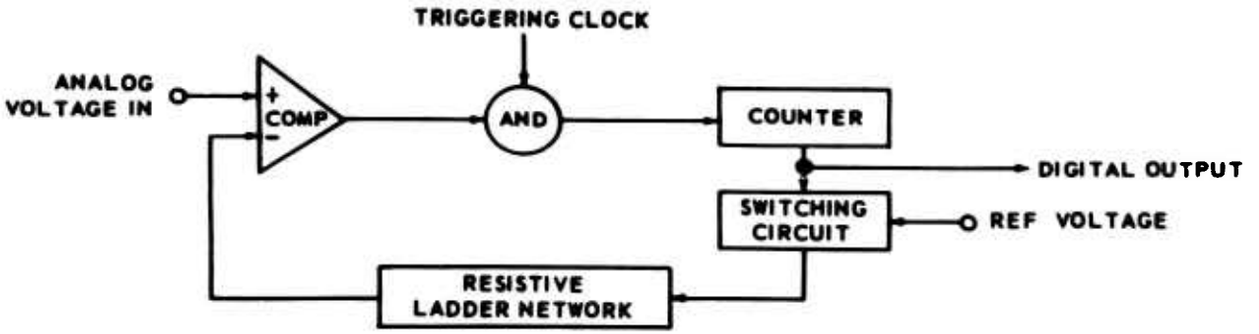

Figure 38. Analog-to-Digital Converter.

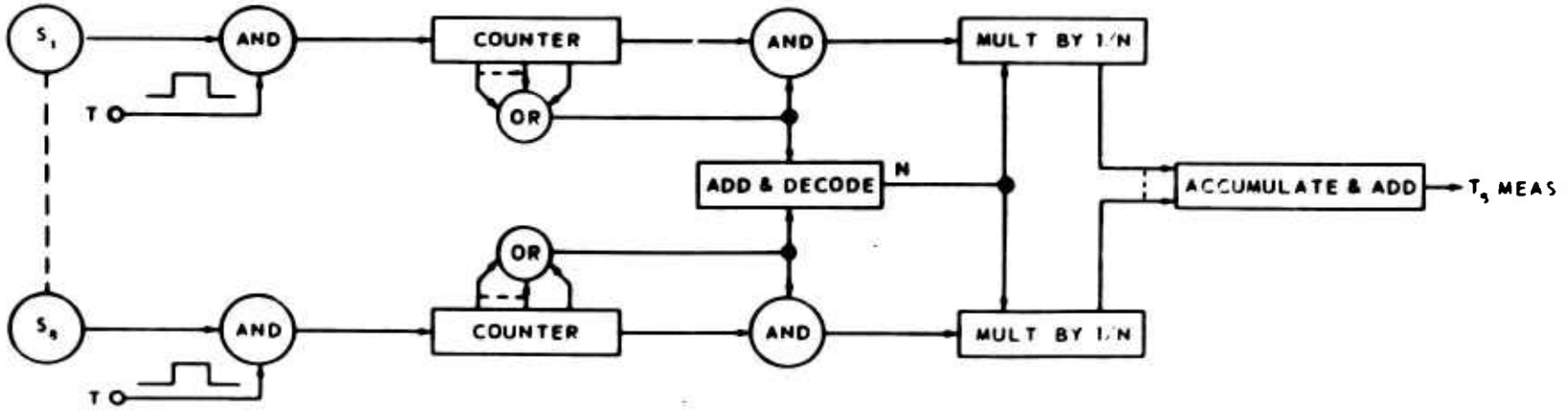

Figure 39. Turbine Inlet Temperature Averaging Circuit (Digital).

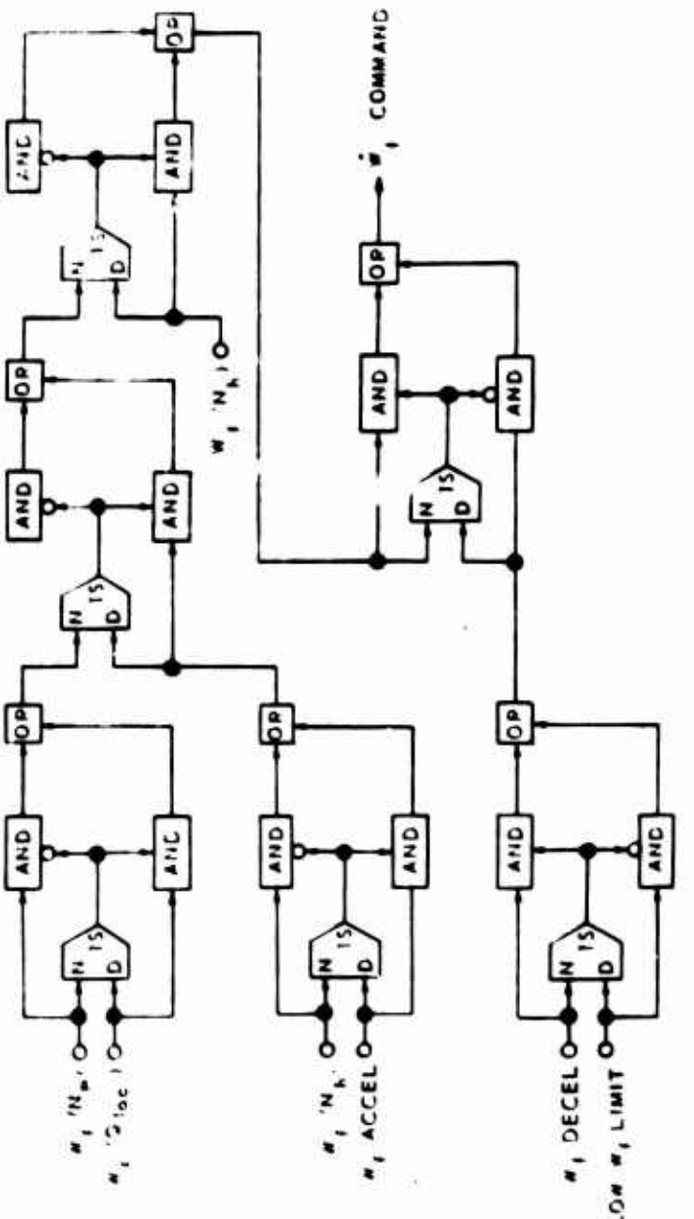

Figure 40. Control Mode Selector (Digital).

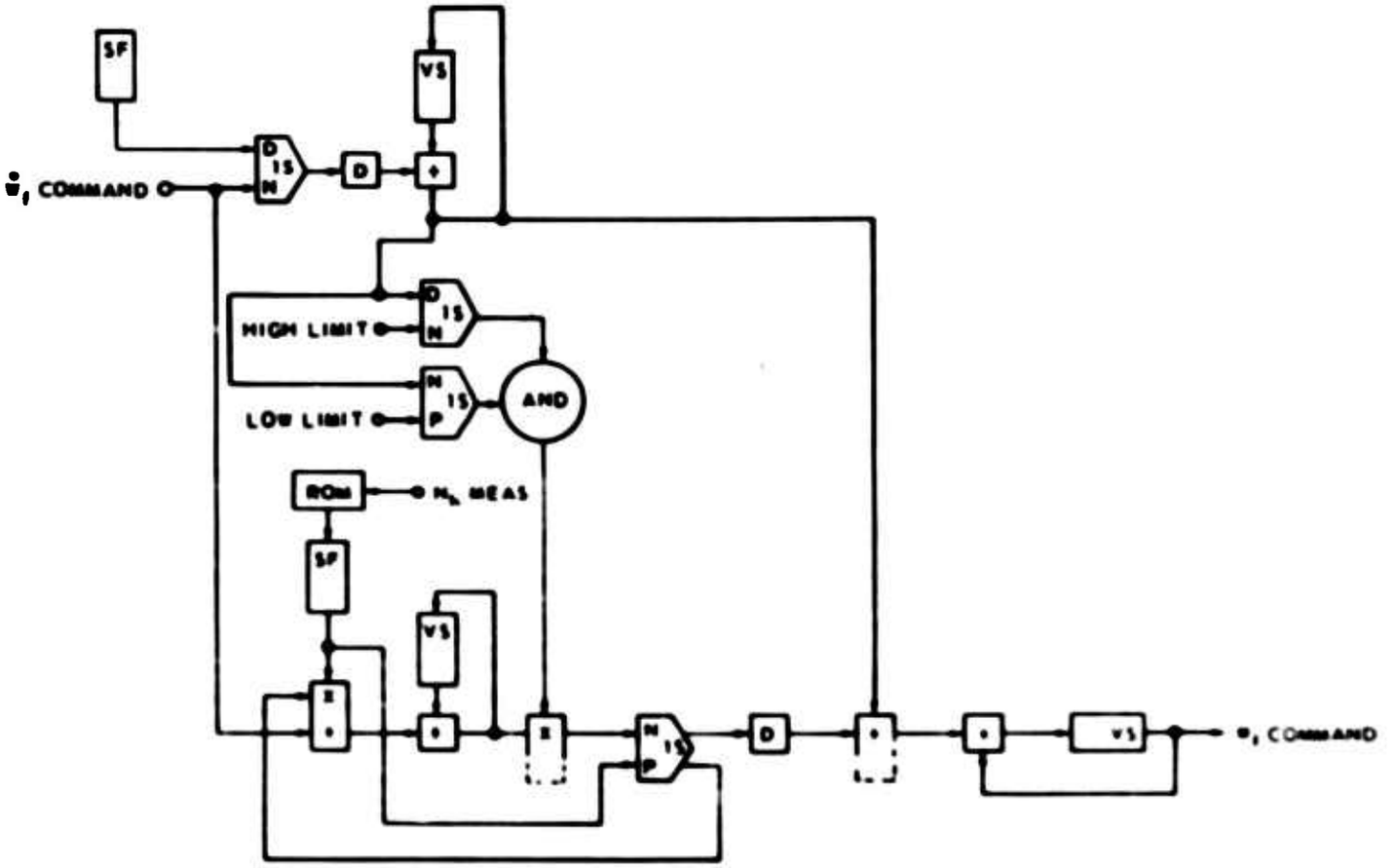

Figure 41. Integrator (Digital).

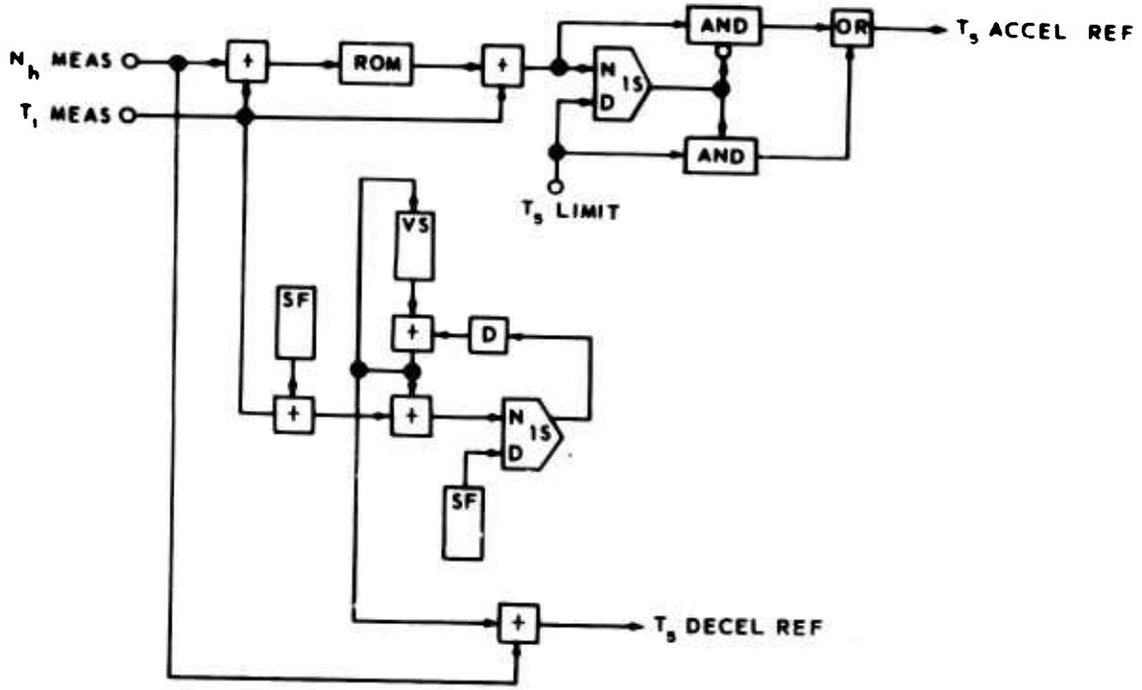

Figure 42. T_5 Acceleration and Deceleration Limit Generators (Digital).

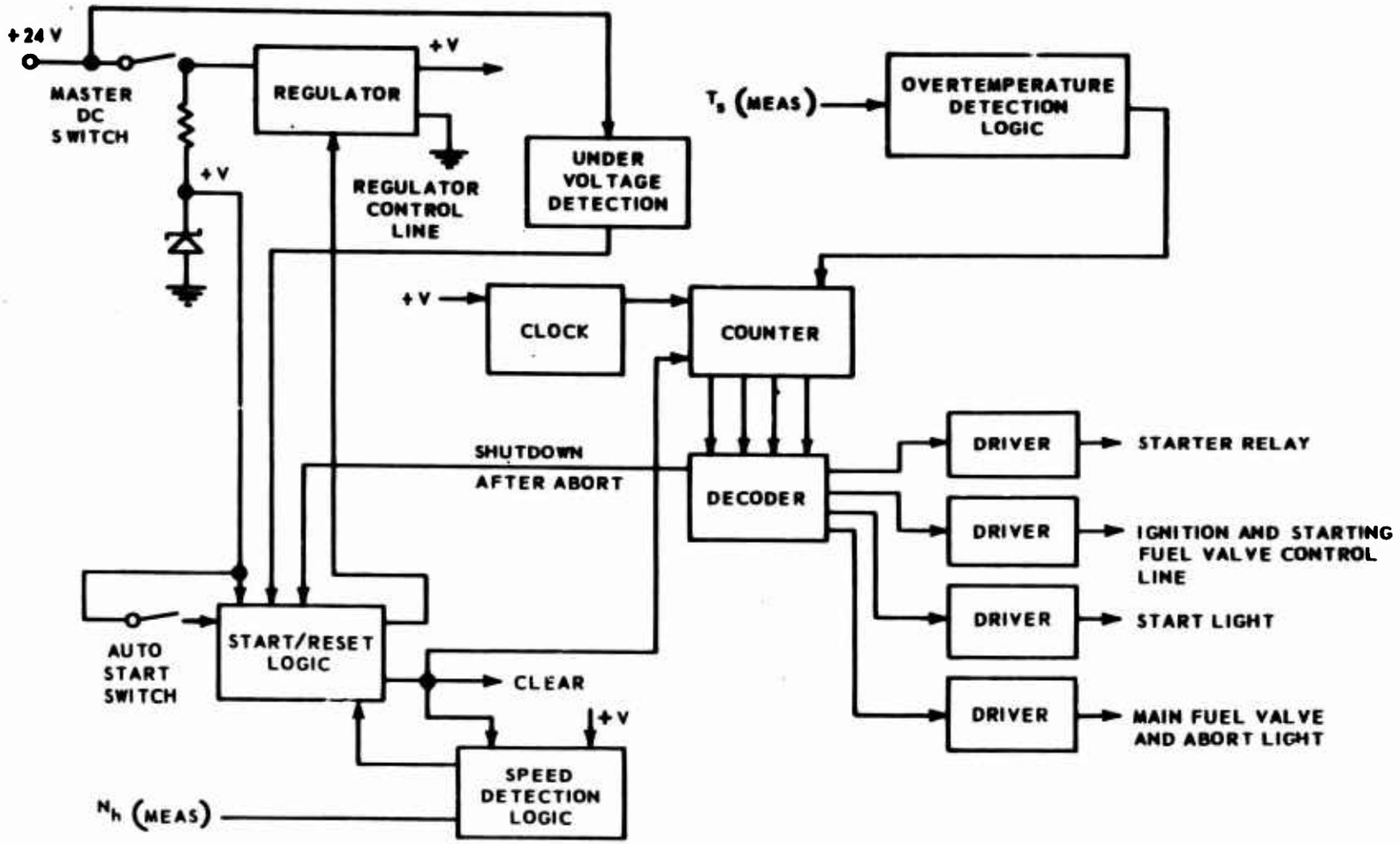

Figure 43. Automatic Starting System Circuit (Digital).

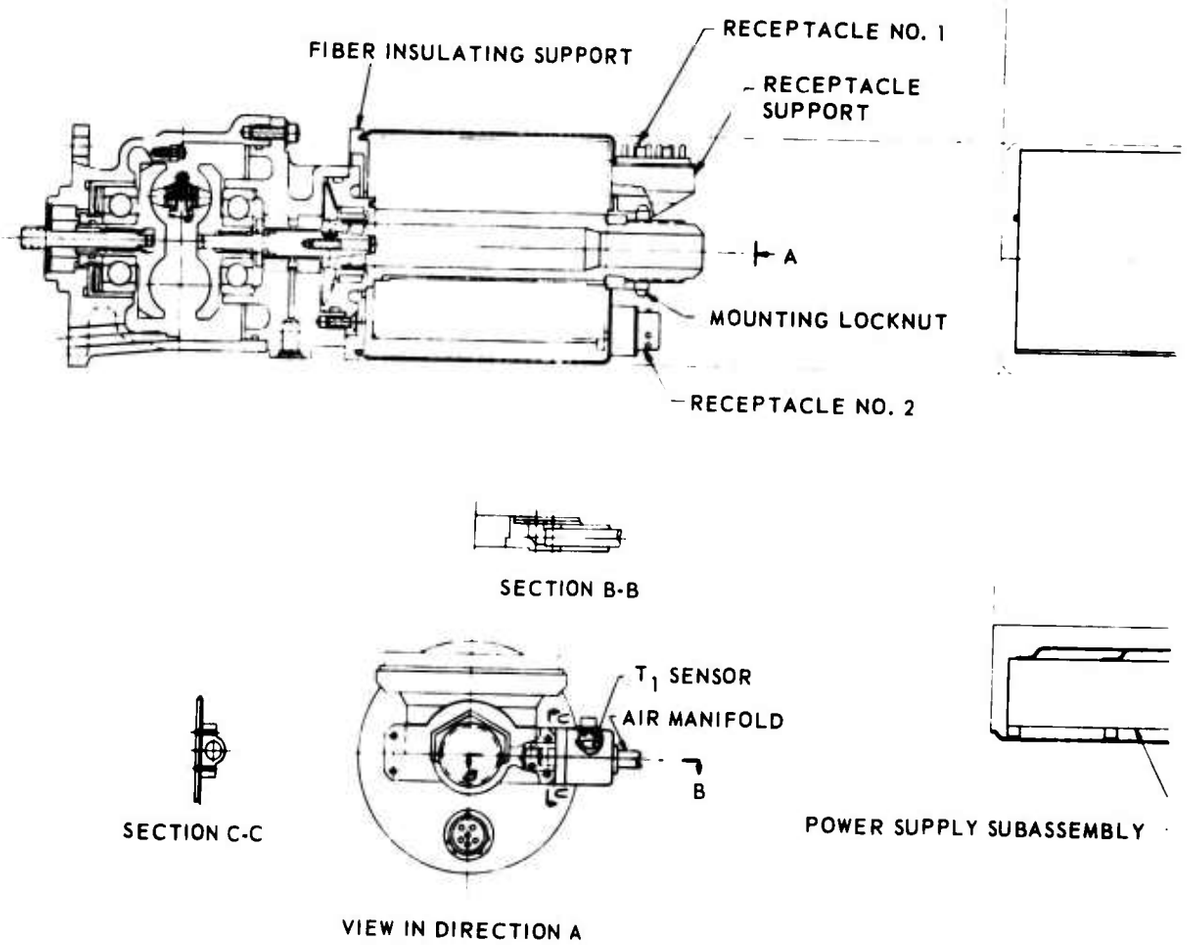

Figure 44. Analog Computer Assembly.

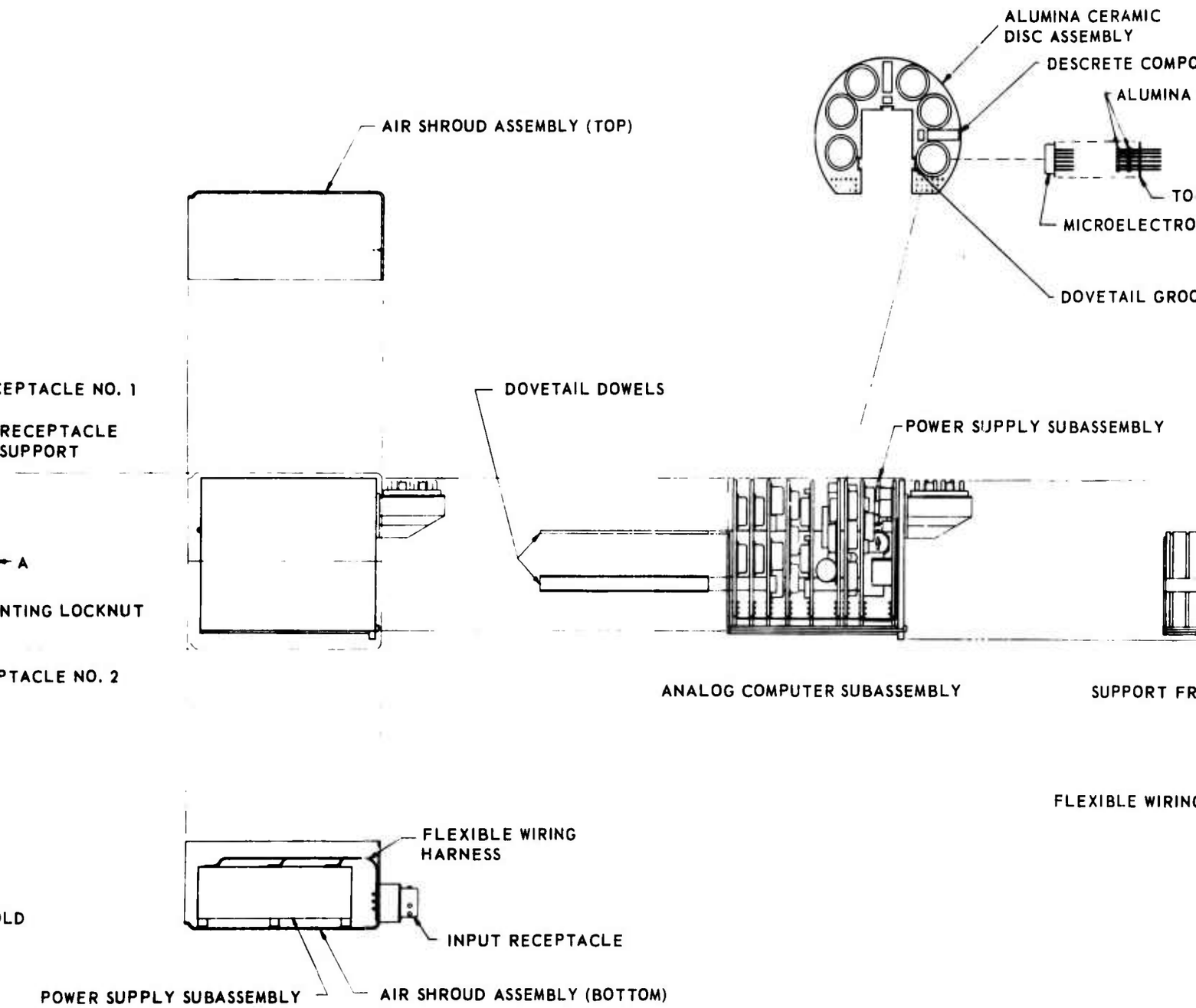
ALUMINA CERAMIC
DISC ASSEMBLY
DESCRETE COMPO
ALUMINA
TO
MICROELECTRO
DOVETAIL GROO
AIR SHROUD ASSEMBLY (TOP)
CEPTACLE NO. 1
RECEPTACLE
SUPPORT
A
NTING LOCKNUT
PTACLE NO. 2
DOVETAIL DOWELS
POWER SUPPLY SUBASSEMBLY
ANALOG COMPUTER SUBASSEMBLY
SUPPORT FR
FLEXIBLE WIRING
FLEXIBLE WIRING
HARNESS
INPUT RECEPTACLE
OLD
POWER SUPPLY SUBASSEMBLY
AIR SHROUD ASSEMBLY (BOTTOM)

mbly.

A

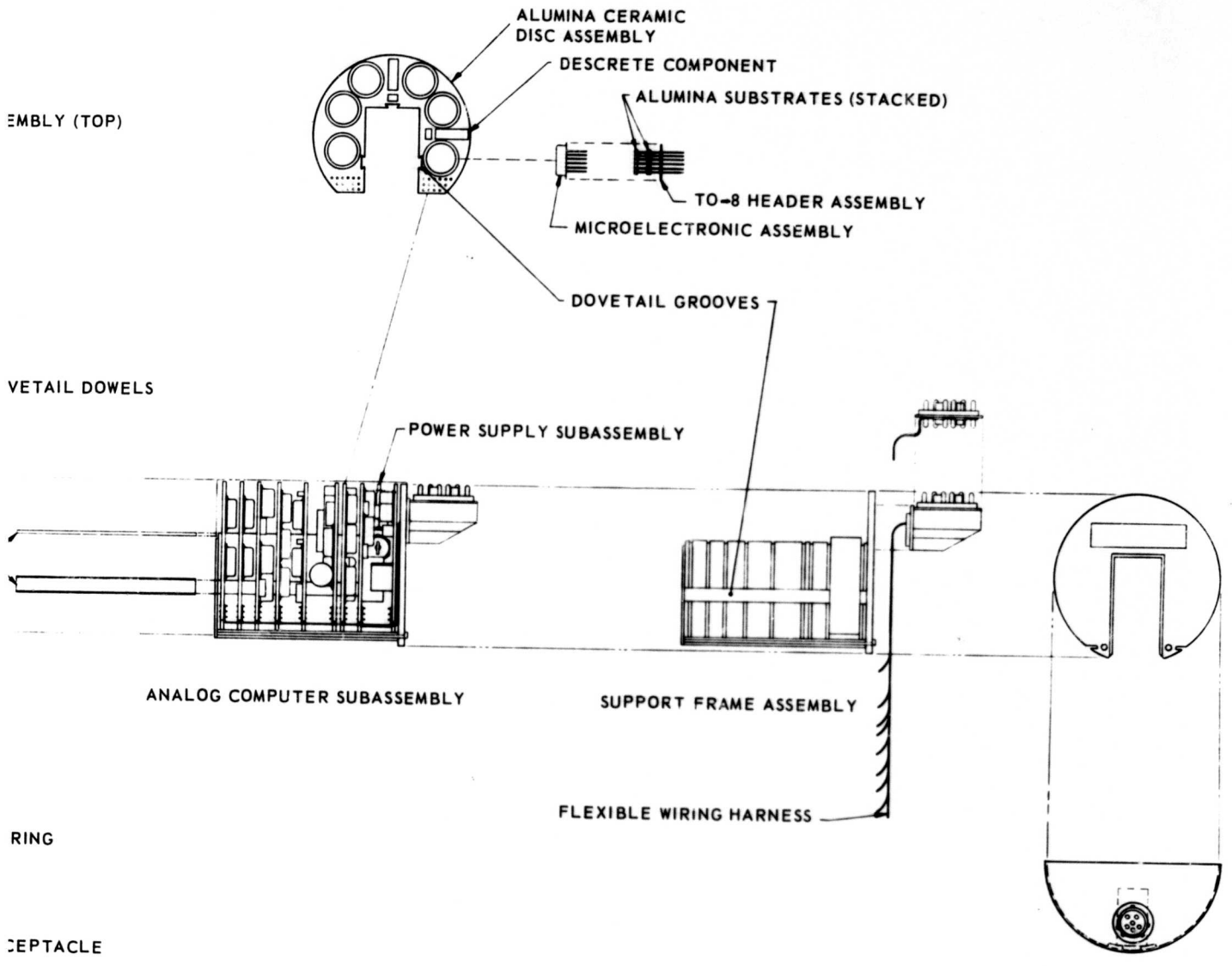

EMBLY (TOP)

VETAIL DOWELS

RING

CEPTACLE

MBLY (BOTTOM)

B

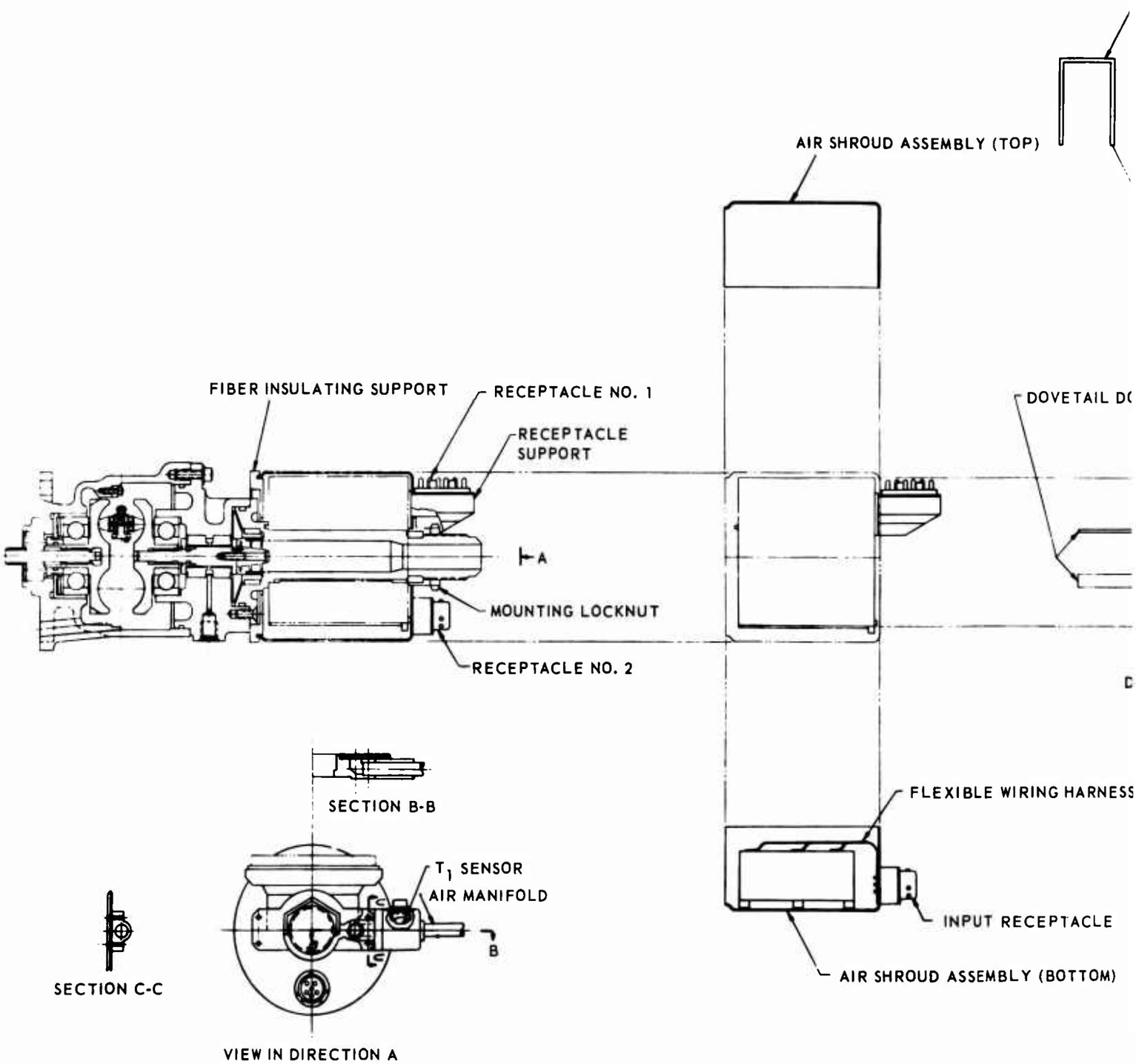

Figure 45. Digital Computer Assembly.

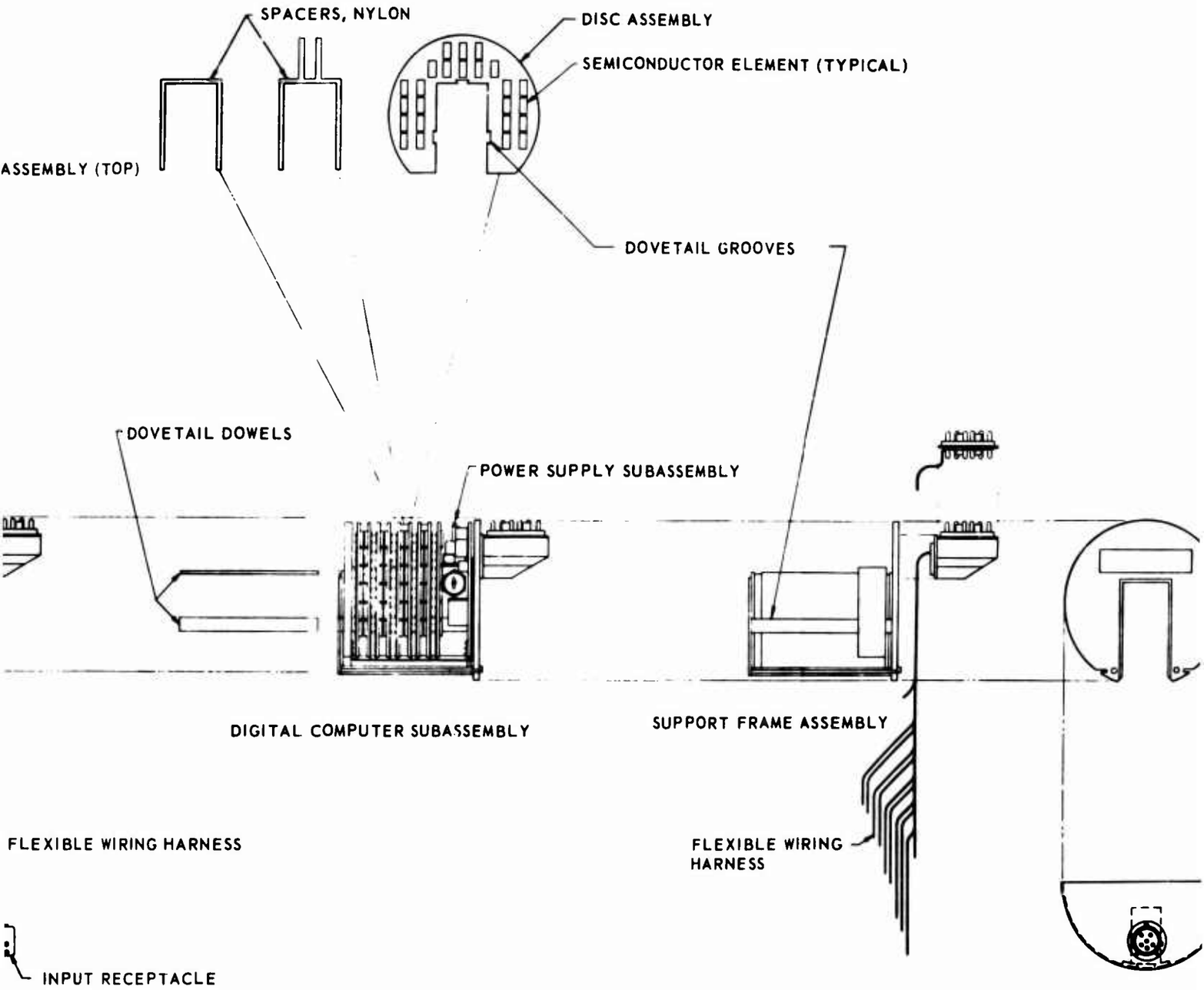
SPACERS, NYLON
DISC ASSEMBLY
SEMICONDUCTOR ELEMENT (TYPICAL)
ASSEMBLY (TOP)
DOVETAIL GROOVES
DOVETAIL DOWELS
POWER SUPPLY SUBASSEMBLY
DIGITAL COMPUTER SUBASSEMBLY
SUPPORT FRAME ASSEMBLY
FLEXIBLE WIRING HARNESS
FLEXIBLE WIRING HARNESS
INPUT RECEPTACLE
OUD ASSEMBLY (BOTTOM)

BLANK PAGE

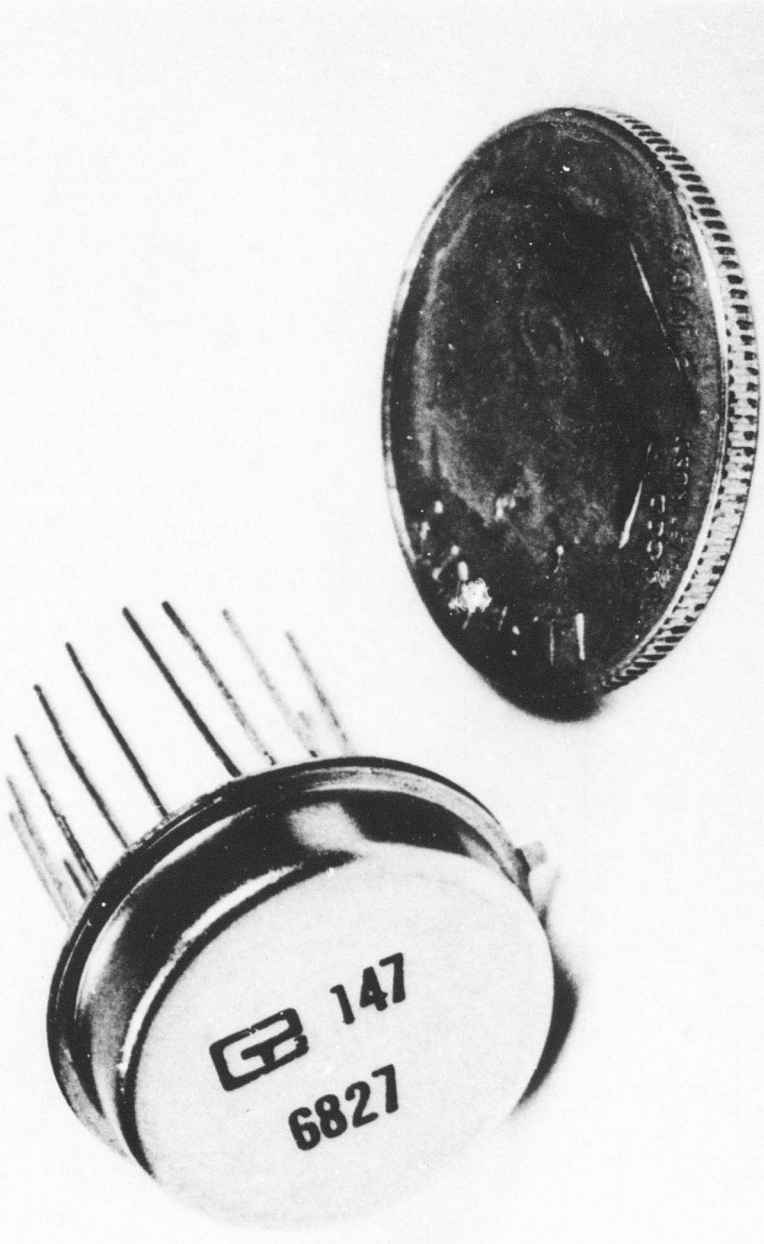

Figure 46. TO-8 Round Package.

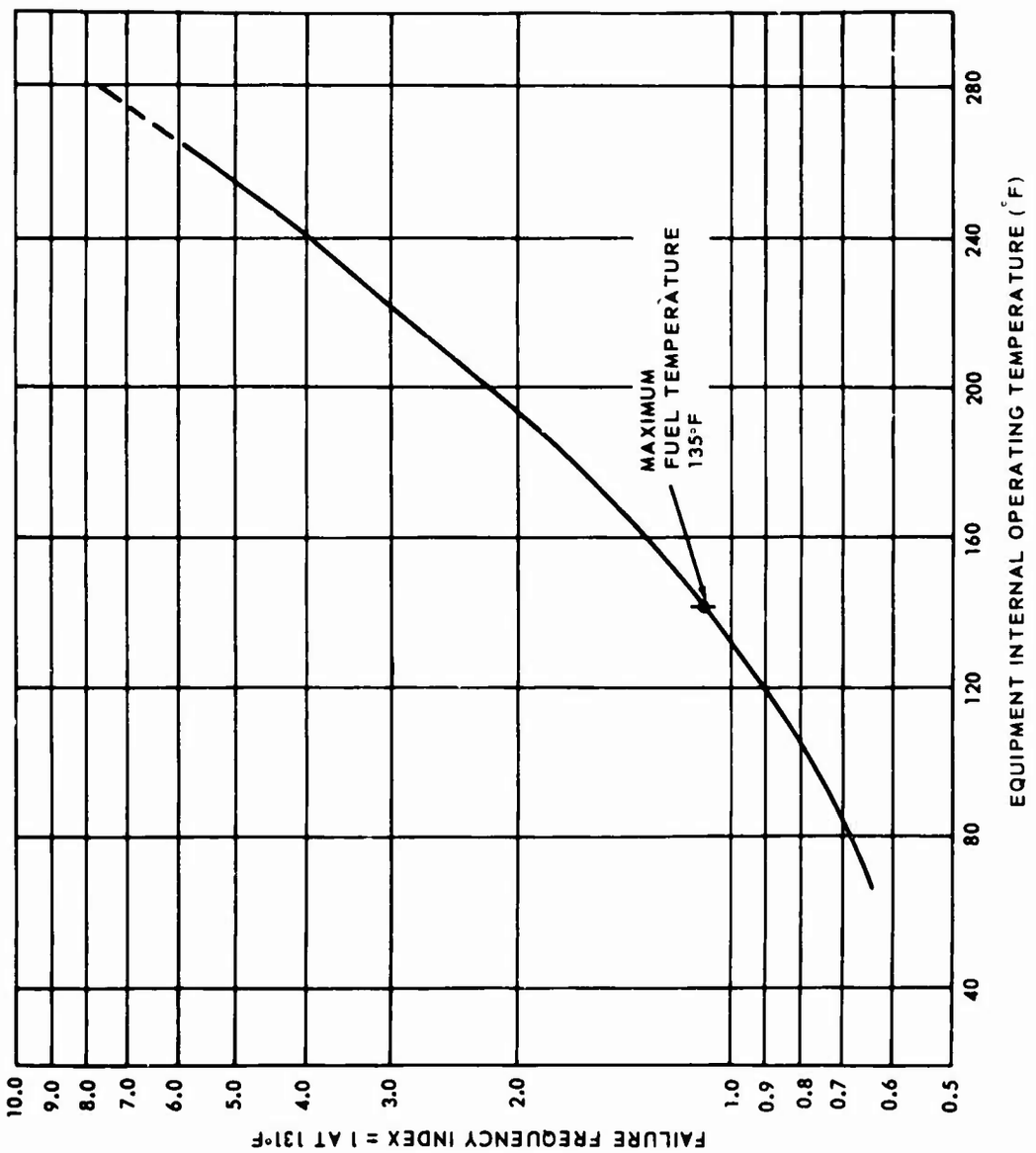

Figure 47. Equipment Reliability Versus Temperature.

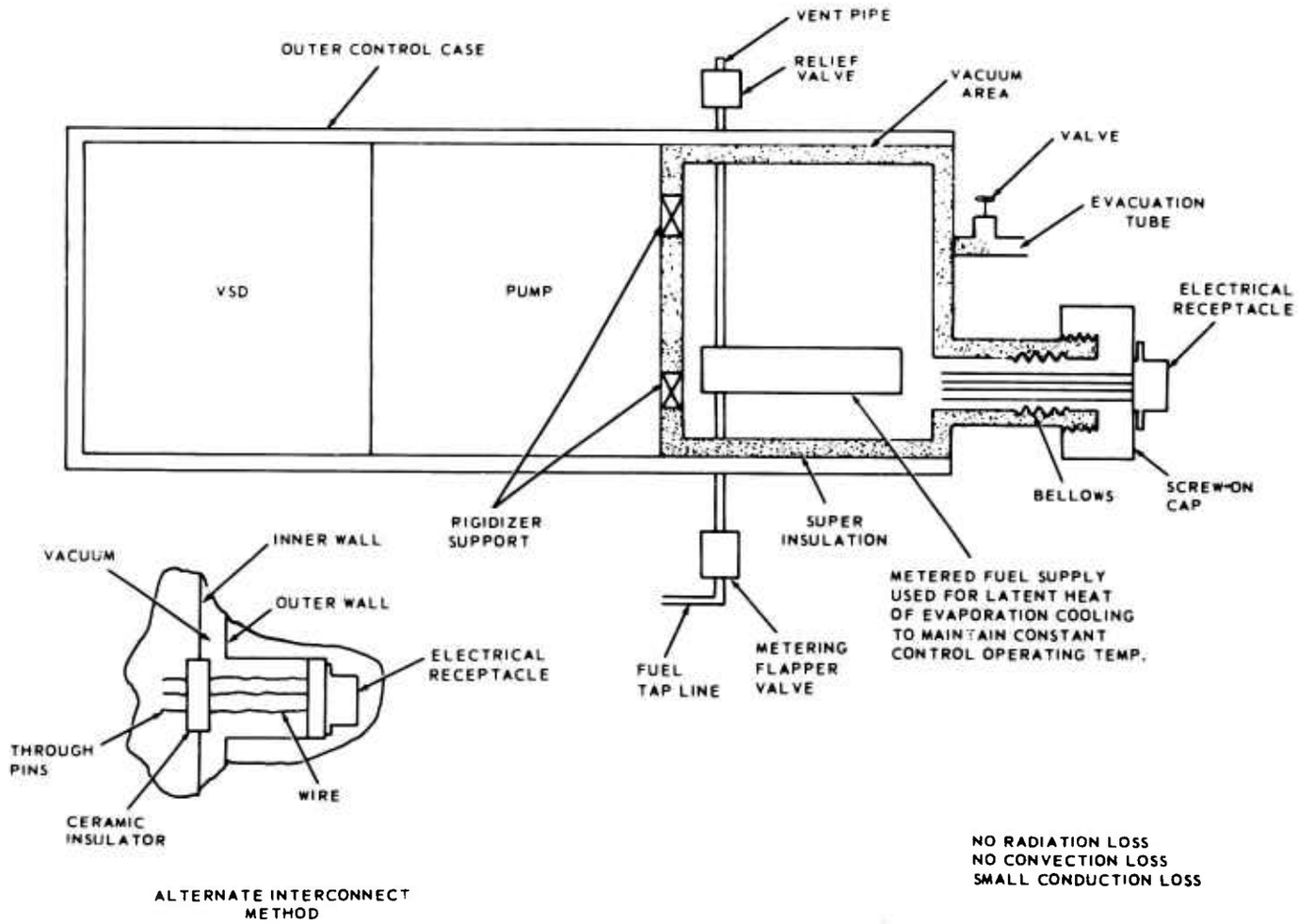

Figure 48. Vacuum-Jacketed Thermal Insulation.

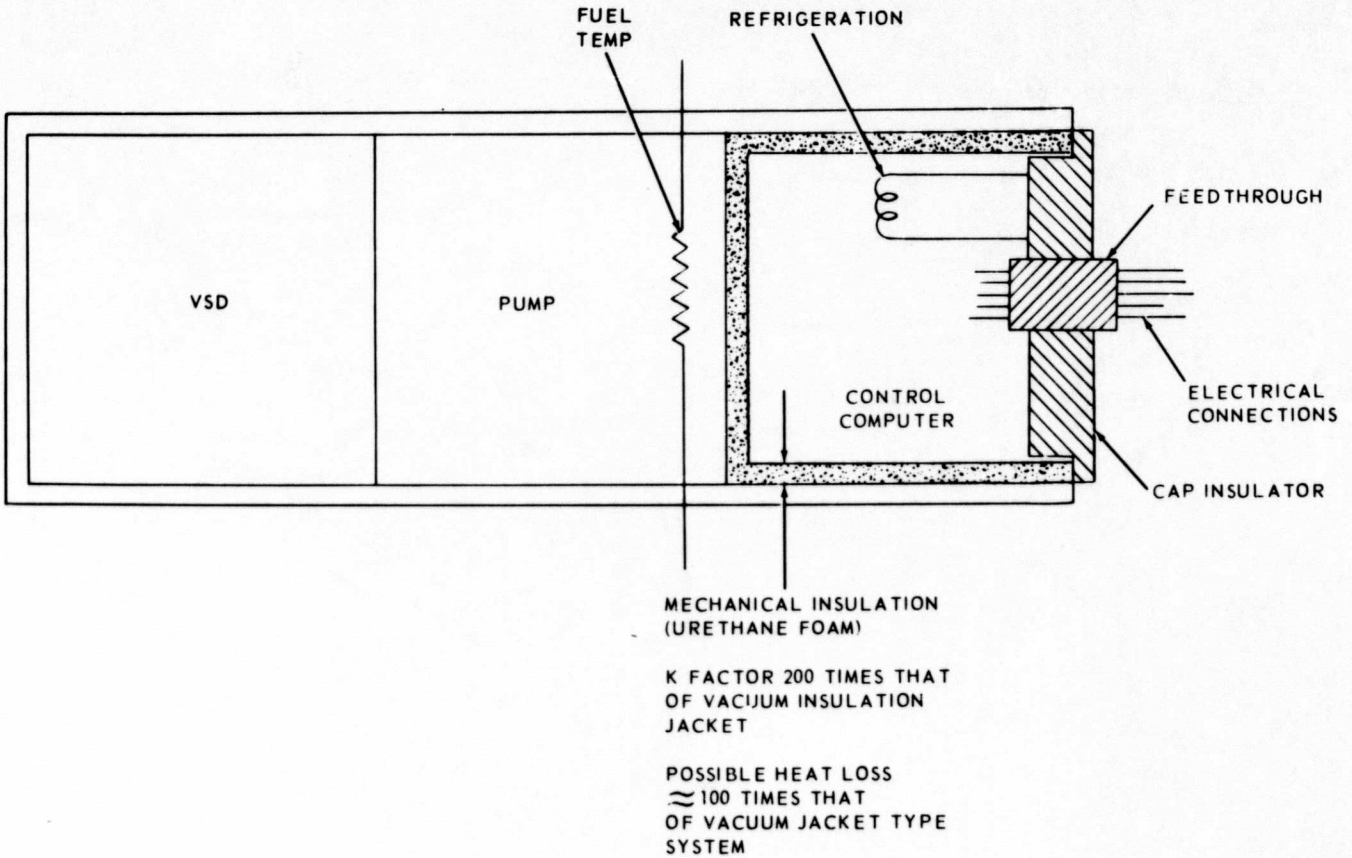

Figure 49. Mechanical Insulation.

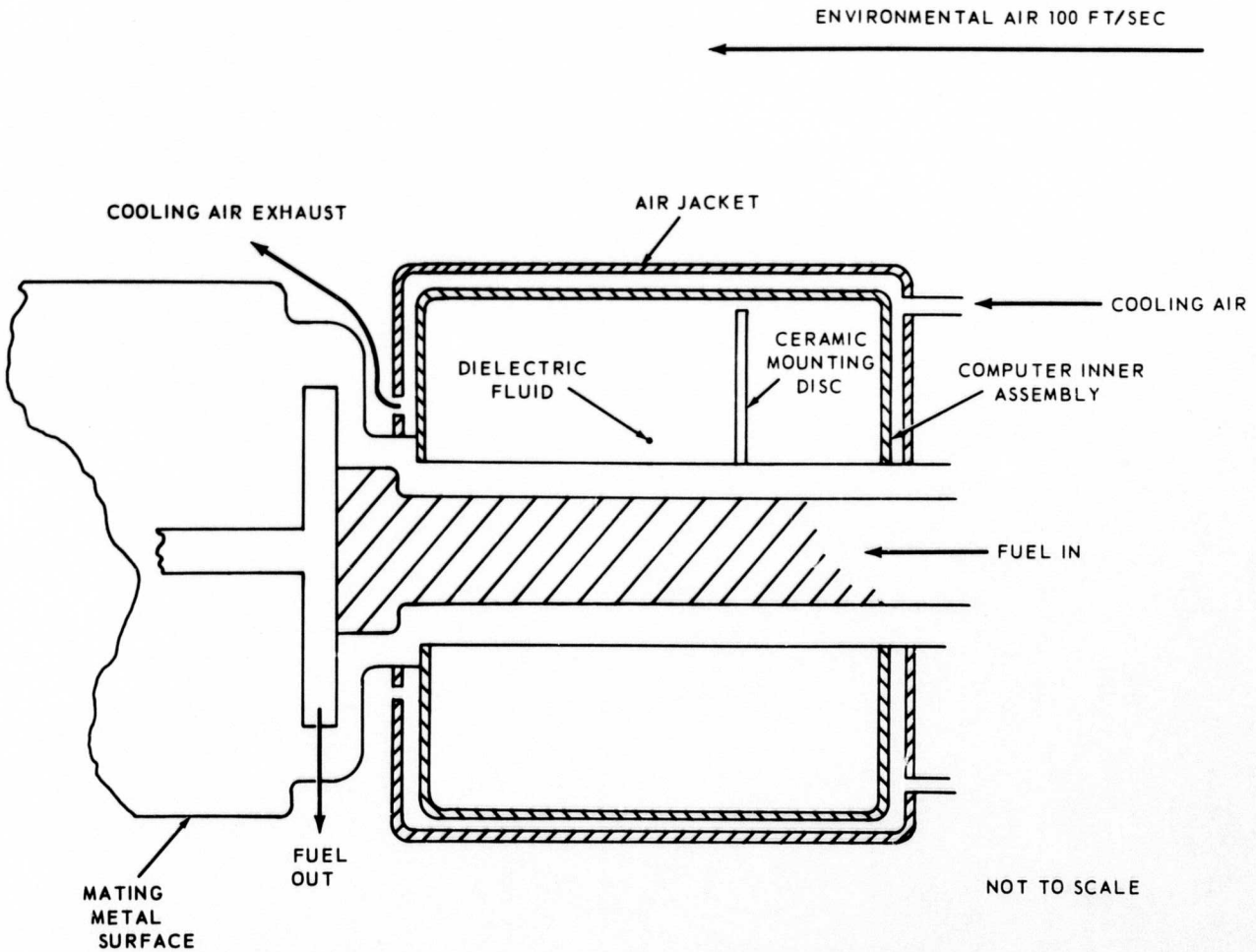

Figure 50. Combined Air, Fuel, and Dielectric Cooling System.

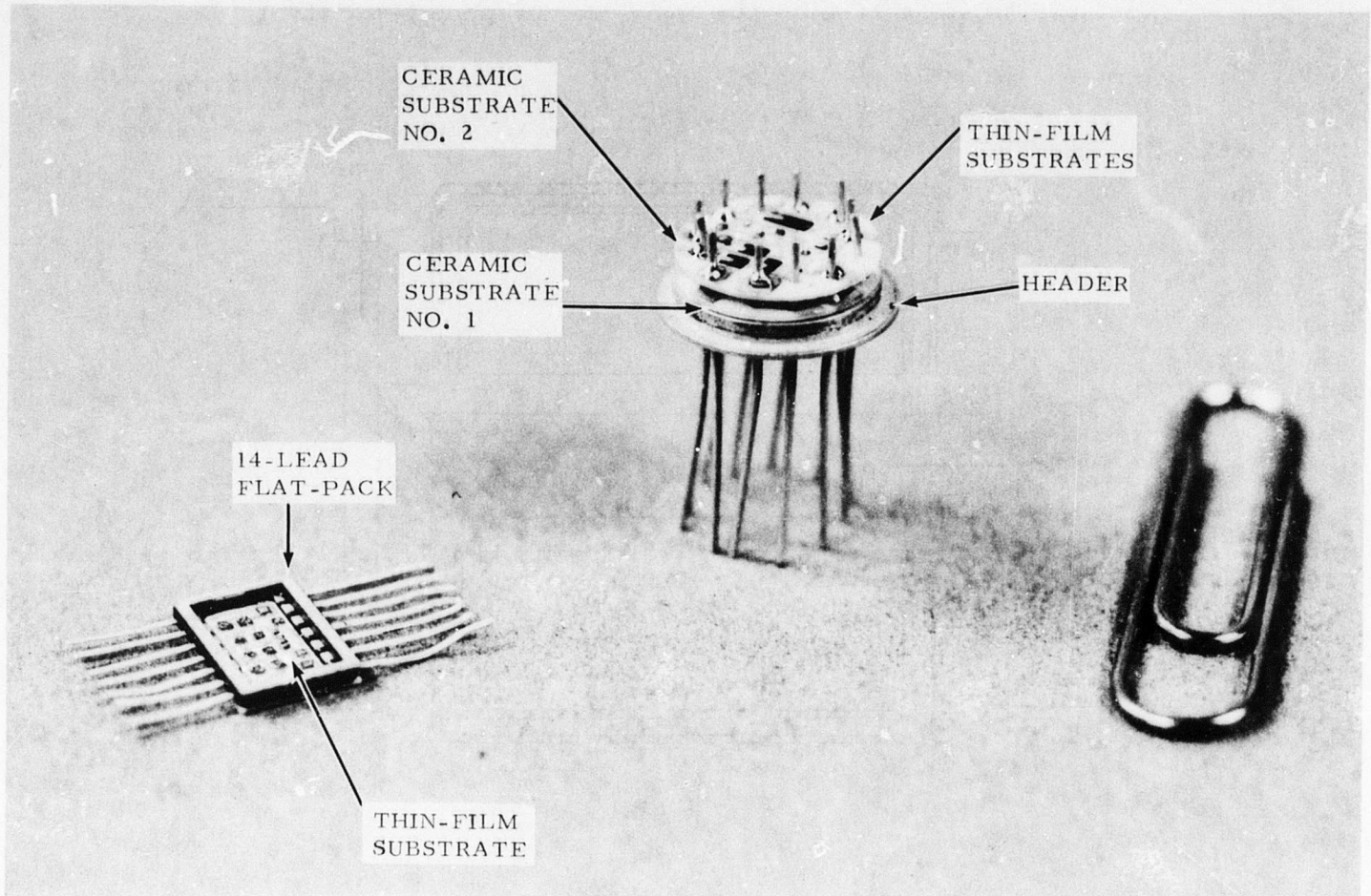

Figure 51. Flat-Pack and Round Can TO-8 With Stacked Substrates.

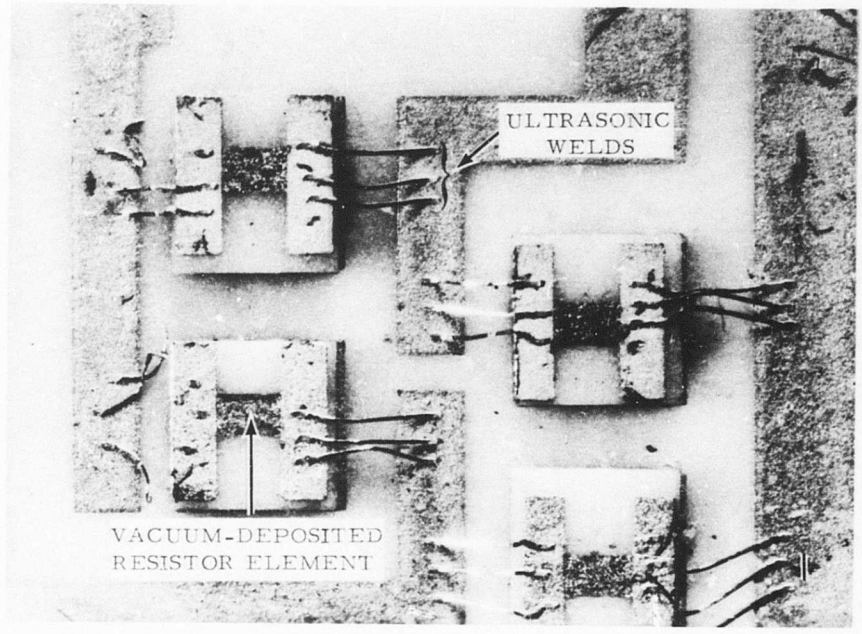

20 X MAGNIFICATION

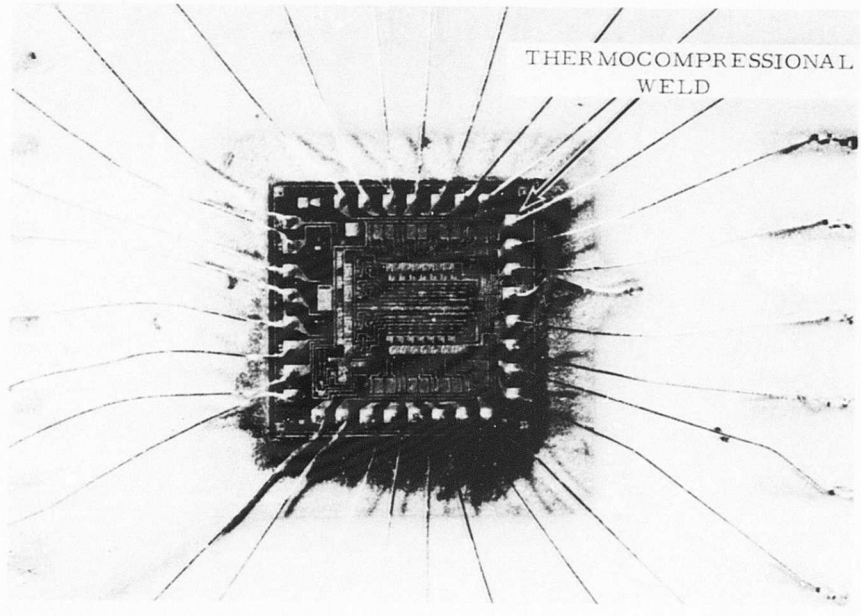

Figure 52. Thermocompressional Versus Ultrasonic Welds.

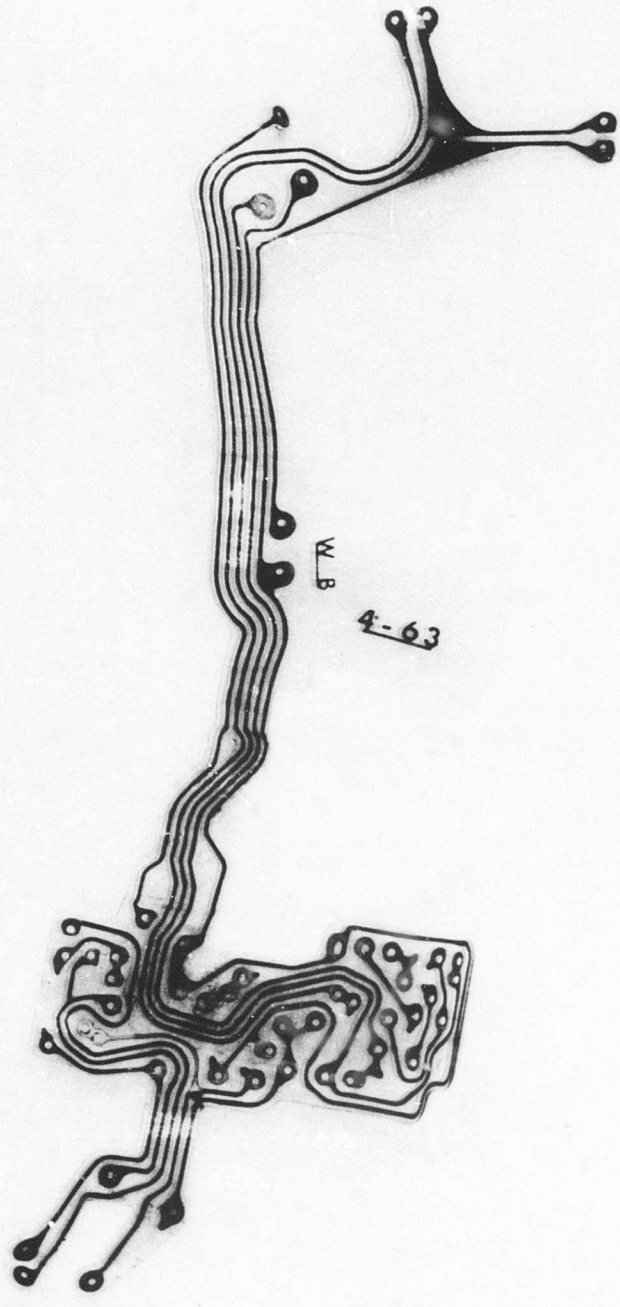

Figure 53. Flexible Wiring Harness.

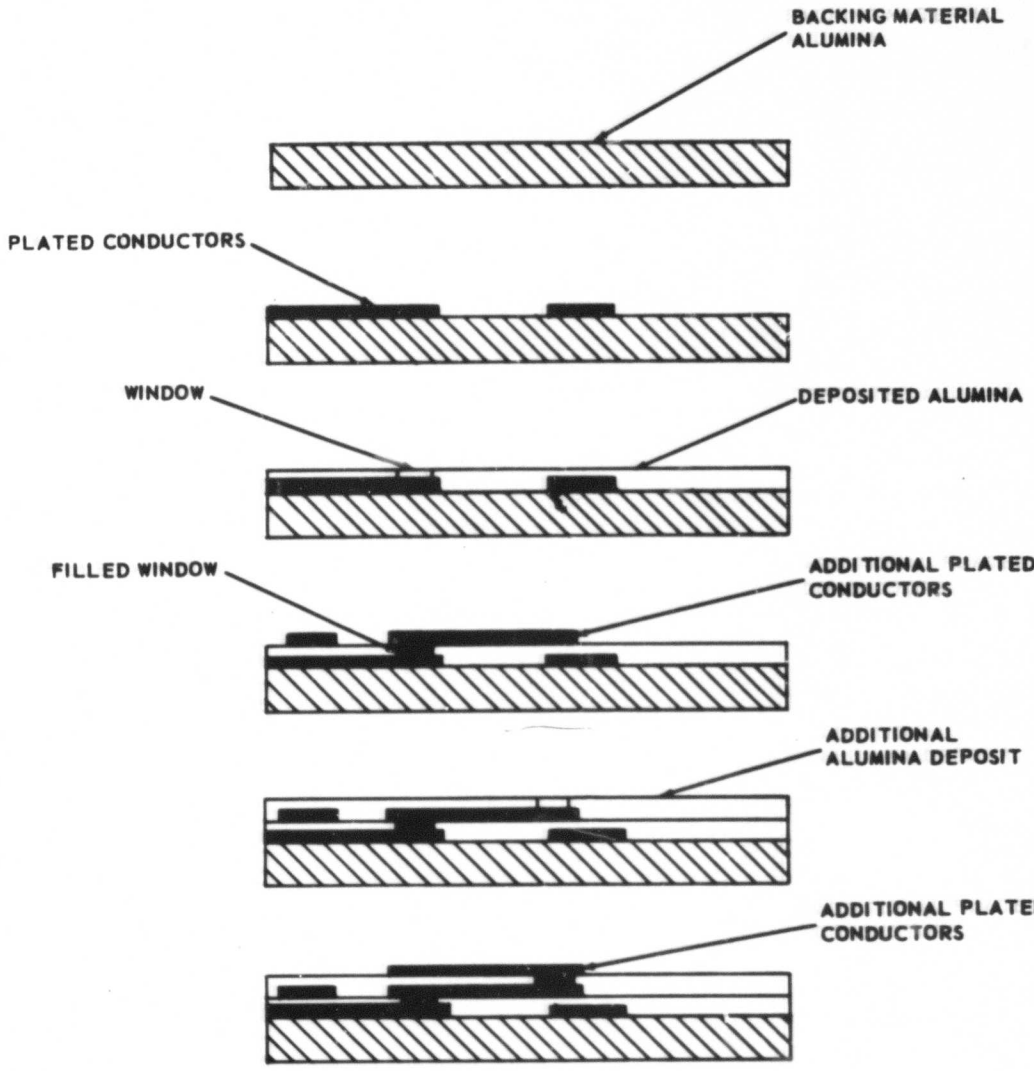

Figure 54. Multilayer Disc Construction.

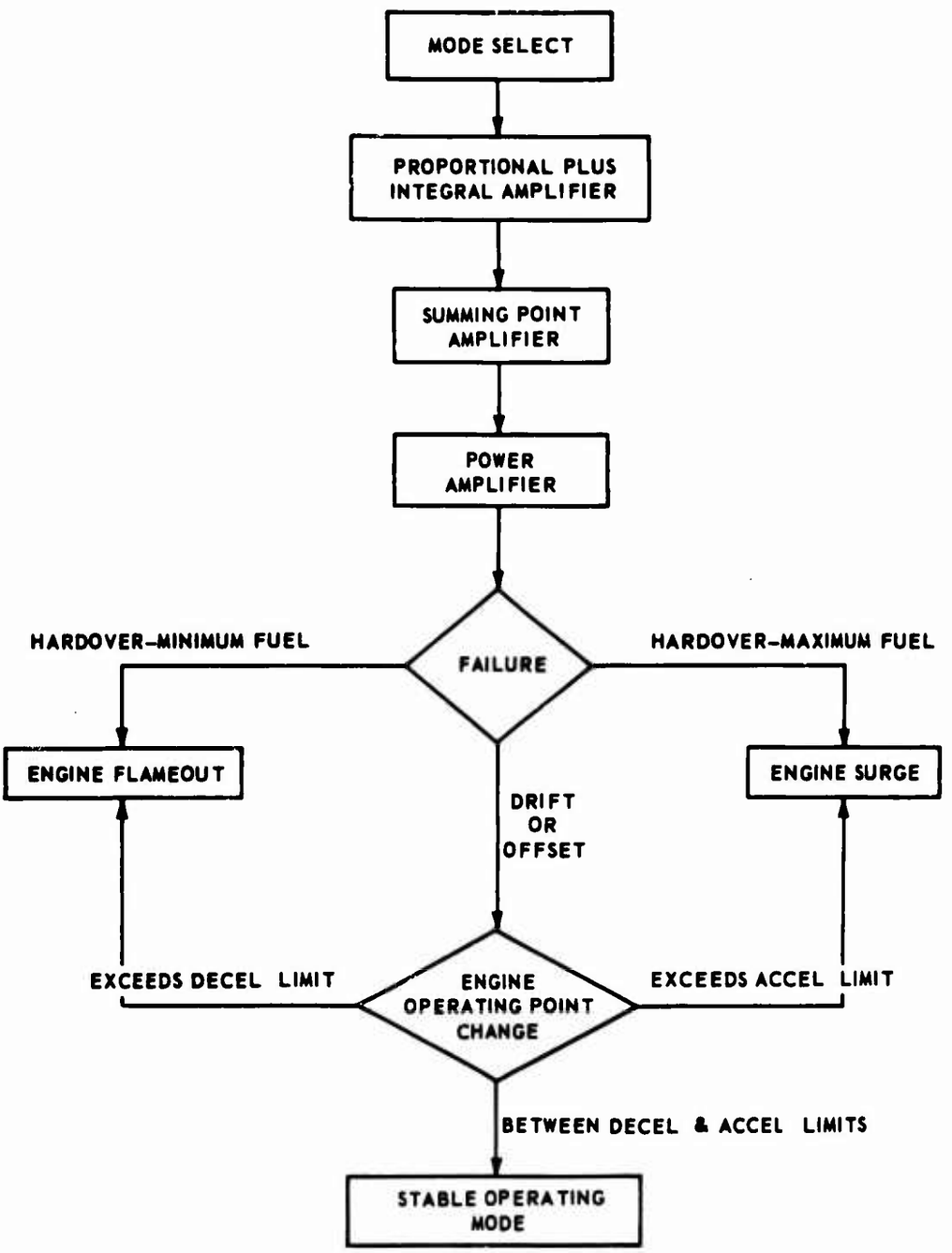

Figure 55. Failure Mode Analysis for the Mode Select and Other Independent System Functions.

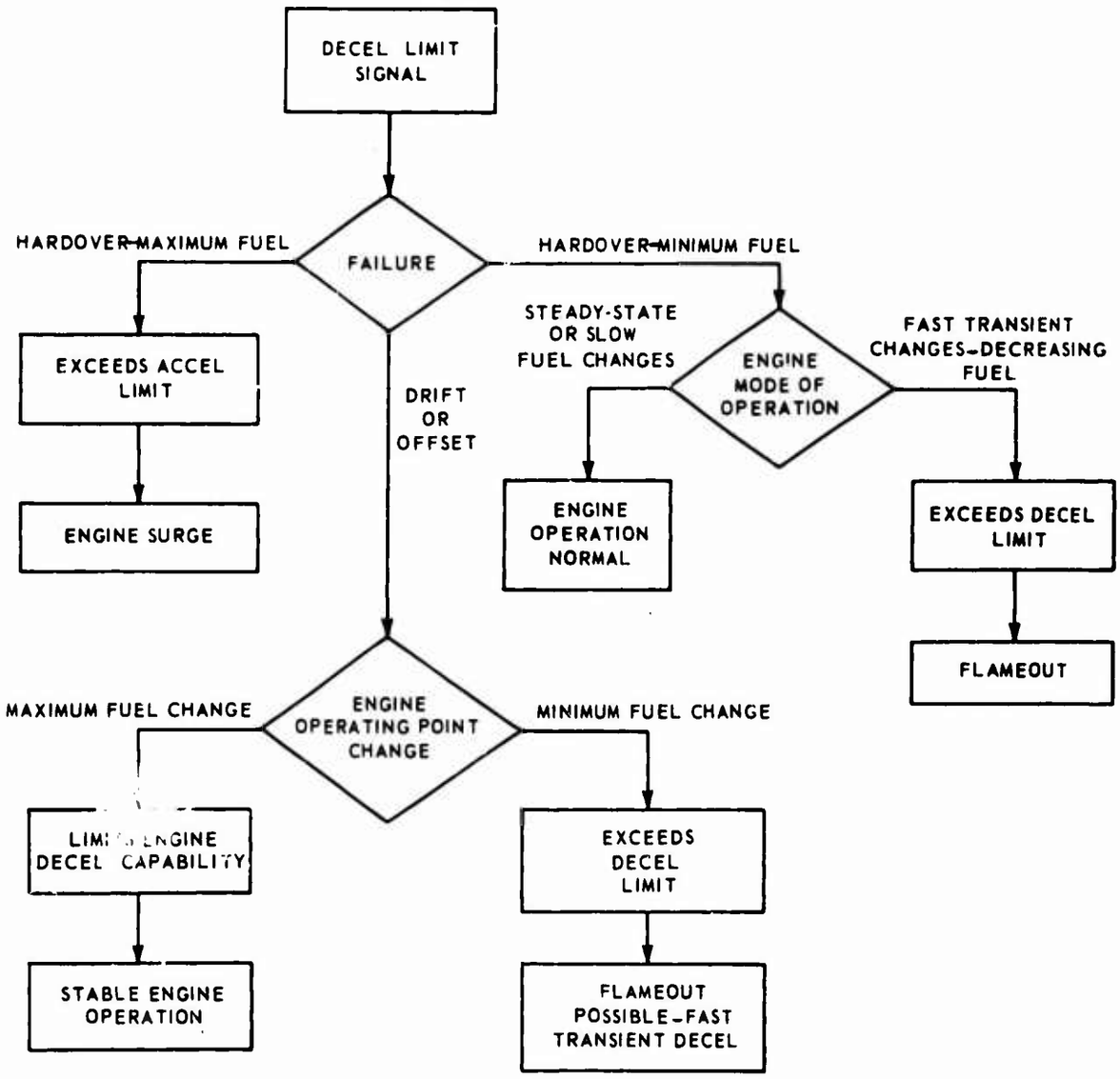

Figure 56. Failure Mode Analysis for the Deceleration Limit System Function.

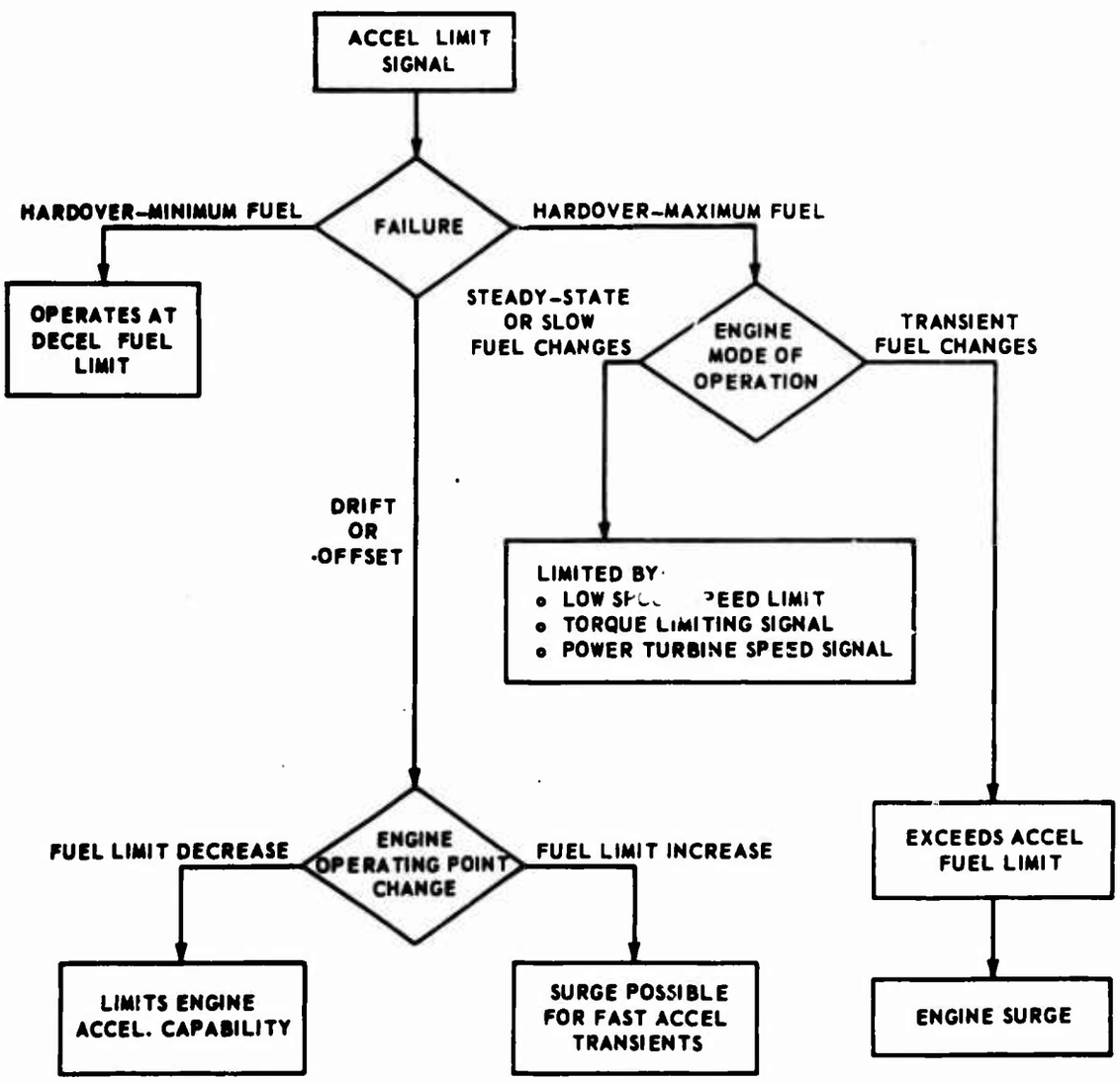

Figure 57. Failure Mode Analysis for the Acceleration Limit System Function.

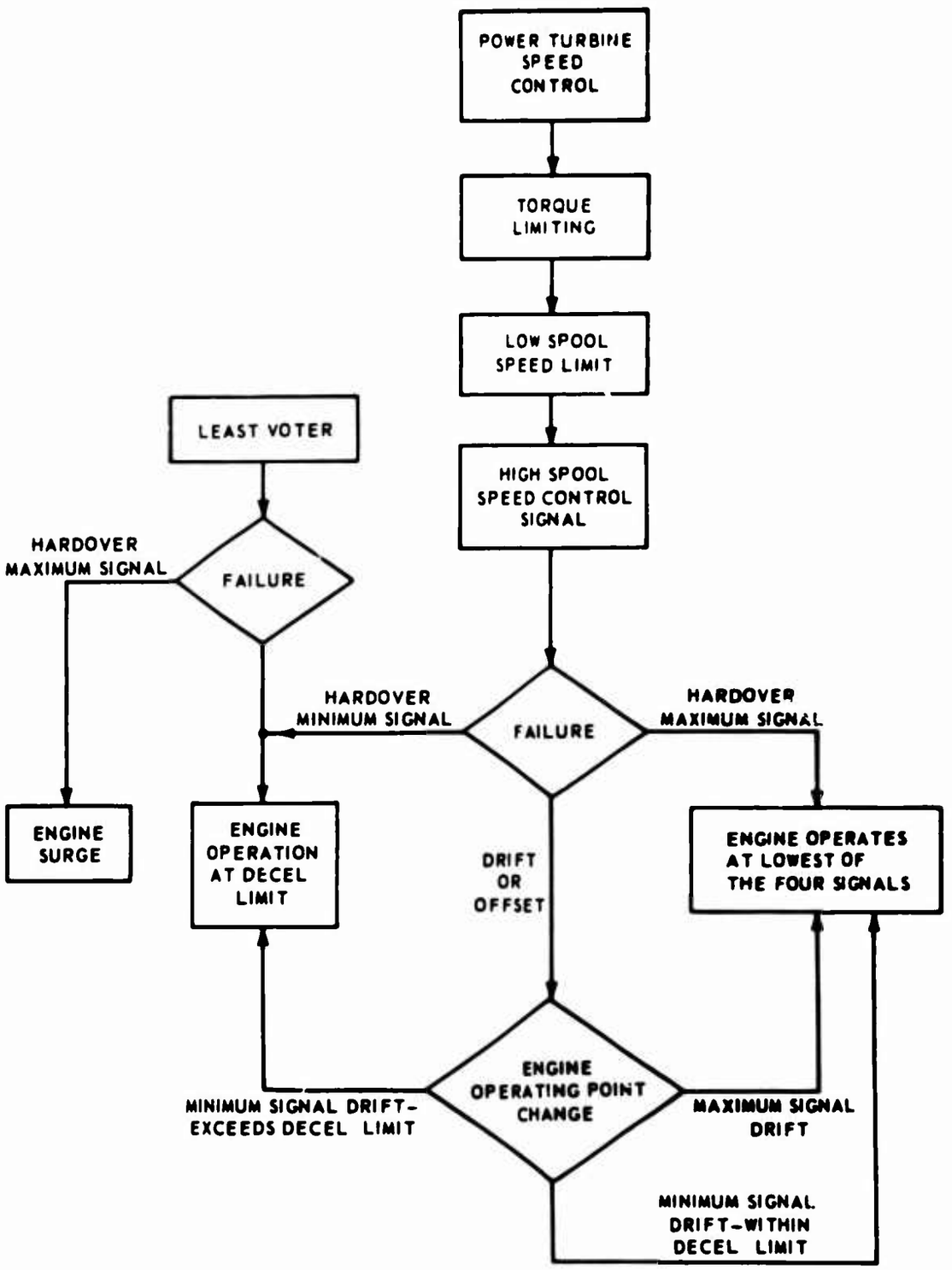

Figure 58. Failure Mode Analysis for Mode-Select-Dominated System Functions.

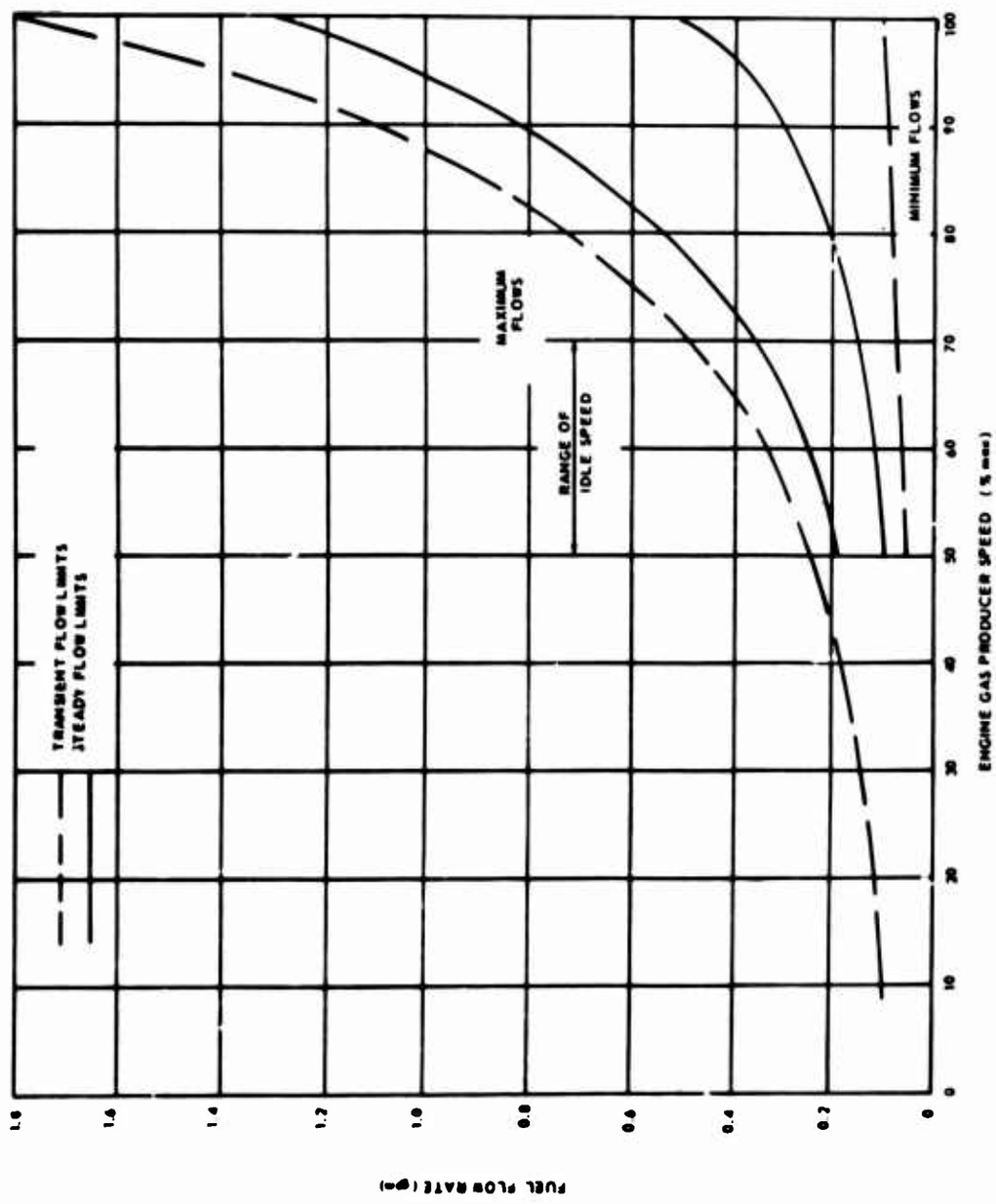

Figure 59. Fuel Pump Discharge Flow Range Versus Gas Producer Speed.

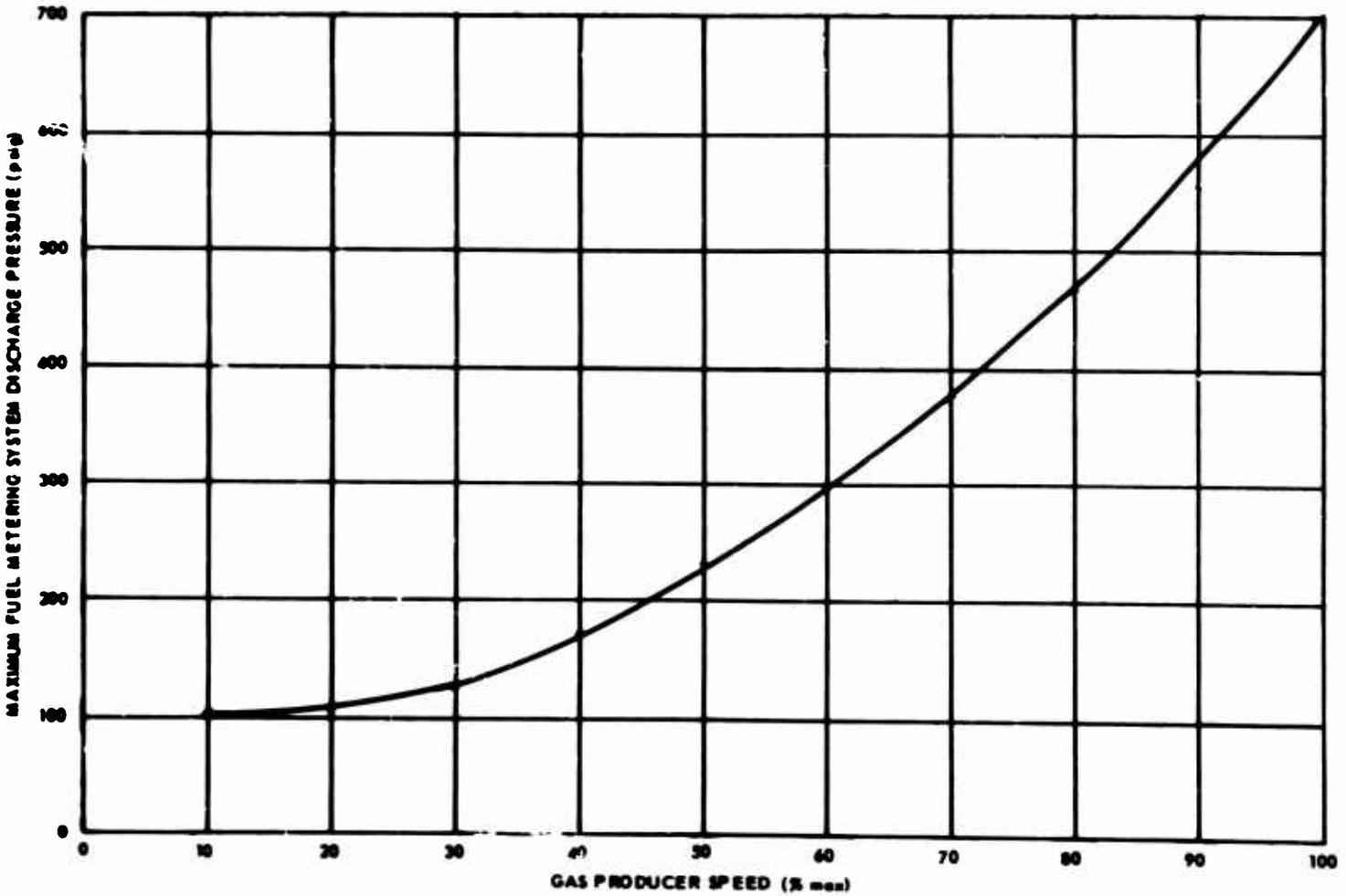

Figure 60. Maximum Required Pump Discharge Pressure Versus Gas Producer Speed.

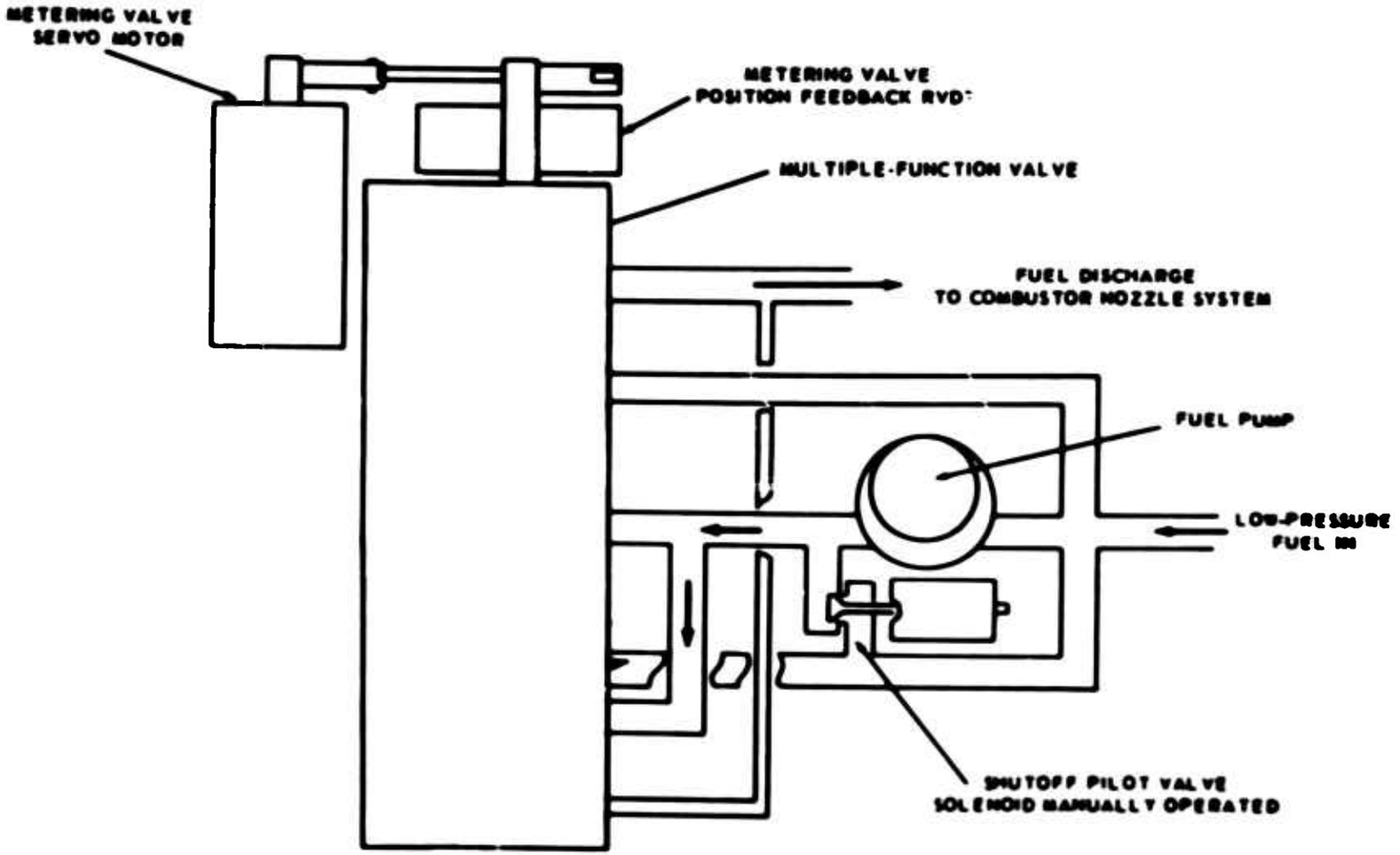

Figure 61. Schematic of Fuel Metering System No. 1.

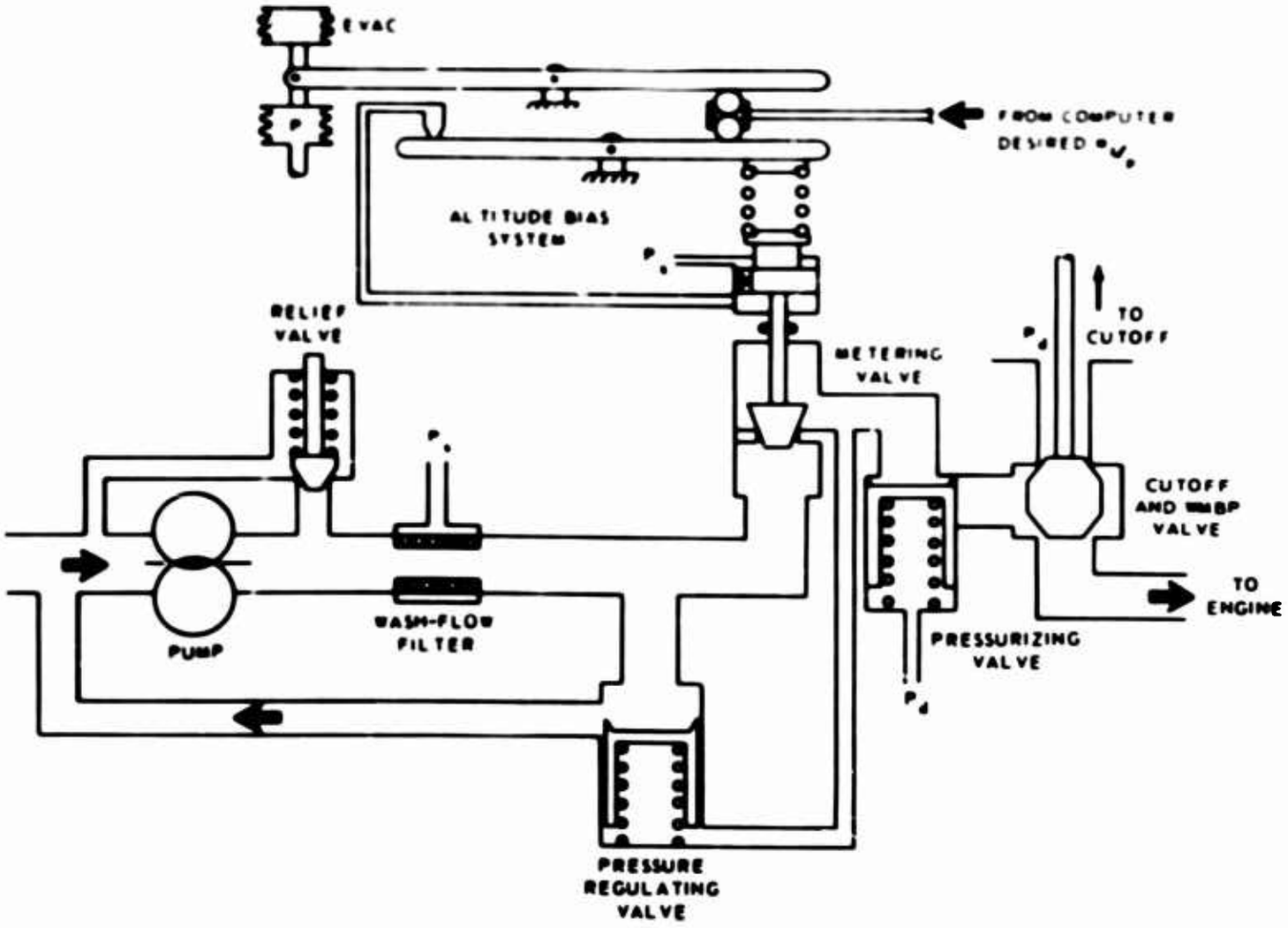

Figure 62. Schematic of Fuel Metering System Functions.

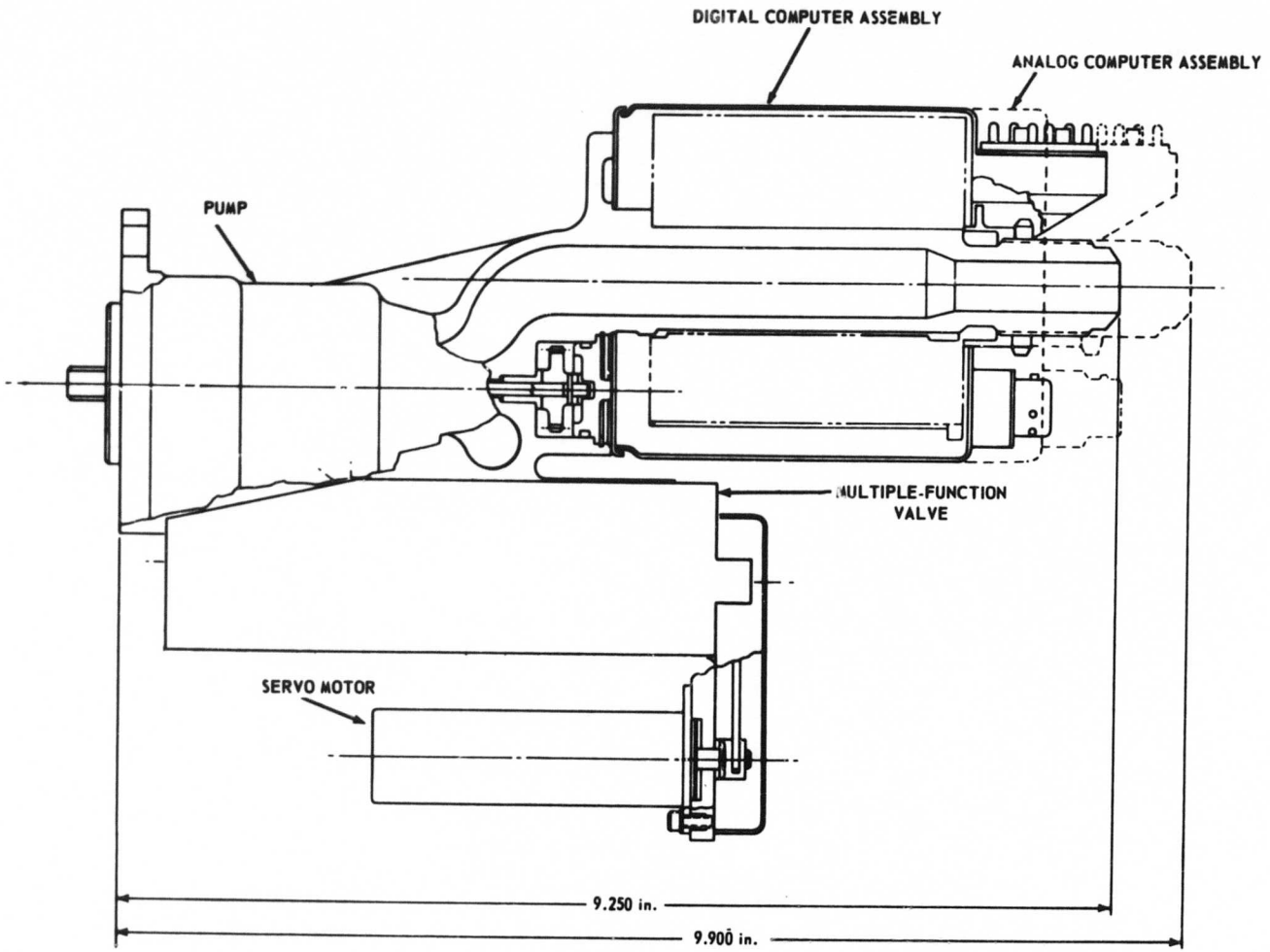

Figure 63. Fuel Metering Section Design, System No. 1.

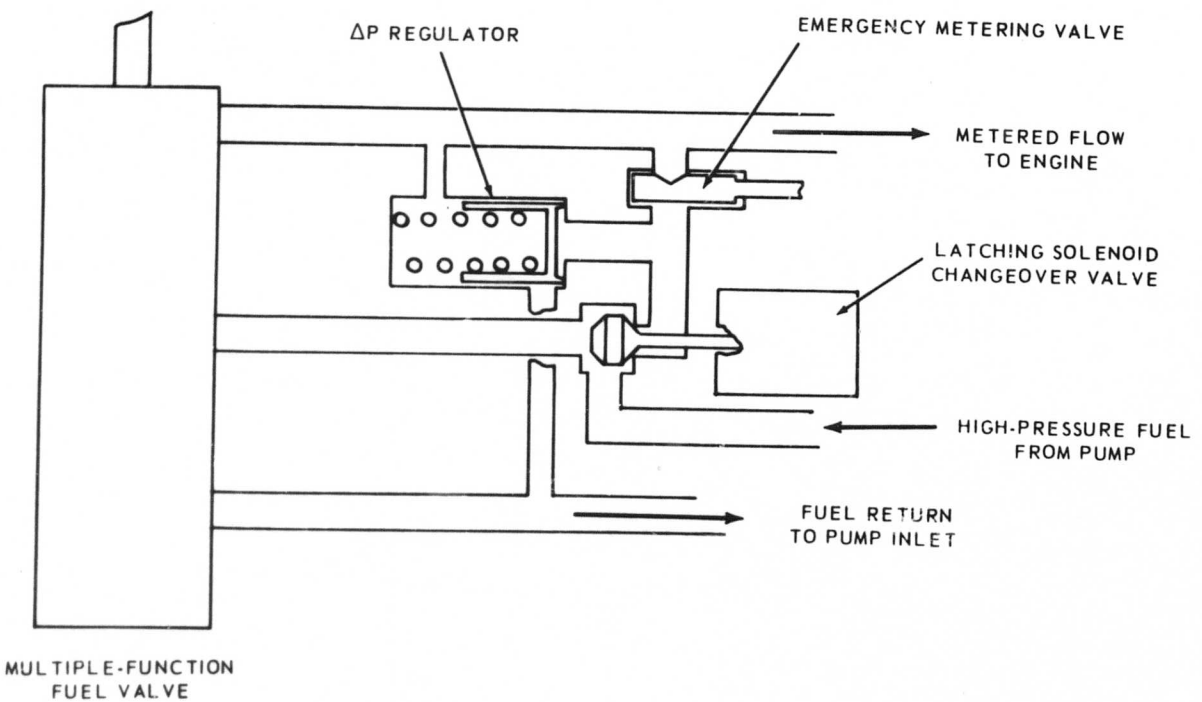

Figure 64. Schematic of Emergency Manual Control, System No. 1.

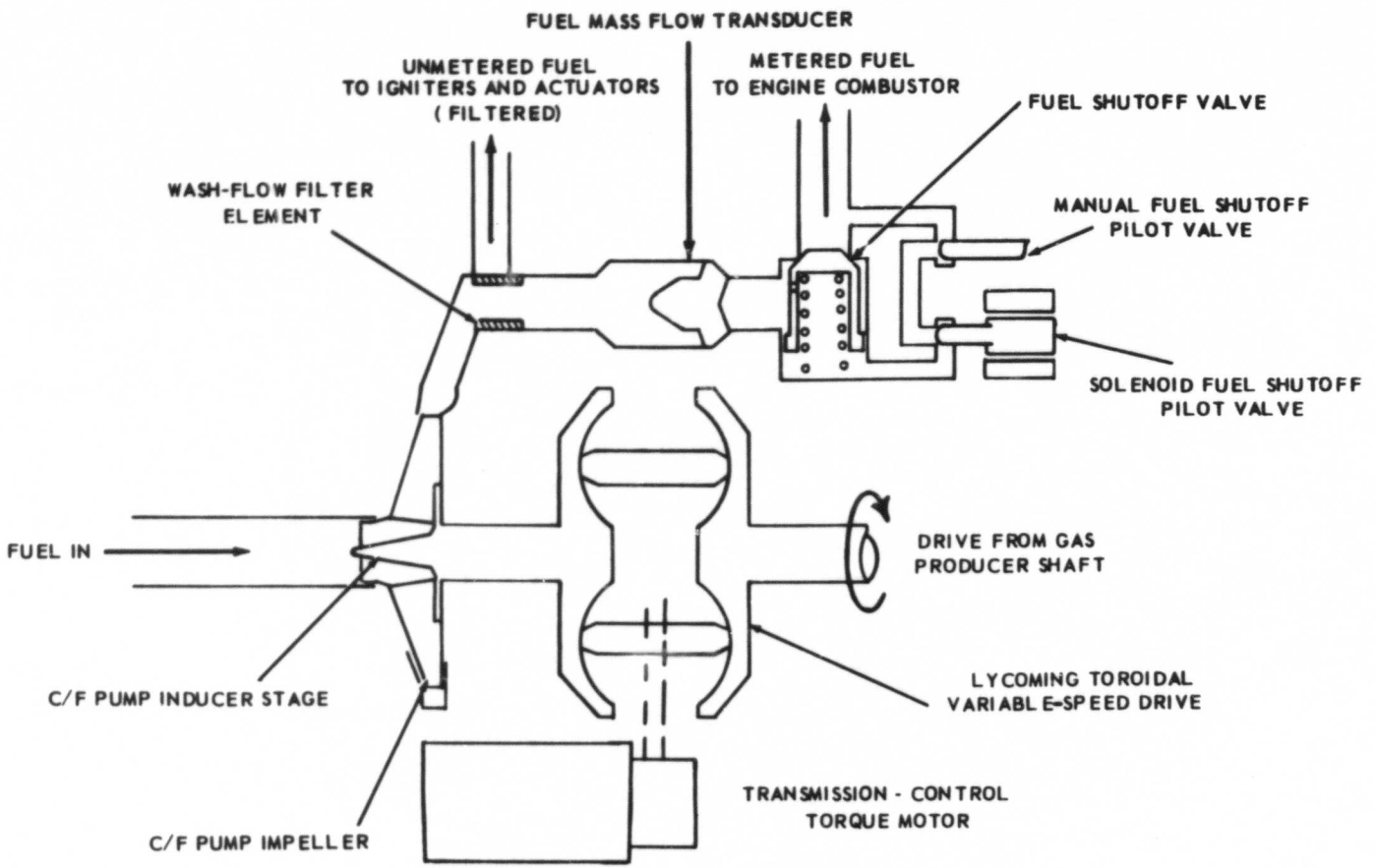

Figure 65. Schematic of Fuel Metering, System No. 2.

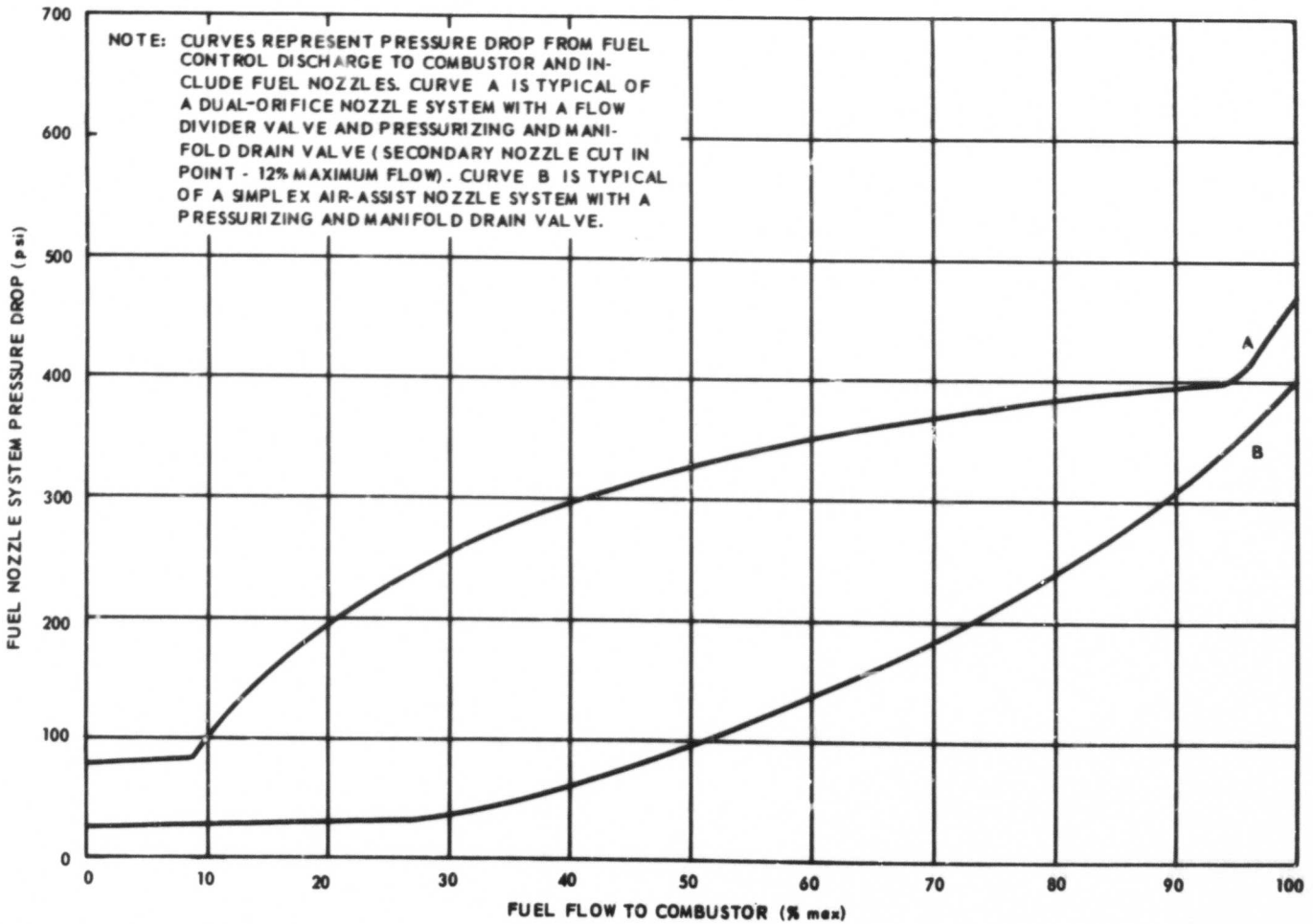

Figure 66. Fuel Nozzle System Pressure Drops Versus Flow.

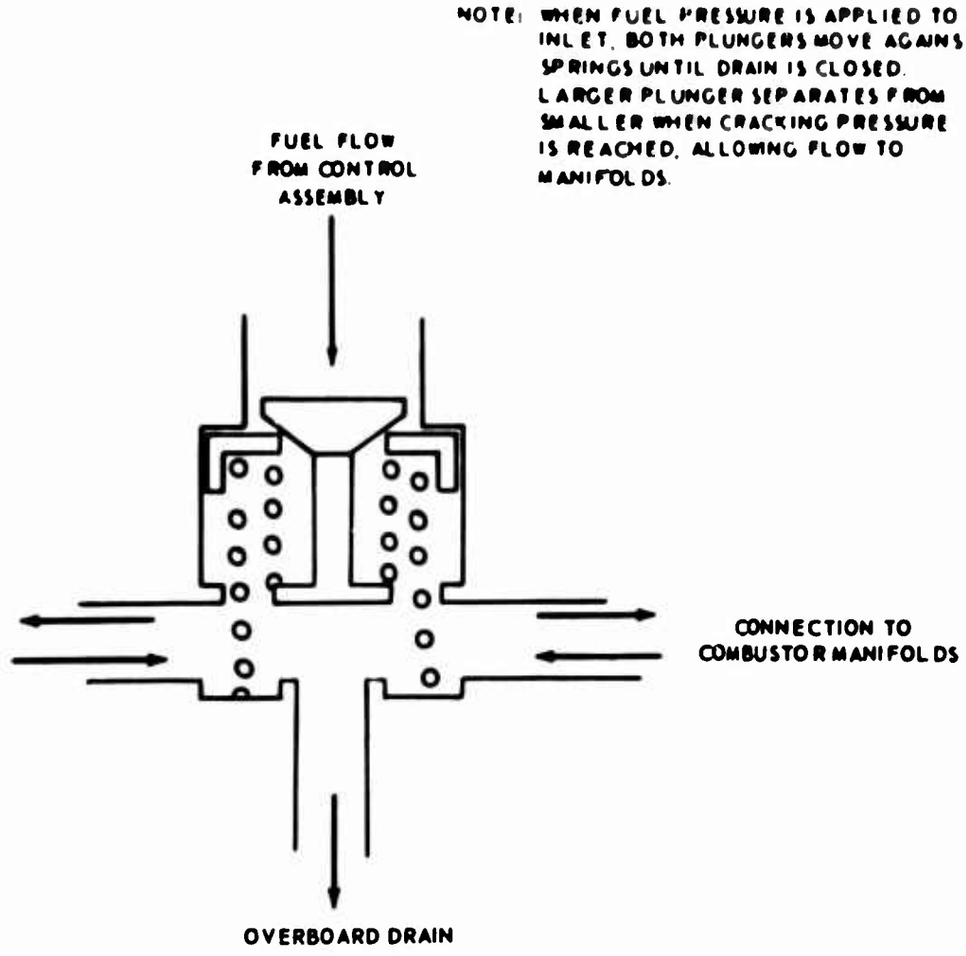

Figure 67. Schematic of Fuel Pressurizing and Manifold Drain Valve.

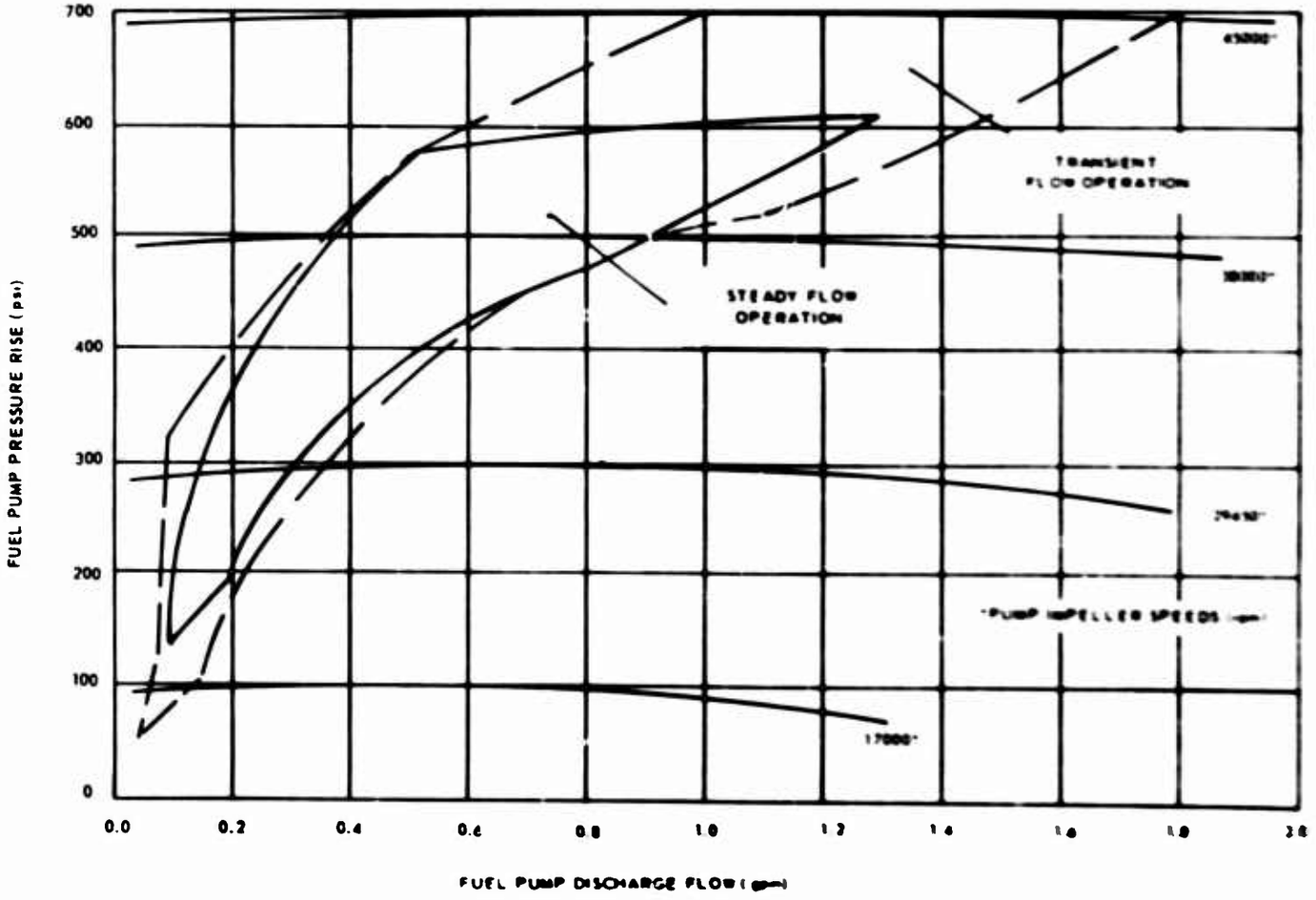

Figure 68. Centrifugal Fuel Pump Pressure Rise Versus Flow and Speed.

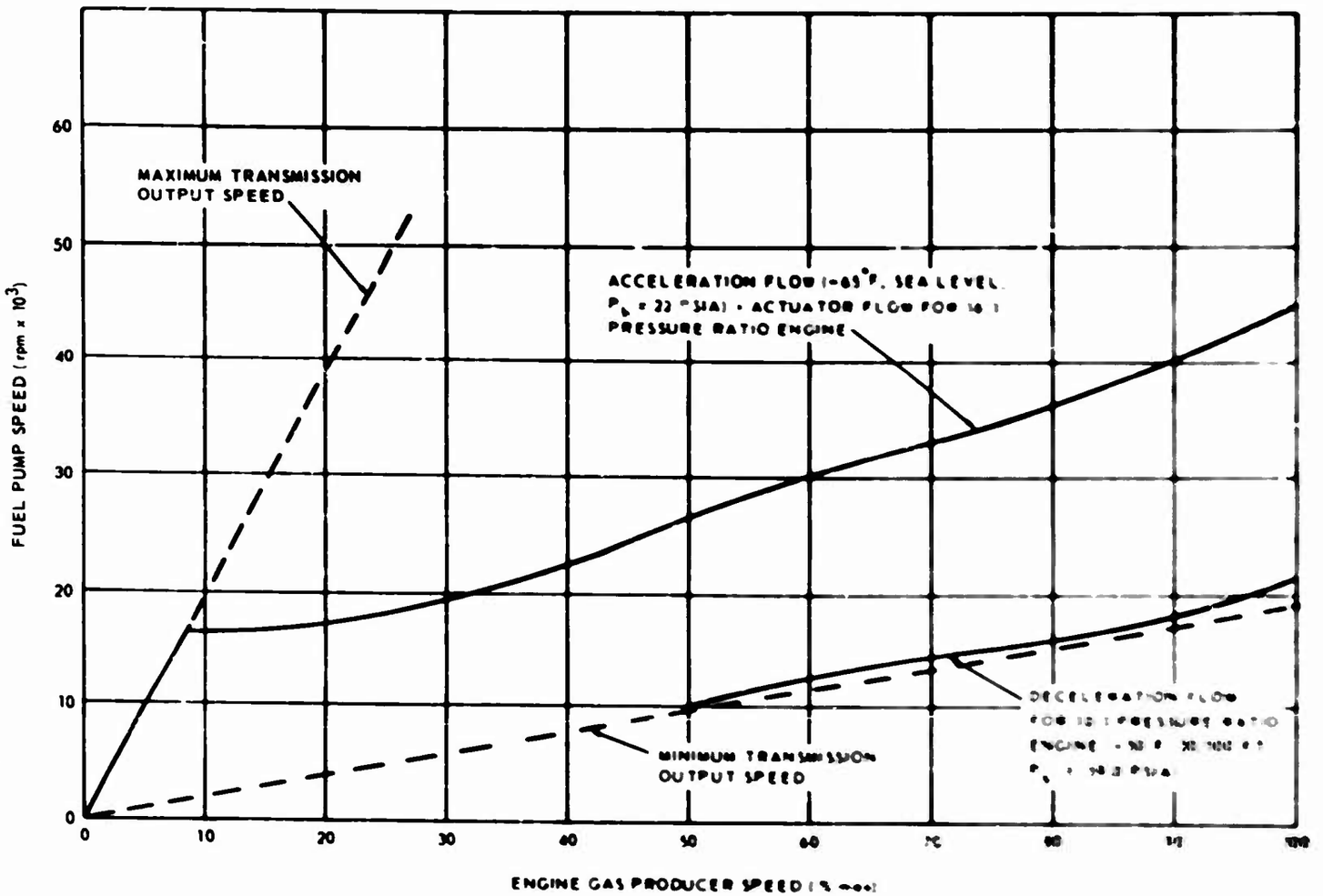

Figure 69. Fuel Pump Speed Range Versus Gas Producer Speed.

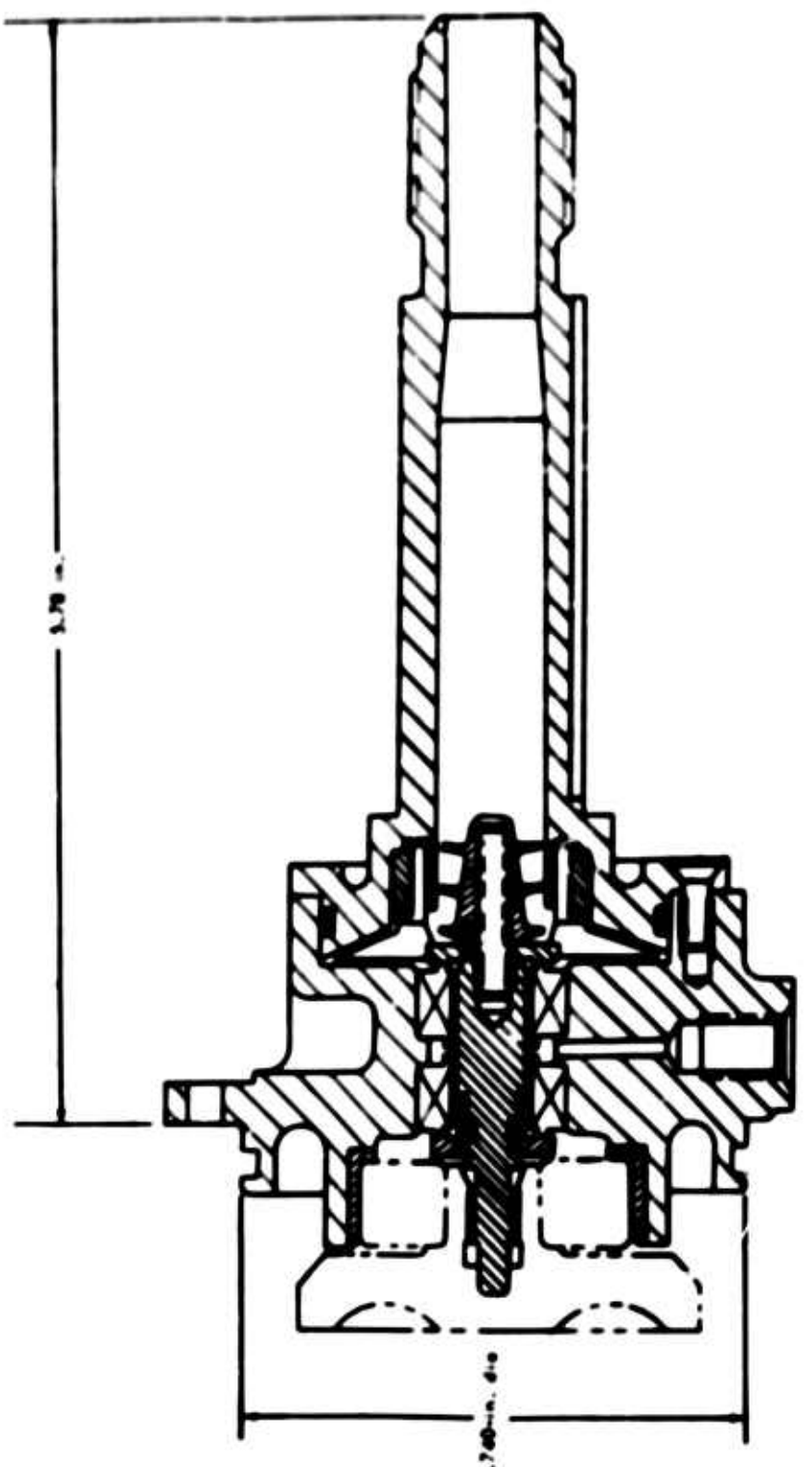

Figure 70. Centrifugal Fuel Pump Design, Vendor A.

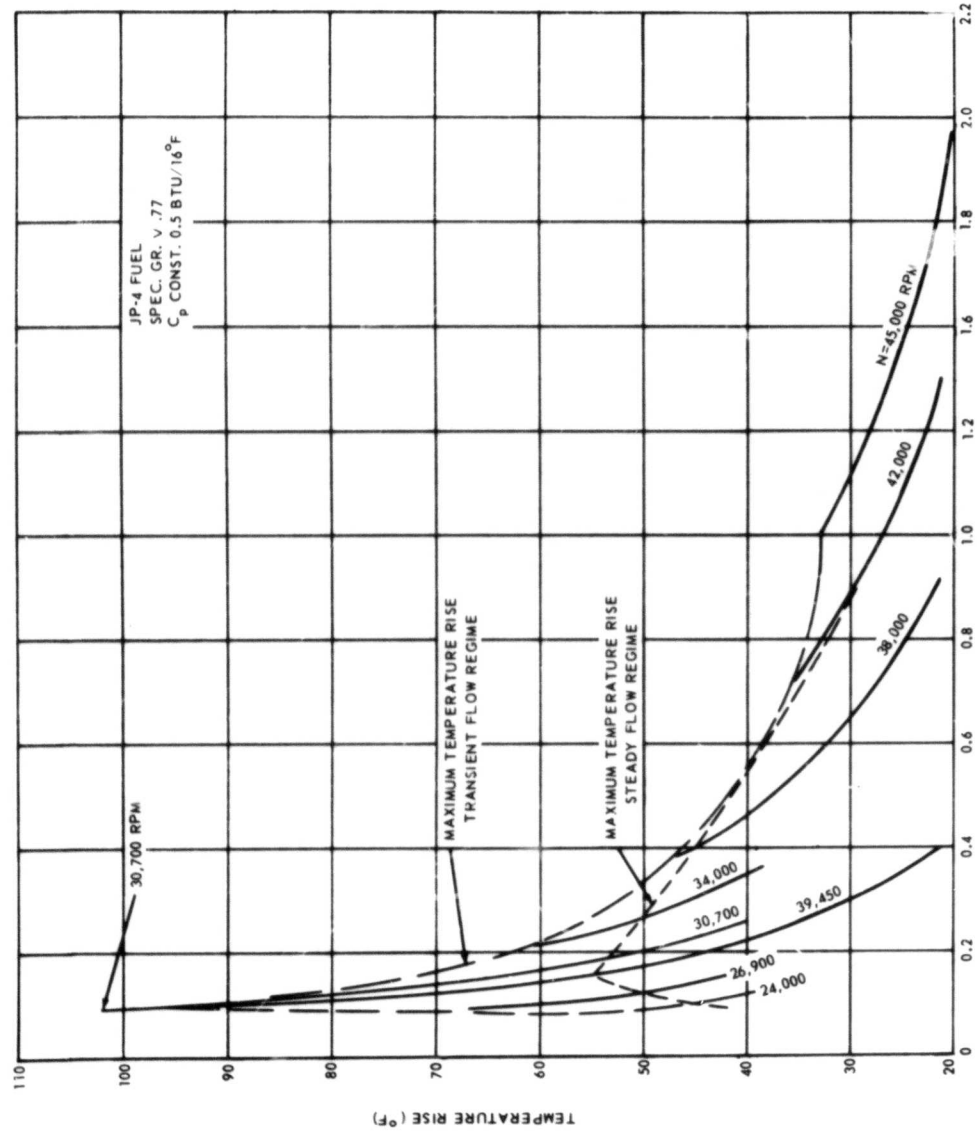

Figure 71. Fuel Temperature Rise Versus Flow and Pump Speed.

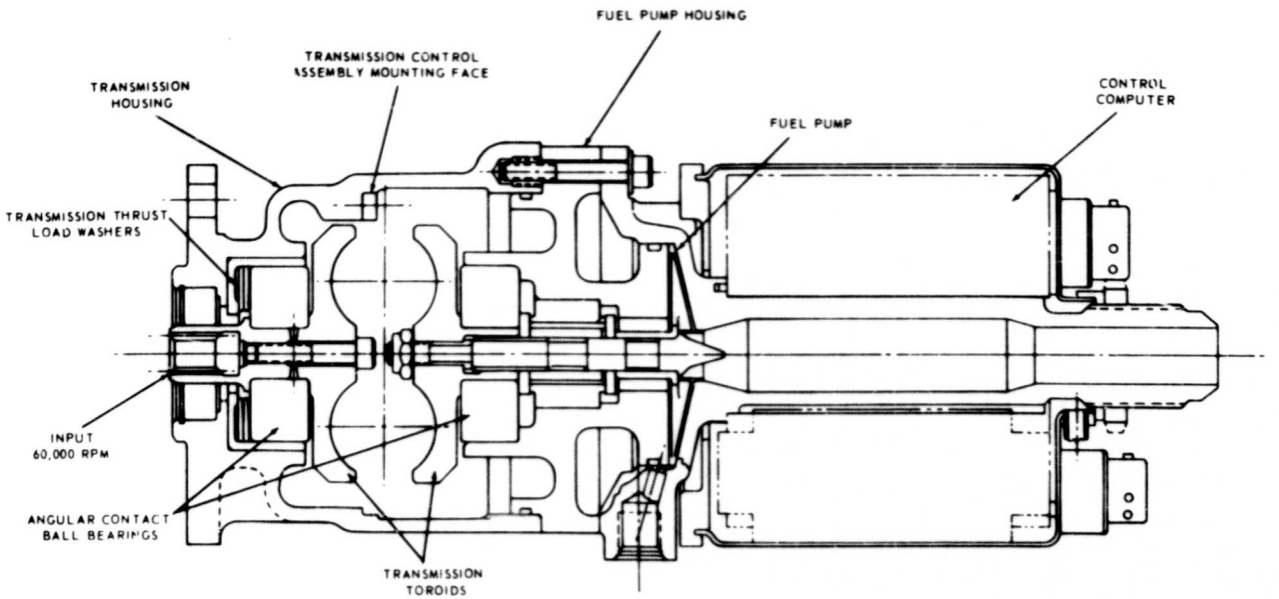

NOTE THE FOLLOWING SYSTEM COMPONENTS ARE NOT SHOWN IN THE DRAWING

- TRANSMISSION CONTROL ASSEMBLY AND ROLLS
- CONTROL TORQUE MOTOR
- N_h SPEED PICKUP
- FUEL SHUTOFF VALVE AND POWER LEVER ASSEMBLY
- FUEL MASS FLOW TRANSDUCER

Figure 72. Fuel Metering System No. 2 With Vendor A Pump.

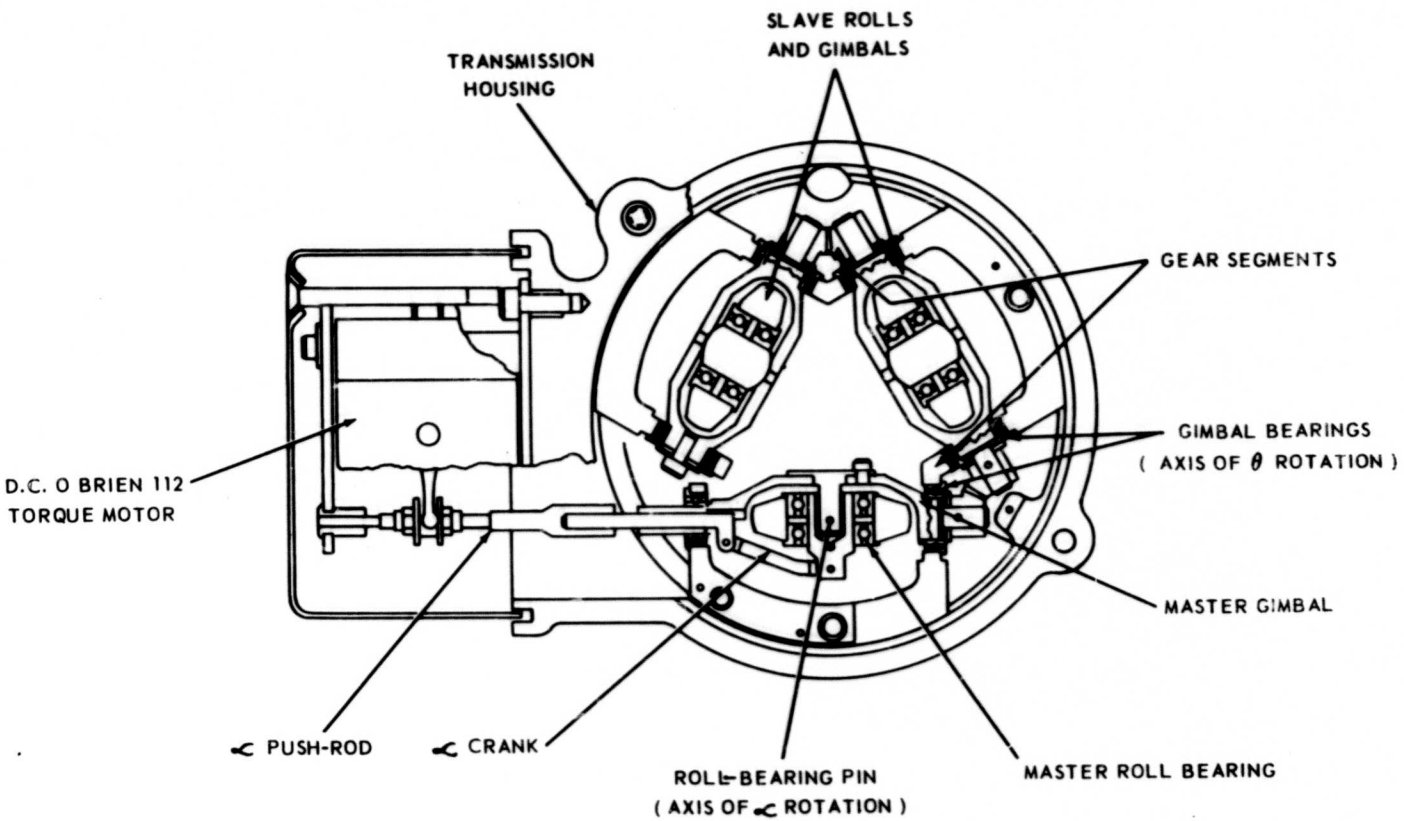

Figure 73. VSD Control Section With α Mode.

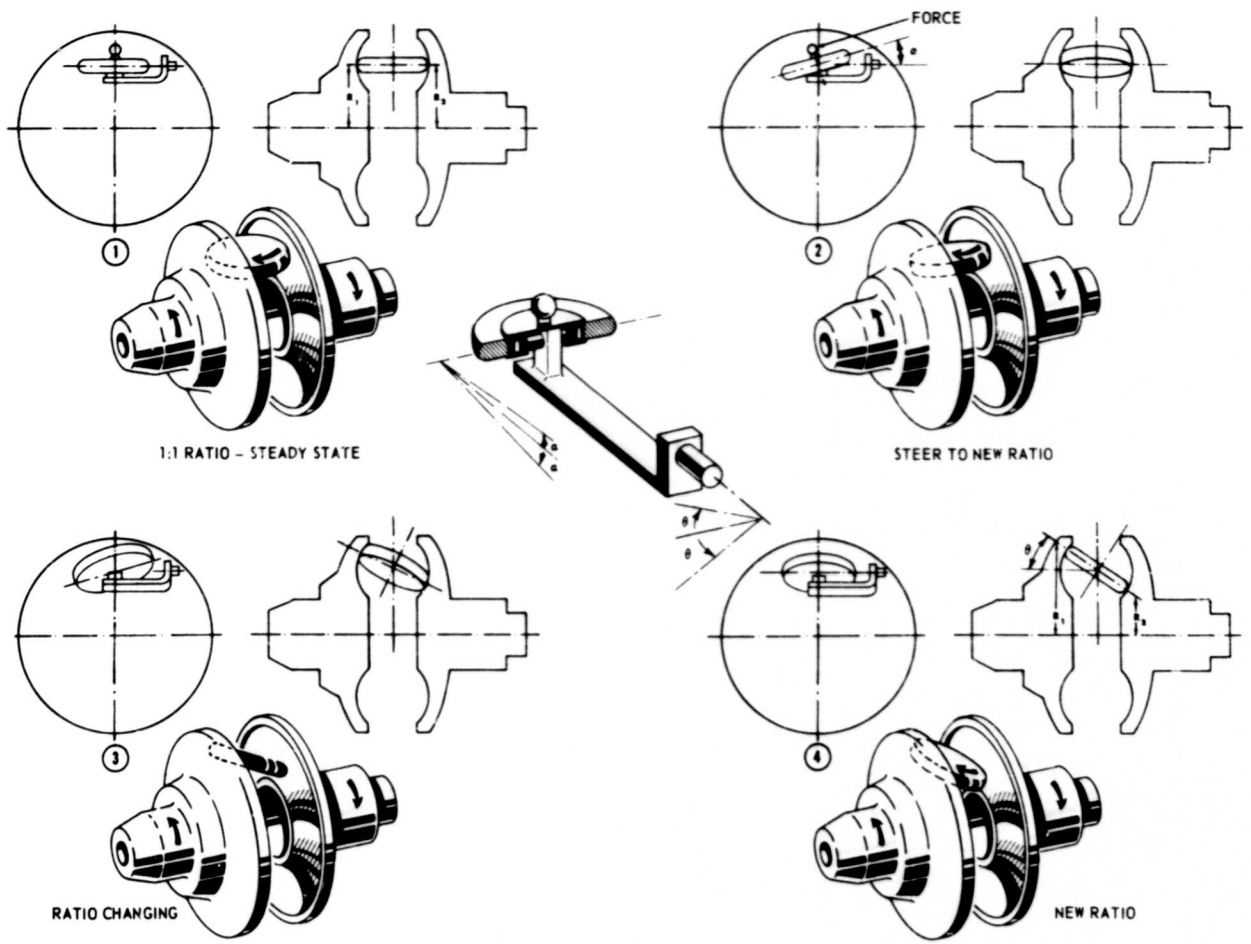

Figure 74. Schematic of Variable-Speed-Drive Control Technique.

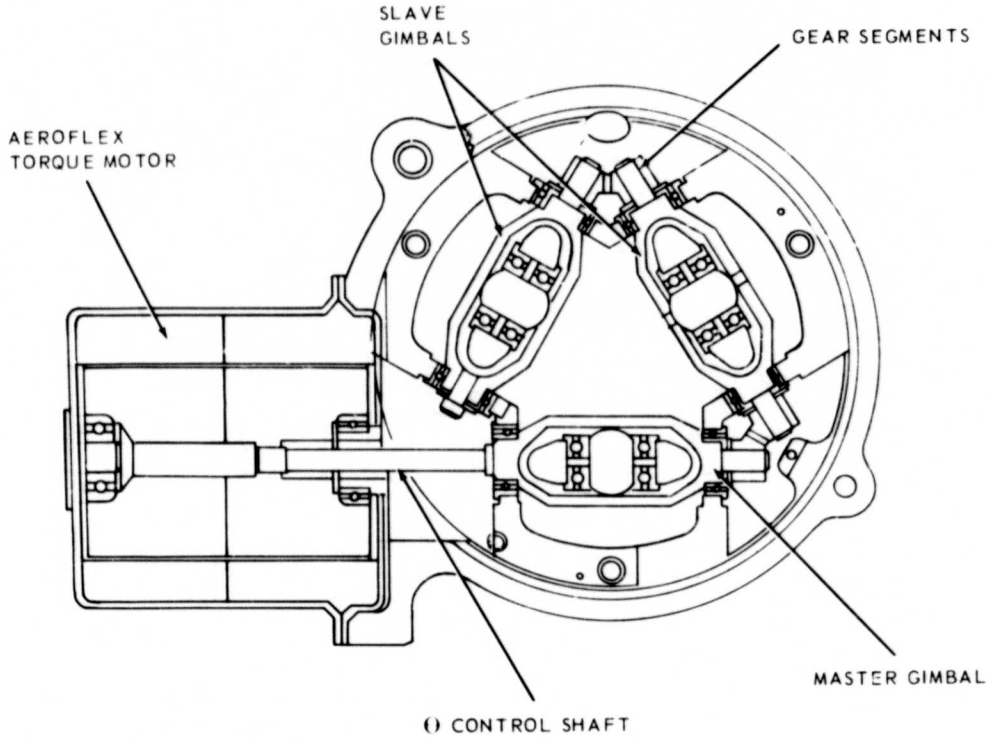

Figure 75. VSD Control Section With θ Control Mode.

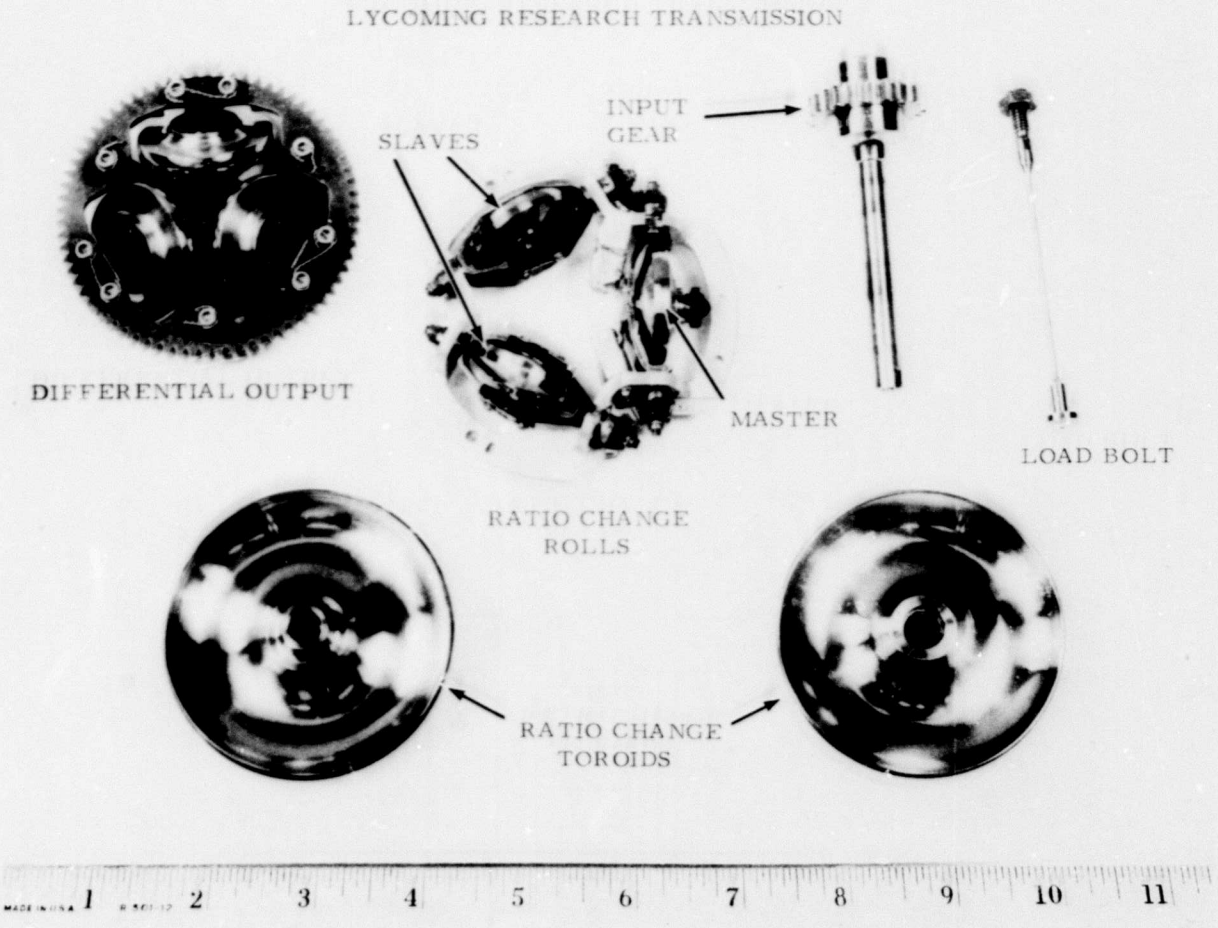

Figure 76. Experimental VSD Components After Test.

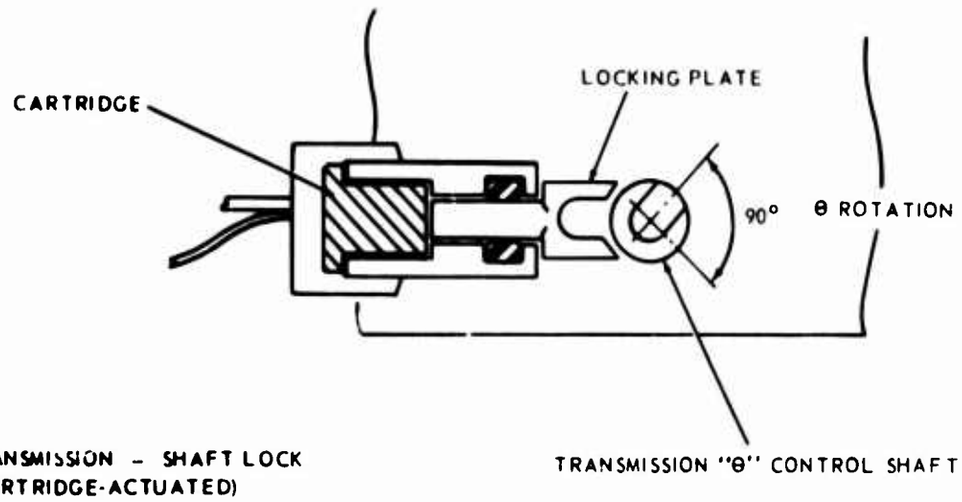

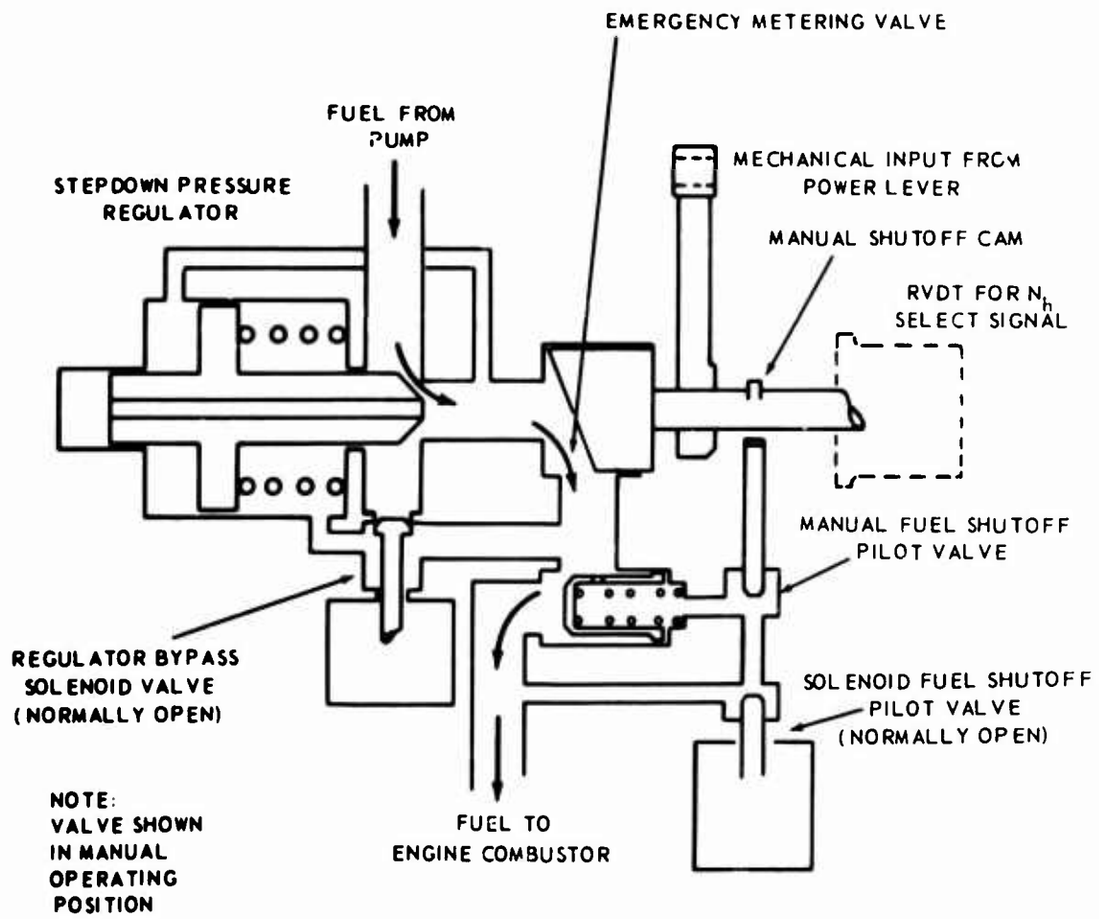

Figure 77. Schematic of Emergency Manual Control System No. 2.

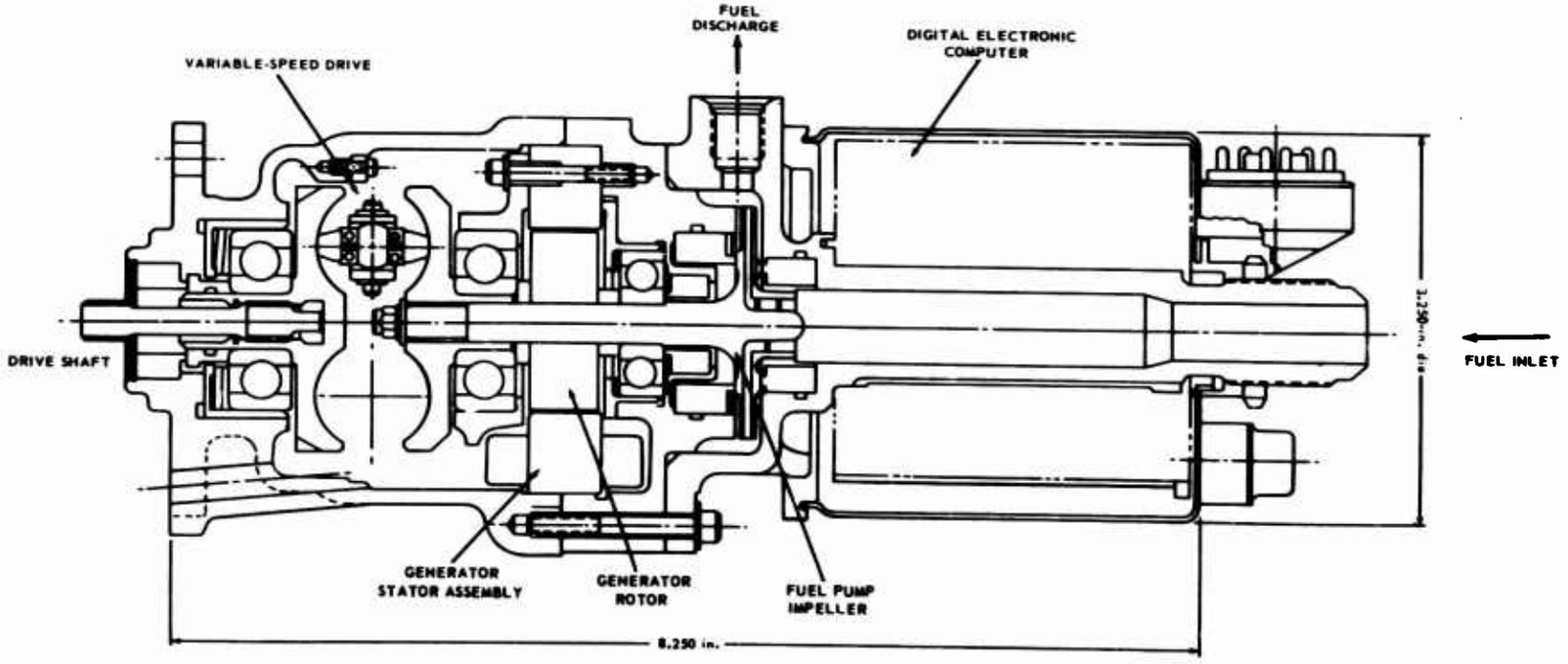

Figure 78. Fuel Metering System No. 2 With Vendor B Pump.

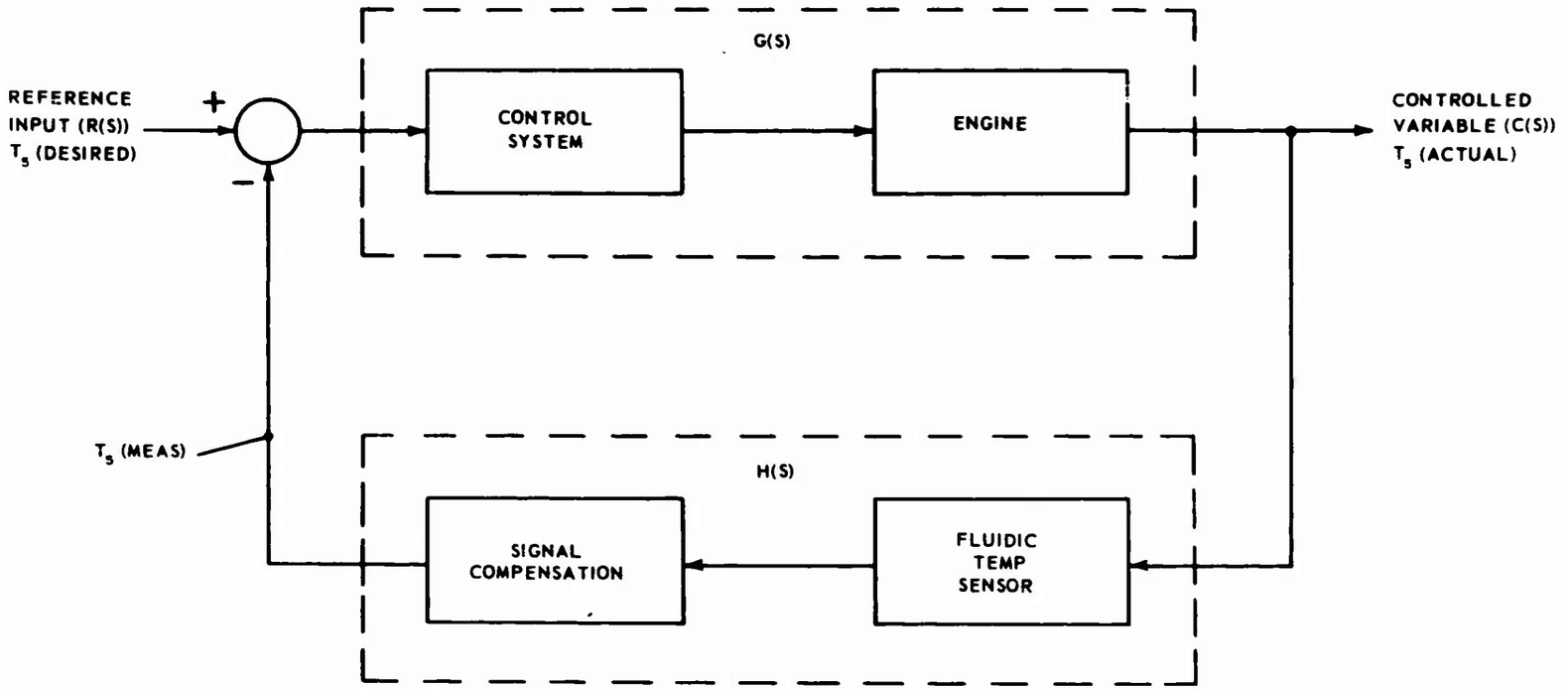

$$\frac{C(S)}{R(S)} = \frac{G(S)}{1 + G(S)\,H(S)} \quad , \text{ IF } G(S) >> 1$$

$$\cong \frac{G(S)}{G(S)\,H(S)} \cong \frac{1}{H(S)}$$

Figure 79. Block Diagram - Turbine Temperature Control.

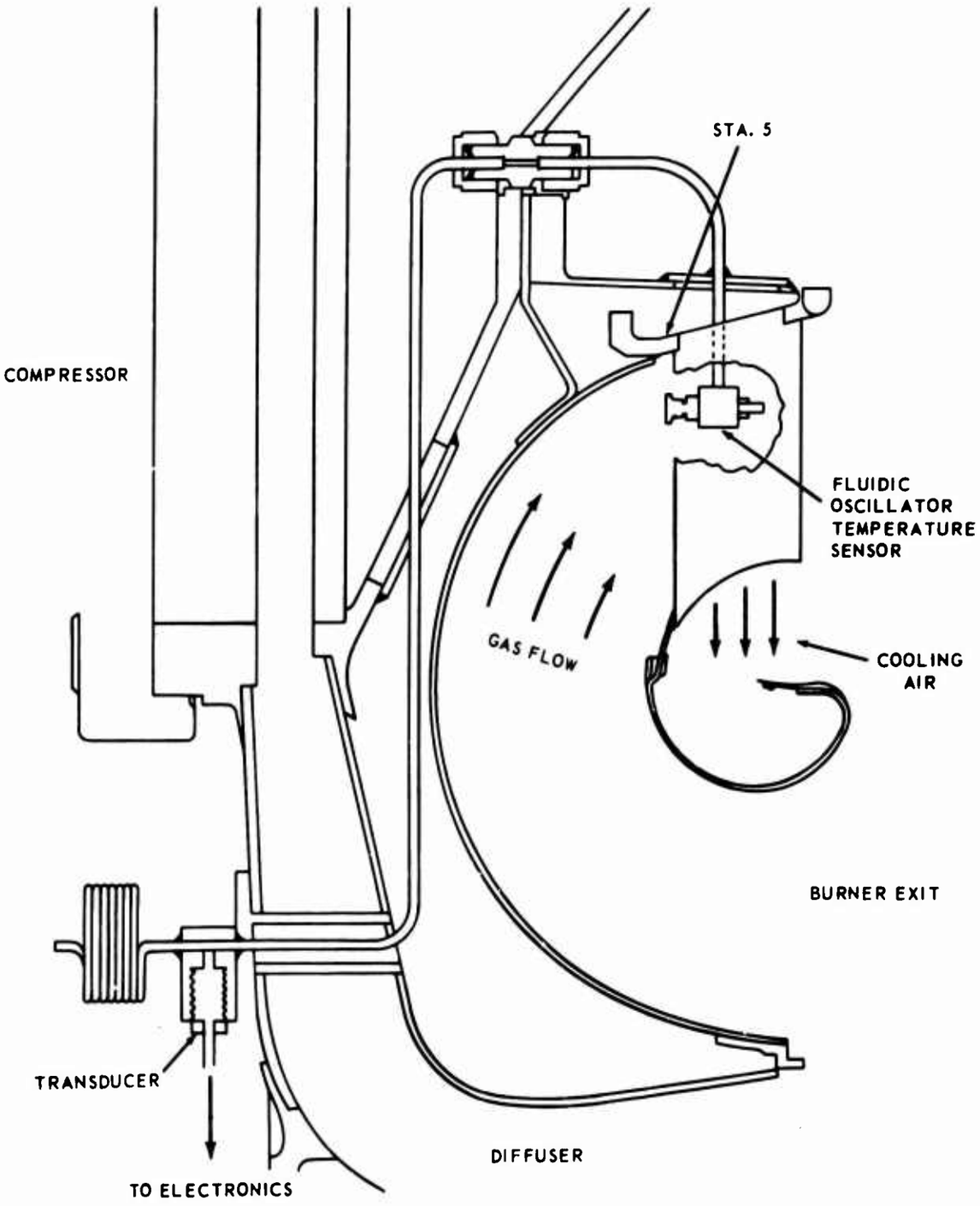

Figure 80. Schematic of Fluidic Sensor Installation on T55-L-7 Engine.

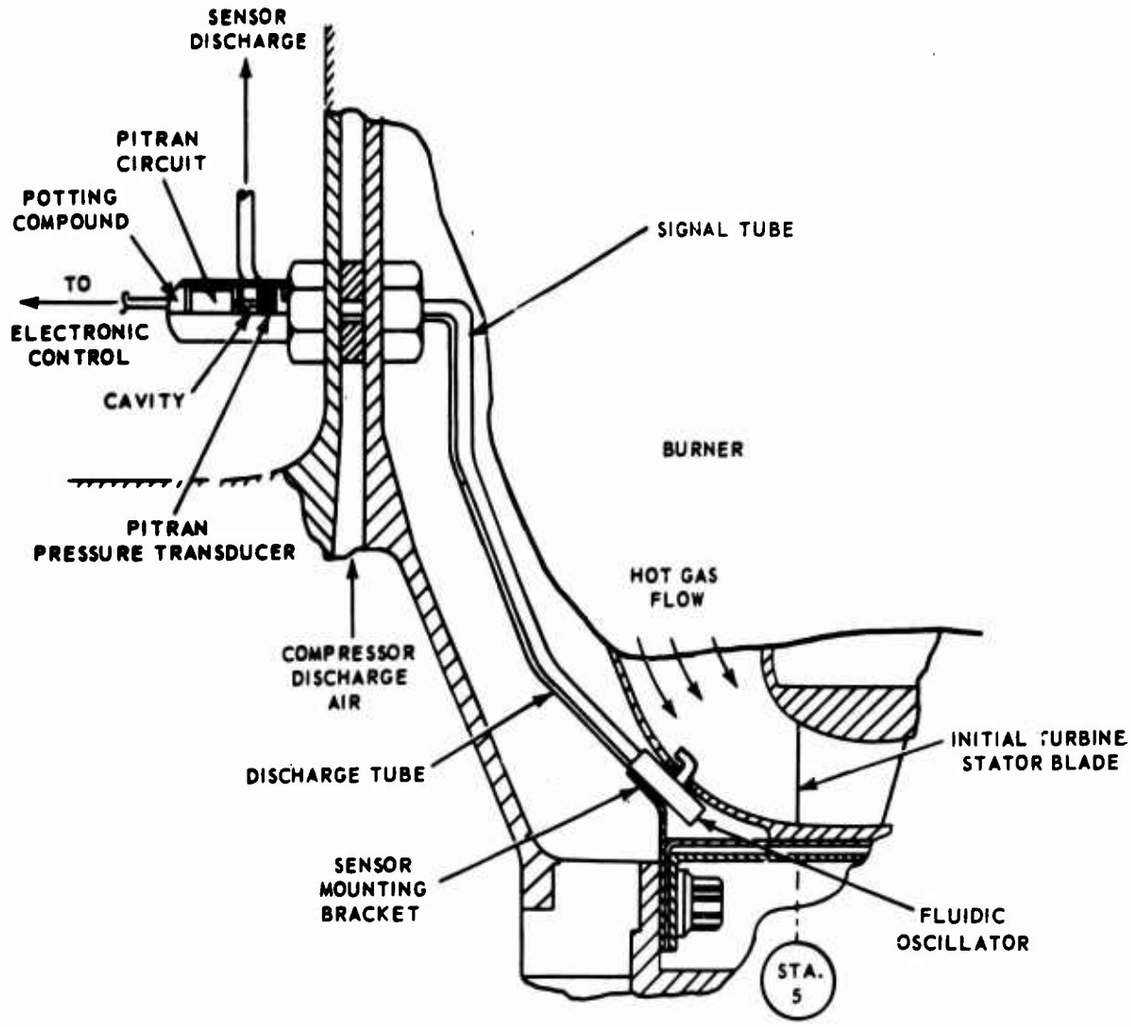

Figure 81. Fluidic Temperature Sensor Installation for a Typical 2- to 5-Lb/Sec W_a Engine.

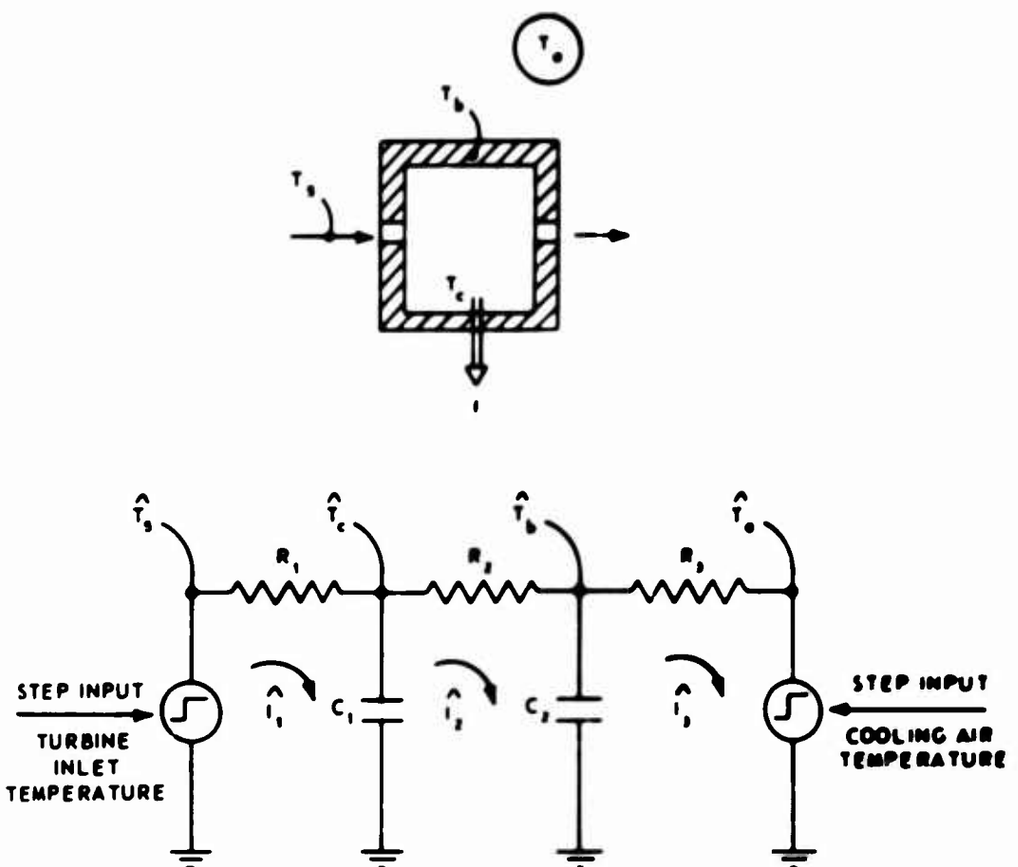

T_s — TURBINE INLET TEMPERATURE (°R)
T_c — SENSOR CAVITY TEMPERATURE
T_b — SENSOR BODY TEMPERATURE
T_o — COOLING AIR TEMPERATURE
R_1 — INLET ORIFICE RESISTANCE (°R/Btu/Sec)
R_2 — INSIDE FILM RESISTANCE
R_3 — OUTSIDE FILM RESISTANCE
C_1 — SENSOR CAVITY CAPACITANCE (Btu/°R)
C_2 — SENSOR MATERIAL CAPACITANCE
$I_{1,2,3}$ — LOOP CURRENTS (HEAT FLOW, Btu/Sec)

Figure 82. Fluidic Oscillator - Electrical Analog.

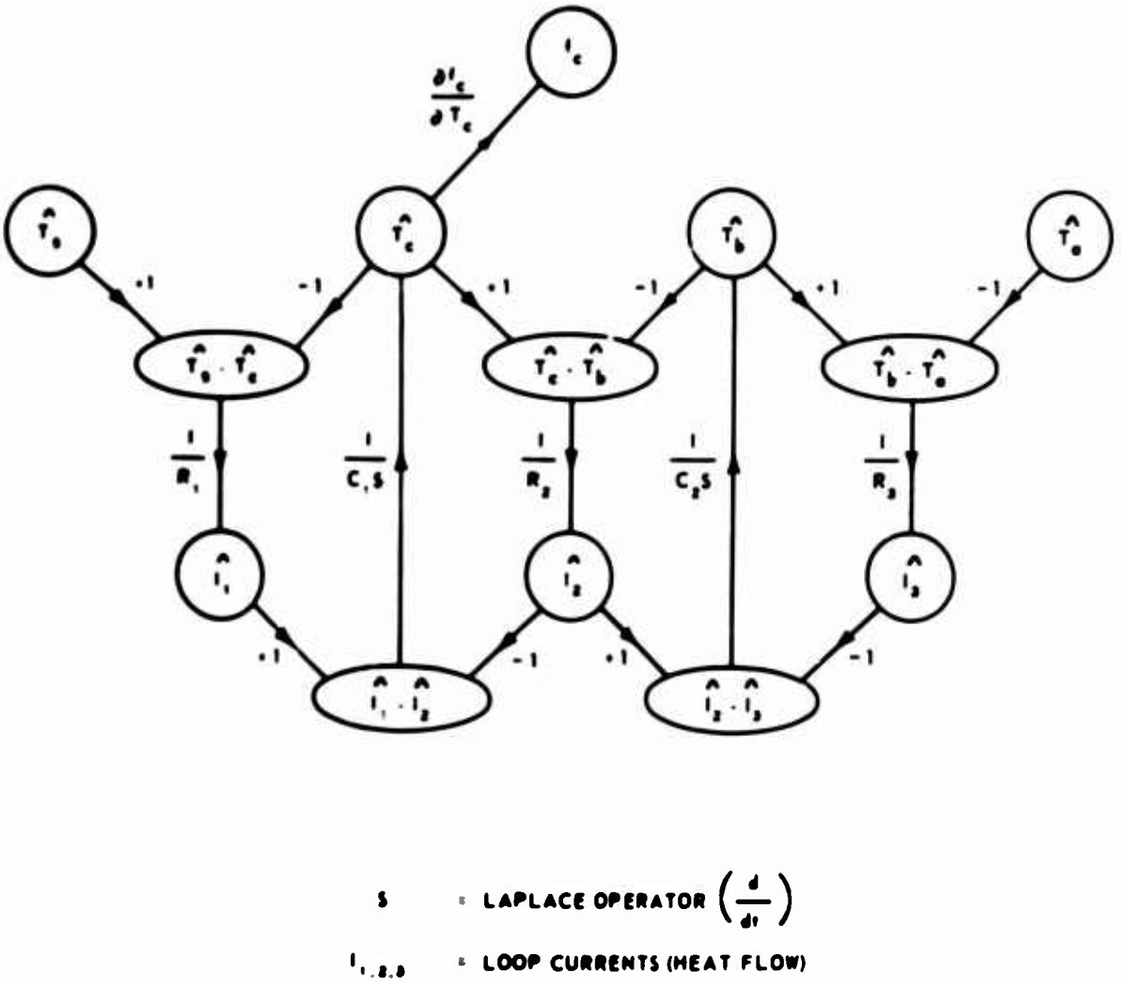

S = LAPLACE OPERATOR $\left(\frac{d}{dt}\right)$

$I_{1,2,3}$ = LOOP CURRENTS (HEAT FLOW)

Figure 83. Fluidic Oscillator - Signal Flow Graph.

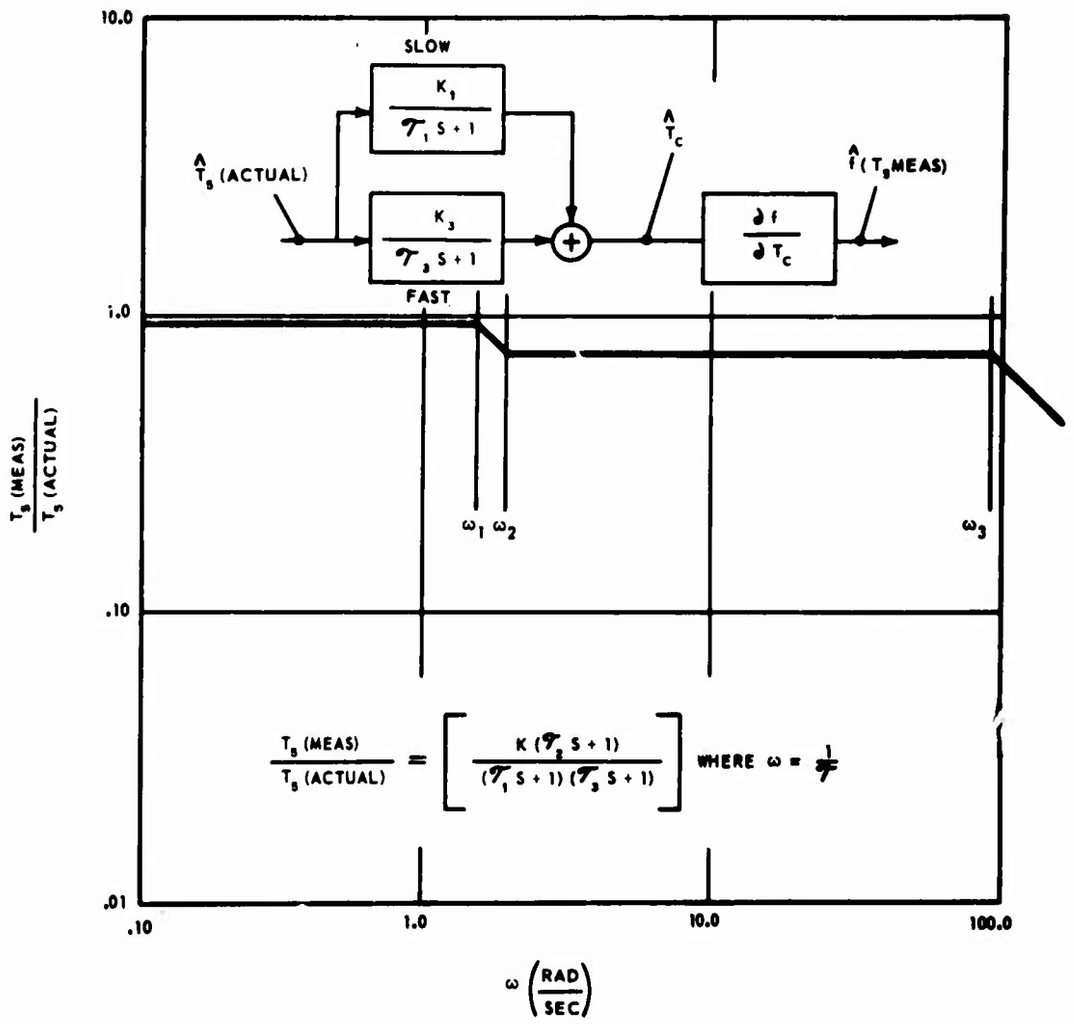

Figure 84. Bode Frequency Response Diagram - T55-L-7 Engine Test Results.

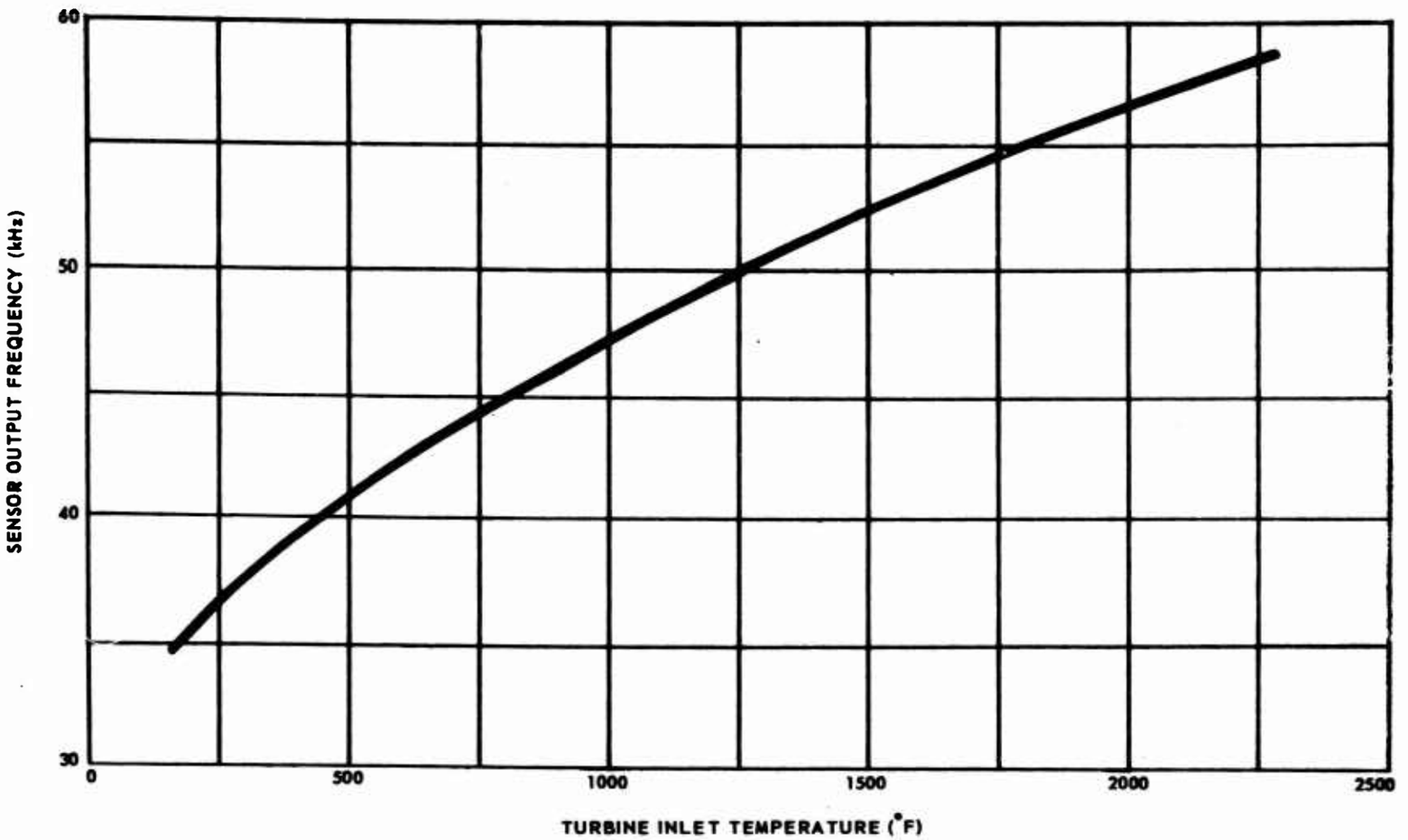

Figure 85. Fluidic Oscillator - Theoretical Frequency Versus Temperature.

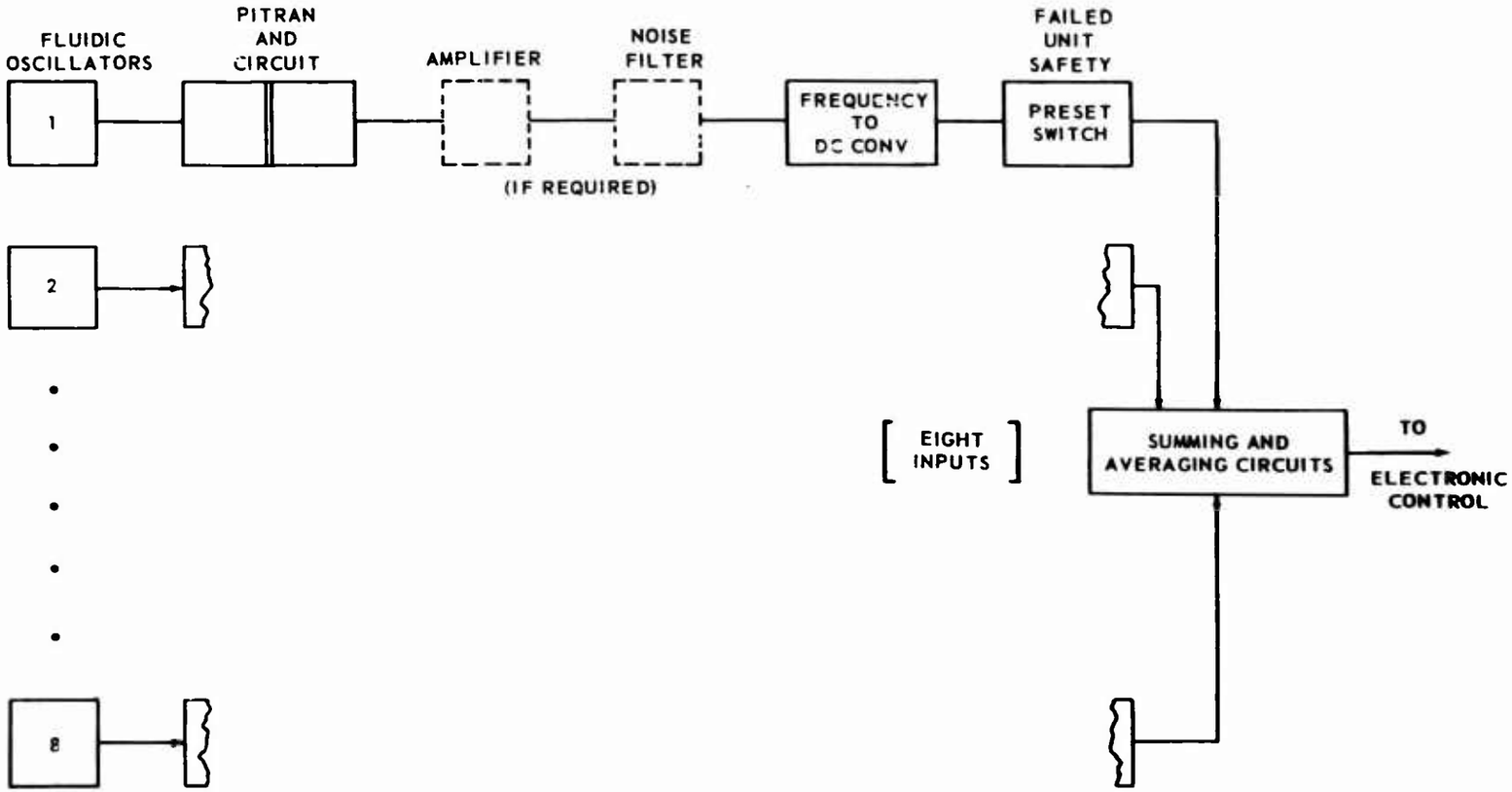

Figure 86. Block Diagram of Multiple Sensor Averaging System.

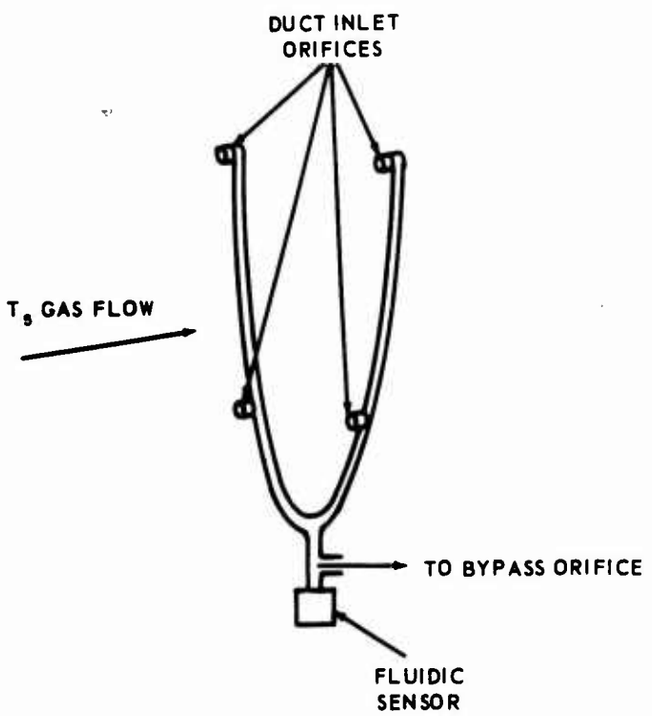

Figure 87. Schematic of Typical Gas Averaging Duct Arrangement.

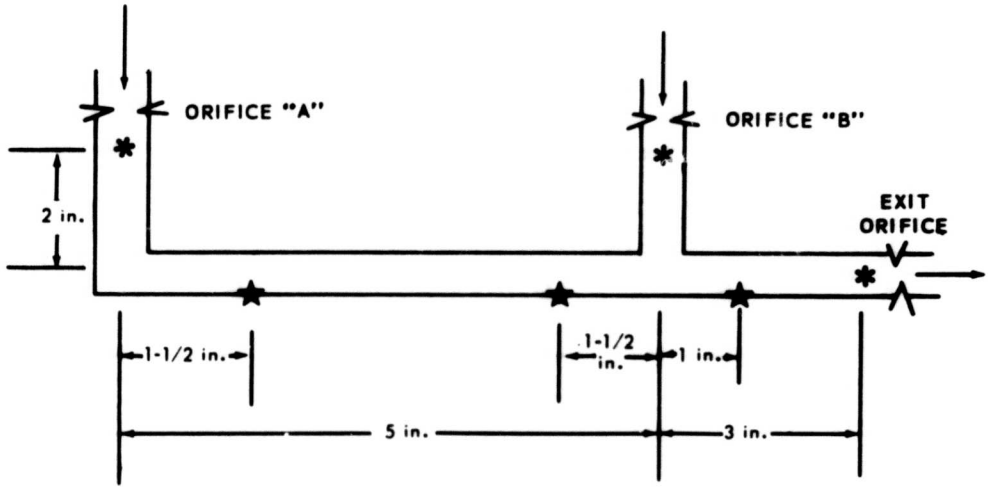

NOTES: GAS ENTERED THE DUCT THROUGH ORIFICES "A" AND "B" AND MIXED WITHIN THE DUCT BEFORE EXITING.

* THERMOCOUPLES MEASURING GAS TEMPERATURE

★ THERMOCOUPLES MEASURING DUCT WALL TEMPERATURE

Figure 88. Gas Averaging Model.

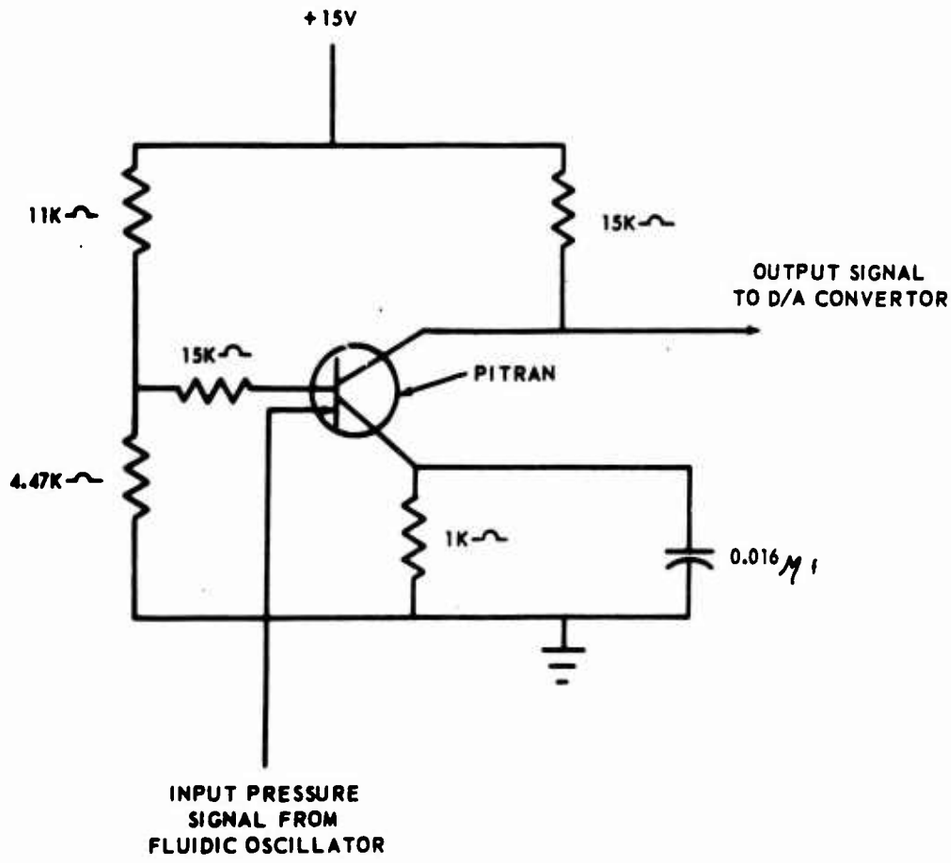

Figure 89. Pitran Circuit.

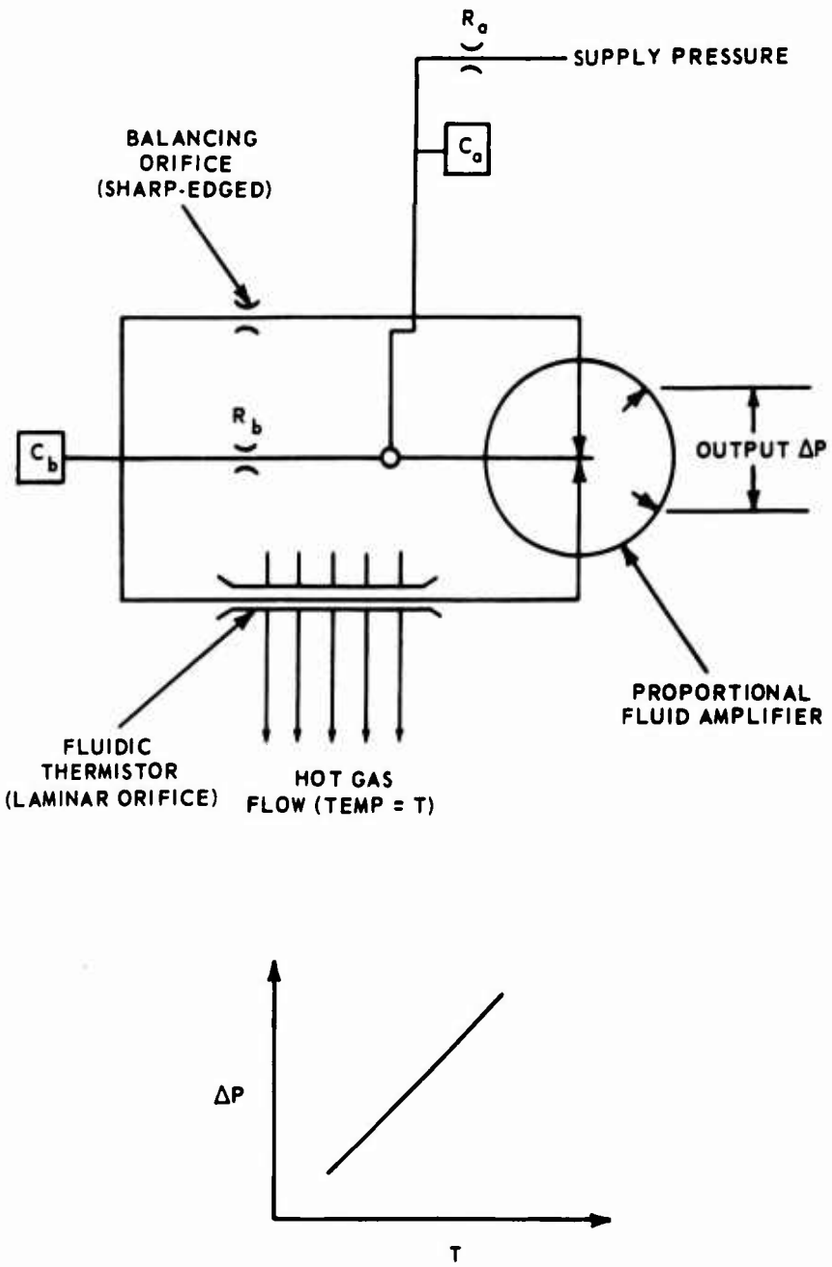

Figure 90. Schematic of Fluidic Thermistor.

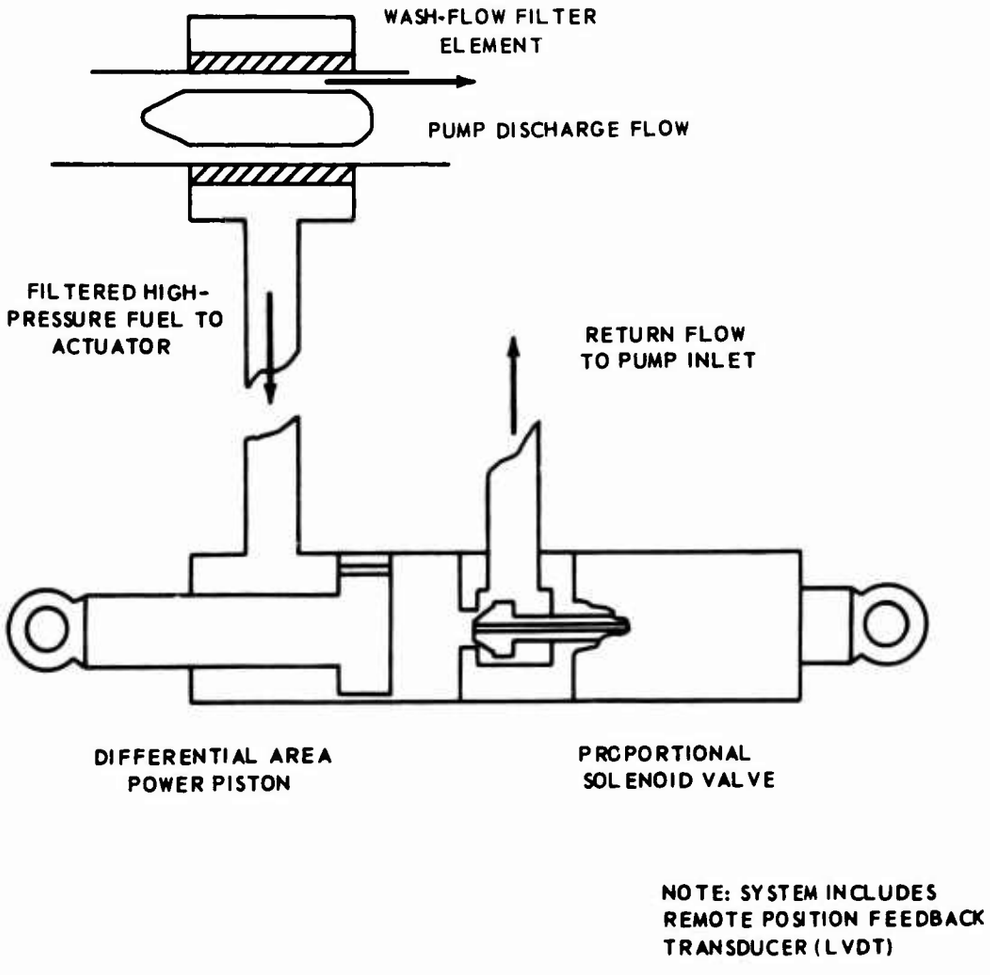

Figure 91. Schematic - Proportional Electrohydraulic Servo System.

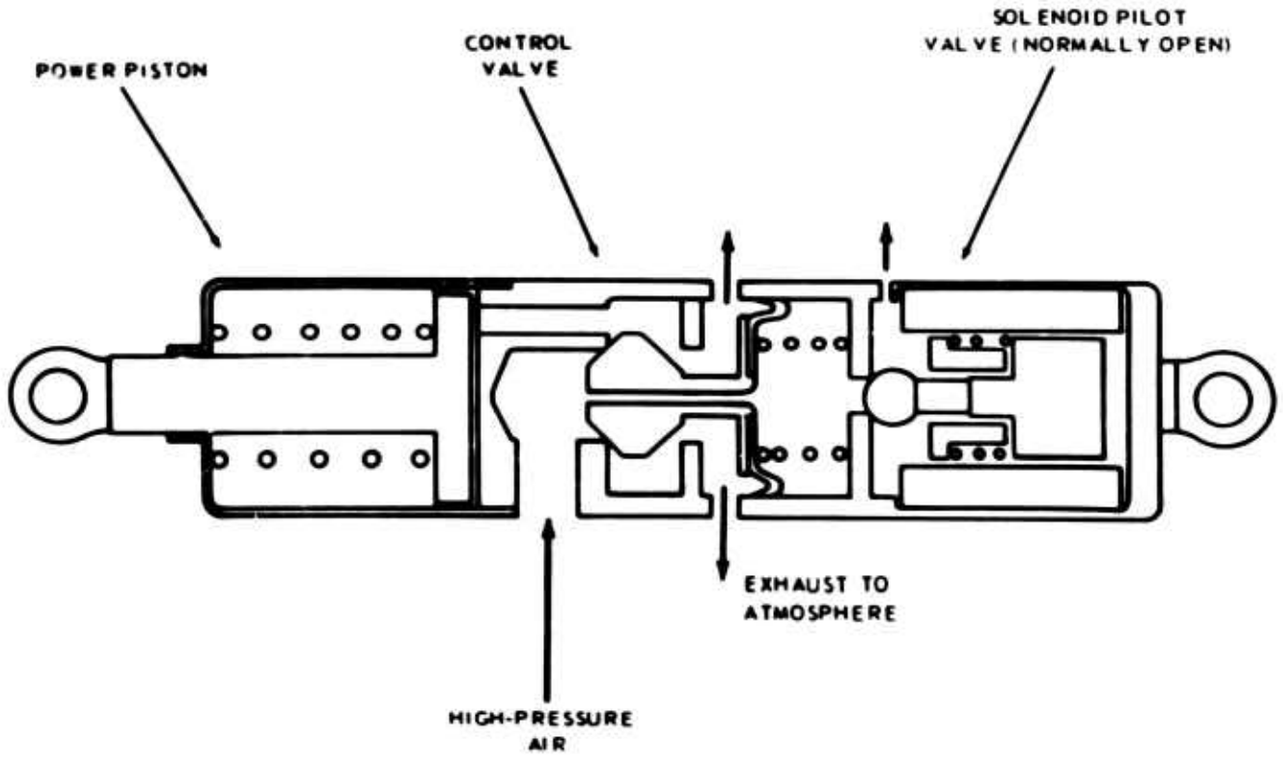

Figure 92. Schematic - Two-Position Electropneumatic Actuator.

APPENDIX I

COMPONENT MAP METHOD OF ENGINE SIMULATION FOR LARGE-SCALE TRANSIENT RESPONSE CONTROL STUDIES

INTRODUCTION

The following text describes the detailed simulation of various engine components such as compressors, turbines, combustors, etc., and the manner in which they are interrelated to assembly the complete engine simulation. These components are defined by either single or bivariant functions and are mutually dependent for their respective inputs. The dynamic elements required to complete the simulation of engine transient response are as follows:

1. Integration of turbine/compressor torque unbalance with a given rotor inertia for calculation of speed changes

2. Integration of the difference between airflow in and out of the volume between components to determine station pressure changes.

3. Fuel scheduling and control lag elements. (This is treated within the Control Mode Study section of this report.)

Figure 93 illustrates the twin-spool gas turbine used for this control study and defines inlet station number for each engine component. Reference to this diagram will aid in an understanding of the following discussion.

Referred speed (NLPRFC) and pressure ratio (P23) are low-spool compressor map inputs, required to obtain GLPC, (the Gamma Function)

$$\frac{W_2\sqrt{\theta_2}}{W_2^* \delta_2}$$

where $\theta_2 = T_2/519$

$\delta_2 = P_2/14.7$

W_2^* = design weight flow

This parameter multiplied by δ_2, an appropriate constant, and divided by $\sqrt{\theta_2}$ yields the actual weight flow W_2. In like manner, W_3 is calculated. The quantity $(W_2 - W_3)$ is integrated and multiplied by the appropriate constant, yielding the interspool pressure changes for the next increment. This calculation is defined in generalized equation (2) on Page 208. Compressor efficiency and average specific heat are given as a function of speed (NLPRFC), from which compressor power (HCLP) is calculated in Btu/sec. Turbine power (HTLP) is calculated in a similar manner to the compressor power. The difference between turbine and compressor power, divided by rotor speed, is unbalanced torque. This torque difference is then integrated and multiplied by the proper constants to define the speed change for the next time increment.

The foregoing procedure takes place on both spools and establishes the major parameters required to define the engine operating conditions during a transient. At steady state, the continuity equation is satisfied where weight flows through each component are equal; hence $dP/dt = 0$. Turbine and compressor work are equal and opposite in polarity; hence $dN/dt = 0$.

COMPRESSOR CHARACTERISTIC SIMULATION

A typical compressor map is usually defined by pressure ratio being a function of referred weight flow and speed. Constant polytropic efficiency loci are also shown.

The following discussion summarizes the major steps and approximations used in the program to calculate the transient performance of each compressor.

A univariant function of polytropic efficiency versus compressor speed was established from the steady-state operating line and used during the transient to calculate the compressor temperature rise. Variable specific heat was treated in a similar manner. The specific heat variation with speed along the operating line of the compressor was assumed to apply during the transient. Thus, the subsequent calculations can be made for each step in the transient, having already stored values of referred airflow, speed, and pressure ratio in the program deck.

All speed values used for inputs to maps and functions are referred to the inlet of that component and normalized

$$N_{Ref} = \frac{N/(T_{IN}/519)^{1/2}}{N^*/(T^*_{IN}/519)^{1/2}} \times 100 \qquad (\%)$$

Where the denominator = constant: T^*_{IN} = Temp. at N^*
N^* = Design Speed

1. Evaluate compressor absolute weight flow:

$$P_r = P_{EX}/P_{IN}$$

$$\text{Gamma} = \Gamma = \frac{W\sqrt{\theta_x}}{\delta_x} = f(P_r, N_{REF})$$

If $\theta_x = T_{IN}/519$ and $\delta_x = P_{IN}/14.7$,

$$\text{then, } W = \left(\frac{(519.0)^{1/2}}{14.7}\right)\Gamma\left(\frac{P_{IN}}{\sqrt{T_{IN}}}\right) \qquad (\text{lb/sec})$$

2. Evaluate temperature rise and power absorbed:

With the computed pressure ratio (P_r), polytropic efficiency (η), and specific heat (C_p) in the form of generated functions, the exit temperature is calculated from basic thermodynamic equations

$$T_{EX} = T_{IN}\left(\frac{P_{EX}}{P_{IN}}\right)^{\frac{R}{J C_p \eta}}$$

$$H_c = W C_p (T_{EX} - T_{IN}) \qquad (\text{Btu/sec})$$

This procedure establishes the compressor performance at any time during the transient.

COMBUSTOR CHARACTERISTICS SIMULATION

The ratio of fuel flow to airflow is first computed. This ratio and burner inlet temperature are inputs to a temperature rise map (based on a particular burner efficiency). This temperature rise ΔT is added to the known inlet temp T_4, giving the burner exit temperature T_5.

$$\Delta T = f\ (W_f/W_a,\ T_4)$$

$$T_5 = \Delta T + T_4$$

Delay time (transport lag) and time constant effects in the combustor were considered to be negligible owing to the small-size atomizing combustor.

TURBINE CHARACTERISTIC SIMULATION

The turbine map was reduced to a univariable function of Γ (weight flow function) versus pressure ratio along a constant speed line, since the speed lines on the map were relatively close in the choked region. This approximation is reasonable for a control study where different modes are being compared.

1. Evaluate turbine absolute weight flow:

$$P_r = P_{EX}/P_{IN}$$

$$\text{Gamma} = \Gamma = \frac{W\sqrt{\theta_x}}{\delta_x} = f\ (P_r)$$

$$\text{If } \theta_x = T_{IN}/519 \text{ and } \delta_x = P_{IN}/14.7,$$

$$\text{then } W = \left(\frac{(519)^{1/2}}{14.7}\right)\Gamma\left(\frac{P_{IN}}{\sqrt{T_{IN}}}\right) \quad \text{(lb/sec)}$$

2. Evaluate temperature drop and power developed with the computed pressure ratio (P_r), given polytropic efficiency (η) and specific heat (C_p) in the form of generated functions. The exit temperature is calculated:

$$T_{EX} = T_{IN} \left(\frac{P_{EX}}{P_{IN}} \right) \frac{R\ (1 + WFAR\ \ (\eta)}{J\ C_p} \qquad (^oR)$$

$$H_T = W\ C_p\ (T_{IN} - T_{EX}) \qquad (Btu/sec)$$

This procedure established the turbine performance at any time during the transient.

ROTOR SPEED SIMULATION

The rotor-accelerating power is equal to the difference between the turbine power and the compressor power. From the following basic equations, the proper integration and conversion are derived to provide the change increments of high and low compressor speed during acceleration or deceleration. It is obvious from equation (1) on Page 207 that the speed assumes a steady-state value when the compressor power is equal and opposite to the turbine power.

$$HP_{acc} = HP_T - HP_c$$

Since $HP = \text{Torque}\ \omega$ where torque $= I\ \omega$

$$HP_T - HP_c = I\ \dot{\omega}\ \omega$$

$$\dot{\omega} = \frac{HP_T - HP_c}{I\ \omega} \quad ; \quad \omega = \frac{Rad}{sec}$$

$$2\ \pi \dot{N} = \frac{HP_T - HP_c}{I\ N\ \ (2\pi)}$$

$$\dot{N} = \frac{HP_T - HP_c}{I\ N\ \ (2\pi)^2} \quad ; N = \frac{Rev}{sec}$$

Converting $HP\ \frac{ft\text{-}lb}{sec}$ to $H\ \frac{Btu}{sec}$; $J = 778\ \frac{ft\text{-}lb}{Btu}$

$$\dot{N} = \frac{(H_T - H_c)\ J}{I\ N\ \ (2\pi)^2} = \frac{19.7}{I} \left[\frac{(H_T - H_c)}{N} \right]$$

$$N = N_{IC} + \frac{19.7}{I} \int_0^t \frac{H_T - H_c}{N} \, dt \qquad (1)$$

	ω	Rotor Speed - rad/sec
	$\dot{\omega}$	Rotor Acceleration - rad/sec^2
	N	Rotor Speed - rev/sec
	$\dot{N}$	Rotor Acceleration - rev/sec^2
	HP	Component Power - (ft - lb)/sec
	I	Rotor Inertia - ft - lb sec^2
	J	Conversion Factor - 778 ft - lb/Btu
	H	Component Power - Btu/sec
Subscript	IC	Initial Condition

PRESSURE - VOLUME SIMULATION

The pressure changes existing between components is determined by differentiation of the Ideal Gas Equation

$$PV = mRT,$$

in which R is the gas constant, V is the volume, and m is the net mass stored in the volume. The summation of airflow entering and leaving a volume is the time rate of change of mass in the volume. During engine transients, the gas state within an interstage volume changes. These changes can be described by differentiating the ideal gas low. Assuming constant temperature, the interstage pressure can be determined by integration of the relative difference of weight flows in and out of this volume. This pressure calculation is defined by equation (2) on Page 208.

Derivation:

$$\frac{dP}{dt} = \frac{R}{V} \left[T \frac{dm}{dt} + m \frac{dT}{dt} \right]$$

Assuming small changes in temperature T over small time increments

$$\frac{dT}{dt} = 0$$

$$\frac{dm}{dt} = \text{mass flow}$$

$$g \frac{dm}{dt} \left(\frac{ft}{sec^2} \cdot \frac{lb_m}{sec} \right) = W = \text{weight flow} \left(\frac{lb_m \, ft}{sec^2} \Big/ sec \right)$$

Substituting $= \frac{dm}{dt} = \frac{W}{g}$

$$P = P_{IC} + \frac{R}{Vg} \int_o^t T \, (W_{IN} - W_{OUT}) \, dt \qquad (2)$$

$$\frac{lb}{in.^2} = \frac{lb_F}{in.^2} + \frac{in.\text{-}lb_F}{lb_m \, {}^oR} \; \frac{1}{in.^3} \; \frac{sec^2}{ft} \; \frac{{}^oR}{1} \; \frac{lb_m \, ft}{sec^3} \; sec$$

$$\frac{lb_F}{in.^2} = \frac{lb_F}{in.^2} + \frac{lb_F}{in.^2}$$

at steady-state the continuity equation is in effect whereby $W_{IN} = W_{OUT}$.

$$\therefore \quad P = P_{IC}$$

where P = Station pressure — $lb_F/in.^2$

R = Gas constant — $640 \; \frac{in.\text{-}lb_F}{lb_m \, {}^oR}$

V = Volume — $in.^3$

g = Constant — $32.2 \; ft/sec^2$

W = Weight flow — $lb_m \; ft/sec/sec = lb_F/sec$

EXHAUST DIFFUSER SIMULATION

For the exhaust diffuser simulation, a univariate function is calculated from steady-state data. This function,

$$GDF = \frac{W_9 \sqrt{T_8}}{P_3 A_D} = f\ (P_9/P_o)$$

was used, and W_9 is extracted by multiplying and dividing GDF by the above parameters available elsewhere in the program.

POWER TURBINE ROTOR SIMULATION

The power turbine rotor is simulated in the same manner as described in the paragraph Rotor Speed Simulation. The accelerating torque T_{Acc} is the difference between load torque (TORQL) and power turbine torque (TORQPT).

$$T_{Acc} = TORQPT - TORQL$$

The load inertia was assumed to be 10 times the power turbine inertia.

$$JL = 10\ JPT$$

Beta (collective pitch) initiated the engine transient by loading the power turbine.

Transient shaft horsepower was also calculated.

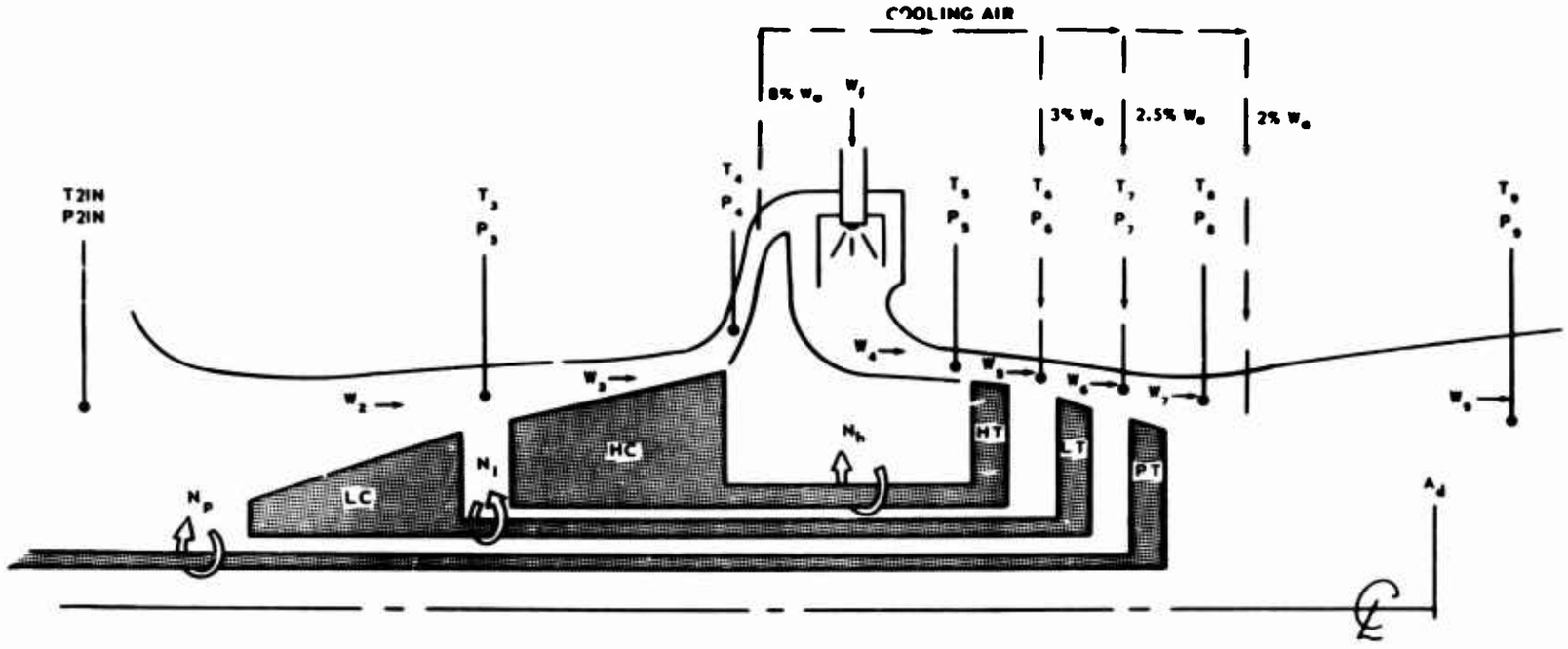

LC = LOW COMPRESSCR
HC = HIGH COMPRESSOR
HT = HIGH TURBINE
LT = LOW TURBINE
W_f = FUEL FLOW
N_h = HIGH SPOOL SPEED
N_l = LOW SPOOL SPEED
N_p = POWER TURBINE SPEED
A_d = DISCHARGE NOZZLE AREA

Figure 93. Engine Station Representation.

APPENDIX II

RELIABILITY APPORTIONMENT

Having established the 30,000-hour MTBF goal, it now becomes necessary to allocate this goal to a lower tier. This allocation or apportionment serves as a guideline in determining the conceptual design's ability to meet the desired goal. The initial apportionment was done for the items depicted on the initial logic diagram. However, as the detailed design progressed, it became more meaningful to represent the apportionment in terms of the developed functional circuits. Figures 94 through 96 and Tables IX and X represent the initial block diagram, apportionment matrices*, and apportionments, respectively, for the analog and digital approach. Table XI and Figure 97 show the realigned apportionment consistent with the developed analog design.

---

* The apportionment is per "A Comprehensive Reliability Engineering Program" by Donald E. Brimley as presented July 5-9, 1966 at UCLA in short course on "Systems Approach to Reliability".

TABLE IX. ANALOG APPORTIONMENT

Block Diagram Designation	Description	Failure Rate (λ) Apportionment in Failures Per 10^6 Hours		
		Per Block	Quant. Per System	Per System
A	Signal Conditioner (N_h, N_l & N_p)	0.908	3	2.724
B	Signal Conditioner (B)	0.532	1	0.532
C	Select (Limit) (N_h & N_p)	0.532	2	1.064
D	Load Sharing (Q_r & Q_l)	0.717	2	1.434
E	Limit Generator (N_l, Q_l & T_5)	0.717	3	2.151
F	Signal Conditioner (T_5 & W_f)	1.090	2	2.180
G	Signal Conditioner (T_l) (Measure)	0.908	1	0.908
H	Function Generator	1.007	4	4.028
J	Operational Amplifier	0.360	13	4.680
K	Summing Point	0.360	14	5.040
L	Least Voter	0.717	1	0.717
M	Most Voter	0.530	1	0.530
N	Integrator	0.717	4	2.868
O	Limiter	0.717	3	2.151
P	Low Limiter	0.717	1	0.717

TABLE IX - Continued

Block Diagram Designation	Description	Failure Rate (λ) Apportionment in Failures Per 10^6 Hours		
		Per Block	Quant. Per System	Per System
O	Proportional Variable Gain	0.717	1	0.717
R	Comparator (Hysteresis)	0.532	1	0.532
S	Wiring and Connections	0.360	1	0.360
TOTAL				33.333

TABLE X. DIGITAL APPORTIONMENT

Block Diagram Designation	Description	Failure Rate (λ) Apportionment in Failures Per 10^6 Hours		
		Per Block	Quant. Per System	Per System
A	Signal Conditioner (N_h, N_1 & N_p)	.856	3	2.568
B	Signal Conditioner (B)	.677	1	0.677
C	Select (Limit) (N_h & N_p)	.677	2	1.354
D	Load Sharing (Q_r & Q_1)	.677	2	1.354
E	Limit Generator (N_1, Q_1 & T_5)	.677	3	2.031
F	Signal Conditioner (T_5 & W_f) (Measure)	.677	2	1.354
G	Signal Conditioner (T_1) (Measure)	.677	1	0.677
H	Function Generator	.500	4	2.000
J	Operational Amplifier	1.92	13	2.496
K	Summing Point	.585	14	8.190
L	Least Voter	1.000	1	1.000
M	Most Voter	.855	1	0.855
N	Integrator	1.106	4	4.424
O	Limiter	.585	3	1.755
P	Low Limiter	.585	1	0.585

TABLE X - Continued

Block Diagram Designation	Description	Failure Rate (λ) Apportionment in Failures Per 10^6 Hours		
		Per Block	Quant. Per System	Per System
Q	Proportional Variable Gain	.720	1	0.720
R	Comparator (Hysteresis)	.855	1	0.855
S	Wiring and Connections	.455	1	0.455
TOTAL				33.35

TABLE XI. DEVELOPED ANALOG DESIGN APPORTIONMENT

Math Model Designation	Description	Failure Rate (λ) Apportionment in Failures Per 10^6 Hours		
		Per Item	Quant. Per System	Per System
A	N_h Actual	0.8	1	0.8
B	Accel Limit Function Generator	1.5	1	1.5
C	Accel Limit Amplifier	0.6	1	0.6
D	Temperature Multiplier	2.5	1	2.5
E	N_h Select	2.6	1	2.6
F	Temperature Amplifier	0.6	1	0.6
G	Decel Limit Function Generator	0.6	1	0.6
H	N_p Select	4.0	1	4.0
J	N_h Expand	0.8	1	0.8
K	Airbleed Trigger Control	2.6	1	2.6
L	Inlet Guide Vane Circuit	1.2	1	1.2
M	N_h Temperature Bias	0.8	1	0.8
N	Authority Circuit	1.0	1	1.0
P	Flow Element Amplifier	3.0	1	3.0
O	N_l Measuring Circuit	1.6	1	1.6
R	Power Supply	2.0	3	6.0

TABLE XI - Continued

Math Model Designation	Description	Failure Rate (λ) Apportionment in Failures Per 10^6 Hours		
		Per Item	Quant. Per System	Per System
S	Torque Amplifier Circuit	1.0	1	1.0
T	T_5 Measuring Circuit	1.6	1	1.6
U	Wiring and Connections	0.5	1	0.5
TOTAL				33.3

$$MTBF = \frac{1}{\lambda} = \frac{1}{33.3 \times 10^{6}} = 30,030 \text{ Hours}$$

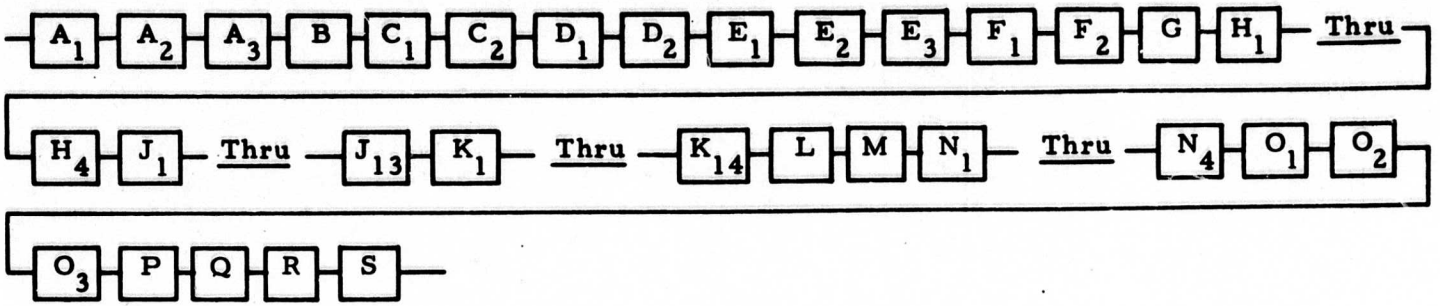

$R_{SYST.} = e^{-\lambda t}$ where: t = Mission/Operating Time and λ = Combined failure rate

or $\lambda = (3\lambda_A + \lambda_B + 2\lambda_C + 2\lambda_D + 3\lambda_E + 2\lambda_F + \lambda_G + 4\lambda_H + 13\lambda_J + 14\lambda_K + \lambda_L + \lambda_M + 4\lambda_N + 3\lambda_O + \lambda_P + \lambda_Q + \lambda_R + \lambda_S)$

Subscript Legend:

A = Signal Conditioner (N_h, N_e & N_p)
B = Signal Conditioner (β)
C = Select, Limit (N_k & N_p)
D = Load Sharing (Q_r & Q_e)
E = Limit Generators (N_1, Q_1 & T_5)
F = Signal Conditioner (T_5 & W_f)
G = Signal Conditioner (T_1)
H = Function Generator
J = Operational Amp
K = Summing Point
L = Least Voter
M = Most Voter
N = Integrator
O = Limiter
P = Low Limiter
Q = Proportional Var. Gain
R = Comparator (Hyster.)
S = Wiring & Connections

Figure 94. Advanced Engine Control System - Computer Portion Reliability Block Diagram.

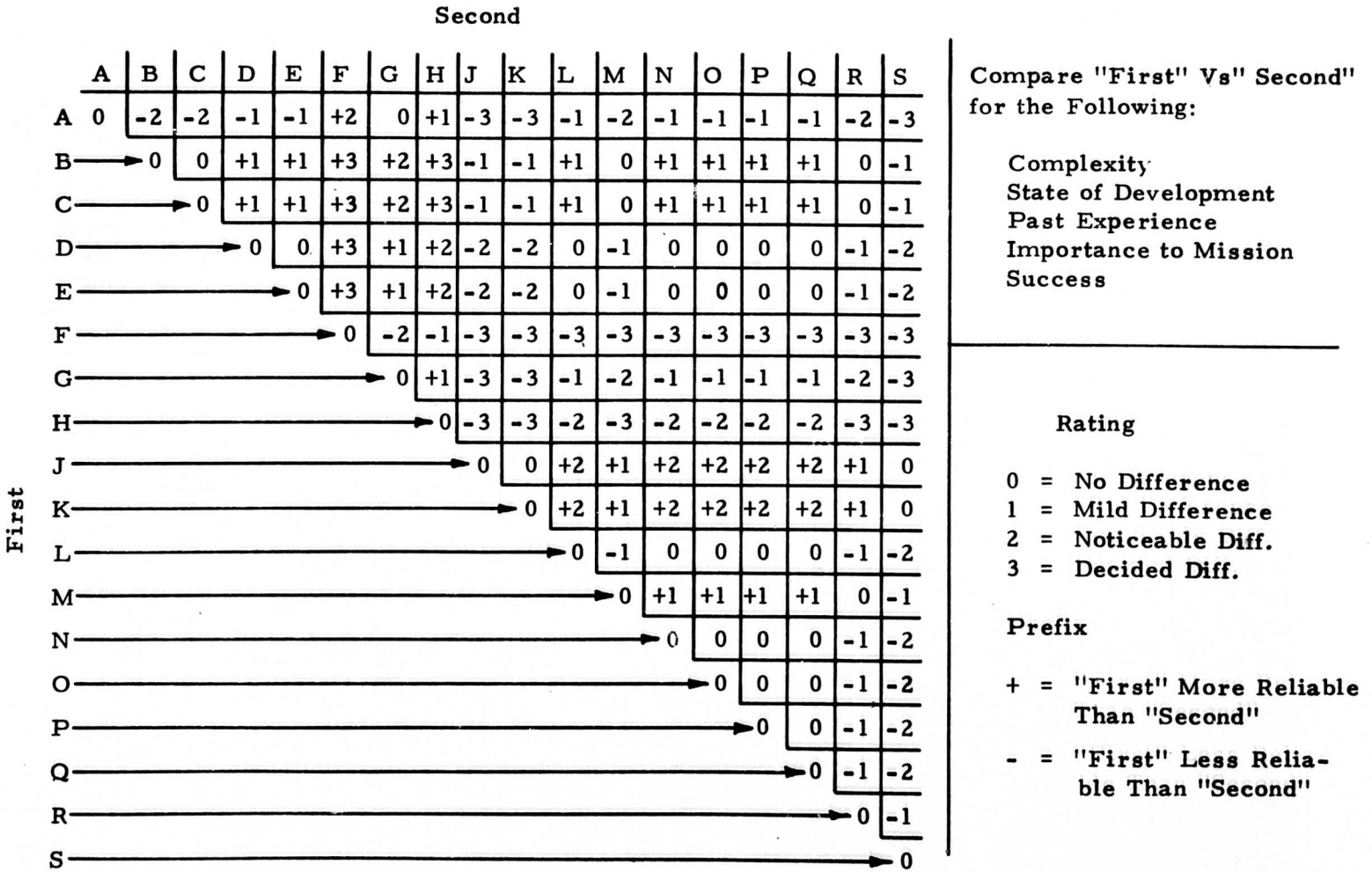

Figure 95 . Analog System - Reliability Apportionment Matrix.

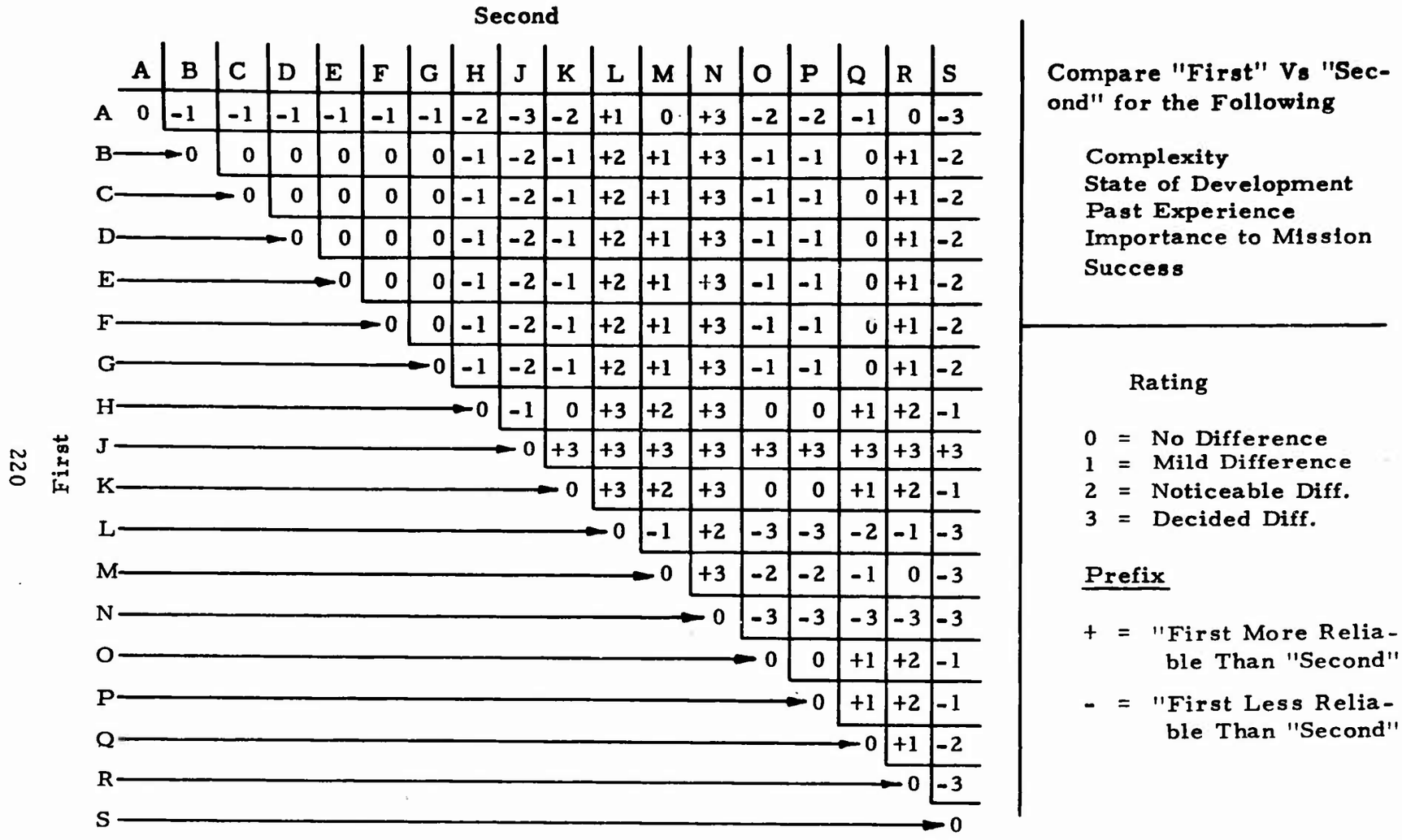

Figure 96 . Digital System - Reliability Apportionment Matrix.

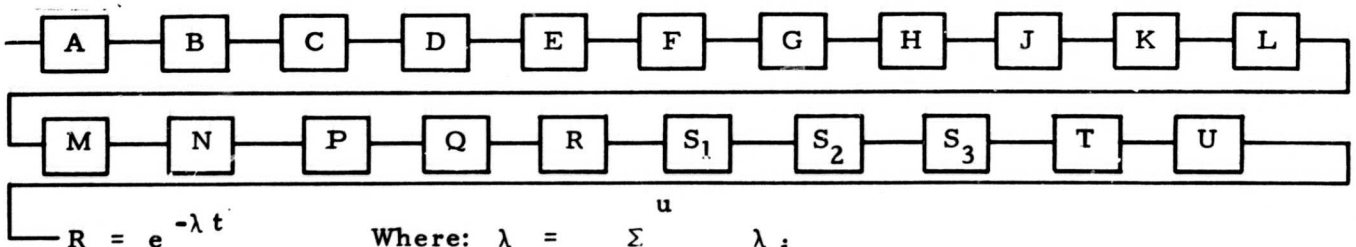

$R = e^{-\lambda t}$ Where: $\lambda = \sum_{i=A}^{u} \lambda_i$

t = Mission Time

A = N_h Actual
B = Accl. Lim. Func. Gen.
C = Accel. Lim. Amp.
D = Temp Multiplier
E = N_h Select
F = Temp. Amplifier
G = Decel Limit Func. Gen.
H = N_p Select
J = N_h Expand
K = Airbleed Trigger Control
L = Inlet Guide Vane Circuit
M = N_h Temp. Bias
N = Authority Circuit
P = Flow Elem. Amp. & Main Metering Circuit
Q = N_i Measuring Circuit
R = Power Supply
S = Torque Amp. Circuit
T = T_5 Measuring Circuit
U = Wiring & Connections

Figure 97 . Reliability Block Diagram - Analog Design.

APPENDIX III

FAILURE RATES AND RELIABILITY PREDICTIONS

FAILURE RATES

Failure rates for components on the microcircuit level are not generally available. However, overall, ten- to fifty-fold improvements are expected to result.* Our assessment is based on a twenty-fold improvement; i. e., the discrete component failure rates obtained from the above-mentioned sources are divided by 20 to give the "equivalent" integrated circuit level failure rate. The ensuing failure rates are primarily based on the latest FARADA Statistically Analyzed Data, which is believed to provide the best estimate due to its broad and varied data base. The failure rates are as follows:

Nomenclature:

λ = Failure rate
λ_d = Discrete component failure rate
λ_{ic} = Integrated circuit level failure rate.

Since there were 369,900 hours of operation with zero failures, the 50 percent confidence level rather than the point estimate is used.

Thus,

$$\lambda \, 50 \text{ percent} = \frac{^2\alpha f}{2T}$$

where $^2\alpha f$ is the value of the chi square deviate with f degrees of freedom, exceeded with the probability $1-\alpha$, and T equals the observed time.

Therefore,

$$\lambda_d = \frac{^2 50.2}{2T} = \frac{1.386}{(2)(369,900)} = 1.873 \times 10^{-6} \text{ failures/hr}$$

---

* "Microelectronic Reliability" by Charles E. Eliot, 1967 Annual Symposium on Reliability Proceedings, pages 349 through 358.

RESISTOR

$\lambda_d = 0.214 \times 10^{-6}$ failures/hr

Source: FARAD* Statistical Group A, Page 4.218
Volume 2, 2nd Edition, March 1968

$$\lambda_{ic} = \frac{0.214 \times 10^{-6}}{20} = 0.0107 \times 10^{-6} \text{ failures/hr}$$

CAPACITOR

$\lambda_d = 0.336 \times 10^{-6}$ failures/hr

Source: Same as above, page 4.29

$$\lambda_{ic} = \frac{0.336 \times 10^{-6}}{20} = 0.0168 \times 10^{-6} \text{ failures/hr}$$

DIODE

$\lambda_d = 0.054 \times 10^{-6}$ failures/hr

Source: Same as above, page 4.295

$$\lambda_{ic} = \frac{0.055 \times 10^{-6}}{20} = 0.0027 \times 10^{-6} \text{ failures/hr}$$

TRANSISTOR

$\lambda_d = 0.340 \times 10^{-6}$ failures/hr

Source: Same as above, page 4.361

$$\lambda_{ic} = \frac{0.340 \times 10^{-6}}{20} = 0.017 \times 10^{-6} \text{ failures/hr}$$

INTEGRATED CIRCUIT

$\lambda_{ic} = 0.4 \times 10^{-6}$ failures/hr

Source: MIL HDBK 217A**, page 7.4-6

INDUCTOR

$\lambda_d =$ Less than 2.7×10^{-6} failures/hr

Source: FARADA page 2.91 - Sept. 1, "68 issue

---

* Bureau of Weapons Failure Rate Data Program

** Military Standardization Handbook, "Reliability Stress and Failure Rate Data for Electronic Equipment".

RELIABILITY PREDICTION

The reliability predictions were made for the various circuits using failure rates from FARADA and MIL HDBK 217A as presented in detail in Appendix I. The reliability block diagram for the analog design is shown in Figure 97 and depicts every item as vital in the proper operation of the system, i.e., this initial prediction does not take into consideration the possibility of using airframe power in case of control power supply failure or the availability of the pilot manual control, a somewhat degraded mode of operation, in case of automatic system malfunction. The predictions based on parts count are as follows for the various computer elements:

Component	Quantity	Failure Rate (λ) X 10^{-6}
(A) N_h ACTUAL		
Resistors	7	0.0749
Capacitors	6	0.1008
Diodes	3	0.0081
Transistors	2	0.0340
Op. Amps	1	0.4000
		0.6178
(B) ACCELERATED LIMIT FUNCTION GENERATOR		
Resistors	13	0.1391
Capacitors	6	0.1008
Diodes	4	0.0108
Op. Amps	3	1.200
		1.4507
(C) ACCELERATED LIMIT AMPLIFIER		
Resistors	4	0.0428
Capacitors	2	0.0336
Op. Amps	1	0.4000
		0.4764

(D) TEMPERATURE MULTIPLIER

Resistors	35	0.3745
Capacitors	12	0.2016
Diodes	6	0.0162
Transistors	5	0.0850
Op. Amps	5	2.0000
		2.6773

(E) N_h SELECT

Resistors	26	0.2782
Capacitors	9	0.1512
Diodes	5	0.0135
Transistors	2	0.0340
Op. Amps	4	1.6000
		2.0769

(F) TEMPERATURE AMPLIFIER

Resistors	5	0.0535
Capacitors	3	0.0504
Diodes	1	0.0027
Op. Amps	1	0.4000
		0.5066

(G) DECELERATED LIMIT FUNCTION GENERATOR

Resistors	12	0.1284
Capacitors	2	0.0336
Op. Amps	1	0.4000
		0.562

(H) N_p SELECT

Resistors	26	0.2782
Capacitors	13	0.2184
Diodes	6	0.0162
Transistors	1	0.0170
Op. Amps	7	2.8000
		3.3298

(J) N_h EXPAND

Resistors	5	0.535
Capacitors	2	0.0336
Op. Amps	1	0.4000
		0.4871

(K) AIRBLEED TRIGGER CIRCUIT

Resistors	24	0.2568
Capacitors	7	0.1176
Diodes	5	0.0135
Transistors	1	0.0170
Transistors (Discrete)	1	0.3400
Op. Amps	4	1.6000
		2.3449

(L) INLET GUIDE VANE CIRCUIT

Resistors	13	0.1391
Capacitors	3	0.0504
Diodes	1	0.0027
Transistors	2	0.0340
Op. Amps	2	0.8000
		1.0262

(N) N_h TEMPERATURE BIAS

Resistors	15	0.1605
Capacitors	2	0.0336
Diodes	4	0.0108
Transistors	4	0.0680
Op. Amps	2	0.8000
		1.0729

(P) AUTHORITY CIRCUIT

Resistors	6	0.0642
Diodes	12	0.0324
Transistors	9	0.1530
		0.2496

(Q) FLOW ELEMENT AMPLIFIER

Resistors	30	0.3210
Capacitors	11	0.1848
Diodes	6	0.0162
Transistors	1	0.0170
Transistors (Discrete)	2	0.6800
Op. Amps	4	1.600
		2.819

(R) N_1 MEASURING CIRCUIT

Resistors	20	0.2140
Capacitors	3	0.0504
Op. Amps	4	1.6000
		1.8644

(S) POWER SUPPLY

Diodes (Bridge) (Discrete)	4	0.776
Diodes (Zener) (Discrete)	2	3.746
Resistors (Discrete)	1	0.214
Capacitors (Discrete)	2	0.672
Inductors (Discrete)	1	1.873
Transistors (Discrete)	1	0.340
		7.621

(T) TORQUE AMPLIFIER CIRCUIT

Resistors	9	0.0963
Diodes	2	0.0054
Op. Amps	2	0.8000
		0.9017

(U) T_5 MEASURING CIRCUIT

Resistors	25	0.2675
Capacitors	3	0.0504
Op. Amps	6	2.4000
		2.7179

(V) WIRING AND CONNECTIONS

Welds	585	0.585

Table XII is a tabulation of the various circuit predictions and depicts an MTBF of 20,363 hours for the present design.

TABLE XII. ANALOG PREDICTION				
		Failure Rate (λ) in Failures Per 10^6 Hours		
Math Model Designation	Description	Per Block	Quantity System	Per System
A	N_h Actual	0.618	1	0.618
B	Accel Limit Function Generator	1.451	1	1.451
C	Accel Limit Amplifier	0.476	1	0.475
D	Temperature Multiplier	2.677	1	2.677
E	N_h Select	2.077	1	2.077
F	Temperature Amplifier	0.507	1	0.507
G	Decel Limit Function Generator	0.562	1	0.562
H	N_p Select	3.330	1	3.330
J	N_h Expand	0.487	1	0.487
K	Airbleed Trigger Control	2.345	1	2.345
L	Inlet Guide Vane Circuit	1.026	1	1.026
M	N_h Temp. Bias	1.073	1	1.073
N	Authority Circuit	0.250	1	0.250
P	Flow Element Amplifier	2.819	1	2.819
Q	N_1 Measure Circuit	1.864	1	1.864
R	Power Supply	7.621	3	22.863
S	Torque Amplifier Circuit	0.902	1	0.902
U	Wiring and Connections	0.585	1	0.585
TOTAL	$MTBF = \frac{1}{48.63 \times 10^{-6}} = 20,563$ Hours			48 63

APPENDIX IV

TEST OF CIRCUITS DIRECTLY EXPOSED TO COOLING FLUID

GENERAL

To evaluate the fluid immersion cooling technique, three separate tests were performed in the laboratory to gather operating performance data on semiconductor chip elements immersed in a dielectric cooling fluid.

The first test performed was temperature-humidity cycling of several integrated circuits and a transistor element. The second series of tests was performed on semiconductor elements which were temperature-cycled over the range of -65° to +250° F. The third test was performed to evaluate the effects on the power dissipation of the semiconductor chips.

Test objectives included evaluating the immediate and long-term physical effects on the performance characteristics of the chip elements.

Results from test data obtained after more than 700 hours of continuous element operation show that the direct fluid immersion of the semiconnector chip elements does not affect either the electrical or the physical properties of those devices and that the fluid immersion approach is sound for the computer application.

FIRST TEST

Six Texas Instruments-type S/N 5400 integrated circuits and one 2N760 general-purpose low-power silicon transistor with several supporting carbon resistors were subjected to the temperature-humidity cycling tests per MIL-STD-810 method 507. These devices were tested in the operating and nonoperating conditions between the temperature limits of +77° and +160° F.

The integrated circuits and 2N760 transistor chips were subjected to the above environment in an unsealed condition while immersed in a thermally conductive high dielectric silicon base fluid. The devices used were first ultrasonically cleaned in a Freon solution and then visually inspected using a microscope. The devices were interconnected and tested electrically at room temperature with the following results:

1. Of 24 outputs available from the S/N 5400 devices, 21 were found to be satisfactory electrically during room-temperature bench

tests. The three bad outputs were caused by physical damage during opening of their hermetically sealed cases and subsequent ultrasonic cleaning operations. The 2N760 transistor was checked and found to be electrically sound.

2. The devices were tested again electrically at room temperature prior to immersing the devices in the fluid. Subsequent tests with the devices immersed at room temperature showed no electrical changes in propagation times.

Although the test was terminated following approximately 28 hours of valid test time, some preliminary conclusions can be drawn from available test data. These conclusions are:

1. Room temperature tests prove that the fluid had not affected the semiconductor "chip" electrical operation.

2. Operation of the "chip" at the elevated temperature limit of 160° F while immersed in the fluid had no effect on the electrical characteristics of "sound" devices.

3. The sound chips would operate satisfactorily in the fluid while subjected to a 90 percent humid environment with temperature cycling for the test time period involved.

Table XIII summarizes the encouraging results of the above test.

SECOND TEST

As a supplement to the above, additional tests were performed with General Instrument Corporation MEM-550C type semiconductor units, which are more representative of the devices chosen for use in the digital control circuit devices.

The type MEM-550 units were received from General Instrument with the cover removed, therefore not requiring they be opened.

The devices were mounted in a brass can,and the can was solder-sealed and subsequently filled with the dielectric coolant fluid during the test described below.

To eliminate premature failures or weak devices, the units, when mounted and sealed in the can, were tested by random application of test power for approximately 4 hours. The units were then subjected to a

subsequent power-applied burn-in at room ambient temperature for a 74-hour period. No failures occurred during this time.

The can containing the chip devices was filled with dielectric coolant and solder-sealed. The test power was applied for a second 48-hour period at room ambient temperature conditions. The performance of the devices was periodically monitored. No changes were noted in performance characteristics, and no failures occurred.

The tests were continued in a temperature test chamber whose temperature was varied between the range of -65° and +250° F for time periods shown in Table XIV. No changes were noted in performance characteristics, and no failures occurred. To date, 740 hours of testing have been accumulated. Testing is continuing with periodic monitoring to gather additional life data. It is of interest to note that a JAN accelerated aging test is performed at temperatures ranging from -35° to +150° F for 14 cycles for a period of 336 hours. This accelerated test is equivalent to and represents five years of normal component usage.

The test results indicate that silicon semiconductor chip elements can be subjected to the direct fluid immersion techniques for prolonged periods without suffering changes to their electrical or physical characteristics.

THIRD TEST

The data below are submitted to point out the power dissipation advantages which are gained by using the direct semiconductor fluid immersion technique. Several silicon transistor "chips", type 2N760, were subjected to power dissipation tests. The units were tested to destruction by deliberately exceeding their power ratings. The units were both in an unsealed condition in ambient air and in the dielectric coolant. It is of interest to note that the power dissipation to induce failure doubled for the immersed units. (See Table XV.)

TABLE XIII. FLUID IMMERSION TEST RESULTS

Device	No. of Initially Good Outputs	No. of Good Outputs at Test Termination	Remarks
A	3	3	No Change
B	4	4	No Change
C	4	3*	Indicated Intermittent Operation
D	2	0	Failed Completely
E	4	4*	Indicated Intermittent Operation
F	4	3*	Indicated Intermittent Operation
Transistor	Good	Good	No Change

* Analysis showed intermittent operation due to test fixture problems.

TABLE XIV. FLUID IMMERSION EVALUATION WITH TEMPERATURE CYCLING

BURN-IN, DRY		
Temperature	**Power-On Time**	**Power-Off Time**
Ambient	74 hours	19 hours
TEMPERATURE CYCLE - IMMERSED		
Temperature	**Power-On Time**	**Power-Off Time**
+259°F	27.5 hours	49.5 hours
Ambient	28.5 hours	150.5 hours
-65°F	14 hours	16.5 hours
Burn-in ON Time	74.0	
ON time in fluid	70.0	
OFF time in fluid	216.5	
TOTAL TIME	360.5 hours	

Devices and Quantity on Test

(6) General Instrument MEM 550C (Dual P Channel-Enhancement Mode Silicon Insulated Gate Field Effect Transistor)

(6) Texas Instrument SN 5451 (Dual 2 Wide 2 Input and/or Invert Gates)

(1) N760A (NPN Silicon Amplifier)

TABLE XV. POWER DISSIPATION TEST

Unit	Normal Rated Wattage	Wattage Dissipation at Failure	
		Unsealed in Ambient Air	Immersed in Fluid
2N760 #1	0.5	1.18 watts	2.16 watts
2N760 #2	0.5	1.45 watts	2.10 watts

APPENDIX V

SOAK TEMPERATURE TIME PROFILE TEST

As background information for the computer thermal design, temperature measurements were made at several locations within the engine nacelle of a Lycoming-based Grumman Mohawk Test Aircraft.

Test results are summarized in Figures 98 through 100. Figure 98 shows the skin temperature changes as a function of time at the 12 o'clock position on the engine inlet housing, 6 inches aft. All temperatures measured with the aircraft facing downwind are slightly higher than those measured facing upwind. A maximum temperature of 133° F was reached 24 minutes after shutdown and remained constant throughout the recording period.

Figure 99 illustrates the ambient temperature changes as measured 1 inch above the compressor first stage. Two minutes after engine shutdown, the temperature peaked to a maximum of 137° F, after which the temperature gradually decreased to a fairly constant level for the entire recording period.

Fuel temperatures measured at the fuel-in and fuel-out ports of the fuel control showed little change throughout the recording period.

Skin temperature changes of the compressor diffuser are shown in Figure 100. There was a marked drop in temperature during the first 2 minutes after shutdown, followed by a slight increase, and then the temperature decreased. Facing upwind, the temperature decreased from 387° to 200° F after 2 minutes from shutdown; while facing downwind, the rate of temperature change was much smaller.

Test results above show that for this particular engine application, the 15-minute soaking period specified in Military Specification MIL-E-5007C is perhaps not adequate for system demonstration. The temperature profiles shown in Figures 98 through 100 demonstrate that the engine nacelle ambient temperatures do not peak and then decrease rapidly after a 15-minute soaking time following engine shutdown, as might be expected, but continue on considerably beyond the 30-minute time shown on the attached curves. With the engine bleed bands open and with a skin temperature on the compressor diffuser of 266° F, the nacelle ambient temperature did not rise above 140° F.

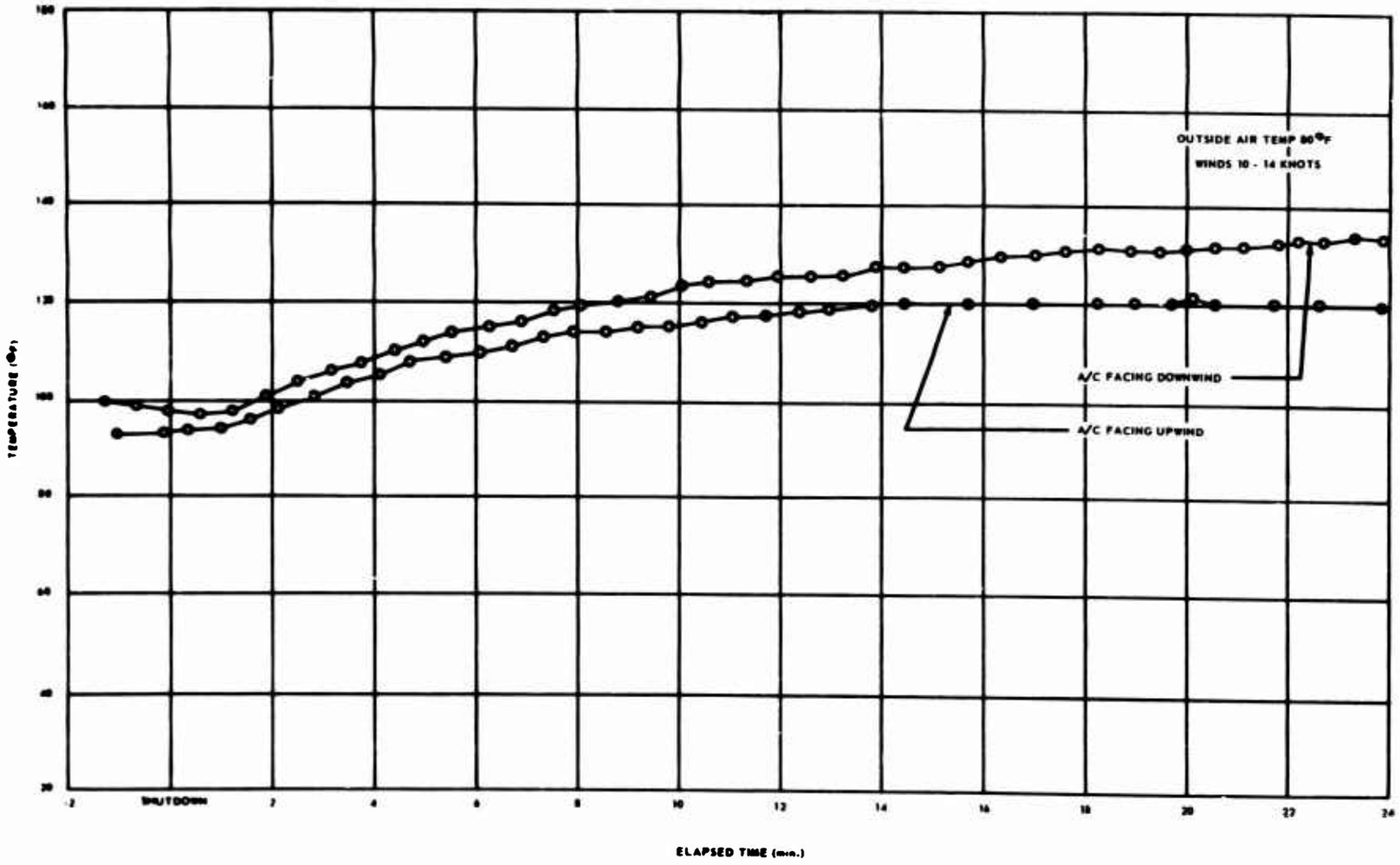

Figure 98. Engine Components Soak Temperature Survey - Engine Inlet Housing Skin Temperature.

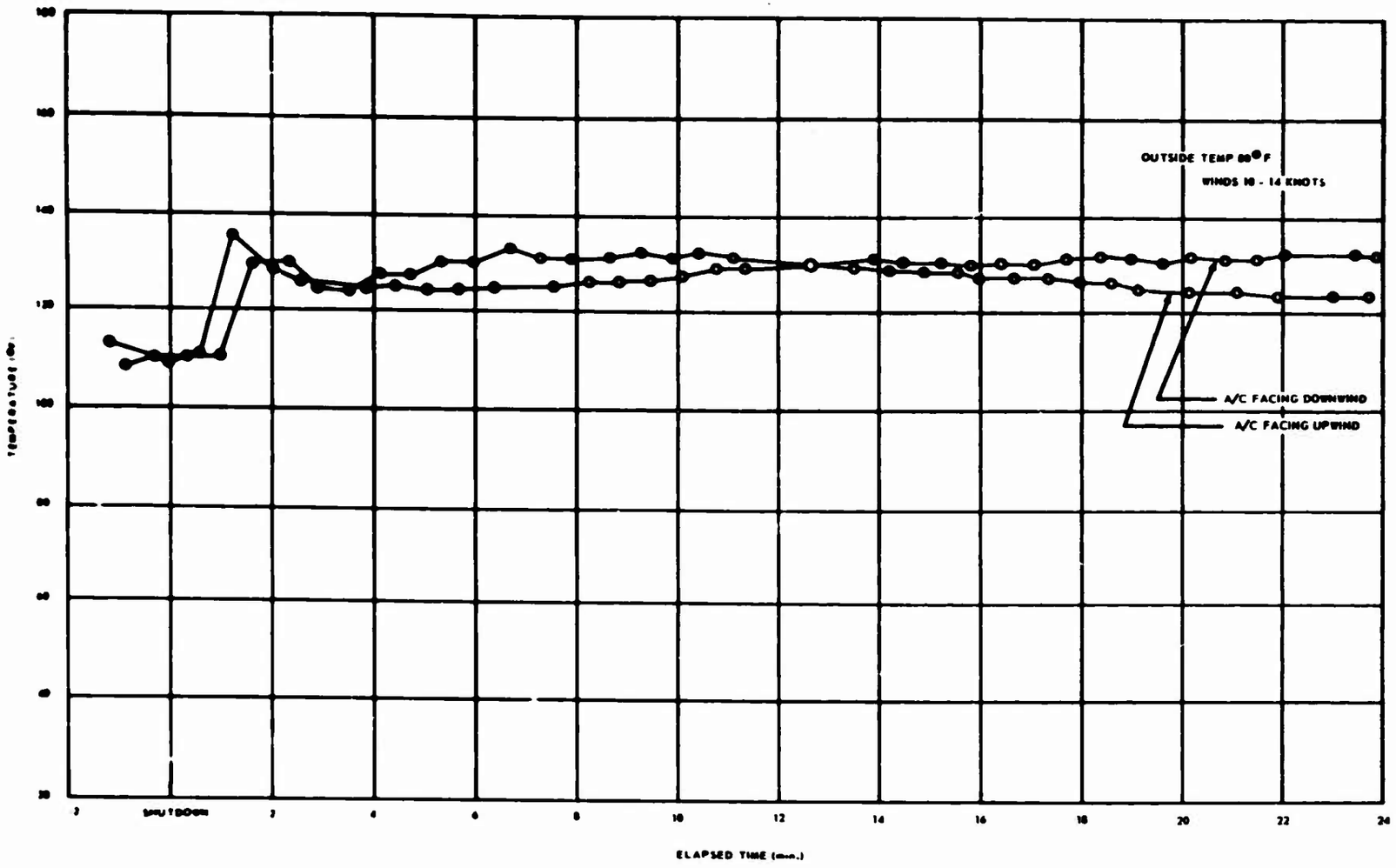

Figure 99. Engine Components Soak Temperature Survey - Nacelle Temperature.

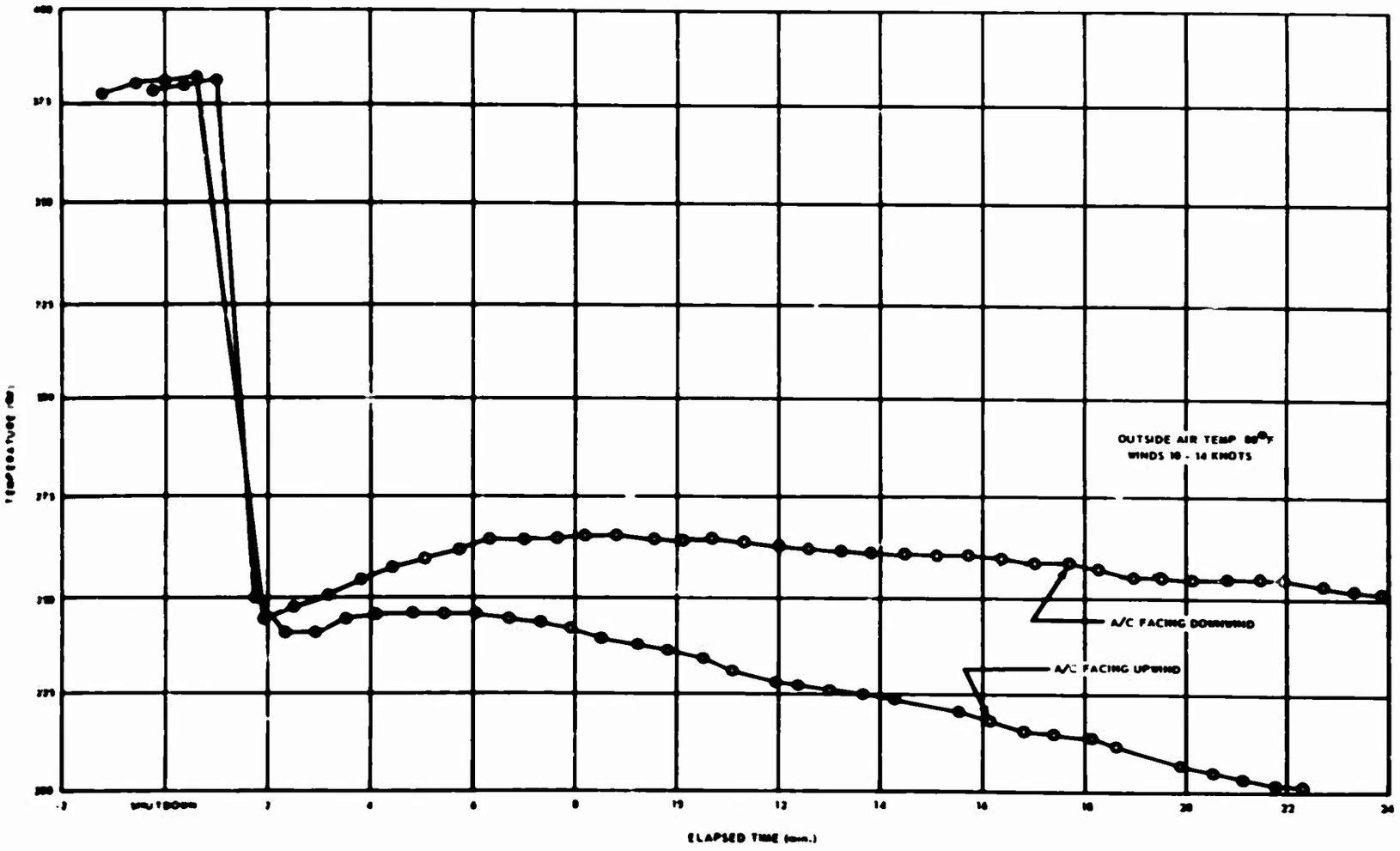

Figure 100. Engine Components Soak Temperature Survey - Compressor Diffuser Skin Temperature.

APPENDIX VI

GENERATOR DESIGN

BACKGROUND

Current military specifications state that the engine control system must be able to provide safe operation and starting capability without assistance from the airframe electrical power system. This implies that an engine-mounted generator must be available for supplying the power requirements of the electronic control system. The concept of Fuel Metering System No. 2 permits a new approach to generator design, and, as an addendum to the program, a study was made of a unit integral with the centrifugal fuel pump.

If the generator is driven directly from the gas producer, it must operate over a 10-to-1 speed range, creating power control problems due to excess output at the higher speeds. At 10-percent engine speed, the generator would turn at 6000 rpm. However, if it were driven at fuel pump speed in System No. 2, the minimum speed would be 19,000 rpm, allowing a significant reduction in size for the same power requirement. Since the speed range is only 2.25 to 1 in this location, the available output is closely related to system requirements and the power control system becomes simpler and more efficient.

REQUIREMENTS

The generator design was determined by the following considerations:

1. Output voltage regulation by control of field excitation is required. Limitations on space and heat dissipation in the computer rule out shunt regulation and other power-wasting methods. Sufficient residual field flux must be retained for the generator to be self-starting.

2. A solid-rotor, brushless machine with encapsulated stator and rotor is mandatory due to the environmental conditions inside the system housing.

3. Four different output voltages are required with $\pm$ 10 percent regulation accuracy. The generator must produce at least 100 watts at 20,000 rpm.

4. Environmental and service life requirements are the same as for the fuel metering section.

GENERATOR DESIGN

A flux-switch generator with wound field excitation was selected for installation in the fuel pump housing. A schematic of the generator is presented in Figure 101. Power generation is achieved by a simple flux-switching action in which the rotor alternately completes one or the other of the two opposing flux paths. Each output winding experiences a complete field reversal when the flux path is changed and produces an alternating current output. Field strength is controlled to obtain output voltage regulation.

A suitable generator was designed and is shown included in the fuel system design (Figure 76). The rotor is an encapsulated, laminated iron sleeve located on the fuel pump shaft. Stator iron and windings are encapsulated to form a cartridge, which is installed in the fuel pump housing. Oil spray cooling of the stator may be provided if necessary.

CONCLUSIONS

The required electrical outputs for the proposed control system can be produced by a flux switch generator located in the fuel pump assembly. The inclusion of the generator would increase package length by 0.25 inch and package weight by 0.50 pound. Additional torque loads imposed on the VSD section during speed changes require further design analysis to determine the final size of the transmission elements.

The advantage of the VSD-driven generator design is that it results in a much smaller unit which operates over a narrow speed range compared to a generator driven directly from the gas producer.

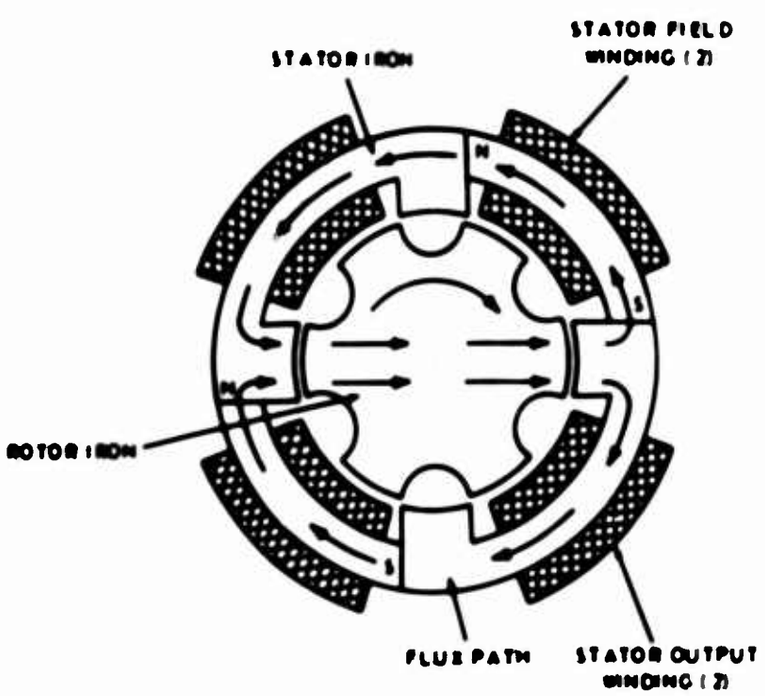

Figure 101. Schematic of Flux Switch Generator Assembly.

Unclassified

Security Classification

DOCUMENT CONTROL DATA - R & D

(Security classification of title, body of abstract and indexing annotation must be entered when the overall report is classified)

1 ORIGINATING ACTIVITY (Corporate author) Avco Lycoming Division Stratford, Connecticut	2a. REPORT SECURITY CLASSIFICATION Unclassified 2b. GROUP

3 REPORT TITLE

ADVANCED ENGINE CONTROL SYSTEM STUDY

4 DESCRIPTIVE NOTES (Type of report and inclusive dates)

Final Report, 1 July through 31 December 1968

5 AUTHOR(S) (First name, middle initial, last name)

Robert Hatch
Joseph Karol

6 REPORT DATE August 1969	7a. TOTAL NO. OF PAGES 262	7b. NO. OF REFS
8a. CONTRACT OR GRANT NO DAAJ02-68-C-0042 b. PROJECT NO 1G162203D144 c. d.	9a. ORIGINATOR'S REPORT NUMBER(S) USAAVLABS Technical Report 69-53 9b. OTHER REPORT NO(S) (Any other numbers that may be assigned this report) Avco Lycoming Report No. 105.5.6	

10 DISTRIBUTION STATEMENT

This document is subject to special export controls, and each transmittal to foreign governments or foreign nationals may be made only with prior approval of US Army Aviation Materiel Laboratories, Fort Eustis, Virginia 23604.

11 SUPPLEMENTARY NOTES	12 SPONSORING MILITARY ACTIVITY US Army Aviation Materiel Laboratories Fort Eustis, Virginia

13 ABSTRACT

This report presents the results of a program conducted to design and evaluate an advanced engine control system for a small (2 to 5 pounds per second airflow) turboshaft engine.

The objective of this program was to evaluate the feasibility of a unique engine control system consisting of closed-loop turbine-inlet-temperature limiting, electronic computation and either of two novel fuel metering systems.

Control mode logic and dynamics were analyzed using computer simulation techniques. Control computer logic and circuitry were established, and all elements of the control system were designed.

It was concluded that a miniaturized advanced control system, weighing 6 to 9 pounds (including pump), is feasible with either of two fuel metering systems and with either analog or digital electronic computation.

All components of the control systems evaluated during this study program are within a reasonable level of technology commensurate with production by the mid-to-late 1970's.

DD FORM 1473

Unclassified

Security Classification

Unclassified

Security Classification

14. KEY WORDS	LINK A		LINK B		LINK C	
	ROLE	WT	ROLE	WT	ROLE	WT
Advanced Engine Control System						
Control System Study for Small Turboshaft Engine						
Engine (2 to 5 pounds per second airflow) Control System						
Study of Control System for Small Turboshaft Engine						

Unclassified

Security Classification